

Electronic Thesis and Dissertation Repository

---

8-21-2020 2:45 PM

## Seismic Hazard Assessment for Mainland China Based on Spatially Smoothed Seismicity and Projected Sets of Ground Motion Models

Chao Feng, *The University of Western Ontario*

Supervisor: Hong, Hanping, *The University of Western Ontario*

A thesis submitted in partial fulfillment of the requirements for the Doctor of Philosophy degree in Civil and Environmental Engineering

© Chao Feng 2020

Follow this and additional works at: <https://ir.lib.uwo.ca/etd>



Part of the [Civil Engineering Commons](#), and the [Structural Engineering Commons](#)

---

### Recommended Citation

Feng, Chao, "Seismic Hazard Assessment for Mainland China Based on Spatially Smoothed Seismicity and Projected Sets of Ground Motion Models" (2020). *Electronic Thesis and Dissertation Repository*. 7222.

<https://ir.lib.uwo.ca/etd/7222>

This Dissertation/Thesis is brought to you for free and open access by Scholarship@Western. It has been accepted for inclusion in Electronic Thesis and Dissertation Repository by an authorized administrator of Scholarship@Western. For more information, please contact [wlsadmin@uwo.ca](mailto:wlsadmin@uwo.ca).

## Abstract

The latest version of the Chinese seismic hazard map (CSHM) (i.e., fifth-generation CSHM) was developed based on the delineated seismic source model, which is defined based on geological and seismological information but also with some subjectivities. The results of the CSHM were presented in terms of peak ground acceleration (PGA) and peak ground velocity. No maps for spectral acceleration (SA) are given. This is partly due to the ground motion models (GMMs) to predict SA for mainland China are unavailable. The unavailability of the GMMs for SA results in the lack of uniform hazard spectra (UHS) that is important for structural seismic design.

There is a gap in the development of the new GMMs and seismicity models for Chinese seismic hazard mapping. This thesis is focused on the evaluation of the seismic hazard and the development of the uniform hazard spectra for mainland China. For the evaluation, a set of GMMs applicable to mainland China is developed by applying the so-called projection method. This method projects the GMMs developed for a reference region with a large number of historical records to a target region where the actual ground motions are scarce. For the projection, the NGA-West2 GMMs developed for California are considered for the reference region, and different regions in mainland China are considered as the target regions.

Rather than using the delineated seismic source model, smoothed seismic source regions based on the historical catalogue and spatial smoothing techniques are considered. Moreover, an analysis is carried out to assess the completeness of the historical Chinese earthquake catalogue. Two smoothed seismic hazard models for mainland China are obtained. The first one is based on cluster analysis and spatial smoothing by considering that a seismic magnitude-recurrence is applicable to a cluster, so the smoothing is carried out for the annual earthquake occurrence rate. The second one considers that the magnitude-recurrence relation is spatially varying, which is obtained by carrying out the smoothing by considering the earthquake magnitude (i.e., the smoothing the cumulative event count as a function of magnitude).

The CSHMs for mainland China are assessed using the newly projected GMMs, which could be used to predict the PGA and SA and the spatially smoothed seismicity models. A parametric investigation is carried out by considering different combinations of GMMs, magnitude-recurrence relations, and smoothed source models. The logic tree approach is used to represent the combinations. The newly developed CSHMs are presented in terms of PGA and SA. In addition, the uniform hazard spectra are developed for different locations within mainland China. A comparison of the newly developed seismic hazard maps to that of the fifth-generation CSHM indicates that they exhibit similar trends, although there are differences in the estimated return period values of PGA. A comparison of the normalized UHS to the standardized design spectrum in Chinese design codes is presented, indicating that the standardized design spectrum is conservative for short and long natural vibration periods.

## Keywords

Seismic hazard assessment; ground motion model; projection method; smoothed seismicity model; magnitude-recurrence relation; logic tree; normalized uniform hazard spectra; Chinese seismic hazard map.

## Summary for Lay Audience

The seismic hazard maps are used as the basis to recommend seismic loads for structural design in codes and standards. The most recent Chinese seismic hazard map (CSHM) (i.e., the 5<sup>th</sup> generation CSHM) has been released. The map presents the estimated peak ground acceleration for a specified probability of exceedance per year. The estimated peak ground acceleration uses the delineated seismic source zones (the considered regions is delineated based on different seismic belts), magnitude frequency distribution relations, and ground motion models (GMMs) that estimates the ground motion for given earthquake events and distance. The presented study is focused on these three aspects of the modelling and assignments in order to assess seismic hazard for mainland China to study the adequacy of the reported seismic hazard by the 5<sup>th</sup> generation CSHM. New sets of the GMMs to predict the peak ground acceleration and spectral acceleration for different regions in mainland China are developed by using the projection method and based on the GMMs developed for the U.S. Spatially smoothed source models based on the historical earthquake catalogue, instead of using the delineated seismic source model, are proposed and examined. Besides, the use of spatially smoothed seismicity allowed the development of regional or site-dependent magnitude-recurrence relations.

By using the newly developed seismic source models, GMMs, and magnitude-recurrence relations, the seismic hazard mapping for mainland China is carried out using numerical simulation techniques. In addition, the site-dependent uniform hazard spectra (UHS), which are currently unavailable for mainland China, are developed. An extensive comparison of the resulting hazard map with the 5<sup>th</sup> generation CSHM is carried out. In general, the results for the peak ground acceleration are in agreement with that given by the 5<sup>th</sup> generation CSHM, although there are differences. The comparison of the UHS with the seismic design spectra recommended in Chinese structural design codes indicates that the latter can be conservative or unconservative depending on the fundamental natural vibration period of the structure.

## Co-Authorship Statement

The material presented in Chapter 2, 3, 4 of this thesis have been published or submitted for potential publication in peer-reviewed journals.

A version of Chapter 2, that is co-authored by H. P. Hong and C. Feng, is published in the *Bulletin of Seismological Society of America*. The publication is “On the Ground Motion Models for Chinese Seismic Hazard Mapping. *Bulletin of the Seismological Society of America*, 109 (5), pp. 2106–2124, 2019, doi: 10.1785/0120180269”.

A version of Chapter 3, that is co-authored by C. Feng, T. J. Liu and H. P. Hong, is published in the *Journal of Seismology*. The publication is “Seismic hazard assessment for mainland China based on spatially smoothed seismicity. *Journal of Seismology*, 24, pp. 613-633, 2020, doi: 10.1007/s10950020099183”.

A version of Chapter 4, that is co-authored by C. Feng, and H. P. Hong, is submitted to a peer-reviewed journal for possible publication.

# **Dedication**

To my parents and my grandmother

## Acknowledgments

I would like to express my greatest appreciation to my supervisor, Professor Hanping Hong, for his guidance, comments and suggestions to this thesis. I can not finish this thesis without his patience and continuous encouragement in the five years Ph.D. study. He taught me the methodology to carry out the research and how to present the work in a logical way. I am grateful for having the opportunity to be his student and work with him in this topic. I would never forget those discussion time with Professor Hanping Hong, he is shape and serious in the research which influenced me deeply, I learnt a lot from him and hopefully I could be a responsible supervisor like him in the future.

I want to give my thanks to my colleges and friends, Ji bao, Xizhong Cui, Jiyang Gu, Qian Tang, Minyu Xiao, Jungmyung Kim, Chao Sheng, and Yongxu Liu and Qian Huang in the research group. When I feel tired from working, the talking with them makes me relaxed, they are nice person and its great fun working with them.

The financial support from Chinese government scholarship is gratefully acknowledged, I also acknowledge the final support from The University of Western Ontario during my study.

Finally, I want to express my appreciation to my family for their love and encouragement. I deeply thank my parents, and my grandmother. The unconditional love that I get from you is priceless in my life.

# Table of Contents

Abstract.....	ii
Summary for Lay Audience.....	iv
Co-Authorship Statement.....	v
Acknowledgments.....	vii
Table of Contents.....	viii
List of Tables.....	xi
List of Figures.....	xiii
Nomenclature.....	xvii
Chapter 1.....	1
1 Introduction.....	1
1.1 Background.....	1
1.2 Objectives and thesis outline.....	3
1.3 References.....	5
Chapter 2.....	10
2 On the Ground Motion Models for Chinese Seismic Hazard Mapping.....	10
2.1 Introduction.....	10
2.2 IPEs and GMMs used for Chinese seismic hazard maps.....	12
2.2.1 IPEs used for the third-generation CSHM.....	12
2.2.2 IPEs and GMMs used for the 4th-generation CSHM.....	16
2.2.3 IPEs and GMMs for developing the fifth-generation CSHM.....	23
2.3 Comparison of the IPEs and GMMs used for the CSHMs.....	27
2.3.1 Comparison of the intensity attenuation and sigma.....	27
2.3.2 Comparison of the GMMs.....	34



2.4	New GMMs and effect of sigma on the UHS.....	38
2.5	Conclusions.....	49
2.6	Data and Resources.....	50
2.7	References.....	51
Chapter 3.....		57
3	Seismic Hazard Assessment for Mainland China Based on Spatially Smoothed Seismicity.....	57
3.1	Introduction.....	57
3.2	Completeness analysis of historical earthquake catalogue .....	59
3.2.1	Chinese historical earthquake catalogue.....	59
3.2.2	Removing aftershocks and completeness analysis of Chinese catalogue.....	61
3.2.3	Estimating magnitude-recurrence relation for a region .....	65
3.3	Seismic hazard mapping for mainland China .....	69
3.3.1	Spatial smoothing of earthquake occurrence .....	69
3.3.2	Spatial smoothing results .....	71
3.4	Seismic hazard mapping .....	76
3.4.1	Ground-motion models.....	76
3.4.2	Hazard maps for PGA, SA and uniform hazard spectra .....	79
3.5	Conclusions.....	86
3.6	References.....	88
Chapter 4.....		92
4	Projecting sets of ground motion models and their use to evaluate seismic hazard and UHS for mainland China.....	92
4.1	Introduction.....	92
4.2	New sets of ground motion models by using projection method.....	95
4.3	Procedure to evaluate UHS and adopted source models .....	107

4.3.1	Spatially smoothed seismic source models .....	107
4.3.2	Seismic hazard assessment procedure .....	112
4.4	Estimated UHS and mapped seismic hazard .....	114
4.4.1	Estimated hazard and UHS for the reference case .....	114
4.4.2	Sensitivity analysis and discussion .....	120
4.5	Conclusions .....	121
4.6	References .....	123
Chapter 5	.....	130
5	Conclusions and Potential for Future Work .....	130
5.1	Conclusions .....	130
5.2	Potential future work .....	132
5.3	References .....	132
Appendix	.....	134
Appendix A:	A summary for the Chinese GMMs .....	134
Appendix B:	k-means cluster analysis results .....	175
Curriculum Vitae	.....	179

## List of Tables

Table 2.1. Model coefficients for Eq. (2.2) used for the third- to fifth-generation CSHMs. .....	15
Table 2.2. Model coefficients for Eq. (2.7) ( $c_3 = 0$ ) (Wang et al. 2000).....	22
Table 2.3. Model coefficients for Eq. (2.7) developed by Yu et al. (2013) for the reference region ( $c_3 = 0$ . The inequality symbols are used as those shown in the reference).....	25
Table 2.4. Model coefficients for EPA and EPV applicable to some regions in China (Yu et al., 2013). .....	25
Table 2.5. Sigma for some selected attenuation relations for macro-intensity $I$ .....	32
Table 2.6. Model coefficients for Eq. (2.2) applicable to regions in China for a random orientation. ....	39
Table 2.7. Effect of sigma on estimated PGA with 63% in 50 years exceedance. ....	47
Table 2.8. Effect of sigma on estimated PGA with 10% in 50 years exceedance. ....	48
Table 3.1. $T_{AS}$ used to classify aftershocks (Gardner and Knopoff 1974).....	62
Table 3.2. Estimated model parameters based on $M_{smin} = 4.75$ for the magnitude-recurrence relation ( $\text{Var}(\ )$ represents the variance of its argument). ....	67
Table 3.3. Location of the selected twelve sites and the estimated PGA (g). For the estimated PGA, the first and second entries correspond to Case C1 = (Case I, nS, $\beta$ -LSF and BSSA14-P) and Case C2 = (Case II, $\lambda$ S and BSSA14-P), respectively. ....	76
Table 3.4. GMMs for PGA for a random orientation estimated based on the geometric mean of the GMMs for long and short axes given in Yu et al. (2013) ( $c_3 = 0$ ). ....	77
Table 4.1. Magnitude scaling term and geometric attenuation anelastic attenuation term for the logarithm of PGA or SA in the GMMs.....	99

Table 4.2. Model coefficients for the projected GMMs for selected  $T_n$ . .....102

Table 4.3. Estimated quantile values by considering 63%, 10% and 2% probability of exceedance in 50 years and 10% in 50 years value given in fifth-generation CSHM (Gao et al. 2015) (COV is calculated from the upper tail distribution fitting for Case 1). .....116

## List of Figures

<p>Figure 2.1. Illustration of the projection method proposed by Hu and Zhang (1984): The subscripts A and B denote the reference and target regions, respectively; circled numbers 1-5 in the figure represent the steps of the projection method. Given a scenario event defined by its magnitude and <math>R_{epi}</math> shown at circled number 1, find its intensity for the target region at circled number 2, find circled number 3 for the reference region based on equal intensity, find the ground motion measure for the reference region at circled number 4, and define the ground motion measure shown at circled number 5. ....</p>	18
<p>Figure 2.2. Comparison of predicted intensity along the major axis (III, IV and V refer to the IPEs used for the third, fourth and fifth-generation CSHM. The notations are also used in Figure 2.3, Figure 2.5 and Figure 2.6. ....</p>	27
<p>Figure 2.3. Comparison of predicted intensity along the minor axis in different regions.</p>	28
<p>Figure 2.4. Comparison of predicted I (i.e., MMI) by using Eqs. (2.6), (2.10), (2.11), and (2.12). ....</p>	30
<p>Figure 2.5. Comparison of predicted EPA, <math>a_E</math>. ....</p>	34
<p>Figure 2.6. Comparison of the GMMs developed for the reference region. ....</p>	36
<p>Figure 2.7. Sigma associated with <math>\ln Y</math> (First row for PGA or SA associated with BSSA14; Second row for PGA considering different target regions; the grey horizontal surface represents the sigma for GMMs used for the fifth-generation CSHM). ....</p>	37
<p>Figure 2.8. Model coefficients for the projected GMMs. ....</p>	41
<p>Figure 2.9. Comparison of the predicted ground motion measures (the model coefficients shown in Table 2.4 for major axis are used to plot the PGA predicted by YLX13). ....</p>	42
<p>Figure 2.10. Considered source zones and sites and estimated uniform hazard spectra for 5% damping ratio and a return period of 50 year (Panel a) and b) shows the source zones and the remaining panels shows the normalized UHS). ....</p>	44

Figure 3.1. Earthquake events with $M_s \geq 4.0$ in the catalogue and after 1500 AD: a) Including the aftershocks and b) Excluding aftershocks. ....	61
Figure 3.2. Cluster analysis results and assigned seismic regions: a) Case I – six seismic regions; b) Cluster analysis results by considering nine clusters; and c) Case II – assigned regions based on the results shown in b). ....	62
Figure 3.3. Identified $t_{C,j,K_{0.25}}$ , $t_{C,j,K_{0.50}}$ and $t_{C,j,K_{0.75}}$ (The plots shown in the first and second rows are for Case I and Case II, respectively. For each set of curves, the upper, middle and lower curves represent $t_{C,j,K_{0.25}}$ , $t_{C,j,K_{0.50}}$ and $t_{C,j,K_{0.75}}$ , respectively.).....	65
Figure 3.4. The magnitude -recurrence relation for different regions and different cases.	68
Figure 3.5. Smoothed cumulative event count (The left plot is for Case I – nS (based on six regions shown in Figure 3.2a), b) Case II – nS (based on nine regions shown in Figure 3.2c). ....	72
Figure 3.6. Fitted bandwidth function for Eq. (3.17) (Criteria 1, 2 and 3 shown in the plots refer to the criteria suggested by Molina et al. (2001), Zuccolo et al. (2013) and Goda et al. (2013), respectively). ....	74
Figure 3.7. Spatially smoothed magnitude-recurrence relations using $\lambda$ S approach. Row 1 shows the estimated $\lambda_{c,k}(M_{smin} = 4)$ for Case I and Case II. Rows 2 and 3 show $\lambda_{c,k}(M_s)$ for twelve sites. Row 2 is for Case I and Row 3 is for Case II. ....	76
Figure 3.8. Comparison of the predicted ground motion measures by using YLX13-G and BSSA14-P for different regions (See Table 3.4). The sigma shown in the first row is for log(PGA) or log(SA) associated with BSSA14-P. ....	79
Figure 3.9. Estimated PGA by using nS for smoothing. : Row 1 for Case I, $\beta$ -LSF and YLX13-G; Row 2 for Case I, $\beta$ -LSF and BSSA14-P; and Row 3 for Case II, $\beta$ -LSF and BSSA14-P. Columns 1 to 3 are for $P_E = 63\%$ , 10% and 2% in 50 years. ....	81

Figure 3.10. Estimated PGA using $\lambda$ S for spatial smoothing. : Row 1 for Case I, $\lambda$ S and YLX13-G; Row 2 for Case I, $\lambda$ S and BSSA14-P; and Row 3 for Case II, $\lambda$ S and BSSA14-P. Columns 1 to 3 are for $P_E = 63\%$ , 10% and 2% in 50 years. ....	82
Figure 3.11. Estimated SA at $T_n = 0.2, 0.5,$ and 2 s and damping ratio of 5% for different exceedance probability $P_E$ in 50 years. ....	84
Figure 3.12. Plots of the obtained UHS normalized with its corresponding PGA (see Table 3.3). $T_g$ is the characteristic period that depends on the site class as well as the site to source distance (GB50011 2010). ....	86
Figure 4.1. Schematic of the projection method by considering different earthquake magnitude and distance measures that are used for different regions. ....	96
Figure 4.2. Identification of the four seismic regions for GMMs and comparison of predicted median PGA. ....	103
Figure 4.3. Comparison of predicted median SA at $T_n = 0.2, 0.5$ and 2 s. ....	105
Figure 4.4. Comparison of the predicted median PGA by using projected GMMs to instrumental ground-motion data (the background data and plots are those from Dangkua et al. (2018)). For plots a) and b) the triangle, diamond, square and circle represent the data from the rock site and the remaining symbols are used to represent data from soil site; for plots c) to e) the circles and cross are used to represent data from rock and soil sites, respectively. a) PGA for ER and $M_s = 4.5$ , b) PGA for ER and $M_s = 6.1$ , c) PGA for MR and $M_s = 6.7$ , d) PGA for TR and $M_s = 6.7$ , and e) PGA for TR and $M_s = 8.0$ ( $M_w = 8.0$ is obtained by using Eqs. (4.9) and (10)). ....	106
Figure 4.5. Sigma for ASK14, BSSA14, CB14, and CY14 and for YLX13-G. ....	107
Figure 4.6. Assigned source regions and considered earthquake catalogue: a) Historical seismic events with $M_s \geq 4.0$ after 1500 AD and excluding aftershocks (See Feng et al. 2020), replotted), b) SM1 with six seismic source regions; and c) SM2 with nine seismic source regions. ....	108

Figure 4.7. Estimated $t_{C,j,p}$ for selected $p$ values: The plots in the first and second rows are for SM1 and SM2.....	109
Figure 4.8. Spatially Smoothed $\lambda_{c,k}(M_s = 4)$ . The first row is for $p = 0.5$ and, SM1 and SM2. The left plot in the second row is for SM1 and $p = 0.16$ , and the right plot for SM2 and $p = 0.84$ . .....	111
Figure 4.9. $\lambda_{c,k}(M_s)$ for Beijing, Shanghai and Chengdu (from left to right) for selected $p$ and seismic source model. ....	111
Figure 4.10. Considered five logic trees (Cases 1 to 5).....	114
Figure 4.11. Empirical probability distributions of the annual maximum PGA at selected locations. ....	117
Figure 4.12. Standardized UHS for a few selected sites.....	118
Figure 4.13. Seismic hazard map for Case 1 based on SA for $P_E = 63\%$ , 10% and 2 % in 50 years. ....	119
Figure 4.14. Seismic hazard map for Case 1 Based on SA $P_E = 63\%$ , 10% and 2 % in 50 years. ....	120
Figure 4.15. Comparison of seismic hazard maps for Cases 2 to 5 $P_E = 10\%$ in 50 years...	121



# Nomenclature

## Chapter 2

$A, B, C$ and $R_0$	Coefficients for intensity prediction equations
$C(T_n)$	Seismic design coefficient curve normalized with respect to its corresponding peak ground acceleration value
$D_h$	Hypocentral distance
$F_{M_s}(m_s)$	Probability distribution for earthquake events with surface-wave magnitude greater or equal to $m_s$
$I_C$	Chinese seismic intensity scale
$I_{ca}$	Intensity along major axis
$I_{cb}$	Intensity along minor axis
$M$	Earthquake magnitude
$M_s$	Surface-wave magnitude
$M_{smax}$	Maximum magnitude considered for a source zone
$M_{s-US}$	$M_s$ reported by the National Earthquake Information Center of the United State Geological Survey
$M_w$	Moment magnitude
$PGA_r$	Median peak horizontal acceleration evaluated based on surface-wave magnitude and epicentral distance with reference velocity
$R_{epi}$	Epicentral distance
$R_{epi-a}$	Distance from epicenter to the points located on the major axis

$R_{\text{epi-b}}$	Distance from epicenter to the points located on the minor axis
$R_{\text{jb}}$	Closest distance to the surface projection of the fault
$T_g$	Characteristic period of response spectrum
$T_n$	Natural vibration period of single degree-of-freedom system
$V_c$	Limiting velocity beyond which ground motions no longer scale with time averaged shear-wave velocity in the top 30 m
$V_{\text{ref}}$	Reference velocity corresponding to NEHRP B/C boundary site conditions
$V_{\text{S30}}$	Time averaged shear-wave velocity in the top 30 m
$Y$	Ground motion intensity measures
$a_E$	Effective peak acceleration
$c_i, i = 1, \dots, 6; e_i, i = 1, \dots, 7; f_1, f_3, f_4, f_5$	Coefficients for ground motion model
$f_1, f_3, f_4, f_5$	Coefficients for soil amplification term of BSSA14-P
$m_{e\text{-jb}}$	Mean of the gamma variate, gamma variate is considered for the difference between epicentral distance and the closest distance to the surface projection of the fault
$v_E$	Effective peak velocity
$v_{e\text{-jb}}$	Coefficient variation of the gamma variate, gamma variate is considered for the difference between epicentral distance and the closest distance to the surface projection of the fault

$z_1$	Basin depth
$\varepsilon_i$	Zero mean residual for intensity prediction equation
$\varepsilon_{ia}$	Residual for intensity prediction equation along major axis
$\varepsilon_{ib}$	Residual for intensity prediction equation along minor axis
$\varepsilon_Y$	Zero mean residual for ground motion model
$\lambda(4)$	Annual earthquake occurrence rate for surface-wave magnitude greater or equal to 4.0
$\sigma_{1a\varepsilon}$	Standard deviation of the residual for intensity prediction equation along major axis
$\sigma_{1b\varepsilon}$	Standard deviation of the residual for intensity prediction equation along minor axis
$\sigma_{1\varepsilon}$	Standard deviation of the residual for intensity prediction equation
$(\sigma_{1\varepsilon})_{\text{Reference}}$	Standard deviation of the residual for reference region intensity prediction equation
$(\sigma_{1\varepsilon})_{\text{Target}}$	Standard deviation of the residual for target region intensity prediction equation
$\sigma_{Ye}$	Standard deviation of the residual for ground motion model
$(\sigma_{Ye})_{\text{Reference}}$	Standard deviation of the residual for reference region ground motion model

### Chapter 3

$C(T_n)$	Seismic design coefficient curve normalized with respect to its corresponding peak ground acceleration value
----------	--

$H(M_{sj})$	Bandwidth for seismic event with magnitude equal to $M_{sj}$
$I_{mj}$	$j$ -th magnitude interval
$M_B$	Body-wave magnitude measured by using P-waves and S-waves
$M_b$	Body-wave magnitude measured by using only P-waves
$M_{smin,j}$	$j$ -th case of lowest $M_s$ for catalogue completeness
$M_{s-obs}$	Maximum observed $M_s$
$N$	Half of the Number for the elementary non-overlapping subintervals
$N_C$	Total number of lowest magnitude cases considered for completeness analysis
$N_{j,k}$	Total number of likely values of $T_{C,j}$
$P_E$	Exceedance probability in 50 years
$P_j(C T_{C,j})$	Probability of completeness for earthquake catalogue after $T_{C,j}$
$R_{AS}$	Radius for the circle that takes the epicenter of the mainshock as center
$T_{AS}$	Occurrence time delay between mainshock and its aftershock
$T_{C,j}$	Considered completeness time for earthquake catalogue with magnitudes not smaller than $M_{smin,j}$
$T_F$	Most recent time for the earthquake catalogue
$T_I$	Earliest time for the seismic event reported by the earthquake catalogue
$T_n$	Natural vibration period of single degree-of-freedom system
$a$	Parameter determining the degree of smoothing

$b_1, b_2$	Model parameters for bandwidth function
$c$	Bandwidth parameter in Gaussian kernel smoothing
$c_i, i = 1, \dots, 6$	Coefficients for ground motion model
$dt$	Non-overlapping subintervals of equal duration considered for catalogue completeness analysis
$k_j$	Number of observed events in the $j$ -th magnitude bin
$m_j$	Representative magnitude of the $j$ -th magnitude interval
$n$	Number of magnitude intervals (or bins)
$n_C$	Total number of cells in the considered seismic source region
$n_E$	Total number of earthquake events in the considered seismic source region
$n_k(M_{\text{smin}})$	Cumulative event count with magnitude greater than or equal to $M_{\text{smin}}$ within the $k$ -th cell
$r_{ik}$	Distance between the $i$ -th cell and the $k$ -th cell
$s_j$	Location for $j$ -th seismic event
$t_{C,j,Kp}$	Completeness time for $P$ -quantile of $P_j(C T_{C,j})$
$t_j$	Observation period for the observed events in the $j$ -th magnitude bin
$\Delta T_j, \Delta T_{C,j}$	Effective observation period calculated from $T_F - T_{C,j}$
$\beta_i$	Slope of the Gutenberg-Richter relation for $i$ -th region or cell
$\hat{\beta}_i$	Estimated $\beta_i$ based on maximum likelihood method

$\varepsilon_Y$	Zero mean residual for ground motion model
$\lambda_i(M_{\text{smin}})$	Annual occurrence rate with magnitude greater than $M_{\text{smin}}$ for $i$ -th region or cell
$\lambda_{c,k}(M_s)$	Annual earthquake occurrence rate for events with magnitude not smaller than $M_s$ at $k$ -th grid cell
$\hat{\sigma}_{\beta_i}^2$	Variance of normal variate $\beta$ for $i$ -th seismic region
$\sigma_{Ye}$	Standard deviation of the residual for ground motion model
$\phi$	A constant equal to or greater than 1

#### Chapter 4

$C(T_n)$	Seismic design coefficient curve normalized with respect to its corresponding peak ground acceleration value
$M_{G\text{ref}}$	Magnitude measures used in the IPE for the reference region
$M_{I\text{ref}}$	Magnitude measures used in the IPE for the reference region
$M_{I\text{tar}}$	Magnitude measures used in the IPE for the reference region
$M_s$	Surface-wave magnitude
$M_{sj}$	Magnitude for $j$ -th seismic event
$M_{\text{smax}}$	Maximum $M_s$ for source region
$M_{\text{smin},j}$	Minimum considered $M_s$ for $j$ -th source region
$M_{\text{s-US}}$	$M_s$ reported by U.S. agency
$M_w$	Moment magnitude

$P_E$	Exceedance probability in 50 years
$R_{\text{epi}}$	Epicentral distance
$R_{G\text{ref}}$	Distance measures used in the IPE for the reference region
$R_{I\text{ref}}$	Distance measures used in the IPE for the reference region
$R_{\text{jb}}$	Closest distance to the surface projection of the fault
$R_{\text{rup}}$	Closest distance to the rupture plane
$T_{Cj}$	Considered completeness time for earthquake catalogue with magnitudes not smaller than $M_{\text{min},j}$
$T_F$	Most recent reporting time for earthquake catalogue
$T_T$	Number of years for a given observation period
$W$	Fault width
$Z_{\text{hyp}}$	Hypocenter depth
$Z_{\text{tor}}$	Depth to the top of the rupture
$a_i, i = 1, \dots, 6, 8,$ $17; c_{4M}$	Regressed coefficients for ASK14-P
$a_i, i = 1, \dots, 5, \beta_1,$ $\beta_2$ and $\gamma$	Regressed coefficients for IM14-P
$b_1, b_2$	Coefficients for bandwidth function
$c_i, i = 0, \dots, 7,$ and $c_{20}$	Regressed coefficients CB14-P
$c_i, i = 1, \dots, 5, c_{4\_a},$	Regressed coefficients for CY14-P

$c_{RB}$ and $c_{r1}$	
$c_6, c_n, c_M, c_{r2}, c_{r3}$ and $c_{HM}$	Regressed coefficients for CY14-P
$m_{e-jb}$	Mean of the gamma variate, gamma variate is considered for the difference between $R_{epi}$ and $R_{rup}$
$s$	A point of interest within the considered seismic source region
$s_j$	Location for $j$ -th seismic event
$s_k$	Location for the center of the $k$ -th cell
$t_{Cj,p}$	$p$ -quantile of $T_{Cj}$
$v_{e-jb}$	Coefficient variation of the gamma variate, gamma variate is considered for the difference between $R_{epi}$ and $R_{rup}$
$\Delta T_{Cj}$	Effective observation period calculated from $T_F - T_{Cj}$
$\Delta t_{Cj,p}$	$p$ -quantile of $\Delta T_{Cj}$
$\varepsilon_{\log W}$	zero-mean normally distributed random variable
$\varepsilon_{Z_{hypo}}$	zero-mean normally distributed random variable
$\lambda_{c,k}(M_s)$	Annual earthquake occurrence rate for events with magnitude not smaller than $M_s$ at $k$ -th grid cell
$\sigma_{\log W}$	Standard deviation for $\varepsilon_{\log W}$
$\sigma_{Z_{hypo}}$	Standard deviation for $\varepsilon_{Z_{hypo}}$
$M_{Iref}$	Magnitude measures used in the IPE for the reference region
$R_{Iref}$	Distance measures used in the IPE for the reference region



$M_{Gref}$	Magnitude measures used in the IPE for the reference region
$R_{Gref}$	Distance measures used in the IPE for the reference region
$M_{I\text{tar}}$	Magnitude measures used in the IPE for the reference region
$R_{Iref}$	Distance measures used in the IPE for the reference region
$M_s$	Surface-wave magnitude
$R_{epi}$	Epicentral distance
$R_{jb}$	Closest distance to the surface projection of the fault
$R_{rup}$	Closest distance to the rupture plane
$W$	Fault width
$Z_{tor}$	Depth to the top of the rupture
$m_{e-jb}$	Mean of the gamma variate, gamma variate is considered for the difference between $R_{epi}$ and $R_{rup}$
$\nu_{e-jb}$	Coefficient variation of the gamma variate, gamma variate is considered for the difference between $R_{epi}$ and $R_{rup}$
$M_w$	Moment magnitude
$Z_{hyp}$	Hypocenter depth
$\varepsilon_{Z\text{hypo}}$	zero-mean normally distributed random variable
$\sigma_{Z\text{hypo}}$	Standard deviation for $\varepsilon_{Z\text{hypo}}$
$\varepsilon_{\log W}$	zero-mean normally distributed random variable
$\sigma_{\log W}$	Standard deviation for $\varepsilon_{\log W}$

# Chapter 1

## 1 Introduction

### 1.1 Background

Seismic hazard maps are often used as the basis for seismic design (NBCC 2015; NEHRP 2003; GB50011 2010). The probabilistic seismic hazard analysis (PSHA) requires the seismic source model, magnitude-recurrence relations, and ground motion models (GMMs) (also known as attenuation relations). The use of PSHA was pioneered by Cornell (1968) and Esteva (1968) (see McGuire 2008) by using the delineated seismic source models. Their analysis framework is still employed at present by many researchers. Other available approaches include those proposed by Milne and Davenport (1965, 1969), Sterescu (1988), Frankel (1995), and Woo (1996). These approaches consider different degrees of spatial smoothing in assigning the seismic hazard model. Hong et al. (2006) compared the differences in the estimated seismic hazard for Canada by using the approaches given by Cornell (1968), Milne and Davenport (1965, 1969), and Sterescu (1988). They found that the estimated seismic hazard based on the considered approaches is similar, but the degree of spatial smoothing can affect the estimated return period values of annual maximum peak ground acceleration (PGA) and spectral acceleration (SA).

The spatial smoothing approaches given in Frankel (1995) and Woo (1996) have been adopted by several researchers (Molina et al. 2001; Beauval et al. 2006; Xu and Gao 2012; Goda et al. 2013; Zuccolo et al. 2013; and Xu 2019). These two methods differ in how the spatial smoothing is carried out. The method proposed by Frankel (1995) emphasizes the smoothing of the occurrence rate and considers that the magnitude-recurrence for a region can be assumed to be the same. The approach proposed by Woo (1996) treats each observed event separately, and the smoothing is carried out by considering the earthquake magnitude. The magnitude-recurrence relation is then developed based on the smoothed cumulative events versus earthquake magnitude.

The Chinese seismic hazard maps (CSHMs) were developed essentially based on the PSHA method proposed by Cornell (1968), except that a two-level delineation of the

seismic source zone is considered (Liu 1987). The first-level delineation is focused on large source area, and the second-level delineation is carried out by considering the localized geological and seismological information. The details of the third-generation and fourth-generation Chinese seismic hazard map (CSHMs) are detailed in CEA (1990) and Hu et al. (2001), respectively. By refining the two-level delineation, a three-level delineation, identifying smaller source zones, was proposed in Pan et al. (2013). The seismic source model based on three levels of delineation was considered in developing the fifth-generation (i.e., most recent) CSHM. One of the advantages of using the delineated seismic source model is that it incorporates seismotectonic information. However, it has been argued such an approach in assigning the seismic source zone involves a circular argument (Hong et al. 2006). Note that the spatial smoothed seismic source model has not been used to map the seismic hazard for mainland China, although its use to investigate the seismic occurrence rate was presented in Xu (2019).

For the development of CSHMs, since there are insufficient quality ground motion records for seismic events that occurred in China to develop GMMs, the projection method is used to develop the needed GMMs for PGA (Hu and Zhang 1984; Hu et al. 1996). This method maps the GMMs developed for a reference region with a large number of historical records to a target region, where the actual ground motions are scarce. The method relies on the availability of the intensity (such as the macro-intensity, MMI) prediction equations (IPEs) and GMMs for reference region, and the IPE for the target region. Firstly, IPEs,  $I_{ref}(M_{Iref}, R_{Iref})$ , and GMMs,  $Y_{ref}(M_{Yref}, R_{Yref})$ , for reference region (the subscript ref denotes reference region), and the IPEs for target region (i.e., a region in mainland China),  $I_{tar}(M_{Itar}, R_{Itar})$  (the subscript tar denotes target region) are selected, where  $M$  and  $R$  with subscript  $I$  and  $Y$  represent the magnitude and distance measures that associated with the IPEs and GMMs. Then, given an earthquake event in the target region with magnitude  $M_{Itar}$  at distance  $R_{Itar}$  that causing intensity  $I_{tar}(M_{Itar}, R_{Itar})$ , there can be found another earthquake event in reference region with  $M_{Iref}$  at distance  $R_{Iref}$  that with intensity  $I_{ref}(M_{Iref}, R_{Iref})$  and  $I_{ref}(M_{Iref}, R_{Iref}) = I_{tar}(M_{Itar}, R_{Itar})$  is satisfied. The projection method assumes that the ground motion for reference region is applicable for a target region if the seismic events in both regions cause the same intensity, the predicted ground motion for the reference region that calculated based on  $Y_{ref}(M_{Iref}, R_{Iref})$  is considered equal to the ground motion in the target

region that is caused by  $(M_{tar}, R_{tar})$ . Lastly, the GMMs for the target region,  $Y_{tar}(M_{tar}, R_{tar})$ , can be developed based on the sampling of  $(M_{tar}, R_{tar})$  and  $Y_{ref}(M_{ref}, R_{ref})$ . It is worth noting that if the magnitude and distance measures for the IPEs and GMMs are not consistent, the conversion relation should be taken into account when applying the projection method. Details on the projection method will be elaborated in the following chapters.

By using the projection method and considering the Western U.S. as a reference region due to the relative rich ground motion recordings and same type of earthquake events as that frequently occurred in mainland China (i.e., shallow crustal earthquake events), the GMMs for PGA are developed by Wang et al. (2000) and used for the development of the fourth-generation of CSHM. In Wang et al. (2000), the IPE given by Chandra (1979) for San Andreas province (Western U.S.), and the GMMs developed based on California ground motion records are used as the IPE and GMMs for the reference regions. Similarly, the GMMs developed in Yu et al. (2013) (hereafter YLX13) are developed by considering the Western U.S. as the reference region. YLX13 is used to develop the fifth-generation CSHM. The IPE for the reference region that is adopted by Yu et al. (2013) is the same as the one used by Wang et al. (2000). As will be discussed, the standard deviation of the residual for YLX13 is not fully elaborated and may not be adequate.

The fourth-generation and fifth-generation CSHMs are given in terms of PGA with 10% exceedance probability in 50 years. No SA values are given due to the unavailability of sets of GMMs for SA that are applicable to mainland China. Moreover, no uniform hazard spectra (UHS) are given, even though there is a clear international trend in implementing UHS for codified structural design (e.g., Canada and the U.S.).

## 1.2 Objectives and thesis outline

The overall objectives for this study are to:

- 1) Develop new GMMs to predict PGA and SA for mainland China by using the projection method;

2) Develop spatially smoothed seismicity models and use the projected GMMs to assess the seismic hazard for mainland China and explore the difference between the standard design spectrum and the normalized UHS;

3) Map seismic hazard for mainland China by considering combinations of seismic source models, magnitude-recurrence relations, and GMMs; and recommend standardized UHS that could be adopted for codified structural design.

To achieve these objectives, in Chapter 2, a summary of the development of the third- to fifth-generation CSHMs is presented. Relevant available IPEs are reviewed, and the use of the projection method is explained. A new set of GMMs is developed based on the NGA-West2 model given by Boore et al. (2013, 2014). The impact of using the new GMMs for seismic hazard mapping for simple hypothetical source models is presented.

In Chapter 3, the use of spatial smoothing techniques to develop spatially smoothed seismic source models is explained. It is used to develop two source models applicable to mainland China based on historical catalogues. For the development, a catalogue completeness assessment is carried out. The developed source models are used to carry out seismic hazard modeling for mainland China. Maps for PGA and SA are presented. A comparison of the mapped seismic hazard for PGA and that given in the fifth-generation CSHM is presented. The discrepancy between the mapped hazard and those given in the fifth-generation CSHM is discussed and explained.

In Chapter 4, the use of the projection method is considered again to map four additional sets of ground motion models based on four sets of GMMs in the NGA-West2 (Abrahamson et al. 2013, 2014; Campbell and Bozorgnia 2013, 2014; Chiou and Youngs 2013, 2014; Idriss 2013, 2014). The projected GMMs are then used to develop seismic hazard maps for China by considering combinations of seismic source models, magnitude-recurrence relations, and GMMs. The comparison of the obtained hazard maps to the fifth-generation CSHM is given. Most importantly, a new seismic hazard map is suggested, and UHS are presented.

The conclusions from Chapters 2 to 4 are summarized in Chapter 5. Suggestions are given with regard to scrutinize the fifth-generation CHSM. Also, the UHS for different sites within mainland China are recommended.

### 1.3 References

- Abrahamson, N.A., Silva, W.J., and Kamai, R. (2013). Update of the AS08 ground motion prediction equations based on the NGA-Wet2 data set. PEER Report No. 2013/04, Pacific Earthquake Engineering Research Center, *University of California, Berkeley*.
- Abrahamson, N.A., Silva, W.J., and Kamai, R. (2014). Summary of the ASK14 ground motion relation for active crustal regions. *Earthquake Spectra*, 30 (3): 1025-1055.
- Beauval, C., Scotti, O., and Bonilla, F. (2006). The role of seismicity models in probabilistic seismic hazard estimation: comparison of a zoning and a smoothing approach. *Geophysical Journal International*, 165(2): 584-595.
- Boore, D. M., J.P. Stewart, E. Seyhan, and G.M. Atkinson (2013). NGA-West2 Equations for Predicting Response Spectral Accelerations for Shallow Crustal Earthquakes, PEER Report No. 2013/05, Pacific Earthquake Engineering Research Center, *University of California, Berkeley*.
- Boore, D.M., Stewart, J.P., Seyhan, E., and Atkinson, G.M. (2014). NGA-west2 Equations for predicting PGA, PGV and 5% Damped PSA for Shallow Crustal Earthquakes. *Earthquake Spectra*. 30 (3): 1057-1085.
- Building Seismic Safety Council (BSSC) (2004). NEHRP Recommended Provisions for Seismic Regulations for New Buildings and Other Structures, Part 1: Provisions (FEMA 450-1/2003 Edition), *Building Seismic Safety Council*, Washington, D.C.
- Campbell, K.W., and Bozorgina, Y. (2013). NGA-West2 Campbell- Bozorgina ground motion model for the horizontal component of PGA, PGV, and 5%-damped elastic pseudo acceleration response spectra for periods ranging from 0.01 to 10 s. PEER

Report No. 2013/06, Pacific Earthquake Engineering Research Center, *University of California, Berkeley*.

Campbell, K.W., and Bozorgina, Y. (2014). NGA-West2 ground motion model for the average horizontal component of PGA, PGV, and 5%-damped linear acceleration response spectra. *Earthquake Spectra*, 30 (3): 1087-1115.

Chandra, U. (1979). Attenuation of intensities in the United States, *Bull. Seismol. Soc. Am.*, 69, 2003-2024.

China Earthquake Administration (CEA) (1990). Introduction to the Intensity Hazard Map of China, *Seismological Press*, Beijing, China.

Chiou, B.S.-J, and Youngs, R. (2013). Update of the Chiou and Youngs NGA ground motion model for average horizontal components of peak ground motion and response spectra. PEER Report No. 2013/07, Pacific Earthquake Engineering Research Center, *University of California, Berkeley*.

Chiou, B.S.-J, and Youngs, R. (2014). Update of the Chiou and Youngs NGA model for the average horizontal components of peak ground motion and response spectra. *Earthquake Spectra*. 30(3): 1117-1153.

Cornell, C.A. (1968). Engineering seismic risk analysis. *Bull. Seism. Soc. Am.*, 58(5): 1583-1606.

Esteva, L. (1968). *Bases para la formulación de decisiones de diseño sísmico*. Ph.D's thesis, Instituto de Ingeniería, Universidad Nacional Autónoma de México. (In Spanish)

Frankel, A. (1995). Mapping seismic hazard in the central and eastern United State. *Seism. Res. Lett.*, 66(4): 8-21.

GB50011-2010. (2010). Code for seismic design of buildings. *Ministry of Housing and Urban-Rural Development of the People's Republic of China* (MOHURD), Beijing, China.

- Goda, K., Aspinall, W., and Taylor, C.A. (2013). Seismic hazard analysis for the UK: Sensitivity to spatial seismicity modelling and ground motion prediction equations. *Seismological Research Letters*, 84(1): 112-129.
- Hong, H.P., Goda, K., and Davenport, A.G. (2006). Seismic hazard analysis: a comparative study. *Canadian Journal of Civil Engineering*, 33(9), 1156-1171.
- Hu, Y.X., Gao, M.T., Du, W., Jin, Y., Zhao, F.X., Zou, Q.J., Tao, Y.L., and Zhou, B.G. (2001). GB18306-2001: Introduction to China ground motion parameter zoning map. *Standards Press of China*, Beijing, China. (in Chinese).
- Hu, Y.X., and Zhang, M.Z. (1984). A method of predicting ground motion parameters for regions with poor ground motion data. *Earthquake Engineering and Engineering Vibration*, 4(1): 1-11. (in Chinese)
- Hu, Y. X., Zhou, K. S., and Yan, X. J. (1996). A method for evaluation of ground motion in regions with few acceleration observation data, *Earthq. Eng. Eng. Vib.* 16(3), 2–10 (in Chinese).
- Idriss, I.M. (2013). NGA-West2 model for estimating average horizontal value of pseudo-absolute spectral accelerations generated by crustal earthquakes. PEER Report No. 2013/08, Pacific Earthquake Engineering Research Center, *University of California, Davis*.
- Idriss, I.M. (2014). An NGA-West2 model empirical model for estimating the horizontal spectral values generated by shallow crustal earthquakes. *Earthquake Spectra*. 30(3): 1155-1177.
- Liu, H.X. (1987). On the seismic zoning map China, *Proceedings of International Seminar on Seismic Zonation*, Guangzhou, China, pp. 35-42, 6-10 December. (in Chinese)
- Milne W.G., and Davenport, A.G. (1969). Distribution of earthquake risk in Canada. *Bull. Seism. Soc. Am.*, 59(2): 729-754.
- Milne, W. G., and Davenport, A. G. (1965). Statistical parameters applied to seismic



regionalization. *Proceedings of the Third World Conference on Earthquake Engineering*, Auckland and Wellington, New Zealand, Volume I, pp. 181-193, 22 January to 1 February .

Molina, S., Lindholm, C.D., and Bungum, H. (2001). Probabilistic seismic hazard analysis: zoning free versus zoning methodology. *Bollettino di Geofisica* (selected papers from the 27th ESC, Lisbon, 2000), 42: 19-39.

NBCC. (2015). National Building Code of Canada 2015. *Institute for Research in Construction*, National Research Council of Canada, Ottawa, Ont.

Pan, H., Gao, M. T., and Xie, F. R. (2013). The earthquake activity model and seismicity parameters in the new seismic hazard map of China. *Technology for Earthquake Disaster Prevention*, 8(1), 11-23. (in Chinese)

Sterescu, A. (1988). *Approaches to seismic risk estimation*. M.A.Sc. thesis, Department of Civil Engineering, The University of Western Ontario, London, Ont.

Wang, S.Y., Yu, Y.X., Gao, A.J., and Yan, X.J. (2000). Development of attenuation relations for ground motion in China. *Earthquake Research in China*, 16(2), 99-106. (in Chinese)

Woo, G. (1996). Kernel estimation methods for seismic hazard area source modeling. *Bull. Seism. Soc. Am.*, 86(2): 353-362.

Xu, W.J. (2019). Probabilistic seismic hazard assessment using spatially smoothed seismicity in North China seismic zone. *Journal of Seismology*, 23(3): 613-622.

Xu, W.J., and Gao, M.T. (2012). Seismic hazard estimate using spatially smoothed seismicity model as spatial distribution function, *Acta Seismologica Sinica*, 34(4): 525-536 (in Chinese).

Yu, Y.X., Li, S.Y., and Xiao, L. (2013). Development of ground motion attenuation relations for the new seismic hazard map of China. *Technology for earthquake disaster prevention*, 8(1): 24-33 (in Chinese).

Zuccolo, E., Corigliano, M., and Lai, C.G. (2013). Probabilistic seismic hazard assessment of Italy using kernel estimation methods. *Journal of Seismology*, 17(3): 1001-1020.

## Chapter 2

# 2 On the Ground Motion Models for Chinese Seismic Hazard Mapping

## 2.1 Introduction

Probabilistic models for seismic hazard mapping are used as the basis to assign the seismic design load, to evaluate seismic risk, and to plan for earthquake disaster reduction. The information needed to develop seismic hazard maps includes the geometries of each seismic source zone, the magnitude dependent occurrence rate (i.e., magnitude-recurrence relations) and ground motion models (GMMs). The most popular probabilistic approach used to estimate seismic hazard at a site was developed by Cornell (1968) and Esteva (1968). Other available approaches include those presented by Milne and Davenport (1969), Liu (1987) and Frankel (1995). The major difference between the approaches given by Milne and Davenport (1969) and Frankel (1995) is how the historical seismicity is smoothed in space to define the seismic source zones.

The approach proposed by Liu (1987) was employed to develop Chinese seismic hazard maps, where the two-level delineation of the source zone was considered. Recently, the fifth-generation Chinese seismic hazard map (CSHM) was developed. Some of the information on the source zones, magnitude-recurrence relations, and GMMs used to map the fifth-generation CSHM were described in GB18306-2015 (Gao et al., 2015). The GMMs were developed based on the projection method that was originally proposed by Hu and Zhang (1984). The projection method is considered because of insufficient instrumental ground motion records available in China to develop the GMMs, although other approaches may be considered (e.g., developing GMMs using a physics-based stochastic model such as was done in Atkinson and Boore (1995)). The projection method basically assumes that for a given scenario event defined by earthquake magnitude and source-to-site distance for a reference region, one can find the source-to-site distance in a target region,  $d_T$ , by equating the predicted macro-intensities such as the modified Mercalli intensity (MMI) and Chinese seismic intensity scale in both regions. It further assumes that the predicted ground motion measures such as PGA or PGV for the scenario event in

the reference region are equal to those for the target region but for the corresponding  $d_T$ . This process of calculating samples of the ground motion measures and  $d_T$  for the target region is repeated for a series of scenarios. These calculated values are then used as the basis to develop GMMs for the reference region. The projection method implicitly assumes that there are consistencies in data used for the reference region to develop the set of intensity prediction equation (IPE) and GMM. The consistency should include site condition, magnitude reporting, and earthquake mechanism in both reference and target regions. However, this may not be the case in practice.

For the development of the fourth- and fifth-generation CSHMs, California was considered as the reference region, and the IPE given by Chandra (1979) was used for the reference region. The justification for using this IPE instead of other available IPEs was not given, especially considering that it is associated with a small standard deviation of residuals (i.e., sigma), and other IPEs are also available (Howell and Schultz, 1975; Atkinson et al., 2014) for the reference region. While the GMMs for the reference region were developed using records from a small number (i.e. 16) of seismic events from 1970 to 2002 (Yu et al., 2013), and their associated standard deviations of the residuals tend to be less than those of new GMMs developed based on the Next Generation of Attenuation (NGA) project (Power et al., 2008). It must be emphasized that the GMMs are also essential for deterministic seismic hazard assessments.

In this chapter, the following tasks are carried out: (1) to provide a critical review of the GMMs used for the CSHMs focused on mainland China, (2) to develop new GMMs for ground motion measures such as PGA and the spectral acceleration (SA) using the projection method, but considering other available IPEs and/or GMMs for the reference region, (3) to investigate the differences between the estimated seismic hazards for simple source zone models by using the developed GMMs and those used for the fifth-generation CSHM, and (4) to elaborate on the influence of the sigma of the GMMs on the estimated seismic hazard and uniform hazard spectra (UHS). The inclusion of the critical review in the present chapter is based on the consideration that the information on the IPEs and GMMs used to assess the third to fifth-generation CSHMs has not been compared in a succinct manner. The application of the projection method to develop new GMMs is

justified because of the insufficiently well-documented Chinese ground motion records in mainland China. The effect of using newly projected GMMs on the estimated seismic hazard and UHS is illustrated.

## 2.2 IPEs and GMMs used for Chinese seismic hazard maps

### 2.2.1 IPEs used for the third-generation CSHM

The catalogue of historical Chinese earthquakes is rich compared with that for other regions in the world. However, the magnitudes of some of the historical events in the catalogue are inferred from the observed Chinese seismic intensity scale,  $I_C$ , since the ground motion records for these events are unavailable. The isoseismal contour lines (i.e., contours with equal  $I_C$  value) of some of the historical seismic events are available.

A procedure was proposed by Chen and Liu (1989) to develop the IPE using the available isoseismal contour lines from historical seismic events. For their development, it was considered that  $I_C$  in two horizontal orthogonal directions differ and  $I_C$  in the horizontal plane can be described using an elliptical model with (semi-) major axis along the fault line and (semi-) minor axis normal to the fault line. Their algorithm ensures that the predicted  $I_C$  values along the two axes converge to a common value when the epicentral distance tends to zero.

The procedure given in Chen and Liu (1989) was adopted by CEA (1990), although it seems that the constraint that “ $I_C$  values converge to a common value when the distance from the source tends to zero.” was neglected. For the analysis, 568 isoseismal lines from 201 earthquakes were employed. Also, it was considered that the characteristics of the isoseismal lines for different regions could differ and, the whole country was separated into eastern and western seismic regions (with the boundary between the two regions defined approximately by the longitude line of  $105^\circ$ ).

In addition, some intensity data were modified to better represent the spatial distribution of intensity for the far-field and near-field. For example, for sites that are within 5 km from the epicenter, the  $I_C$  value was increased about 0.1 to 1 as compared to the intensity given by the nearest isoseismal lines since these sites were associated with severe damage. For

the far-field, data for sites with  $I_C$  of V were available and data for lower intensity were considered inaccurate even though the lowest  $I_C$  of IV was employed in estimating the seismic hazard. Therefore, to develop IPE that is applicable for the intensity scale below  $I_C$  of V, some data points with an  $I_C$  equal to 3.5 were imposed at locations with the epicentral distance given by,

$$\log R_{\text{epi}} = 0.22M + 1.11 \quad (2.1)$$

where  $R_{\text{epi}}$  (km) is the epicentral distance and magnitude is within  $M5$  to  $8.5$ . It was inferred from CEA (1990) that  $M$  represents surface wave magnitude  $M_s$ . This interpretation and the use of  $M_s$  to replace  $M$  in Eq. (2.1) is considered in the following. Unless otherwise indicated,  $M$  in several studies that were reviewed and described below was also interpreted as  $M_s$ .

It was considered that the IPE, along the major and minor axes, can be expressed as (CEA 1990),

$$I_C = A + B \times M_s + C \times \ln(R_{\text{epi}} + R_0) + \varepsilon_I \quad (2.2)$$

in which  $A$ ,  $B$ ,  $C$  and  $R_0$  are model parameters to be determined based on regression analysis, and  $\varepsilon_I$  is zero mean residual term. The developed IPE for the eastern region of China are:

$$I_{Ca} = 6.046 + 1.480M_s - 2.081 \times \ln(R_{\text{epi}-a} + 25) + \varepsilon_{Ia} \quad (2.3)$$

for the major axis with the standard deviation of the residual  $\varepsilon_{Ia}$ ,  $\sigma_{Ia\varepsilon}$ , equal to 0.49; and

$$I_{Cb} = 2.617 + 1.435M_s - 1.441 \times \ln(R_{\text{epi}-b} + 7) + \varepsilon_{Ib} \quad (2.4)$$

for the minor axis with the standard deviation of the residual  $\varepsilon_{Ib}$ ,  $\sigma_{Ib\varepsilon}$ , equal to 0.56. In Eqs. (2.3) and (2.4),  $I_{Ca}$  and  $I_{Cb}$  represent the intensities along major and minor axes, respectively;  $R_{\text{epi}-a}$  and  $R_{\text{epi}-b}$  represent the distances from the epicenter to the points located on the major and minor axes, respectively. For easy reference, the model coefficients for

Eqs (2.3) and (2.4) are shown in Table 2.1. Similarly, the IPEs were developed for the western region of China, and the model coefficients are also listed in Table 2.1.

Table 2.1. Model coefficients for Eq. (2.2) used for the third- to fifth-generation CSHMs.

Reference	Region	Axis	$A$	$B$	$C$	$R_0$	$\sigma_{Ia\varepsilon}$ or $\sigma_{Ib\varepsilon}$
Used for 3 <sup>rd</sup> -generation CSHM (CEA 1990)	Eastern seismic region	Major	6.046	1.480	-2.081	25	0.49
		Minor	2.617	1.441	-1.441	7	0.56
	Western seismic region	Major	5.643	1.538	-2.109	25	0.64
		Minor	2.941	1.363	-1.494	7	0.61
Used for 4 <sup>th</sup> -generation CSHM (Wang et al. 2000)	Eastern seismic region	Major	5.019	1.446	-4.136	24	0.517
		Minor	2.240	1.446	-3.070	9	0.517
	Western seismic region	Major	5.253	1.398	-4.164	26	0.632
		Minor	2.019	1.398	-2.943	8	0.632
Used for 5 <sup>th</sup> -generation CSHM (Yu et al., 2013)	Eastern seismic region	Major	5.7123	1.3626	-4.2903	25	0.583
		Minor	3.6588	1.3626	-3.5406	13	0.583
	Median seismic region	Major	5.8410	1.0710	-3.6570	15	0.520
		Minor	3.9440	1.0710	-2.8450	7	0.520
	Xinjiang seismic region	Major	5.6018	1.4347	-4.4899	25	0.592
		Minor	3.6113	1.4347	-3.8477	13	0.592
	Tibet seismic region	Major	6.4580	1.2746	-4.4709	25	0.664
		Minor	3.3682	1.2746	-3.3119	9	0.664

CEA, China Earthquake Administration



The contour line with an intensity equal to  $I_C$  is therefore given by the coordinates  $(x, y)$  satisfying,

$$\left(x/R_{\text{epi-}a}(I_C)\right)^2 + \left(y/R_{\text{epi-}b}(I_C)\right)^2 = 1 \quad (2.5)$$

where  $R_{\text{epi-}a}(I_C)$  and  $R_{\text{epi-}b}(I_C)$  are the values of  $R_{\text{epi-}a}$  and  $R_{\text{epi-}b}$  calculated for  $I_{Ca} = I_C = I_{Cb}$  using Eqs. (2.3) and (2.4), respectively; and the  $X$ - and  $Y$ -axes for the coordinate system are oriented along the major and minor axes with the origin placed at the epicenter, respectively.

The IPEs were used to develop seismic intensity zonation maps that were employed as the basis to infer PGA. For seismic hazard assessment, it was considered that the directions of the major and minor axes for a source zone could be defined as follows (CEA 1990):

1. For faults with single strike direction, the direction of the major axis follows the fault strike of the geology structure;
2. For conjugate faults, the probability of the earthquake occurring along each fault is the same;
3. For the faults made up of main faults and branch faults, the probability of earthquake occurring along the main fault is 0.7 and along the branch faults is 0.3; and
4. For faults with unclear strike direction, the probability of the direction of major axis of an earthquake is uniformly distributed between 0 to 360°.

### 2.2.2 IPEs and GMMs used for the 4th-generation CSHM

Instead of relying on the intensity, the use of the PGA was considered to develop the fourth-generation CSHM. The GMMs for PGA developed based on Chinese ground motion records were not robust because of insufficient ground motion records from Chinese earthquakes. To overcome this problem, a projection method proposed by Hu and Zhang (1984) was employed by Wang et al. (2000) to develop GMMs. In the projection method, it is assumed that the PGA or any other ground motion measures  $Y$  in different

regions in the world must be the same for events with the same  $M_s$  and  $I_C$  near the epicenter. Based on this equality assumption, their method to develop GMMs for a region with an available IPE is illustrated in Figure 2.1. It is considered that the IPE and GMM applicable to a region A (i.e., reference region), denoted as  $I_{CA}(M_s, R_{\text{epi}})$  and  $Y_A(M_s, R_{\text{epi}})$ , are already available, and the GMM for  $Y$  applicable to a region B (i.e., target region),  $Y_B(M_s, R_{\text{epi}})$ , can be inferred or evaluated once the IPE applicable to the region B,  $I_{CB}(M_s, R_{\text{epi}})$ , is given. More specifically, by assuming  $(M_s, I_{\text{epi}})_A = (M_s, I_{\text{epi}})_B$ , given an event with  $M_s$  and  $R_{\text{epi}} = R_1$ , one finds  $R_2$  from  $I_{CB}(M_s, R_1) = I_{CA}(M_s, R_2)$ . The calculated  $Y_A(M_s, R_2)$  is assigned to  $Y_B(M_s, R_1)$ . By repeating this calculation for a range of  $R_{\text{epi}}$  values, the relation  $Y_B(M_s, R_{\text{epi}})$  was established and the functional relation for  $Y_B(M_s, R_{\text{epi}})$  was developed.

A variant of this projection procedure was also proposed in Hu et al. (1996), which assumes that there exists an event in the region A with magnitude and epicentral distance  $(M_s, R_{\text{epi}})_A$ , and an event in the region B with  $(M_s, R_{\text{epi}})_B$  such that  $I_C$  and  $Y$  are equal in both cases. One of the advantages of this procedure as compared with that given in Figure 2.1 is that there is no need to know the functional relations of  $I_C$  or  $Y$  to  $M_s$  and  $R_{\text{epi}}$  which were not always available. In this approach, it is considered that the information on  $I_C$  and  $Y$  is rich for the region A, and the objective was to find  $Y$  in terms of  $M_s$  and  $R_{\text{epi}}$  if the information on  $I_C$  for the region B was adequate. Given  $I_{CA}$  for an event defined by  $(M_s, R_{\text{epi}})_A$ , denoted as  $I_{CA}((M_s, R_{\text{epi}})_A)$ , the method basically assumes that  $(M_s, R_{\text{epi}})_B$  can be identified by minimizing the differences between  $I_{CA}((M_s, R_{\text{epi}})_A)$  and  $I_{CB}((M_s, R_{\text{epi}})_B)$ .  $Y$  for the region B is then obtained using the attenuation relation for  $Y$  applicable to the region A and the relation established between  $(M_s, R_{\text{epi}})_A$  and  $(M_s, R_{\text{epi}})_B$ . However, no optimum assumption for the projection method was identified.

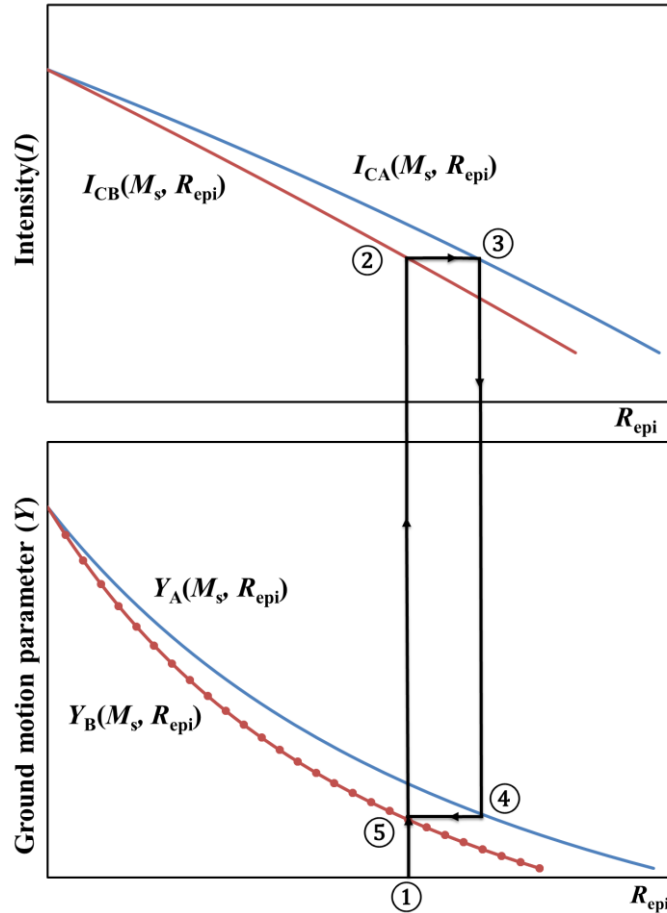


Figure 2.1. Illustration of the projection method proposed by Hu and Zhang (1984): The subscripts A and B denote the reference and target regions, respectively; circled numbers 1-5 in the figure represent the steps of the projection method. Given a scenario event defined by its magnitude and  $R_{epi}$  shown at circled number 1, find its intensity for the target region at circled number 2, find circled number 3 for the reference region based on equal intensity, find the ground motion measure for the reference region at circled number 4, and define the ground motion measure shown at circled number 5.

Using the projection method illustrated in Figure 2.1, Wang et al. (2000) developed a set of GMMs. For the development, it was assumed that the GMMs for the eastern and western seismic regions of China differ and that IPE can be modeled using Eq. (2.2) with model coefficients shown in Table 2.1 for the fourth-generation CSHM that were obtained using the procedure given in Chen and Liu (1989). In this case, in addition to the seismic events and isoseismal lines that were considered to develop the IPE used in mapping the

third-generation CSHM, 169 isoseismal lines from 66 earthquakes were considered (see Chapter 2; page 54; Hu et al., 2001).

Wang et al. (2000) used the western U.S. as the reference region, and considered that the IPE developed by Chandra (1979),

$$I - I_0 = 2.014 - 0.00659R_{\text{epi}} - 2.014\log(R_{\text{epi}} + 10) + \varepsilon_I, \text{ for } R_{\text{epi}} < 330 \text{ km} \quad (2.6a)$$

or,

$$I = 0.514 + 1.5000M_s - 0.00659R_{\text{epi}} - 2.014\log(R_{\text{epi}} + 10) + \varepsilon_I, \text{ for } R_{\text{epi}} < 330 \text{ km} \quad (2.6b)$$

is adequate for the reference region, where  $\sigma_{I\varepsilon} = 0.274$ , and the relation  $M_s = 1 + 2I_0 / 3$  is employed in writing Eq. (2.6b), where  $I$  denotes the intensity.

For the reference and target regions, it was considered that the GMMs for the effective peak acceleration (EPA), denoted as  $a_E$ , or effective peak velocity (EPV), denoted as  $v_E$ , can be expressed as (Wang et al., 2000),

$$\log Y = c_1 + c_2M_s + c_3M_s^2 + c_4 \log(R_{\text{epi}} + c_5 \exp(c_6M_s)) + \varepsilon_Y, \quad (2.7)$$

where  $Y$  denotes  $a_E$  (cm/s<sup>2</sup>) or  $v_E$  (cm/s), and  $c_i, i = 1, \dots, 6$ , are the model coefficients,  $\varepsilon_Y$  is the residual with zero mean and the standard deviation  $\sigma_{Y\varepsilon}$ . In evaluating  $a_E$  or  $v_E$ , it was considered that  $a_E$  equals 40% (i.e., 1/2.5) of the average of the ‘‘plateau’’ of the SA for a damping ratio of 5% and the period between the corner periods  $T_0$  and  $T_1$ , and that  $v_E$  equals 40% (1/2.5) of the average of the plateau of the spectral velocity (SV) for a damping ratio of 5% and the period between the corner periods  $T_1$  and  $T_2$  (see Chapter 2; page 53; Hu et al., 2001). However, a value of  $2.25 \times a_E$  instead of  $2.5 \times a_E$  is recommended in the design code (GB50011-2010, 2010) to evaluate the ‘‘plateau’’ of the SA for a damping ratio of 5%, resulting in an inconsistency. The characteristic period of the response spectrum  $T_g$  equals  $2\pi v_E / a_E$  (the significance of  $T_g$  will be discussed in the following sections). The functional

form shown in Eq. (2.7) for the ground motion measures was also considered by others, including Huo and Hu (1992).

The model coefficients for Eq. (2.7) were developed based on 187 ground motion records from 21 mainshocks that occurred from 1933 to 1994 in the western U.S, (Wang et al., 2000). The coefficients are shown in Table 2.2. By assuming that the intensity measure  $I_c$  is equivalent to the intensity measure  $I$ , and using the projection method, the developed model coefficients by Wang et al. (2000) for Eq. (2.7) are also presented in Table 2.2. The table shows that  $\sigma_{Y\varepsilon}$  for the target region is assigned to be the same as that for the reference region, although no justification for such an assignment was elaborated. The  $\sigma_{Y\varepsilon}$  value shown in Table 2.2 is for  $\log Y$ ; it should be multiplied by 2.30 ( $= \ln(10)$ ) to represent the sigma of  $\ln Y$ .

$\sigma_{Y\varepsilon}$  for the target region should be a function of  $\sigma_{I\varepsilon}$  and  $\sigma_{Y\varepsilon}$  for the reference region and of  $\sigma_{Ia}$  (or  $\sigma_{Ib}$ ) for the target region (Wang and Wu, 1988). Huo et al. (1992) also emphasized that the use of theoretically-derived equations by some simplifying assumptions, including the independence of  $\varepsilon_I$  and  $\varepsilon_Y$  for the same region, overestimates  $\sigma_{Y\varepsilon}$  for the target region. To overcome this, it was suggested that (Huo et al., 1992),

$$\left(\sigma_{Y\varepsilon}\right)_{\text{Target}} = \frac{\left(\sigma_{I\varepsilon}\right)_{\text{Target}}}{\left(\sigma_{I\varepsilon}\right)_{\text{Reference}}} \times \left(\sigma_{Y\varepsilon}\right)_{\text{Reference}} \quad (2.8)$$

where the subscripts Target and Reference refer to the target and reference regions, respectively.

If Eq. (2.8) is used for projecting the GMMs shown in Table 2.2,  $\sigma_{Y\varepsilon}$  for the target region is about twice of the values shown in Table 2.2. This large increase is due to the small sigma for Eq. (2.6). The effect of changing sigma on the estimated seismic hazard is discussed in the following sections.

In addition, according to Liu et al. (2006), the reported  $M_s$  by the U.S. and China differ.  $M_s$  reported by the Institute of Geology, China Earthquake Administration, is related to  $M_s$

reported by the National Earthquake Information Center of the United State Geological Survey (denoted as  $M_{s-US}$  in the remaining part of this chapter) by,

$$M_{s-US} = 1.07M_s - 0.61 \quad (2.9)$$

By considering this difference,  $M_s$  shown in Eqs. (2.6) and (2.7) for the reference region should be interpreted as  $M_{s-US}$ . Since this reporting difference was only available in 2006, it was not mentioned in developing the GMM for the target region in Wang et al. (2000).

Table 2.2. Model coefficients for Eq. (2.7) ( $c_3 = 0$ ) (Wang et al. 2000).

Parameter	Region	Axis	$c_1$	$c_2$	$c_4$	$c_5$	$c_6$	$\sigma_{Y\varepsilon}$
Effective peak acceleration (EPA) (cm/s <sup>2</sup> )	Western USA		1.204	0.631	-1.928	1.046	0.451	0.242
	Eastern China	Major	2.304	0.747	-2.59	2.789	0.451	0.242
		Minor	1.184	0.585	-1.764	1.046	0.451	0.242
	Western China	Major	2.492	0.786	-2.787	3.269	0.451	0.242
		Minor	1.093	0.591	-1.794	1.046	0.451	0.242
Effective peak velocity (EPV) (cm/s)	Western USA		0.907	0.698	-1.674	1.046	0.451	0.327
	Eastern China	Major	0.013	0.793	-2.212	2.789	0.451	0.327
		Minor	0.943	0.655	-1.506	1.046	0.451	0.327
	Western China	Major	0.207	0.829	-2.408	3.269	0.451	0.327
		Minor	1.002	0.661	-1.55	1.046	0.451	0.327

### 2.2.3 IPEs and GMMs for developing the fifth-generation CSHM

The GMMs used to assess the fifth-generation CSHM were developed for four subregions covering the mainland China by considering regional differences in the intensity attenuation and seismic activity (Yu et al., 2013; Gao et al., 2015). The historical earthquake data used to develop the intensity attenuation are 973 isoseismal lines from 377 earthquakes (with magnitude greater than  $M_s 4.0$ ), where those before 1990 are the same as the ones used to develop the fourth-generation CSHM. Using the data, the model coefficients for Eq. (2.2) developed by Yu et al. (2013) and applied for the fifth-generation CSHM are shown in Table 2.1 for four zones: (a) Eastern seismic region (i.e., “Eastern strong seismic region”); (b) Median seismic region (i.e., “Median-strong seismic region”); (c) Tibet seismic region; and (d) Xinjiang seismic region.

The geographical region for the “Median-strong seismic region” coincides with part of the eastern China region considered to develop the fourth-generation CSHM. For this region, it was indicated that the IPE is only applicable for up to  $M_s 7.0$  (Yu et al., 2013). The “Tibet seismic region” and “Xinjiang seismic region” coincide with part of the western region of China considered to develop the fourth-generation CSHM.

For the development of the GMMs, Yu et al. (2013) followed the same approach used by Wang et al. (2000). Again, Eq. (2.6) was used as the IPE for the reference region. However, to develop the GMMs for  $a_E$  and  $v_E$  applicable to the reference region, Yu et al. (2013) considered records from 16 seismic events from 1970 to 2002: 13 occurred in California, one in Taiwan and two in Iran. This resulted in a total of 268 ground motion records obtained at sites with  $V_{S30}$  (i.e., the time averaged shear-wave velocity in the top 30 m) greater than 500 m/s, corresponding to site Class I defined in GB50011-2010 (2010). These records were grouped into records from seismic events with magnitude smaller than  $M_s 6.5$ , and with magnitude greater than  $M_s 6.5$ , although it is not clear how the event with magnitude equal to  $M_s 6.5$  (e.g., 1983 Coalinga earthquake) was grouped. The estimated model coefficients of the GMMs by using the records are presented in Table 2.3. A simple calculation indicated that at  $M_s 6.5$ , the predicted  $a_E$  or  $v_E$  by the developed model for



magnitude less than or equal to  $M_s6.5$  differs from, but is very close to that predicted by the model for the magnitude greater than or equal to  $M_s6.5$ .

Based on the GMMs for the reference region (i.e., Eq. (2.7)) with model coefficients depicted in Table 2.3, the IPE shown in Eq. (2.6) for the reference region, and the IPE for the target region (i.e., Eq. (2.2) with model coefficients as shown in Table 2.1), the GMMs applicable to site Class I for the four target regions in China were developed by Yu et al. (2013) and shown in Table 2.4 based on the projection method. The equations for magnitude equal to  $M_s6.5$  does not always lead to the same value, especially for the Tibet seismic region, which may affect the estimated seismic hazard.

Table 2.3. Model coefficients for Eq. (2.7) developed by Yu et al. (2013) for the reference region ( $c_3 = 0$ . The inequality symbols are used as those shown in the reference).

Ground motion measure	Magnitude	$c_1$	$c_2$	$c_4$	$c_5$	$c_6$	$\sigma_{Y\epsilon}$
EPA ( $\text{cm/s}^2$ )	$M_s \leq 6.5$	0.561	0.746	-1.925	0.956	0.462	0.236
	$M_s \geq 6.5$	2.501	0.448	-1.925	0.956	0.462	0.236
EPV ( $\text{cm/s}$ )	$M_s \leq 6.5$	-1.819	0.879	-1.731	0.956	0.462	0.271
	$M_s \geq 6.5$	0.425	0.533	-1.731	0.956	0.462	0.271

Table 2.4. Model coefficients for EPA and EPV applicable to some regions in China (Yu et al., 2013).

Parameter and Region	Sub-region	Magnitude range	Axes	$c_1$	$c_2$	$c_4$	$c_5$	$c_6$	$\sigma_{Y\epsilon}$
EPA ( $\text{cm/s}^2$ ), Eastern region of China	Eastern seismic region	$M_s < 6.5$	Major	1.979	0.671	-2.315	2.088	0.399	0.236
			Minor	1.176	0.660	2.004	0.944	0.447	0.236
		$M_s \geq 6.5$	Major	3.533	0.432	-2.315	2.088	0.399	0.236
			Minor	2.753	0.418	2.004	0.944	0.447	0.236
	Median seismic region	$M_s < 6.5$	Major	2.417	0.498	-2.079	2.802	0.295	0.236
			Minor	1.715	0.471	-1.723	1.295	0.331	0.236
		$M_s \geq 6.5$	Major	3.706	0.298	-2.079	2.802	0.295	0.236
			Minor	2.690	0.321	-1.723	1.295	0.331	0.236
EPA, ( $\text{cm/s}^2$ ), Western region of China	Xinjiang seismic region	$M_s < 6.5$	Major	1.791	0.72	-2.389	1.772	0.424	0.236
			Minor	0.983	0.713	-2.118	0.825	0.465	0.236
		$M_s > 6.5$	Major	3.403	0.472	-2.389	1.772	0.424	0.236
			Minor	2.610	0.463	-2.118	0.825	0.465	0.236
	Tibet seismic region	$M_s < 6.5$	Major	2.387	0.645	-2.416	2.647	0.366	0.236
			Minor	1.003	0.609	-1.854	0.612	0.457	0.236
		$M_s \geq 6.5$	Major	3.807	0.411	-2.416	2.647	0.366	0.236
			Minor	2.457	0.388	-1.854	0.612	0.457	0.236

EPV (cm/s), Eastern region of China	Eastern seismic region	$M_s < 6.5$	Major	-0.363	0.791	-2.103	2.088	0.399	0.271
			Minor	-1.147	0.788	-1.825	0.944	0.447	0.271
		$M_s \geq 6.5$	Major	1.437	0.513	-2.103	2.088	0.399	0.271
			Minor	0.712	0.502	-1.825	0.944	0.447	0.271
	Median seismic region	$M_s < 6.5$	Major	0.093	0.621	-1.889	2.802	0.295	0.271
			Minor	-0.589	0.601	-1.559	1.295	0.331	0.271
		$M_s \geq 6.5$	Major	1.640	0.382	-1.889	2.802	0.295	0.271
			Minor	0.671	0.407	-1.559	1.295	0.331	0.271
EPV (cm/s), Western region of China	Xinjiang seismic region	$M_s < 6.5$	Major	-0.547	0.840	-2.181	1.772	0.424	0.271
			Minor	-1.351	0.843	-1.945	0.825	0.465	0.271
		$M_s \geq 6.5$	Major	1.310	0.544	-2.181	1.772	0.424	0.271
			Minor	0.569	0.549	-1.945	0.825	0.465	0.271
	Tibet seismic region	$M_s < 6.5$	Major	-0.064	0.766	-2.205	2.647	0.366	0.271
			Minor	-1.301	0.741	-1.696	0.612	0.457	0.271
		$M_s \geq 6.5$	Major	1.714	0.491	-2.205	2.647	0.366	0.271
			Minor	0.443	0.474	-1.696	0.612	0.457	0.271

Again, no justification was provided to the assigned  $\sigma_{Y\varepsilon}$  shown in Table 2.4, even though values of  $\sigma_{Ia\varepsilon}$  and  $\sigma_{Ib\varepsilon}$  for different target regions differ, and  $\sigma_{I\varepsilon}$  for the reference region is much smaller than those for the target regions. The impact of this assumption on the seismic hazard mapping was not elaborated. Also, the difference between  $M_s$  and  $M_{s-US}$  was not included to derive the GMM for the target region.

## 2.3 Comparison of the IPEs and GMMs used for the CSHMs

### 2.3.1 Comparison of the intensity attenuation and sigma

A comparison of the reviewed IPEs considered for the CSHM in the previous sections is given in this section to aid the understanding of the differences among the three generations CSHM. The comparison of the IPEs used for the three generations of the CSHM is presented in Figure 2.2 for locations along the major axis and magnitudes ranging from  $M_s$  5 to 8. The figure indicates that the differences in the predicted intensity increase as  $M_s$  increases. Moreover, it can be observed that:

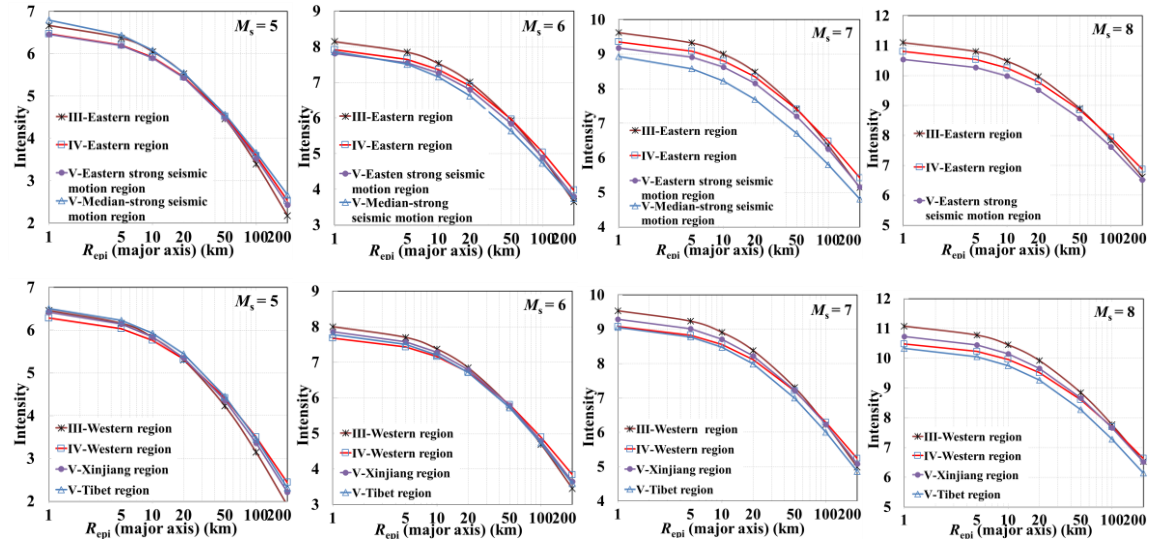


Figure 2.2. Comparison of predicted intensity along the major axis (III, IV and V refer to the IPEs used for the third, fourth and fifth-generation CSHM. The notations are also used in Figure 2.3, Figure 2.5 and Figure 2.6.

1. The differences in the predicted intensities are not very large for  $M_s$  5 and  $M_s$  6.0.

2. The model for the Median seismic region provides the lowest predicted intensity for  $M_s7.0$ . However, it is unclear why this is not the case for  $M_s5.0$ .

3. The differences between the predicted intensity for eastern and western seismic regions are not very large, especially considering the larger uncertainty in these IPEs. For example,  $\sigma_{Ia\varepsilon}$  and  $\sigma_{Ib\varepsilon}$  range from 0.49 to 0.64 for the IPEs developed for the third-generation CSHM, 0.52 to 0.63 for the IPEs developed the fourth-generation CSHM, and 0.52 to 0.66 for the IPEs developed the fifth-generation CSHM. The lower sigma values are for the eastern seismic region and the higher values are for the western seismic region. Moreover, these sigma values are about twice of the sigma value of 0.274 for the IPE shown in Eq. (2.6) that was adopted for the reference region for the fourth and fifth-generation CSHMs.

Similarly, a comparison of the IPEs used for the three generations of the CSHM is presented in Figure 2.3 for the locations along the minor axis. The observations made from the results shown in Figure 2.2 are also applicable to the results presented in Figure 2.3. As expected, the intensity attenuates faster along the minor axis than along the major axis. It must be emphasized that the curves for  $M_s8$  are not plotted in Figure 2.2 and Figure 2.3 for the median-strong seismic region since the IPEs, in this case, are only applicable for up to  $M_s7$  (Yu et al., 2013).

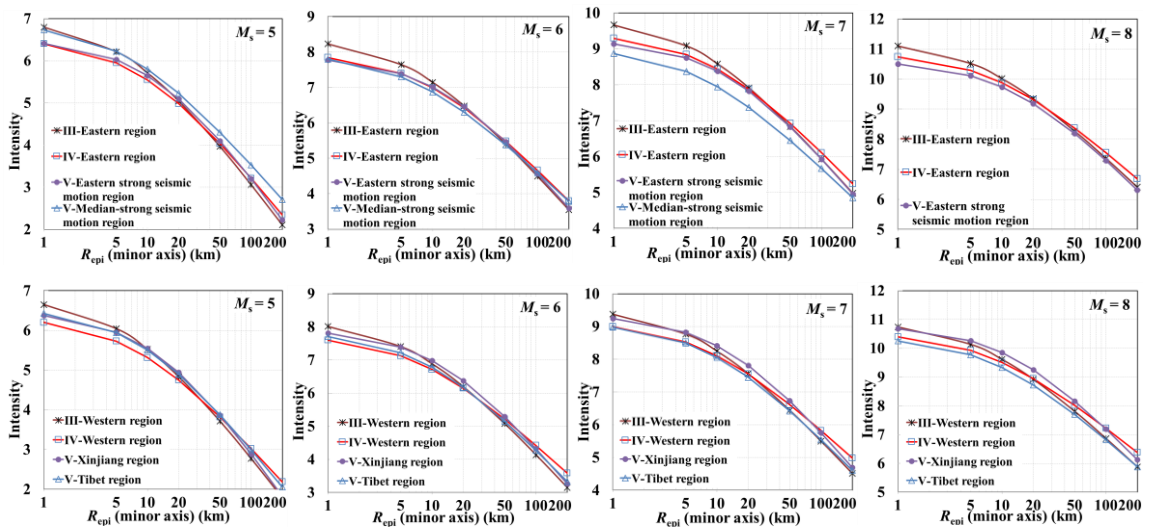


Figure 2.3. Comparison of predicted intensity along the minor axis in different regions.

A literature search focused on the IPEs applicable to the reference region was carried out. Three additional relevant equations are found: two given by Howell and Schultz (1975) and one given by Atkinson et al. (2014). The IPEs given by Howell and Schultz (1975) are,

$$\ln(I / I_0) = 0.364 - 0.130 \ln R_{\text{epi}} - 0.0019 R_{\text{epi}} + \varepsilon_I, \quad (2.10)$$

and,

$$I - I_0 = 0.874 - 0.422 \ln R_{\text{epi}} - 0.0186 R_{\text{epi}} + \varepsilon_I, \quad (2.11)$$

that were developed using almost the same set of data as those used in Chandra (1979), where  $I$  represents the MMI and  $I_0 = 3(M_{\text{s-US}} - 1) / 2$ . It was indicated that the standard deviation of  $\varepsilon_I$  (i.e., the root-mean-square-error in  $I$ ) equals 0.43 for Eq. (2.10) and 0.64 for Eq. (2.11). These sigma values are much greater than that given by Chandra (1979) but are comparable to those shown in Table 2.1. Eq. (2.10) was developed based on the concept of energy decay and, is associated with a smaller standard deviation of residuals, and Eq. (2.11) has the same functional form as Eq. (2.6).

The IPE given by Atkinson et al. (2014) is,

$$I = 0.309 + 1.864 M_w - 1.672 \log R - 0.00219 R + 1.77 \max\left(0, \log\left(\frac{R}{50}\right)\right) - 0.383 M_w \log R + \varepsilon_I, \quad (2.12)$$

where  $M_w$  is the moment magnitude,  $R = \sqrt{D_h^2 + 14^2}$ ,  $D_h$  is the hypocentral distance in km, and the residual  $\varepsilon_I$  is a random variable with zero mean and standard deviation of 0.50.

A comparison of Eqs. (2.6), (2.10) to (2.12) is plotted in Figure 2.4. For the plotting of Eq. (2.12), it is considered that  $D_h = \sqrt{R_{\text{epi}}^2 + 8^2}$  (Atkinson and Wald, 2007),  $M_w = (2/3) \times \log M_0 - 10.73$  (Kanamori, 1977), and (Ekström and Dziewonski, 1988),

$$\log M_0 = \begin{cases} 19.24 + M_{s-US} & M_{s-US} < 5.3 \\ 30.20 - \sqrt{92.45 - 11.40M_{s-US}} & 5.3 \leq M_{s-US} \leq 6.8. \\ 16.14 + 3/2 M_{s-US} & M_{s-US} > 6.8 \end{cases} \quad (2.13)$$

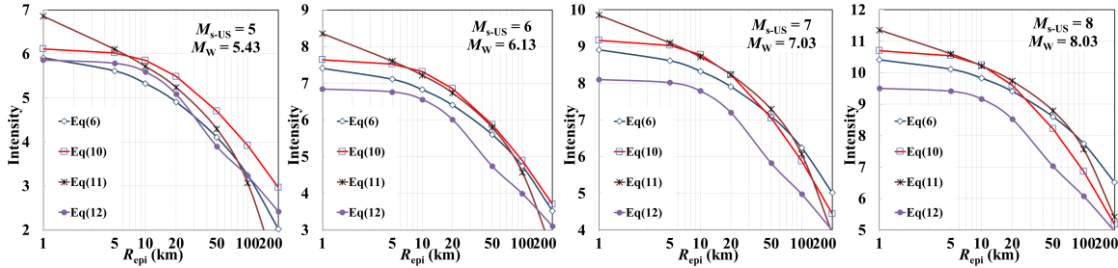


Figure 2.4. Comparison of predicted  $I$  (i.e., MMI) by using Eqs. (2.6), (2.10), (2.11), and (2.12).

The comparison shown in Figure 2.4 indicates that the considered IPEs provide relatively consistent predicted intensity for events with  $M_{s-US} \leq 5$  and  $R_{epi}$  within 10 to 100 km. However, as  $M_{s-US}$  increases, the use of Eq. (2.12) leads to the lowest predicted  $I$ . In general, Eq. (2.11) provides the steepest decrease in the predicted  $I$  as  $R_{epi}$  increases. An inspection of the curves shown in Figure 2.4 and those presented in Figure 2.2 and Figure 2.3 indicates that if  $I_C$  is assumed to be equivalent to  $I$  as was done by Wang et al. (2000) and Yu et al. (2013), the predicted  $I$  values by using Eq. (2.11) compare favorably to those predicted by using Eq. (2.2) with the model coefficients shown in Table 2.1. This implies that, on average, the differences in the predicted intensities are not very large; at least for intensities that are of importance for engineering applications.

It is noteworthy that Howell and Schultz (1975) showed that the IPE with both the geometric spreading and exponential absorption provides a better fit than the equation with geometric spreading only for San Andreas province (i.e., California). An inspection of the IPEs for the western U.S. indicates that the consideration of exponential absorption is important especially for large  $R_{epi}$  values. Whether such an observation is applicable to regions in China is unknown. It can be of value to re-examine the attenuation of  $I_C$  using the isoseismal contour lines used in Yu et al. (2013) (when such data become accessible) by considering the geometric spreading and exponential absorption and other functional

forms, including those derived based on energy decay given by Howell and Schultz (1975), and the one used in Atkinson et al. (2014).

The values of  $\sigma_{I\epsilon}$  equal to 0.43 and 0.64 for Eqs. (2.10) and (2.11) (Howell and Schultz, 1975), and  $\sigma_{I\epsilon}$  of 0.5 for Eq. (2.12) (Atkinson et al., 2014) are comparable to the sigma values reported in Table 2.1 and are much greater than  $\sigma_{I\epsilon} = 0.274$  for Eq. (2.6) reported by Chandra (1979). This is important since Eq. (2.8) indicates that  $(\sigma_{Y\epsilon})_{\text{Target}}$  is directly proportional to  $(\sigma_{I\epsilon})_{\text{Target}} / (\sigma_{I\epsilon})_{\text{Reference}}$ . To see whether the values of  $(\sigma_{I\epsilon})_{\text{Target}}$  for Eq. (2.2) and of  $(\sigma_{I\epsilon})_{\text{Reference}}$  for Eqs. (2.6), (2.10), (2.11), and (2.12) are consistent with those applicable to other regions in the world, the sigma values for a few IPEs found in the literature are presented in Table 2.5. The table indicates that the sigma values for most cases agree with those shown in Table 2.1 for the IPEs applicable to China. The sigma values for the IPEs given by Chandra (1979) are lower than other studies.

The earlier observations indicate that the most likely values of sigma are those associated with Eqs. (2.10), (2.11), or (2.12) instead of that associated with Eq. (2.6) for the reference region. The closeness of the predicted intensity values by using Eqs. (2.6), (2.10), and (2.11) and Eq. (2.2) implies that the GMMs for  $a_E$  and  $v_E$  applicable to the target region should not differ strongly from those applicable to the reference region. For a general discussion on the regional dependence and similarity of earthquake response spectra, the reader is referred to Douglas (2007).



Table 2.5. Sigma for some selected attenuation relations for macro-intensity  $I$ .

Reference	Region	Sigma	Notes
Howell and Schultz (1975)	San Andreas province	0.43, 0.64	Intensity = MMI. The first entry is for Eq. (2.10). The second entry is for Eq. (2.11).
	Cordillera province	0.46, 0.61	
	Eastern province	0.42, 0.64	
Anderson (1978)	USA	0.2 to 0.4	Intensity = MMI. This range is based on Figure 2.6 in the reference.
Chandra (1979)	San Andreas province	0.27, 0.27	Intensity = MMI. First entry is obtained using all the listed event in the reference. Second one is for the case with a few events removed.
	Cordillera province	0.25, 0.26	
	Eastern province	0.36, 0.32	
	Central United States	0.24	
Chavez and Castro (1988)	Mexico	0.67 to 0.95	Intensity = MMI.
Casado et al. (2000)	Iberian Peninsula and adjacent areas	0.86 to 0.94	Intensity = MSK. Sigma depends on the considered earthquakes.
Chandler and Lam (2002)	South China	0.7	Intensity = MMI. The reason for the suggested value was not clear.
Dowrick and Rhoades (2005)	New Zealand (NZ), Focal Mechanisms	0.43	Intensity = MMI. The developed attenuation relations are for major and minor axes.
	NZ, Main seismic region	0.43	
	NZ, Deep region	0.50	
Bakun (2006)	Western North America	0.58	Intensity = MMI. (for Basin & Range province of interior North America)
Atkinson and Wald (2007)	California, USA	0.4	Intensity = MMI.
Pasolini et al. (2008)	Italy	0.69	Intensity = MCS.
Sørensen et al. (2009)	Marmara region, northwest Turkey	0.67	Intensity = EMS-98.

Sørensen et al. (2010)	Campania region in southern Italy	0.94 to 0.97	Intensity = MCS. Sigma depends on whether the epicentral distance or Joyner-Boore distance is used.
Atkinson et al. (2014)	Western North America	0.5	Intensity = MMI.

Note: EMS-98 = European Macroseismic Scale - 98, MCS = Mercalli–Cancani–Sieberg scale.

### 2.3.2 Comparison of the GMMs

Comparison of EPA predicted by using the GMMs employed for the fourth- and fifth-generation CSHMs (see Tables 2.2 and 2.4) is presented in Figure 2.5.

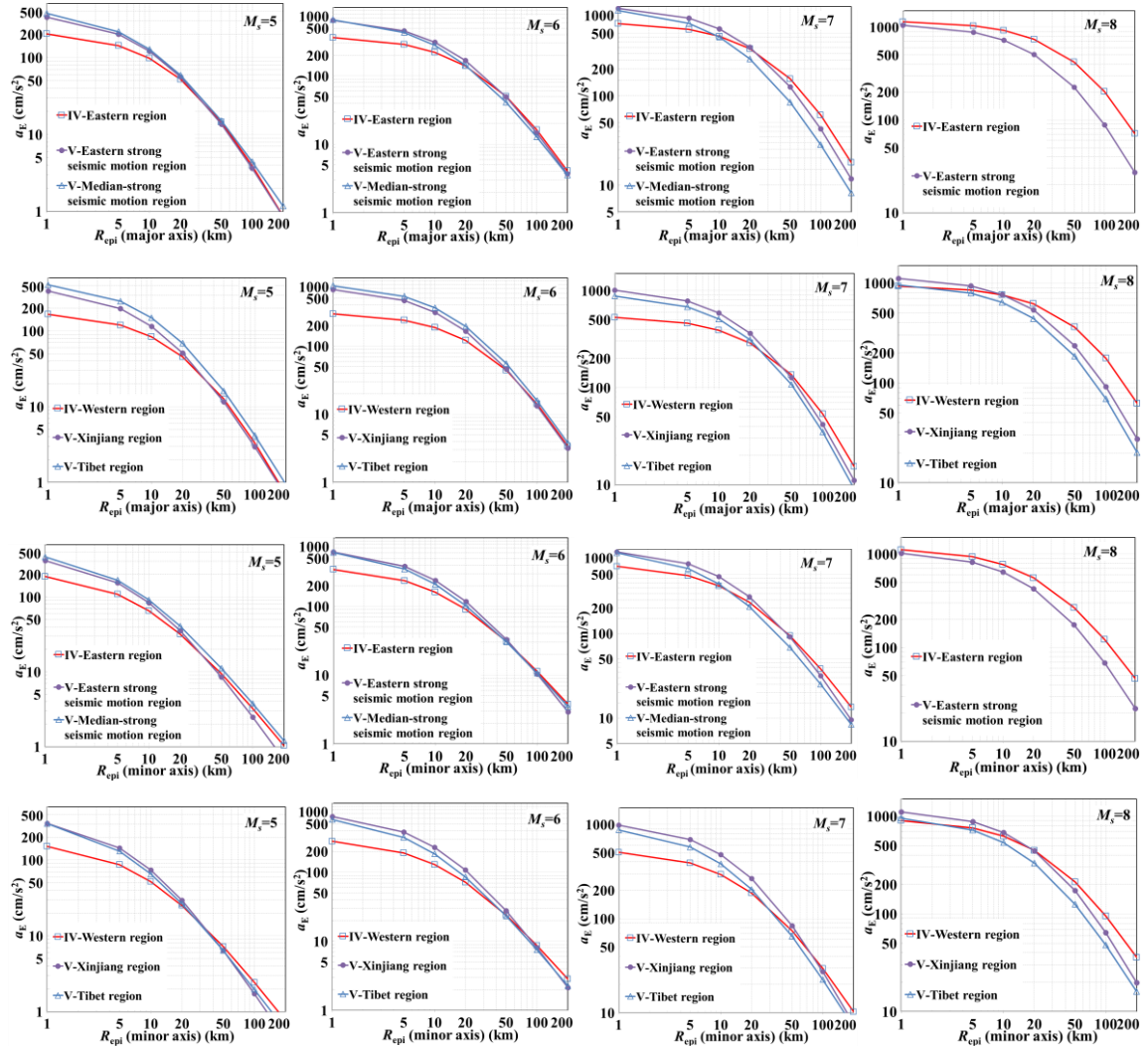


Figure 2.5. Comparison of predicted EPA,  $a_E$ .

The results shown in Figure 2.5 indicate that:

- 1) For the eastern seismic region, the predicted  $a_E$  by using the GMM given by Yu et al. (2013) is greater than that by using the GMM given by Wang et al. (2000) for  $R_{epi}$  less than about 10 km and the magnitude less than or equal to  $M_{s7}$ . However, this trend is reversed for  $M_{s8}$ .

2) For the western seismic region and for small or moderate  $R_{\text{epi}}$ , the predicted  $a_E$  by using the relation given in Wang et al. (2000) is lower or similar to that by using the relation given in Yu et al. (2013). This trend is reversed for  $R_{\text{epi}}$  in the tens or hundreds km.

Since the predicted  $v_E$  values follow the trends similar to those observed from Figure 2.5, the plots of  $v_E$  values are not presented.

The predicted  $a_E$  by using Eq. (2.7) with the model coefficients shown in Tables 2.2 and 2.3 for the reference region is shown in Figure 2.6. The predicted  $a_E$  by using GMMs given in Boore et al. (2014) (referred to as BSSA14 thereafter) which were developed using a large number of records is also shown in Figure 2.6. BSSA14 (which will be discussed further in the next section) is given in terms of  $M_W$ ,  $R_{\text{jb}}$  distance (i.e., Joyner-Boore distance defined as the closest distance to the surface projection of the fault), basin depth  $z_1$ , and  $V_{S30}$ . In plotting BSSA14, it is considered that (1) the fault type is unspecified; (2) the basin depth is treated as unknown (i.e., basin effect is turned off); (3) the relation between  $M_W$  and  $M_{\text{s-US}}$  shown in Eq. (2.13) and the relation between the  $M_{\text{s-US}}$  and  $M_s$  shown in Eq. (2.9) are applicable; and (4)  $V_{S30}$  equal to 500 m/s is adequate since  $V_{S30} > 500$  m/s was used by Yu et al. (2013). To present BSSA14 in terms of  $R_{\text{epi}}$ , it is noted that Scherbaum et al. (2004) suggested that the difference between  $R_{\text{jb}}$  to  $R_{\text{epi}}$  could be considered to be a gamma variate, and that the mean and coefficient of variation of  $R_{\text{epi}} - R_{\text{jb}}$ , denoted as  $m_{e\text{-jb}}$  and  $v_{e\text{-jb}}$ , can be estimated using the following empirical relations (Goda et al., 2010),

$$m_{e\text{-jb}} = \left[ 1 - \exp\left(- (0.458 - 0.0549M_W) \times R_{\text{epi}}^{1.046 - 0.0361M_W}\right) \right] \times \exp\left(-1.297 - 0.138M_W + 0.105M_W^2\right) \quad (2.14a)$$

and,

$$v_{e\text{-jb}} = \left[ 1 + (0.227 - 0.0488M_W) \exp\left(1.921R_{\text{epi}}^{-0.0566}\right) \right] \exp\left(-2.109 - 0.0331M_W\right) \quad (2.14b)$$

These relations are adopted in the present chapter, and  $R_{\text{jb}} = \max(0, R_{\text{epi}} - m_{e\text{-jb}})$  is used for the plot shown in Figure 2.6. Also, the PGA and PGV predicted by using BSSA14 are interpreted as  $a_E$  and  $v_E$ , respectively.

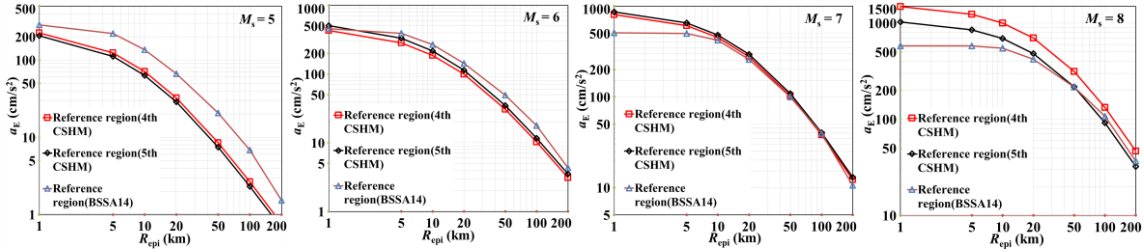
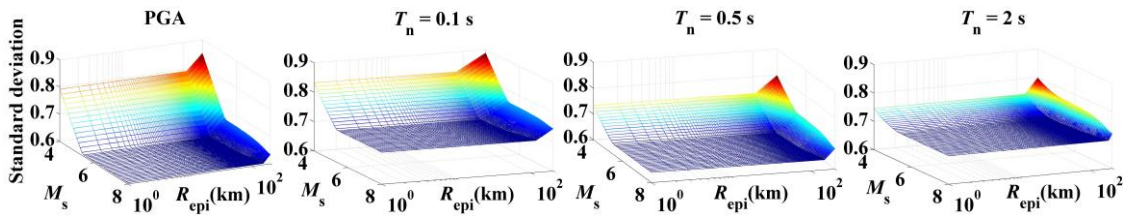


Figure 2.6. Comparison of the GMMs developed for the reference region.

Figure 2.6 shows that the predicted  $a_E$  by using the GMMs developed by Wang et al. (2000) and Yu et al. (2013) are in close agreement. However, they differ from the predicted values by using BSSA14 for  $M_s$  5 or  $M_s$  8. The plateau associated with BSSA14 is controlled by Eq. (2.14). Two additional points on BSSA14 are worth mentioning. The first one is that the sigma values for BSSA14, depends on  $M_w$ , and the distance to the source and vibration period  $T_n$  (see the plots in the first row in Figure 2.7) are greater than those for the GMMs for the EPA used for the fourth- and fifth-generation CSHMs, especially if the magnitude is small. The sigma for BSSA14 decreases as the magnitude increases; it varies slowly with the distance and it varies with  $T_n$ . Second, a variant of BSSA14 that is applicable to China and Turkey, referred to thereafter as BSSA14-CT, was suggested. This variant will be compared to those derived through the projection method in the present chapter in the following section.



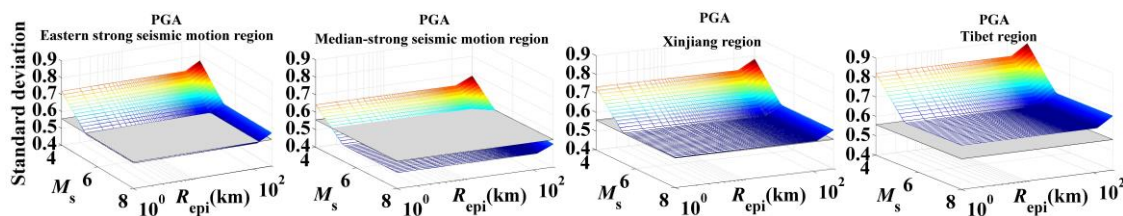


Figure 2.7. Sigma associated with  $\ln Y$  (First row for PGA or SA associated with BSSA14; Second row for PGA considering different target regions; the grey horizontal surface represents the sigma for GMMs used for the fifth-generation CSHM).

In addition to the GMMs developed and used for the CSHMs, other GMMs reported in the literature focused on Chinese sites include those given by Lei et al. (2007), Wang et al. (2013), Tao et al. (2014), and Wen et al. (2018). Lei et al. (2007) focused on the development of the GMMs applicable to the Sichuan region. They followed the same procedure used in Yu et al. (2013), considered the difference in the earthquake magnitude interpretation as shown in Eq. (2.9), and used an IPE developed based on a dataset selected for Sichuan region. Wang et al. (2013) considered limited ground motion records obtained for Chinese earthquakes, including those for the Wenchuan earthquake, to assess the GMMs for PGA and SA. They suggested that the use of major response axis (i.e., the axis corresponding to maximum ground motion measure) could be beneficial. However, unlike in Hong and Goda (2006) and Hong et al. (2009) showing that the major response axis depends on the vibration period, Wang et al. (2013) assumed that the major response axis for the PGA is applicable for SA at different vibration periods. The maximum sigma values for their GMMs are 0.368 for  $\log(\text{PGA})$  and 0.410 for  $\log(\text{SA})$  that are greater than those given by Yu and Wang (2006) (which are 0.240 for  $\log(\text{PGA})$  and 0.388 for  $\log(\text{SA})$ ) estimated by using California records. It suggests that the sigma of the GMMs developed based on Chinese ground motion records is greater than or comparable to those obtained based on California records, although the observational data in terms of the site conditions, number of records, the spatial distribution of the recording station, and the number of earthquakes for Chinese records that are used may not be adequate. It also suggests that the assigned sigma values for the GMMs used in the fourth- and fifth-generation CSHMs shown in Tables 2.2 and 2.4 could be low.

In all cases, the lack of a good number of well-documented historical ground motion records for large earthquakes that have occurred in China hampers the development of the applicable GMMs. Sets of GMMs for SA that are applicable to the regions shown in Tables 2.1 or 2.4 are not available. To overcome this, Tao et al. (2014) explored the use of the records simulated by employing the physics-based stochastic model to develop the GMMs applicable to China. This approach can be valuable and has been used for eastern North America (e.g., Atkinson and Boore, 1995). However, there are difficulties in the selection of the model parameters of the physics-based stochastic model that are most suitable a region of interest where there is no ground motion records.

## 2.4 New GMMs and effect of sigma on the UHS

A set of new GMMs are developed in this section by considering California as the reference region and a region in China as the target region. For the development, it considers the difference in the reported earthquake magnitude for the reference and target regions as shown in Eq. (2.9), and applying the projection method (Hu and Zhang, 1984) but modified to include the uncertainty in IPEs, GMMs and relating  $R_{\text{epi}}$  and  $R_{\text{jb}}$ . More specifically, (1)  $R_{\text{epi}} - R_{\text{jb}}$  that is considered to be truncated gamma variate with an upper bound equal to  $R_{\text{epi}}$ , (see Eqs. (2.14a) and (2.14b)), (2) the residuals for the IPE and GMM applicable to the reference region, and (3) the residuals for the IPE applicable to the target region are sampled. The samples are included in their corresponding equations; and, the procedure shown in Figure 2.1 is applied for a given  $M_s$  and  $R_{\text{epi}}$  to obtain a value of  $Y$  for the target region that corresponding to the given  $M_s$  and  $R_{\text{epi}}$ . This process is repeated so sufficient samples of  $(Y, M_s, R_{\text{epi}})$  are obtained, and the regression analysis is then carried out by using the samples to develop the GMM for the target region. The inclusion of sigma in this process is aimed at having a large number of samples so stable model coefficients for the GMMs can be obtained using the projection method.

The IPE shown in Eq. (2.11) is adopted for the reference region since it is based on a commonly employed functional form including the one used by Chandra (1979), and its sigma value is consistent with most studies summarized in Table 2.5. For a target region, the IPEs applicable for a random orientation are derived using the IPEs employed in the fifth-generation CSHM for the major and minor axes. The use of IPEs for random

orientation is aimed at developing fault orientation independent GMMs so they can be used to assess seismic hazard without assuming the fault orientations of seismic events. The derivation is based on the procedure in Wang and Wu (1988), and the obtained IPEs are shown in Table 2.6. Comparison of the coefficients shown in Tables 2.1 and 2.6 for a given region indicates that the coefficients shown in Table 2.6 are approximately equal to the average of the coefficients applicable to major and minor axes for a given region.

Table 2.6. Model coefficients for Eq. (2.2) applicable to regions in China for a random orientation.

Region	$A$	$B$	$C$	$R_0$	$\sigma_{\mathcal{E}}$
Eastern seismic region	4.5703	1.3626	-3.8746	17.9123	0.5826
Median seismic region	4.7523	1.0710	-3.1934	10.1365	0.5200
Xinjiang seismic region	4.5182	1.4347	-4.1406	17.9531	0.5924
Tibet seismic region	4.6437	1.2746	-3.7933	14.7675	0.6636

BSSA14 (Boore et al. 2013, 2014) is adopted for the reference region. The functional form of BSSA14 expressed in terms of  $M_s$  and  $R_{\text{epi}}$  is,

$$\ln Y = F_M(M_s) + F_P(R, M_s) + F_S(V_{S30}, R, M_s) + \varepsilon_Y \quad (2.15)$$

where  $Y$  represents the PGV, PGA or SA,  $\varepsilon_Y$  is the residual for  $\ln(Y)$  that followed a normal distribution with zero mean and  $\sigma_{Y\varepsilon}$  standard deviation,  $F_M$ ,  $F_P$  and  $F_S$  are given by,

$$F_M(M_s) = \begin{cases} e_1 U + e_2 S_S + e_3 N_S + e_4 R_S + e_5 (M_s - M_{\text{sh}}) \\ + e_6 (M_s - M_{\text{sh}})^2, & \text{for } M_s \leq M_{\text{sh}} \\ e_1 U + e_2 S_S + e_3 N_S + e_4 R_S + e_7 (M_s - M_{\text{sh}}), & \text{for } M_s > M_{\text{sh}} \end{cases}, \quad (2.16)$$

$$F_P(R, M_s) = [c_1 + c_2 (M_s - M_{\text{sref}})] \ln(R / R_{\text{ref}}) + c_3 (R - R_{\text{ref}}) \quad (2.17)$$

and

$$F_S(V_{S30}, R, M_s) = \ln(F_{\text{lin}}) + \ln(F_{\text{nl}}) \quad (2.18)$$



where  $U$ ,  $S_s$ ,  $N_s$  and  $R_s$  take the value of 1.0 if the fault type is unspecified, strike-slip, normal-slip and reverse-slip, respectively, and zero otherwise;  $R = \sqrt{R_{\text{epi}}^2 + h^2}$ ;  $e_i, i = 1, \dots, 7$ ,  $c_1$ ,  $c_2$ ,  $c_3$  and  $h$ , are model coefficients to be determined based on regression analysis;  $\ln(F_{\text{lin}})$  and  $\ln(F_{\text{nl}})$  are linear component of the site amplification and non-linear component of the site amplification, respectively.  $\ln(F_{\text{lin}})$  is given by,

$$\ln(F_{\text{lin}}) = \begin{cases} c \ln(V_{\text{S30}} / V_{\text{ref}}), & \text{for } V_{\text{S30}} \leq V_c \\ c \ln(V_c / V_{\text{ref}}), & \text{for } V_{\text{S30}} > V_c \end{cases} \quad (2.19)$$

where  $V_{\text{S30}}$  is the time-averaged shear-wave velocity in the top 30 m,  $c$  describes the  $V_{\text{S30}}$ -scaling,  $V_c$  is the limiting velocity beyond which ground motions no longer scale with  $V_{\text{S30}}$ , and  $V_{\text{ref}}$  is the specified reference velocity corresponding to NEHRP B/C boundary site conditions (BSSC 2003),  $V_{\text{ref}} = 760$  m/s.  $\ln(F_{\text{nl}})$  is given by,

$$\ln(F_{\text{nl}}) = f_1 + f_2 \ln((PGA_r + f_3) / f_3) \quad (2.20)$$

where  $f_1$ ,  $f_2$ , and  $f_3$  are model coefficients and  $PGA_r$  is the median peak horizontal acceleration evaluated based on given  $M_s$  and  $R$  with  $V_{\text{S30}} = 760$  m/s. Parameter  $f_2$  represents the degree of nonlinearity as a function of  $V_{\text{S30}}$  and is given by:

$$f_2 = f_4 [\exp(f_5 (\min(V_{\text{S30}}, 760) - 360)) - \exp(f_5 (760 - 360))] \quad (2.21)$$

Based on the above consideration and procedure, the obtained coefficients of the GMMs for Eqs. (2.16) and (2.17) are shown in Figure 2.8 for the unspecified fault type, unknown basin depth and  $V_{\text{S30}} = 760$  m/s. The model coefficients  $R_{\text{ref}}$ ,  $c$ ,  $V_{\text{ref}}$ ,  $V_c$ ,  $f_1$ ,  $f_3$ ,  $f_4$  and  $f_5$  are considered to be the same as those given for BSSA14.  $M_{\text{sref}}$  and  $M_{\text{sh}}$  are calculated based on  $M_{\text{ref}}$  and  $M_{\text{h}}$  given for BSSA14. The applicable  $\sigma_{Y\varepsilon}$  is calculated using Eq. (2.8), where  $(\sigma_{I\varepsilon})_{\text{Target}}$  is shown in Table 2.6,  $(\sigma_{I\varepsilon})_{\text{Reference}}$  equals 0.64 (see Eq. (2.11)), and  $(\sigma_{Y\varepsilon})_{\text{Reference}}$  given by Boore et al. (2013) ranges from 0.61 to 0.86 (see Figure 2.7).

If only earthquakes with magnitude greater than  $M_s 6.0$  that are likely to influence the seismic design are considered,  $(\sigma_{Y\varepsilon})_{\text{Reference}}$  shown in Figure 2.7 ranges about 0.61 to 0.66 for PGA. Since the ratio  $(\sigma_{I\varepsilon})_{\text{Target}} / (\sigma_{I\varepsilon})_{\text{Reference}}$  equals 0.910, 0.813, 0.926 and 1.037 for Eastern, Median, Xinjiang and Tibet seismic regions, respectively, the suggested  $\sigma_{Y\varepsilon}$  for the projected GMMs to predict PGA ranges from 0.56 to 0.60 for Eastern seismic region, from 0.50 to 0.54 for Median seismic region, from 0.56 to 0.61 for Xinjiang seismic region, and from 0.63 to 0.68 for Tibet seismic region (see the plots in the second row in Figure 2.7). If the lower motion magnitude events are considered, the increase in the average of sigma for the newly projected GMMs can be about 10% to 20% greater than that for the GMMs used for the fifth-generation CSHM, which equals 0.543 ( $= 0.236 \times \ln(10)$ ).

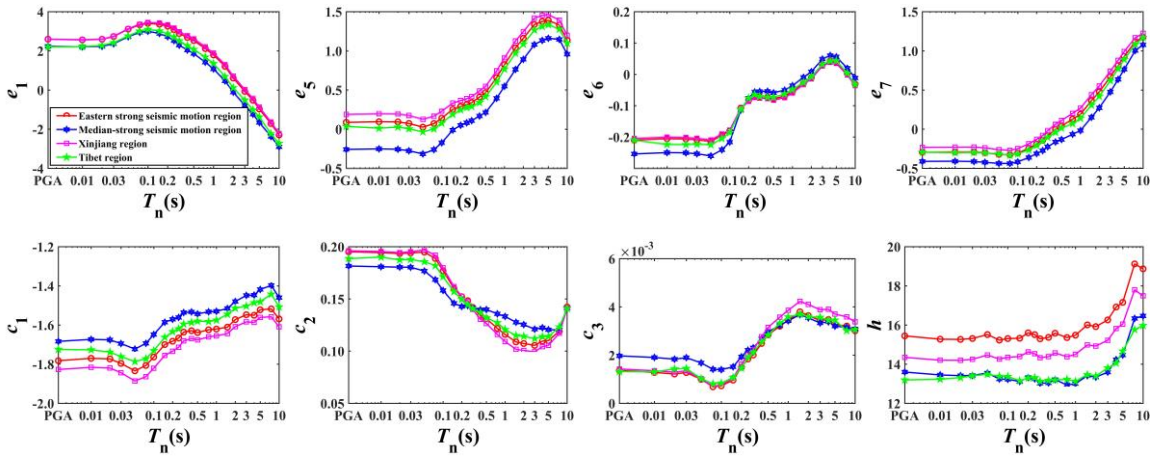


Figure 2.8. Model coefficients for the projected GMMs.

A comparison of the ground motion measures predicted using the projected GMMs, BSSA14-CT, and the GMMs adopted for the fifth-generation of CSHM (Yu et al., 2013) (denoted as YLX13) is presented in Figure 2.9. The GMMs for Median seismic region are not plotted for  $M_s 8.0$  since they are only applicable for magnitude less than or equal to  $M_s 7.0$ . The comparison shown in Figure 2.9 indicates that the values predicted using the newly projected GMMs are relatively close to those predicted by using BSSA14-CT for most cases. However, there are differences between BSSA14-CT and the projected GMMs, especially for  $R_{\text{epi}}$  less than 10 km. The differences are attributed to the differences in the adopted IPEs for the target and reference regions. In general, the predicted PGA

values by using BSSA14-CT or its projected version do not agree with those predicted by using YLX13, especially for  $R_{epi}$  less than 10 km.

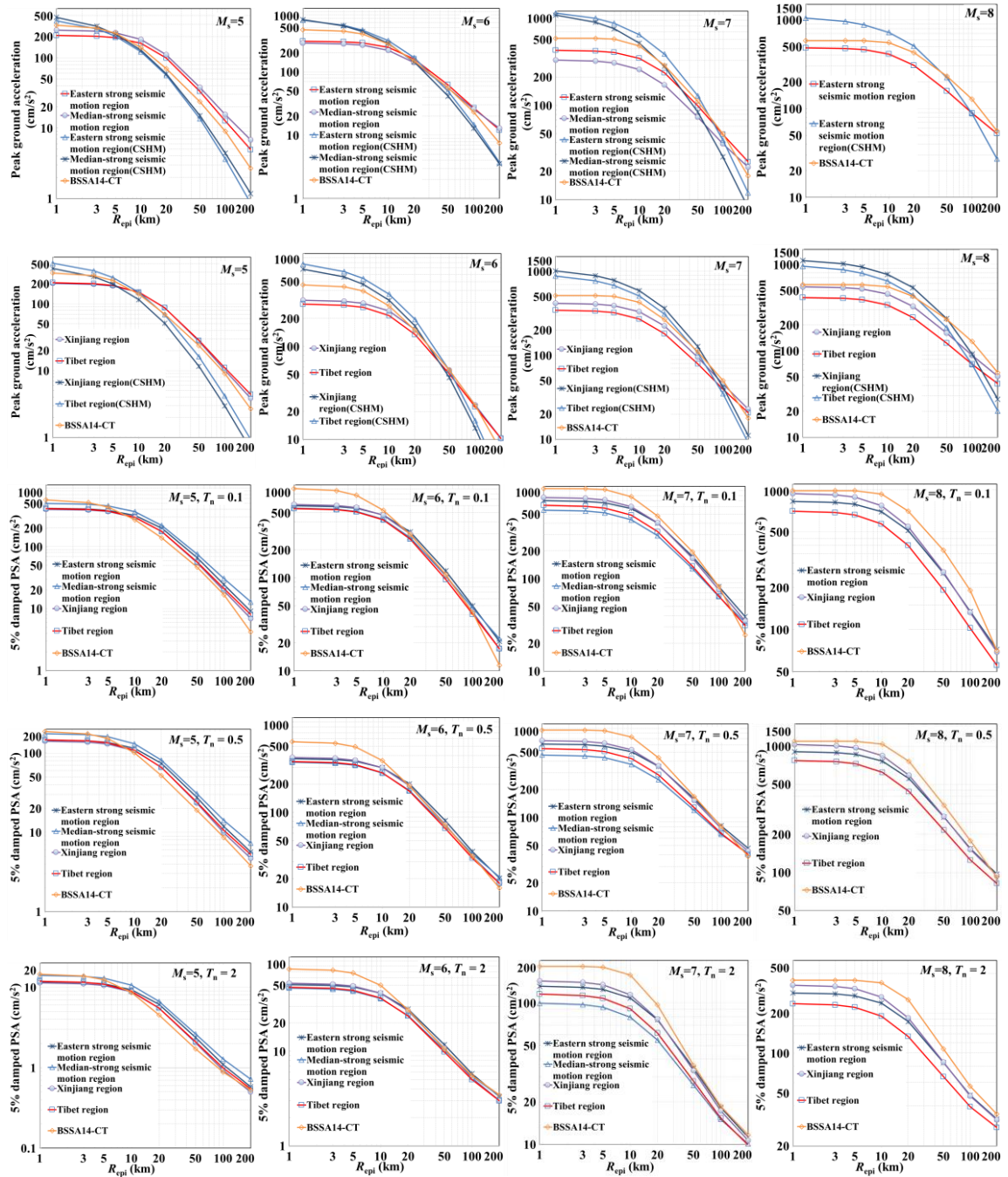


Figure 2.9. Comparison of the predicted ground motion measures (the model coefficients shown in Table 2.4 for major axis are used to plot the PGA predicted by YLX13).

Since  $\varepsilon_Y$  in Eq. (2.15) is normally distribution with zero mean and standard deviation  $\sigma_{Y\varepsilon}$ ,  $\ln Y$  is normally distributed. The  $q$ -fractile of  $Y$ ,  $y_q$ , equals  $m_{\ln Y} \exp(\Phi^{-1}(q)\sigma_{Y\varepsilon})$ , where  $m_{\ln Y}$  is the mean of  $\ln Y$  and  $\Phi^{-1}(\cdot)$  is the inverse of the standard normal distribution function. For a single random seismic event and given  $\sigma_{Y\varepsilon} = 0.6$ , a decrease in  $\sigma_{Y\varepsilon}$  by 10% results in a decrease in  $y_q$  by 7% to 20% for  $q$  equal to  $1-10^{-1}$  to  $1-10^{-4}$ . Similarly, an increase in  $\sigma_{Y\varepsilon}$  by 10% results in an increase in  $y_q$  by 8% to 24% for  $q$  equal to  $1-10^{-1}$  to  $1-10^{-4}$ .

To make a more realistic comparison that considers the seismicity, the estimation of the UHS is carried out for two simple cases: a single fault line source zone and a rectangular source zone as shown in Figure 2.10. The 5% damping ratio is considered based on GB50011 (2010). The earthquake occurrence over a specified source zone is considered to be uniformly distributed with the annual earthquake occurrence rate for magnitude greater than or equal to  $M_s 4.0$ ,  $\lambda(4)$ , shown in the figure. The probability distribution function of  $M_s$  is defined by,

$$F_{M_s}(m_s) = \frac{\exp(-0.86 \times 4) - \exp(-0.86 \times m_s)}{\exp(-0.86 \times 4) - \exp(-0.86 \times M_{s\max})} \quad (2.22)$$

where  $M_{s\max}$  is the maximum magnitude considered for a source zone. For Median–strong seismic region,  $M_{s\max} 7.0$  is used, and for the remaining regions  $M_{s\max} 8.0$  is used.

The estimated UHS by using simulation procedure (Hong et al., 2006) for the identified sites illustrated in Figure 2.10 are also shown in the figure by using the projected GMMs with the model coefficients shown in Figure 2.8 and  $V_{S30}$  equal to 500 m/s. The UHS is estimated for a return period of 50 years (i.e., 63% of exceedance in 50 years) corresponding to the “frequent earthquake” defined in GB50011-2010 (2010). For the plot, each UHS is normalized with its corresponding PGA value that is obtained for site Class II (GB50011-2010, 2010). Also, the code recommended “seismic design coefficient curve” (GB50011-2010, 2010) normalized with respect to its corresponding PGA value

(i.e.,  $0.45a_E$ ), denoted as  $C(T_n)$ , is shown in the figure for the characteristic period  $T_g = 0.35, 0.40$  and  $0.45$  (s).

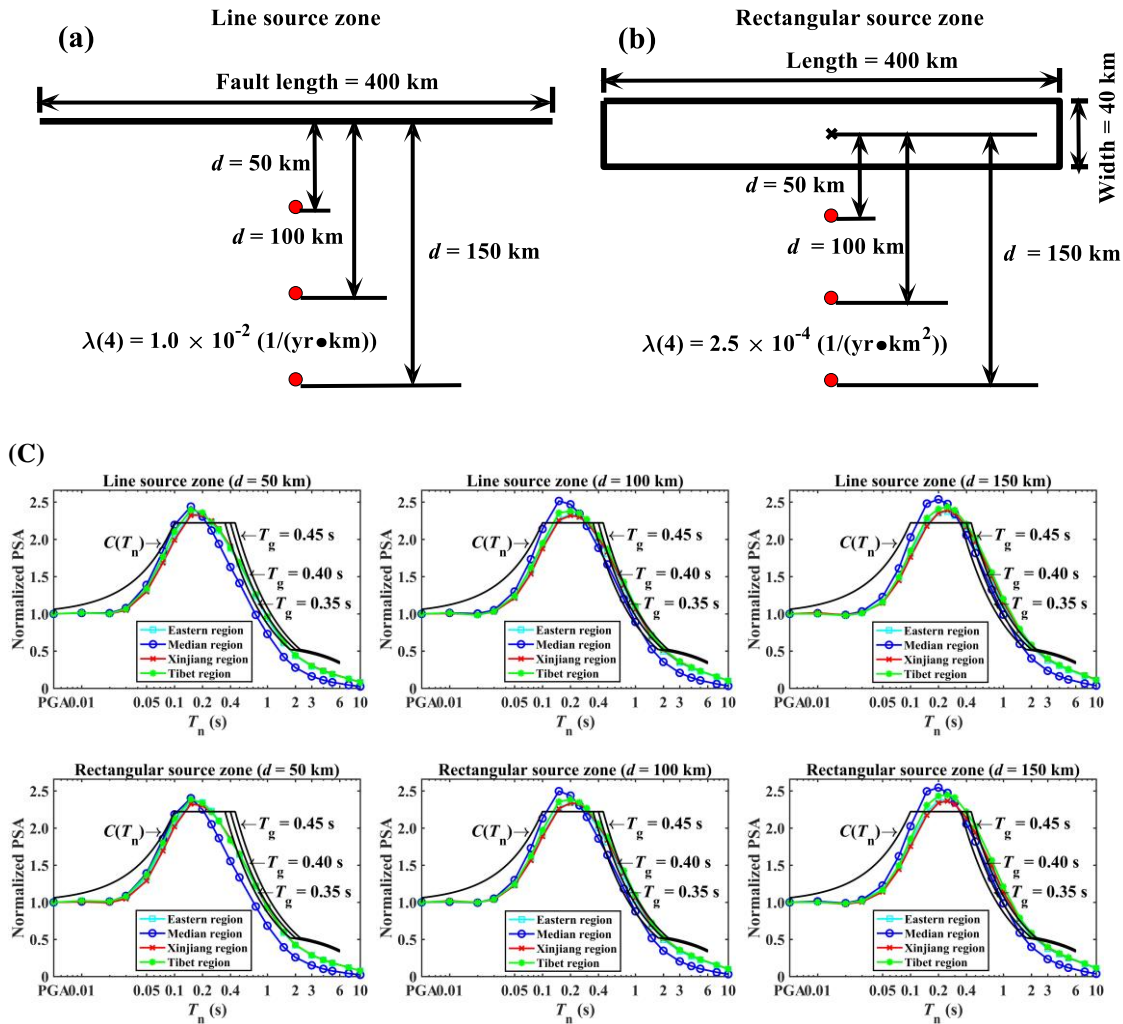


Figure 2.10. Considered source zones and sites and estimated uniform hazard spectra for 5% damping ratio and a return period of 50 year (Panel a) and b) shows the source zones and the remaining panels shows the normalized UHS).

Results shown in Figure 2.10 indicate that the overall trend of  $C(T_n)$  is similar to that of the normalized UHS, and that the shape of UHS is almost identical for each of the four regions considered for the fifth-generation CSHM. The lower values of the normalized UHS for Median seismic region can be explained by noting that  $M_{\text{smax}}7.0$  is used for this region, while  $M_{\text{smax}}8.0$  is used for the remaining regions. However, there are distinct characteristics between the normalized UHS and  $C(T_n)$ . First, for  $T_n \leq 0.2$  s, the normalized

UHS is smaller than  $C(T_n)$ , and is shifted towards the right as compared to  $C(T_n)$ . This implies that the use of  $C(T_n)$  overestimates the seismic design load for stiff structures if the PGA values for  $C(T_n)$  and the normalized UHS are the same. Second, the “plateau” for the normalized UHS is not as pronounced as that for  $C(T_n)$ , and the maximum value of normalized UHS can be greater than that of  $C(T_n)$ , depending on the considered  $T_g$ . Third, the slope of  $C(T_n)$  changes drastically for  $T_n$  near 2 s, this behaviour is not present for the normalized UHS. Also, the normalized UHS is smaller than that of  $C(T_n)$  for  $T_n$  greater than about 2 s. This implies that for a given PGA value the use of  $C(T_n)$  overestimates the seismic load for very flexible structures and structures with base isolations as compared to that obtained from the normalized UHS. Figure 2.10 also indicates that the shape of the UHS by considering the area source is consistent with that by considering the line source.

To investigate the effect of sigma on the UHS, the above analysis is carried out again but with the sigma equal to 0.9 or 1.1 times  $\sigma_{y\epsilon}$  used for Figure 2.10. Since the obtained shapes of the UHS are similar to those presented in Figure 2.10, they are not plotted. The relative differences in the estimated PGA caused by varying the sigma values are also included in Table 2.7. By increasing or decreasing  $\sigma_{y\epsilon}$  by 10%, the estimate PGA is decreased or increased, on average, by 9% or 10%, respectively. This observation is important for CSHM since  $\sigma_{y\epsilon}$  for the newly developed GMMs to predict PGA is increased as compared to that of YLX13.

For comparison purpose, the estimation of the 50-year return period value of PGA is also carried out by using YLX13 (i.e., using the geometric mean of YLX13 for the major and minor axes). Since YLX13 is only applicable for site Class I, the calculated value needs to be multiplied by a scaling factor to obtain that applicable for Class II (Gao et al., 2015). The scaling factor equals 1.25 for PGA equal to 0.05g, it decreases as the value of PGA increases and tends to 1.0 for PGA greater than or equal to 0.4g. The scaled PGA values are compared in Table 2.7. The comparison shown in Table 2.7 indicates that the values obtained by using projected BSSA14 for most regions and considered distances are greater than those obtained by using YLX13. The average of the ratio of the former to the latter is about 1.37. As mentioned previously,  $\sigma_{y\epsilon}$  for the projected GMMs, on average, could be

10% to 20% greater than that for YLX13 for a selected region. If 10% and 20% increase in  $\sigma_{Y_\varepsilon}$  for YLX13 is considered, the increase in the return period value of PGA is, on average, about 6% and 14%, respectively. This explains some of the observed differences between the estimated PGA by using the newly projected GMMs and YLX13. This increase needs to be seriously considered and scrutinized as it impacts the reliability-based structural design code making and economic demand for developing new and retrofitting of existing infrastructure system (Madsen et al., 2006; Goda and Hong, 2006).

Table 2.7. Effect of sigma on estimated PGA with 63% in 50 years exceedance.

Region and source model	Site defined in the figure	50-year return period value of PGA or $a_E$ (g)		Relative error using projected GMMs		Relative error using YLX13	
		projected GMMs	YLX13	Decreasing $\sigma_{Y\epsilon}$ by 10%	Increasing $\sigma_{Y\epsilon}$ by 10%	Increasing $\sigma_{Y\epsilon}$ by 10%	Increasing $\sigma_{Y\epsilon}$ by 20%
Eastern line source	50 km	0.1778	0.2021	-7.6%	9.4%	4.8%	11.2%
	100 km	0.1107	0.0921	-8.3%	8.7%	6.2%	13.7%
	150 km	0.0867	0.0529	-8.1%	9.4%	6.9%	14.9%
Median Line source	50 km	0.1129	0.1015	-8.7%	10.1%	5.9%	14.3%
	100 km	0.0632	0.0428	-8.9%	10.2%	8.8%	17.5%
	150 km	0.0485	0.0243	-9.5%	11.2%	8.8%	18.6%
Xinjiang, Line source	50 km	0.1700	0.1949	-7.5%	9.0%	4.9%	11.2%
	100 km	0.1052	0.0863	-7.5%	8.8%	6.1%	13.2%
	150 km	0.0816	0.0485	-7.5%	10.3%	5.4%	13.7%
Tibet, line source	50 km	0.1612	0.1582	-9.7%	11.8%	5.8%	12.8%
	100 km	0.1012	0.0702	-10.3%	12.2%	6.7%	13.8%
	150 km	0.0804	0.0394	-10.4%	10.7%	7.3%	15.2%
Eastern, area source	50 km	0.1870	0.2133	-7.8%	9.9%	5.7%	11.1%
	100 km	0.1120	0.0946	-7.6%	8.9%	6.6%	13.4%
	150 km	0.0869	0.0538	-8.0%	9.8%	6.3%	14.4%
Median area source	50 km	0.1245	0.1105	-7.6%	9.3%	7.2%	14.2%
	100 km	0.0649	0.0444	-9.1%	9.9%	7.6%	17.2%
	150 km	0.0488	0.0246	-9.4%	10.9%	8.1%	18.3%
Xinjiang, area source	50 km	0.1808	0.2076	-8.4%	6.7%	5.4%	11.5%
	100 km	0.1057	0.0888	-6.7%	9.4%	5.6%	12.4%
	150 km	0.0825	0.0495	-8.8%	8.5%	5.6%	13.1%
Tibet, area source	50 km	0.1704	0.1699	-9.1%	12.2%	5.5%	12.7%
	100 km	0.1018	0.0723	-9.3%	12.0%	6.0%	13.3%
	150 km	0.0802	0.0403	-10.3%	11.7%	6.8%	15.8%



Table 2.8. Effect of sigma on estimated PGA with 10% in 50 years exceedance.

Region and source model	Site defined in the figure	475-year return period value of PGA or $a_E$ (g)		Relative error using projected GMMs		Relative error using YLX13	
		Projected GMMs	YLX13	Decreasing $\sigma_{Y_E}$ by 10%	Increasing $\sigma_{Y_E}$ by 10%	Increasing $\sigma_{Y_E}$ by 10%	Increasing $\sigma_{Y_E}$ by 20%
Eastern, line source	50 km	0.3210	0.3461	-10.5%	13.4%	10.2%	19.7%
	100 km	0.2000	0.1747	-12.2%	12.9%	9.0%	22.4%
	150 km	0.1569	0.0988	-11.4%	13.1%	11.1%	23.4%
Median Line source	50 km	0.1796	0.1875	-12.4%	13.6%	10.6%	22.8%
	100 km	0.0996	0.0777	-12.4%	13.0%	10.4%	24.3%
	150 km	0.0769	0.0424	-12.6%	16.2%	13.6%	30.1%
Xinjiang, Line source	50 km	0.3136	0.3472	-9.7%	15.0%	9.1%	17.4%
	100 km	0.1959	0.1679	-13.0%	11.6%	9.7%	19.0%
	150 km	0.1522	0.0936	-12.0%	16.0%	8.0%	22.0%
Tibet, line source	50 km	0.3058	0.2899	-14.6%	15.6%	6.0%	15.7%
	100 km	0.1901	0.1327	-14.4%	17.1%	11.1%	21.1%
	150 km	0.1516	0.0726	-13.7%	16.1%	12.1%	27.0%
Eastern, area source	50 km	0.3482	0.3854	-11.0%	12.3%	8.6%	20.0%
	100 km	0.2027	0.1814	-11.5%	12.1%	11.5%	21.5%
	150 km	0.1577	0.1015	-10.9%	15.1%	10.7%	23.5%
Median area source	50 km	0.2063	0.2181	-10.6%	12.6%	9.9%	18.6%
	100 km	0.1026	0.0803	-11.7%	13.0%	12.4%	27.6%
	150 km	0.0774	0.0436	-12.7%	14.9%	12.0%	28.7%
Xinjiang, area source	50 km	0.3430	0.3824	-11.2%	11.6%	6.6%	20.5%
	100 km	0.1966	0.1752	-10.1%	12.6%	9.7%	21.4%
	150 km	0.1531	0.0939	-12.4%	12.6%	9.3%	24.1%
Tibet, area source	50 km	0.3268	0.3141	-12.0%	16.7%	9.4%	17.0%
	100 km	0.1913	0.1407	-12.5%	16.6%	9.2%	20.2%
	150 km	0.1523	0.0762	-13.8%	18.0%	11.2%	21.2%

Since the “seismic fortification intensity” (a term used in the Chinese design code) is selected by using the 475 year return period value, the analysis carried out for Figure 2.10 and Table 2.7 is repeated for the return period equal to 475 years. Since the shapes of the normalized UHS obtained in this case are almost identical to those shown in Figure 2.10, they are not plotted. The obtained PGA values are shown in Table 2.8. Comparison of the results shown in Tables 2.7 and 2.8 indicates that the conclusions drawn from results shown in Table 2.7 are also applicable to the results presented in Table 2.8. By increasing or decreasing  $\sigma_{y\epsilon}$  by 10%, the estimated PGA by using the projected GMMs is decreased or increased, on average, by 12% or 14%, respectively. The ratio of the PGA obtained by using the projected GMMs to that obtained by using YLX13, on average, is about 1.32. If 10% and 20% increase in  $\sigma_{y\epsilon}$  for YLX13 is considered, the increase in the 475-year return period value of PGA is, on average, about 10% and 22%, respectively. The observed larger increase in the 475-year return period caused by an increased sigma is expected because the quantile estimation in the tail is very sensitive to the degree of uncertainty. In addition, since according to GB50011-2010 (2010) the design checking requires the use of the 2475-year return period values of PGA, analysis leading to Table 2.8 is carried out again but for a return period of 2475 years. In this case, the average ratio of the PGA obtained by using the projected GMMs to that obtained by using YLX13 is about 1.32. The average increase in the 2475-year return period value of PGA is about 13% and 28% for 10% and 20% increase in  $\sigma_{y\epsilon}$  for YLX13, respectively.

## 2.5 Conclusions

A critical review is carried out for the GMMs used to develop CSHMs focused on mainland China. It indicates that these GMMs are all developed based on the projection method. The use of such a method is necessary because sufficient ground motion records of large earthquakes are lacking in mainland China, although the catalogue of historical Chinese earthquakes is relatively rich as compared with that for other regions in the world. It must be emphasized that the projection method implicitly assumes that there are consistencies in data used for the reference region to develop the set of IPE and GMM. The

consistency should include site condition, magnitude reporting and earthquake mechanism in both reference and target regions. However, this may not be the case in practice.

It was found that justifications for the adopted values of the standard deviation ( $\sigma$ ) for the developed GMMs for the PGA used for the fourth- and fifth-generation CSHMs were not provided and that these  $\sigma$  values may be low. The differences in reporting  $M_s$  by the Institute of Geology, CEA, and by the USGS National Earthquake Information Center are not considered in developing these GMMs. Moreover, the GMMs for spectral acceleration were not given for the fourth- and fifth-generation CSHMs. By considering these facts, a new set of GMMs for different regions in mainland China is developed based on the projection method and the GMMs given by Boore et al. (2013, 2014). Depending on the considered region, the  $\sigma$  for the projected GMMs,  $\sigma_{y_e}$ , is about 10% to 20% greater than that for the GMMs used for the fifth-generation CSHM.

The increase in  $\sigma$  is likely to cause an increase in the estimated return period value of the annual maximum PGA and affecting the seismic hazard mapping. Through simple seismic hazard assessment, it is shown that the use of the newly projected GMMs is likely to cause about 35% increase in the estimated 50-, 475- and 2475-year return period values of PGA as compared to those obtained by using the GMMs adopted for the fifth-generation CSHM. Part of the increase is attributed to the differences in the  $\sigma$  values between the newly projected GMMs and those used to map seismic hazard for mainland China. Moreover, the shape of the standardized UHS obtained in the present chapter differs from that of the normalized response spectrum recommended by the Chinese seismic design code. These observations need to be further investigated by mapping seismic hazard for mainland China and seriously considered for structural design code-making.

## 2.6 Data and Resources

The coefficients for BSSA14 was obtained from Boore et al. (2013), webpage (<https://peer.berkeley.edu/research/nga-west-2/final-products>, last accessed September 2017).

## 2.7 References

Anderson, J. G. (1978). On the attenuation of Modified Mercalli Intensity with distance in the United States, *Bull. Seismol. Soc. Am.* **68**,1147-1179.

Atkinson G.M., and D.J. Wald (2007). "Did You Feel It?" intensity data: A surprisingly good measure of earthquake ground motion, *Seismol. Res. Lett.* **78**, 362-368.

Atkinson, G.M., and D.M. Boore (1995). Ground-motion relations for eastern North America, *Bull. Seismol. Soc. Am.* **85**, 17-30.

Atkinson, G.M., C.B. Worden, and D.J. Wald (2014). Intensity prediction equations for North America, *Bull. Seismol. Soc. Am.* **104**, 3084-3093.

Bakun, W.H. (2006). MMI attenuation and historical earthquakes in the Basin and Range province of western North America, *Bull. Seismol. Soc. Am.* **96**, 2206-2220.

BSSC (Building Seismic Safety Council) (2004). NEHRP Recommended Provisions for Seismic Regulations for New Buildings and Other Structures, Part 1: Provisions (FEMA 450-1/2003 Edition). Building Seismic Safety Council, Washington, D.C

Boore, D. M., J.P. Stewart, E. Seyhan, and G.M. Atkinson (2013). NGA-West2 Equations for Predicting Response Spectral Accelerations for Shallow Crustal Earthquakes, PEER Report No. 2013/05, Pacific Earthquake Engineering Research Center, University of California, Berkeley, CA.

Boore, D.M., J.P. Stewart, E. Seyhan, and G.M. Atkinson (2014). NGA-west2 Equations for predicting PGA, PGV and 5% Damped PSA for Shallow Crustal Earthquakes, *Earthq. Spectra*, **30**, 1057-1085.

Casado, C.L., S.M. Palacios, J. Delgado, and J.A. Peláez (2000). Attenuation of intensity with epicentral distance in the Iberian Peninsula, *Bull. Seismol. Soc. Am.* **90**, 34-47.

CEA (China Earthquake Administration) (1990). Introduction to the intensity hazard map of China. Seismological press, Beijing, China.

Chandler, A.M., and N. Lam (2002). Intensity attenuation relationship for the South China Region and comparison with the component attenuation model, *Journal of Earth Sciences*, **20**(7), 775-790.

Chandra, U. (1979). Attenuation of intensities in the United States, *Bull. Seismol. Soc. Am.* **69**, 2003-2024.

Chávez, M., and R. Castro (1988). Attenuation of modified Mercalli intensity with distance in Mexico, *Bull. Seismol. Soc. Am.* **78**, 1875-1884.

Chen, D.S., and X.H. Liu (1989). Elliptical attenuation relationship of earthquake intensity, *North China earthquake sciences*, **17**(3), 31-42. (in Chinese)

Cornell, C.A. (1968). Engineering seismic risk analysis, *Bull. Seismol. Soc. Am.* **58**, 1583-1606.

Douglas J. (2007). On the regional dependence of earthquake response spectra, *ISET Journal of Earthquake Technology*. **44**(1), 71-99.

Dowrick, D.J., and D.A. Rhoades (2005). Revised models for attenuation of Modified Mercalli intensity in New Zealand earthquakes, *Bulletin of the New Zealand Society for Earthquake Engineering*, **38**(4), 185-214.

Ekström. G, and A.M. Dziewonski (1988) Evidence of bias in estimation of earthquake size, *Nature*, **332**, 319-324.

Esteva, L. (1968). Bases para la formulación de decisiones de diseño sísmico, Ph.D's thesis, Instituto de Ingeniería, Universidad Nacional Autónoma de México. (In Spanish)

Frankel, A. (1995). Mapping seismic hazard in the central and eastern United State, *Seismol. Res. Lett.*, **66**, 8-21.

Gao M.T., X.J. Li, X.W. Xu, K.B. Wei, Y.X. Yu, B.G. Zhou, F.X. Zhao, H. Pan, Y.J. Lv, Q. Zhou, J. Wu, D.W. Lu, K. Chen, Y.X. Li and Z.W. Gao (2015). GB18306-2015:

Introduction to the seismic hazard map of China. Standards press of China, Beijing, China. (in Chinese).

GB50011-2010. 2010. Code for seismic design of buildings, Ministry of Housing and Urban-Rural Development of the People's Republic of China (MOHURD), Beijing, China.

Goda, K., and H.P. Hong (2006). Optimal seismic design considering risk attitude, societal tolerable risk level, and life quality criterion. *Journal of Structural Engineering*, **132**(12), 2027-2035.

Goda, K., H.P. Hong, and G.M. Atkinson (2010). Impact of using updated seismic information on seismic hazard in Western Canada, *Canadian Journal of Civil Engineering*, **37**, 562-575.

Hong, H.P., and K. Goda (2007). Orientation-dependent ground motion measure for seismic hazard assessment, *Bull. Seismol. Soc. Am.* **97**, 1525-1538.

Hong, H.P., K. Goda, and A.G. Davenport (2006). Seismic hazard analysis: a comparative study, *Canadian Journal of Civil Engineering*, **33**, 1156-1171.

Hong, H.P., A. Pozos-Estrada, and R. Gomez (2009) Orientation effect on ground motion measure for Mexican subduction earthquakes, *Earthquake Engineering and Engineering Vibration*, **8**(1), 1-16.

Howell, B. F., and T.R. Schultz (1975). Attenuation of modified Mercalli intensity with distance from the epicenter, *Bull. Seismol. Soc. Am.* **65**, 651-665.

Hu, Y. X., M. T. Gao, W. Du, Y. Jin, F.X. Zhao, Q.J. Zou, Y.L. Tao, and B.G. Zhou (2001) GB18306-2001: Introduction to China ground motion parameter zoning map. Standards press of China, Beijing, China. (in Chinese).

Hu, Y.X., and M.Z. Zhang, (1984). A method of predicting ground motion parameters for regions with poor ground motion data, *Earthquake Engineering and Engineering Vibration*, **4**(1), 1-11. (in Chinese)

Hu, Y.X., K.S. Zhou, and X.J. Yan (1996). A method for evaluation of ground motion in regions with few acceleration observation data, *Earthquake Engineering and Engineering Vibration*, **16**(3), 2-10. (in Chinese)

Huo, J.R., and Y.X. Hu (1992). Study on attenuation laws of ground motion parameters, *Earthquake Engineering and Engineering Vibration*, **12**(2), 1-11. (in Chinese)

Huo, J.R., Y.X. Hu, and Q.M. Feng (1992). Study on estimation of ground motion from seismic intensity, *Earthquake Engineering and Engineering Vibration*, **12**(3), 1-15. (in Chinese)

Kanamori, H. (1977). The energy release in great earthquakes, *Journal of Geophysical Research*, **82**(20), 2981-2987.

Lei, J.C., M.T. Gao, and Y.X. Yu (2007). Seismic motion attenuation relations in Sichuan and adjacent areas, *ACTA Seismologica Sinica*, **29**(5), 500-501, (in Chinese)

Liu, H.X. (1987). On the seismic zoning map China, Proceedings of International Seminar on Seismic Zonation, Guangzhou, China, pp. 35-42.

Liu, R.F., Y.T. Chen, P. Bormann, X. Ren, J.M. Hou, L.Y. Zou, and H. Yang (2006). Comparison between earthquake magnitudes determined by China seismograph network and U.S. seismograph network (II): surface wave magnitude, *ACTA Seismologica Sinica*, **28**(1), 1-7. (in Chinese)

Madsen, H.O., S. Krenk, and N.C. Lind (2006). Methods of structural safety. Courier Corporation.

Milne, W.G., and A.G. Davenport (1969). Distribution of earthquake risk in Canada, *Bull. Seismol. Soc. Am.* **59**, 729-754.

Pasolini, C., D. Albarello, A. D' Amico, and B. Lolli (2008). The Attenuation of Seismic Intensity in Italy, Part II: Modeling and Validation, *Bull. Seismol. Soc. Am.* **98**, 692-708.

- Power, M., Chiou, B., Abrahamson, N., Bozorgnia, Y., Shantz, T., and Roblee, C. (2008). An overview of the NGA project, *Earthq. Spectra*, **24**,3-21.
- Scherbaum, F., J. Schmedes, and F. Cotton (2004). On the conversion of source-to-site distance measures for extended earthquake source models, *Bull. Seismol. Soc. Am.* **94**, 1053-1069.
- Sørensen, M.B., D. Stromeyer, and G. Grünthal (2009). Attenuation of macroseismic intensity: A new relation for the Marmara Sea region, northwest Turkey, *Bull. Seismol. Soc. Am.* **99**, 538-553.
- Sørensen, M.B., D. Stromeyer, and G. Grünthal (2010). Intensity attenuation in the Campania region, Southern Italy, *Journal of Seismology*, **14**(2), 209-223.
- Tao, Z.R., X.X. Tao, and W.Q. Li (2014). Strong ground motion attenuation relationship for North China from small earthquake records by earthquake monitoring networks, *Earthquake Engineering and Engineering Dynamics*. **34** suppl, pp. 202-205. (in Chinese)
- Wang, S.Y., and H.Y. Wu (1988). Ground motion relationship for Lunan region, *Earthquake Research in China*, **4**(3), 182-186. (in Chinese)
- Wang, S.Y., Y.X. Yu, A.J. Gao, and X.J. Yan (2000). Development of attenuation relations for ground motion in China, *Earthquake Research in China*, **16**(2), 99-106. (in Chinese)
- Wang, Y.S., X.J. Li, and Z.H. Zhou (2013). Research on attenuation relationships for horizontal strong ground motions in Sichuan – Yunnan region, *ACTA Seismologica Sinica*, **35**(2), 238-249. (in Chinese)
- Wen, R., P. Xu, H. Wang, and Y. Ren (2018). Single - station standard deviation using strong - motion data from Sichuan region, China. *Bull. Seismol. Soc. Am.* **108**, 2237-2247.
- Yu, Y.X., and S.Y. Wang (2006). Attenuation relations for horizontal peak ground acceleration and response spectrum in Eastern and Western China, *Technology for Earthquake Disaster Prevention*. **1**(3), 206-217. (in Chinese)



Yu, Y.X., S.Y. Li, and L. Xiao (2013). Development of ground motion attenuation relations for the new seismic hazard map of China, *Technology for Earthquake Disaster Prevention*, **8**(1), 24-33. (in Chinese)

## Chapter 3

### 3 Seismic Hazard Assessment for Mainland China Based on Spatially Smoothed Seismicity

#### 3.1 Introduction

Results from probabilistic seismic hazard analysis (PSHA) are used as the basis for codified seismic design, seismic risk analysis, emergency preparedness, and disaster reduction. The essential information required to develop probabilistic seismic hazard maps includes the seismic source zones, the magnitude-recurrence relations and ground-motion models (i.e., attenuation relations). The popular probabilistic approach used to estimate seismic hazard is the one developed by Cornell (1968) and Esteva (1968) (see McGuire 2004). An example application of this approach to estimate seismic hazard at a site in Mexico City was presented in Liu et al. (2016), where such estimates are compared with those directly obtained by using ground motion records at the same site. Other available approaches include the ones presented by Milne and Davenport (1969), Liu (1987), Frankel (1995), and Woo (1996). The major differences between these approaches are the ways in which the historical seismicity is spatially smoothed to define the seismic source models and to characterize the magnitude-recurrence relations. A comparison of using three approaches with different degrees of smoothing to define the seismic source models to develop seismic hazard maps was presented in Hong et al. (2006) for regions in Canada.

The procedures proposed by Frankel (1995) and Woo (1996) leads to spatially smoothed seismic source representations. The main difference in these two procedures is how a historical earthquake catalogue is used in the kernel smoothing processes. In Frankel (1995), the cumulative event count is spatially smoothed and, a probabilistic model of magnitude-recurrence relation is assigned to the region. In Woo (1996), the occurrence rate of each event or a group of events within a magnitude bin in a catalogue is spatially smoothed, and the assignment of a magnitude-recurrence relation is not required. The application of the procedure to map seismic hazard for regions in different countries were presented by Molina et al. (2001), Beauval et al. (2006), Xu and Gao (2012), Goda et al. (2013), Zuccolo et al. (2013) and Xu (2019). The overall conclusion from these studies is

that the use of such a procedure to define the seismicity could lead to underestimation of seismic hazard. Xu and Gao (2012) applied several kernel smoothing techniques to obtain spatially smoothed seismic source assess, and estimated the seismic hazard in terms of peak ground acceleration (PGA) for some regions in the mainland China; their estimated seismic hazard compares favourably to that reported in a version of Chinese seismic hazard map obtained using the delineated source zone models.

The temporal coverage of the historical Chinese earthquake catalogue is relatively long as compared with that for other regions in the world. The historical catalogue is used to aid the assignment of the delineated seismic source zones. The approach based on the delineated source zones proposed was employed to map Chinese seismic hazard by considering a broad source zone with sufficient historical seismic events and localized seismic source areas that incorporate the geological and seismological information (Liu 1987). Following the same approach but with three-level delineation of the source zones, the fifth-generation Chinese seismic hazard map (CSHM) was developed; the general information on the seismicity and ground-motion models (GMMs) for long and short (or major and minor) axes used for mapping was described in GB18306-2015 (Gao et al. 2015). For the development, regions, subregions and delineated source zones were considered; hazard maps of PGA were developed but no attempt was made to develop hazard maps of spectral acceleration (SA) or uniform hazard spectrum (UHS).

Assessment of completeness of the Chinese earthquake catalogue was carried out by Huang et al. (1994), and Xu and Gao (2014). The assessment in Huang et al. (1994) was partly based on the changes of the slope in the G-R relation and of historical reporting characteristics. In Xu and Gao (2014), the aftershocks in the catalogue were removed using the approach proposed by Gardner and Knopoff (1974); the completeness of mainshocks was assessed using a statistical procedure (Albarello et al. 2001). It was concluded that the catalogue is complete since the 1970s for earthquakes with a magnitude greater than 4.0. The observation period of completeness for earthquakes with a magnitude greater than 5.0 varies from region to region.

The present chapter is focused on PSHA for mainland China. The main objectives of this chapter are to assess the completeness of the Chinese earthquake catalogue, evaluate the spatially distributed seismicity using two kernel smoothing techniques, estimate the seismic hazard for mainland China in terms of the PGA and SA, and develop UHS. For the completeness assessment, the method proposed by Albarello et al. (2001) is employed. The results of the k-means cluster analysis are used to aid the assignment of seismic regions and two kernel smoothing techniques are applied to obtain geographically distributed occurrence rate for each region. Both the maximum likelihood method (MLM) (Weichert 1980) and least-squares fitting are used to estimate the  $\beta$ -value (i.e.,  $b$ -value) of the G-R relation for unequal observation periods, where the least-squares fitting is carried out for the observation period adjusted occurrence rate. It appears such use of the least-squares fitting has not been explored previously. The seismicity models together with the two sets of adopted GMMs are used to map the seismic hazard and UHS for mainland China.

## 3.2 Completeness analysis of historical earthquake catalogue

### 3.2.1 Chinese historical earthquake catalogue

The historical Chinese earthquake catalogue used is obtained by merging two catalogues: the compiled catalogue by Gu et al. (1983) and the catalogue available from China earthquake data center (CEDC) (<http://data.earthquake.cn/>). The catalogue in Gu et al. (1983) contains 5160 destructive historical earthquake events that occurred from 1831 BC to 1969 AD. The epicenter location, occurrence time and magnitude of each event are reported in the catalogue. The magnitudes (considered as surface-wave magnitude) of the events are greater than or equal to 4.0.

The catalogue from CEDC is for the seismic events that occurred from 1970 to August 2017, and contains data for 32290 events. The occurrence time, epicentral location, focal depth, and magnitude for each event are provided. Different earthquake magnitude scales are used in the reporting, including the local magnitude  $M_L$ , body-wave magnitude  $M_b$

measured by using only P-waves, body-wave magnitude  $M_B$  measured by using the P- and S-waves, surface-wave magnitude  $M_s$ , and the surface-wave magnitude based on the record in the vertical direction  $M_{s7}$  (Liu et al. 2007; Bormann et al. 2007). In most cases,  $M_s$  is reported; the GMMs employed for the fifth-generation CSHM are based on  $M_s$  (Gao et al. 2015).

For an earthquake whose magnitude is not given in  $M_s$ , the following magnitude conversion equations are adopted for the numerical analysis to be carried out,

$$M_s = 0.932M_L + 0.295, \quad (3.1)$$

$$M_s = 1.01M_{s7} + 0.11, \quad (3.2)$$

and,

$$M_s = 1.33M_B - 2.07, \quad (3.3)$$

where,

$$M_B = 1.22M_b - 0.86. \quad (3.4)$$

Eq. (3.1) (Wang and Yu 2009) was based on the earthquake events reported by the Chinese seismological agency from 1990 to 2007. Eqs. (3.2) to (3.4) (Liu et al. 2007; Bormann et al. 2007) were based on earthquake events reported by CEDC from 1983 to 2004.

If  $M_s$  is not reported but  $M_L$  and any other magnitude scale are given for an event in the catalogue, Eq. (3.1) is used to convert  $M_L$  to  $M_s$  since this was considered to develop the fifth-generation CSHM (Gao et al. 2015). Eq. (3.2) is used if  $M_s$  and  $M_L$  are not available but  $M_{s7}$  and other magnitude scales are given. If  $M_s$ ,  $M_L$ , and  $M_{s7}$  are not provided, Eqs. (3.3) and (3.4) are employed to obtain  $M_s$ . In other words, when converting from other magnitudes to  $M_s$ , the preference is given to  $M_L$ ,  $M_{s7}$ ,  $M_B$ , and  $M_b$  in decreased order.

Since the development of the fifth-generation CSHM and several other studies (Huang et al. 1994; Xu and Gao 2014; Gao et al. 2015) considered that the Chinese earthquake

catalogue is reliable after 1500, only those events observed after 1500 are considered and processed below. A plot of the events in the catalogue with  $M_s \geq 4.0$ , including aftershocks, is shown in Figure 3.1a.

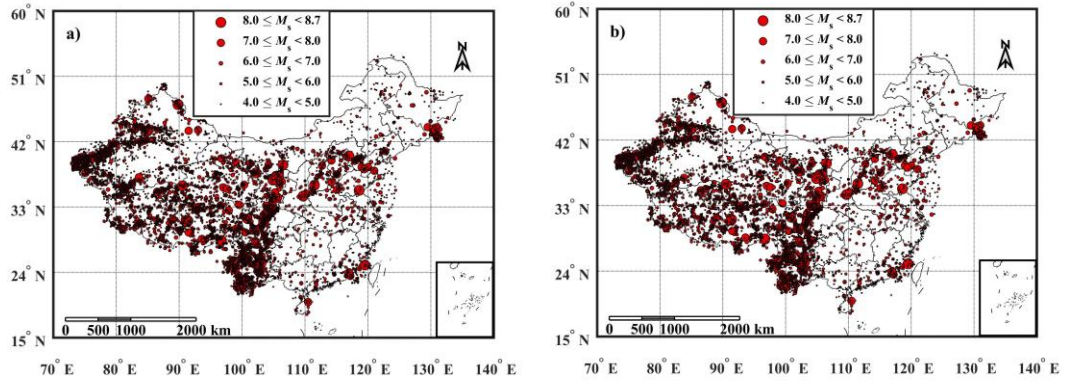


Figure 3.1. Earthquake events with  $M_s \geq 4.0$  in the catalogue and after 1500 AD: a) Including the aftershocks and b) Excluding aftershocks.

### 3.2.2 Removing aftershocks and completeness analysis of Chinese catalogue

The criteria and procedure proposed by Gardner and Knopoff (1974) are adopted to remove the aftershocks from the considered catalogue. Given the occurrence of a mainshock, the criteria consider that the events occurred within a time delay from the mainshock less than  $T_{AS}$  and with an epicentral distance from the epicenter of the mainshock less than  $R_{AS}$  are classified as aftershocks, where  $R_{AS}$  (km) is calculated using (Liu et al. 1996),

$$\log R_{AS} = 0.5M_s - 1.78, \quad (3.5)$$

and the values of  $T_{AS}$  are given in Table 3.1.

By applying the criteria to the considered catalogue, the location and magnitude of the events with aftershock removed are shown in Figure 3.1b. The spatial pattern shown in Figure 3.1b is very similar but not identical to that shown in Xu and Gao (2014) that was obtained for seismic events up to 2014. The Figure 3.1 also shows that the seismic

occurrences are geographically clustered.

To assess the completeness of the catalogue and seismicity, Xu and Gao (2014) assigned six seismic regions. In this chapter, two cases in assigning seismic regions, named Case I and Case II, are considered. Case I mimics the six regions assigned by Xu and Gao (2014) which is shown in Figure 3.2a.

Table 3.1.  $T_{AS}$  used to classify aftershocks (Gardner and Knopoff 1974).

$M_s$	$T_{AS}$ (days)	$M_s$	$T_{AS}$ (days)
3.5	22	6.0	510
4.0	42	6.5	790
4.5	83	7.0	915
5.0	155	7.5	960
5.5	290	8.0	985

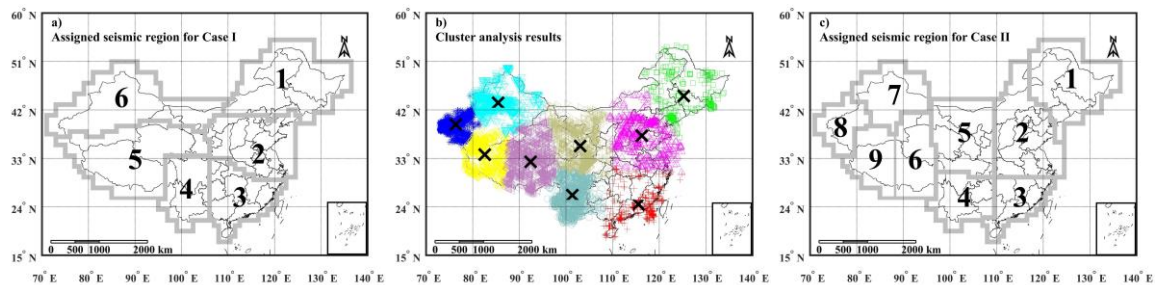


Figure 3.2. Cluster analysis results and assigned seismic regions: a) Case I – six seismic regions; b) Cluster analysis results by considering nine clusters; and c) Case II – assigned regions based on the results shown in b).

For Case II, the k-means cluster analysis (MacQueen 1967) for the catalogue with aftershocks removed is carried out to assign the regions. The number of clusters ranging from 4 to 10 is considered in the analysis and the results are given in Appendix B. Inspection of the analysis results indicates that the use of nine regions provides a reasonable spatial cluster classification as illustrated in Figure 3.2b, where X marks the center of the cluster. Consequently, the identified clusters are used as a guide to assign the regions as shown in Figure 3.2c. The consideration of 9 regions is an attempt to reduce the inhomogeneity of geographically varying seismicity within each region.

Since a seismic catalogue that has unequal observation periods for different earthquake magnitude intervals affects the estimation of the magnitude recurrence relations (Weichert 1980), an analysis of the catalogue completeness needs to be carried out. Consider that the catalogue is reported up to a most recent time  $T_F$ , and the earliest time when an event is reported is  $T_I$ . The completeness analysis of the catalogue for events with magnitude greater than  $M_{\text{sm},j}$  after the time  $T_{C,j}$  is to be carried out for  $j = 1, \dots, N_C$ , where  $N_C$  is the total number of lowest magnitude cases considered for completeness analysis, and  $T_{C,j} \in [T_I, T_F)$ . For a given  $M_{\text{sm},j}$ , the procedure given by Albarello et al. (2001) requires that  $\Delta T_{C,j} = T_F - T_{C,j}$  is to be divided into  $2N$  elementary non-overlapping subintervals of equal duration  $\delta t$  ( $\delta t = \Delta T_{C,j} / (2N)$ ), and that a comparison of the earthquake occurrence rates in the  $i$ -th and  $(N+i)$ -th intervals, denoted as  $\lambda_i$  and  $\lambda_{N+i}$ , is carried out. The procedure assumes that a complete and representative catalogue exhibits similar statistical properties in its first and second halves. The probability of completeness of the catalogue for a given value of  $T_{C,j}$  (i.e., within the specific time span  $\Delta T_{C,j}$ ),  $P_j(C|T_{C,j})$ , is given by,

$$P_j(C|T_{C,j}) = \frac{\Delta T_{C,j}}{\phi \Delta T_{\text{max}}} \times (0.5)^{N'} \times \sum_{k=m}^{N'} \frac{N'}{k!(N'-k)!}. \quad (3.6)$$

In Eq. (3.6),  $\Delta T_{\text{max}} = T_F - T_I$ ;  $\phi$  is a constant equal to or greater than 1;  $N'$  denotes the total number of cases where  $\lambda_i \neq \lambda_{N+i}$  for  $i = 1, \dots, N$ ;  $m$  represents the observed number of cases where  $\lambda_i < \lambda_{N+i}$ ; and the sum represents the probability of observing  $m$  or more cases with  $\lambda_i < \lambda_{N+i}$ . In writing Eq. (3.6), it is assumed that the probability that the catalogue within  $\Delta T_{C,j}$  is statistically representative or captures the basic relevant seismogenic process is directly proportional to  $\Delta T_{C,j} / \Delta T_{\text{max}}$ . An estimate of  $p$ -quantile of  $T_{C,j}$ ,  $t_{C,j,K_p}$ , is obtained by solving,

$$\sum_{k=1}^{K_p} P_j^*(C|t_{C,j,k}) = p, \quad K_p \in [1, N_{j,K}] \quad (3.7)$$

where



$$P_j^*(C|t_{C,j,k}) = P_j(C|t_{C,j,k}) / \sum_{k=1}^{N_{j,K}} P_j(C|t_{C,j,k}); \quad (3.8)$$

in which  $N_{j,K}$  is the total number of likely values of  $T_{C,j}$ ,  $t_{C,j,k}$ , considered; and  $p$  is the non-exceedance probability. The 0.5-quantile of  $T_{C,j}$ ,  $t_{C,j,K_{0.5}}$ , is considered as the point estimate of  $T_{C,j}$ . The inter-quantile range,  $|t_{C,j,K_{0.25}} - t_{C,j,K_{0.75}}|$ , is used as a measure of the uncertainty in  $T_{C,j}$ . It is further considered that  $T_{C,j} > T_{C,k}$  for  $M_{\text{min},j} < M_{\text{min},k}$ .

No additional guideline to select  $N$  or  $\delta t$  was given in Albarello et al. (2001). By considering a range of  $N$  values, it was found that  $N = 1$  is preferred for the analysis of events with  $M_s < 4.75$ , and  $N = 60$  is preferred for the events with  $M_s \geq 4.75$ . Using these values of  $N$  and the procedure given by Albarello et al. (2001), the completeness analysis is carried out for each identified region shown in Figures 3.2a and 3.2c. The obtained  $p$ -quantiles of  $T_{C,j}$  for each region is shown in Figure 3.3 for  $p = 0.25, 0.5$  and  $0.75$ . The results indicate that the uncertainty in  $T_{C,j}$  is small for  $M_{\text{min},j}$  below 4.5 and its value is consistent for different regions whether Case I or Case II is considered. As  $M_{\text{min},j}$  increases the deviation of the values  $t_{C,j,K_{0.25}}$  and  $t_{C,j,K_{0.75}}$  from  $t_{C,j,K_{0.50}}$  increases. This suggests that there is significant uncertainty in the time after which the earthquake catalogue for events with  $M_s \geq 5.0$  is complete.

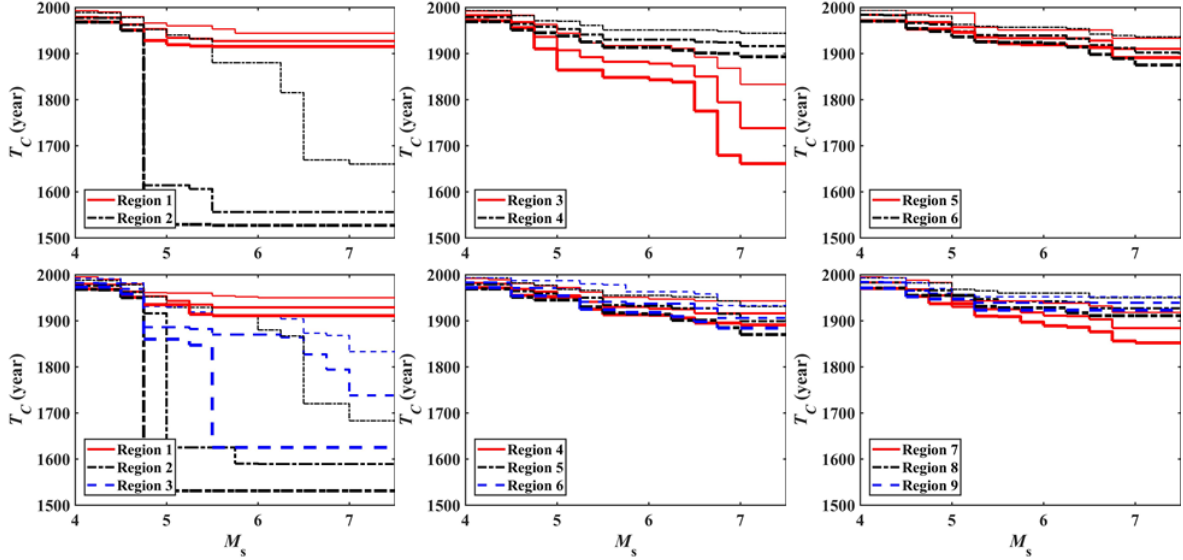


Figure 3.3. Identified  $t_{C,j,K_{0.25}}$ ,  $t_{C,j,K_{0.50}}$  and  $t_{C,j,K_{0.75}}$  (The plots shown in the first and second rows are for Case I and Case II, respectively. For each set of curves, the upper, middle and lower curves represent  $t_{C,j,K_{0.25}}$ ,  $t_{C,j,K_{0.50}}$  and  $t_{C,j,K_{0.75}}$ , respectively.)

In the following,  $t_{C,j,K_{0.50}}$  is employed in the seismic hazard assessment for the reference case. This is based on the suggestion given by Albarello et al. (2001) and that a preliminary analysis by varying  $p$  from 0.25 to 0.75 indicates that the estimated seismic hazard is not very sensitive to the selected  $p$  value. It is noteworthy that by adopting this criterion several large historical events are not considered. This includes the events located at (34.5°N, 109.7°E) near Xi'an with magnitude  $M_s = 8.0$  in 1556, and the event located at (20.0°N, 110.5°E) near Haikou (Hainan island) with  $M_s = 7.5$  occurred in 1605.

### 3.2.3 Estimating magnitude-recurrence relation for a region

The unequal observation periods for different earthquake magnitudes need to be considered to estimate the  $\beta$ -value (Weichert 1980) in the G-R relation with upper and lower bounds, denoted as  $M_{smax}$  and  $M_{smin}$ ,

$$n_i(M_s) = n_i(M_{smin}) \frac{\exp(-\beta_i M_s) - \exp(-\beta_i M_{smax})}{\exp(-\beta_i M_{smin}) - \exp(-\beta_i M_{smax})} \quad (3.9)$$

or

$$\lambda_i(M_s) = \lambda_i(M_{smin}) \frac{\exp(-\beta_i M_s) - \exp(-\beta_i M_{smax})}{\exp(-\beta_i M_{smin}) - \exp(-\beta_i M_{smax})} \quad (3.10)$$

where  $n_i(M_s)$  is the cumulative event count,  $\lambda_i(M_{smin})$  is the annual occurrence rate with magnitude greater than  $M_{smin}$ , the subscript  $i$  indicates that the estimated parameters are for the  $i$ -th region or cell. The estimates of  $\beta_i$  and  $\lambda_i(M_{smin})$ ,  $\hat{\beta}_i$  and  $\hat{\lambda}_i(M_{smin})$ , by using MLM (Weichert 1980) are obtained by solving,

$$\left( \sum_{j=1}^n \tau_j m_j e^{-\hat{\beta}_i m_j} \right) / \left( \sum_{j=1}^n \tau_j e^{-\hat{\beta}_i m_j} \right) - \left( \sum_{j=1}^n k_j m_j \right) / K_i = 0, \quad (3.11)$$

and,

$$\hat{\lambda}_i(M_{smin}) = K_i \left( \sum_{j=1}^n e^{-\hat{\beta}_i m_j} \right) / \left( \sum_{j=1}^n \tau_j e^{-\hat{\beta}_i m_j} \right) \quad (3.12)$$

where  $n$  is the number of magnitude intervals (or bins),  $m_j$  is the representative magnitude of the  $j$ -th magnitude interval defined by  $I_{mj}$ , (e.g.,  $I_{mj} = (m_j - \Delta m/2, m_j + \Delta m/2]$ ), and  $\Delta m = (M_{smax} - M_{smin})/n$ ;  $\tau_j$  and  $k_j$  represent the observation period for and number of observed events in the  $j$ -th magnitude bin respectively; and  $K_i = \sum_{j=1}^n k_j$ . If  $K_i$  is sufficiently large,  $\beta_i$

can be approximated by a normal variate with a variance,  $\hat{\sigma}_{\beta_i}^2$ , given by,

$$\hat{\sigma}_{\beta_i}^2 = \frac{1}{K_i} \left[ \left( \sum_{j=1}^n \tau_j e^{-\hat{\beta}_i m_j} \right)^2 / \left( \left( \sum_{j=1}^n \tau_j e^{-\hat{\beta}_i m_j} \right) \left( \sum_{j=1}^n \tau_j m_j^2 e^{-\hat{\beta}_i m_j} \right) - \left( \sum_{j=1}^n \tau_j m_j e^{-\hat{\beta}_i m_j} \right)^2 \right) \right]. \quad (3.13)$$

The variance of  $\lambda_i(M_{smin})$  equals  $\hat{\lambda}_i(M_{smin}) / K_i$ .

The obtained estimates of  $\beta_i$  and  $\lambda_i(M_{smin})$ , referred to as  $\beta$ -MLM, are shown in Table 3.2 for  $M_{smin} = 4.75$  by considering the identified regions shown in Figure 3.2 with the bin width of the magnitude ( $\Delta m$ ) equal to 0.25. This consideration is justified since the seismic hazard at a site is most likely dominated by events with  $M_s \geq 4.75$ . Table 3.2 indicates that

$\hat{\beta}_i$  varies from 0.83 to 2.05 for Case I and from 0.78 to 1.87 for Case II, and the standard deviation of  $\beta_i$  varies from 0.063 to 0.225 for Case I and from 0.071 to 0.241 for Case II.  $\hat{\lambda}_i(M_{smin})$  for each region shown in the Table 3.2 ranges from about 0.40 to 9.62. This large variation agrees with the spatial pattern of historical seismic events shown in Figure 3.1b.

Table 3.2. Estimated model parameters based on  $M_{smin} = 4.75$  for the magnitude-recurrence relation ( $\text{Var}(\cdot)$  represents the variance of its argument).

Case	Region	MLM				LSF		
		$\beta_i$	$\text{Var}(\beta_i)$	$\lambda_i(M_{smin})$	$\text{Var}(\lambda_i)$	$\beta_i$	$\lambda_i(M_{smin})$	$M_{smax}$
I	1	0.83	0.029	0.83	0.004	0.85	0.80	7.6
	2	1.26	0.008	0.72	0.001	1.14	0.62	8.6
	3	2.05	0.051	0.66	0.002	1.92	0.57	8
	4	1.41	0.004	5.92	0.004	1.45	5.78	8.7
	5	1.67	0.004	9.62	0.004	1.70	9.04	8.5
	6	1.86	0.007	6.04	0.003	1.73	5.12	8.5
II	1	0.78	0.028	0.85	0.004	0.75	0.80	7.6
	2	1.38	0.011	0.59	0.001	1.21	0.48	8.6
	3	1.82	0.058	0.40	0.002	1.71	0.35	8
	4	1.46	0.005	5.11	0.005	1.56	5.19	8.7
	5	1.46	0.008	3.31	0.004	1.32	2.86	8.6
	6	1.76	0.009	4.58	0.005	1.83	4.51	8.5
	7	1.79	0.016	2.16	0.003	1.63	1.81	8.5
	8	1.87	0.014	4.00	0.003	1.79	3.47	8.5
	9	1.59	0.015	2.91	0.004	1.56	2.59	8.5

Plots of the fitted and empirical magnitude-recurrence relation are shown in Figure 3.4. For the plot,  $M_{smax}$  is considered as the maximum of a) the overall maximum magnitude for the seismic source regions suggested by Gao et al. (2015) and b) the observed maximum magnitude for the historical earthquake catalogue plus a tolerance of 0.1. The use of that given in Gao et al. (2015) is justified since it is used to assess the fifth-generation CSHM. The consideration of tolerance is to ensure that there is a non-zero probability of occurrence of the observed maximum earthquake magnitude. It is acknowledged that the assignment of the maximum magnitude could be subjective and affect the estimated

seismic hazard (Rosenblueth and Ordaz 1990). The consideration of the uncertainty in the maximum magnitude on the estimated seismic hazard is beyond the scope of the present chapter.

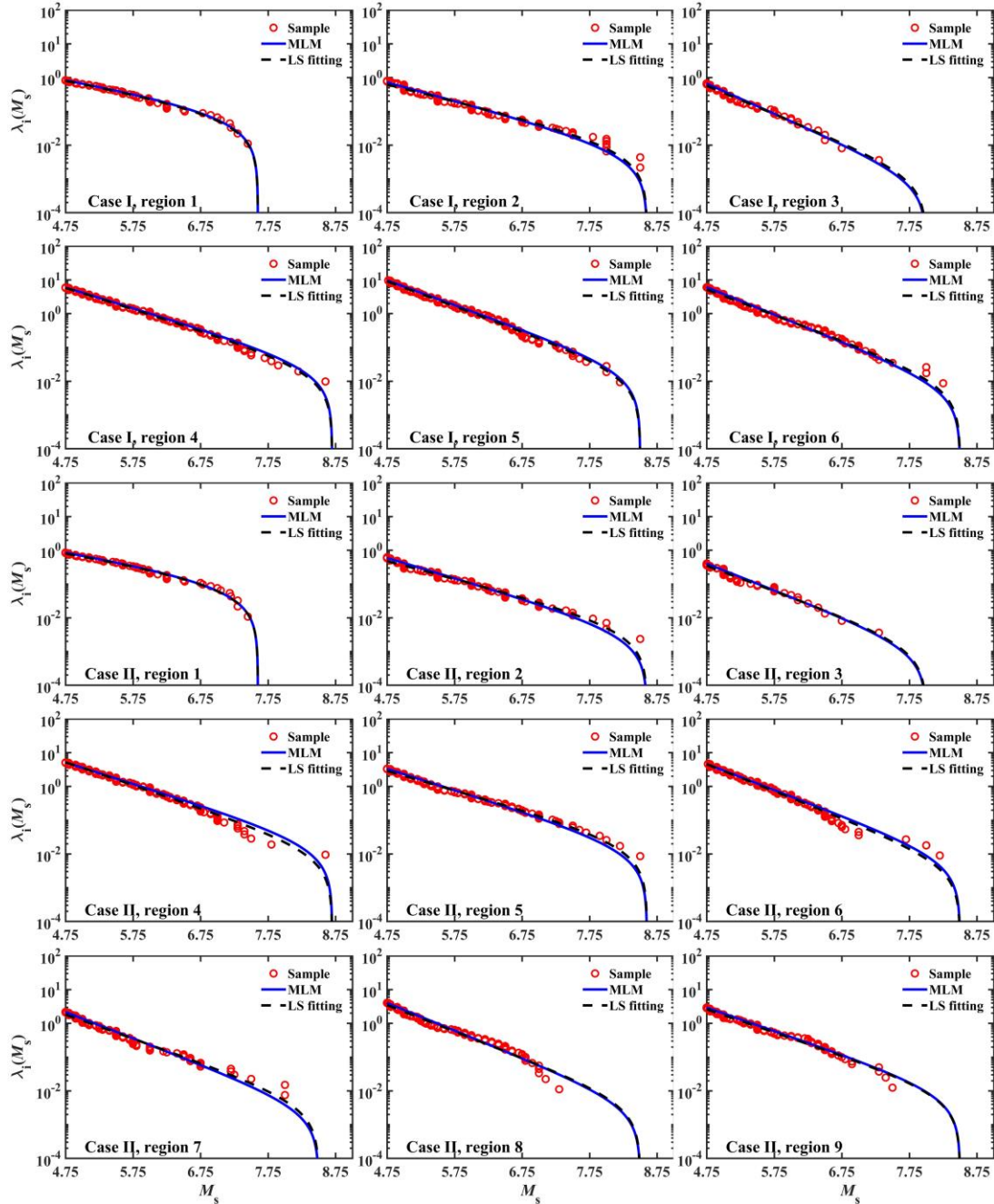


Figure 3.4. The magnitude -recurrence relation for different regions and different cases.

The plots depicted in Figure 3.4 indicate that the fitted relation follows well the empirical

relation that is calculated using,

$$\lambda_i(M_s) = \sum_{j=1}^{n_E} I(M_{sj} > M_s) / \Delta T_j \quad (3.14)$$

where  $n_E$  is the total number of observed seismic events in a region with the magnitude of the  $j$ -th event denoted as  $M_{sj}$ ,  $I(M_{sj} > M)$  is an indicator function and equals 1 and 0 if  $M_{sj} > M_s$  and  $M_{sj} \leq M_s$ , respectively, and  $\Delta T_j$  is the effective observation time period which is considered equal to  $\Delta T_{C,j} = T_F - T_{C,j}$  (see Figure 3.3 for  $T_{C,j}$ ). This is partly due to the nature of a greater number of small magnitude events.

For a comparison purpose, the least-squares fitting (LSF) to the adjusted occurrence rate calculated according to Eq. (3.14) is also carried out by using the model shown in Eq. (3.10). The obtained model parameters, denoted as  $\beta$ -LSF, are shown in Table 3.2 and the fitted relations are plotted in Figure 3.4 as well. The values of the model parameters obtained based on LSF differ slightly from those obtained by using MLM but the fitted curves obtained by the LSF and MLM are almost identical as shown in Figure 3.4. The Figure 3.4 shows that the fitted curves for Region 6 in Case I and for Region 6 and 7 in Case II underestimates the empirical occurrence rates slightly and that the underestimation is even less severe for Region 1 in Case I and Regions 1, 2 and 5 in Case II.

### 3.3 Seismic hazard mapping for mainland China

#### 3.3.1 Spatial smoothing of earthquake occurrence

Consider that the historical earthquake catalogue for a region containing  $n_E$  earthquakes with location and magnitude denoted as  $(s_j, M_{sj}), j = 1, \dots, n_E$ . Two smoothing techniques are considered to obtain spatially smoothed source models in this section. The first one used is the Gaussian kernel smoothing (Frankel 1995). The region of interest is covered by a regular square grid and the cumulative event count with magnitude greater than or equal to  $M_{\text{min}}$  within the  $k$ -th cell,  $n_k(M_{\text{min}})$ ,  $k = 1, \dots, n_C$ , is obtained, where  $n_C$  is the total number of cells. The application of Gaussian kernel smoothing technique to  $n_k(M_{\text{min}})$

over the region results in,

$$\tilde{n}_k(M_{\text{smin}}) = \frac{1}{\sum_{i=1}^{n_c} \exp(-r_{ik}^2 / c^2)} \sum_{i=1}^{n_c} n_i(M_{\text{smin}}) \times \exp(-r_{ik}^2 / c^2), \quad (3.15)$$

where  $\tilde{n}_k(M_{\text{smin}})$  is the number of events with magnitude greater than or equal to  $M_{\text{smin}}$  in the  $i$ -th cell after smoothing,  $r_{ik}$  denotes the distance between the  $i$ -th and the  $k$ -th cells, and  $c$  is bandwidth parameter. For this chapter,  $c$  is determined by using R (R Development Core Team 2014) for each considered region. For simplicity, this procedure is referred to as nS ( $n_k(M_{\text{smin}})$  smoothing) in the following. The seismicity is then defined by the smoothed  $\tilde{n}_k(M_{\text{smin}})$  for each cell within a region, and the  $\beta$ -value for magnitude-recurrence relation applicable to the region.

The second smoothing technique considered is the one proposed by Woo (1996) – which is referred to as  $\lambda$ S. The epicenter of each seismic event in the catalogue is smoothed spatially using a kernel function, capturing spatial clustering of earthquake epicenters. Several kernel functions could be considered for the smoothing (Woo 1996), and the one suggested by Vere-Jones (1992) that is preferred by several studies (Molina et al. 2001; Beauval et al. 2006; Xu and Gao 2012; Goda et al. 2013; Zuccolo et al. 2013),  $K(M_{s_j}, s - s_j)$ , is expressed as,

$$K(M_{s_j}, s - s_j) = \frac{\alpha - 1}{\pi [H(M_{s_j})]^2} \left[ 1 + \frac{|s - s_j|^2}{(H(M_{s_j}))^2} \right]^{-\alpha}, \quad (3.16)$$

where  $M_{s_j}$  is the earthquake magnitude for the  $j$ -th event;  $s$  denotes a point of interest;  $\alpha$  is the parameter controlling the degree of smoothing ranging from 1.5 to 2.0; and the bandwidth parameter reflecting the degree of smoothing,  $H(M_{s_j})$ , is defined by,

$$H(M_{s_j}) = b_1 \exp(b_2 M_{s_j}), \quad (3.17)$$

in which  $b_1$  and  $b_2$  are model parameters. As the choice of  $\alpha$  has a negligible influence on seismic hazard mapping (Beauval et al. 2006) and  $\alpha = 1.8$  (Xu and Gao 2012) is employed below.

The earthquake occurrence rate at the  $k$ -th grid cell,  $\lambda_{c,k}(M_s)$  (per year for the  $k$ -th cell), with its center defined by  $s_k$  is calculated using,

$$\lambda_{c,k}(M_s) = \sum_{j=1}^{n_E} I(M_{s_j} > M_s) \times K(M_{s_j}, s_k - s_j) / \Delta T_j, \quad (3.18)$$

There is no need to estimate  $\beta$ -value in  $\lambda S$  as one can directly use the empirical magnitude-recurrence relation shown in Eq. (3.18) for each cell. Since the average return period of a potentially extremely large earthquake in a zone could be greater than the observation period of the considered earthquake catalogue, the use of  $\lambda S$  could lead to the estimated seismic hazard lower than that obtained based on the delineated source zone models. This underestimation was observed in Molina et al. (2001), Beauval et al. (2006) and Goda et al. (2013). To reduce such a potential underestimation, a modification to  $\lambda S$ , is employed throughout this chapter. The modification considers that an upper bound  $M_{smax}$ , which is greater than or equal to the observed maximum magnitude for a cell or a region, is imposed and the occurrence rate model defined by Eq. (3.18) is to be extended or extrapolated to  $\lambda_{c,k}(M_{smax}) = 0$ . The assigned  $M_{smax}$  values based on Gao et al. (2015) are site-dependent and are the same as those shown in Table 3.2.

### 3.3.2 Spatial smoothing results

Before carrying out spatial smoothing using  $nS$ , it is noted that a complete historical catalogue for events with magnitude greater than  $M_{smin}$  is required. If a very small  $M_{smin}$ , say 4, is selected,  $T_{Cj}$  is very near present (i.e.,  $\Delta T_{C,j}$  is very small) and the historical catalogue to be used is likely to have a poor temporal coverage for events with large magnitude. If a very large  $M_{smin}$ , say 6, is selected,  $\Delta T_{C,j}$  can be adequate but the influence of events with  $M_s < M_{smin}$  on the seismic hazard is neglected. In addition, the event with  $M_s = 4.75$  is considered to be the lowest earthquake magnitude event that can cause damage to



engineered structures (Gao et al. 2015). Therefore,  $M_{\text{smin}} = 4.75$  is used for the numerical analysis in the following.

By adopting  $M_{\text{smin}} = 4.75$  and using nS, the optimal bandwidth parameter  $c$  for each region can be determined by carrying out cross-validation analysis (Wand and Jones 1994; Silverman 2018). Using these optimal values of  $c$ , the obtained  $\tilde{n}_k(M_{\text{smin}})$  for a grid system with  $0.5^\circ \times 0.5^\circ$  cells are shown in Figures 3.5a and 3.5b for Case I and Case II, respectively. As expected, the smoothed cumulative event count is spatially varying and mimics the spatial trends observed from historical seismic events shown in Figure 3.1b. A comparison of the results presented in Figures 3.5a and 3.5b indicates that the smoothness by using six regions is more extended than that by using nine regions shown in Figure 3.2. The difference in  $\tilde{n}_k(M_{\text{smin}})$  is most pronounced for Regions 4 and 8 shown in Figure 3.2c.  $\tilde{n}_k(M_{\text{smin}})$  shown in Figure 3.5 and, the estimated  $\beta_i$  and  $\lambda_i(M_{\text{smin}})$  shown in Table 3.2 that define the seismic source models are to be used in the next section to carry out seismic hazard assessment.

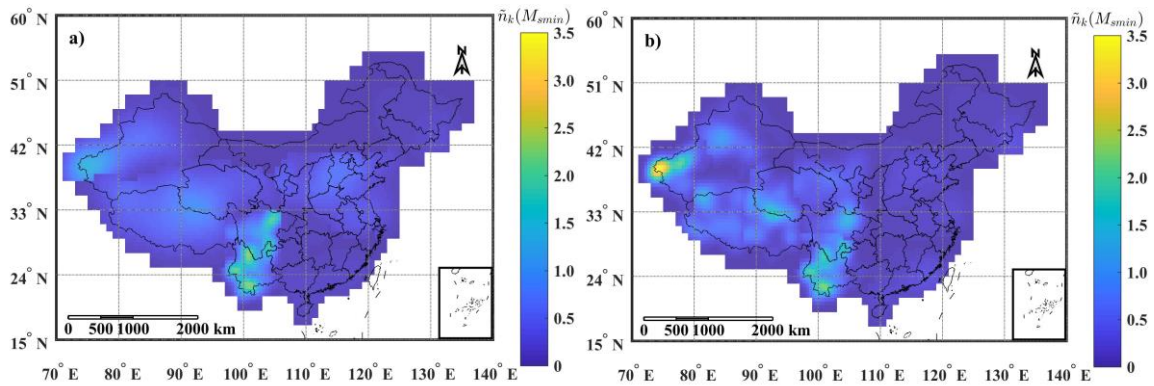


Figure 3.5. Smoothed cumulative event count (The left plot is for Case I – nS (based on six regions shown in Figure 3.2a), b) Case II – nS (based on nine regions shown in Figure 3.2c).

To apply  $\lambda$ S,  $M_{\text{smin}} = 4$  is adopted. Unlike the use of nS approach, the use of  $M_{\text{smin}} = 4$  in  $\lambda$ S approach does not limit the consideration of relative old historical seismic events with larger magnitudes. First, the parameters of the bandwidth function  $H(M_s)$  shown in Eq.

(3.17) need to be estimated. This is done by grouping the seismic event in magnitude bins with bin width of 0.25, evaluating the shortest distance  $H$  ( $H = H(M_s)$ ) between events within each bin and the representative magnitude  $M_s$  of each bin, and carrying out regression analysis between  $H$  and  $M_s$  for all bins to estimate values of  $b_1$  and  $b_2$  (Molina et al. 2001). The fitted Eq. (3.17) for each region is shown in Figure 3.6. Instead of using the shortest distance between events within each of the bins, Zuccolo et al. (2013) used the average of minimum distance for all the earthquake events in the bin, while Goda et al. (2013) used the magnitude of the  $j$ -th event and its minimum distance to an event within the bin for the fitting, where  $j$  varies from 1 to the total number of events within the bin. By using the criteria suggested by Zuccolo et al. (2013) and by Goda et al. (2013), the fitting exercise is carried out with the results shown in Figure 3.6 as well. It is observed from the Figure 3.6 that the number of samples that can be used for the fitting by using the criteria suggested by Molina et al. (2001) and by Zuccolo et al. (2013) is much smaller than that obtained by using the criterion suggested by Goda et al. (2013). A comparison of the fitted curves indicates that in general the fitted curve by using the criterion suggested by Goda et al. (2013) is between those obtained by using the criteria suggested by Molina et al. (2001) and Zuccolo et al. (2013). The model parameters obtained for the former is adopted for the seismic hazard assessment.

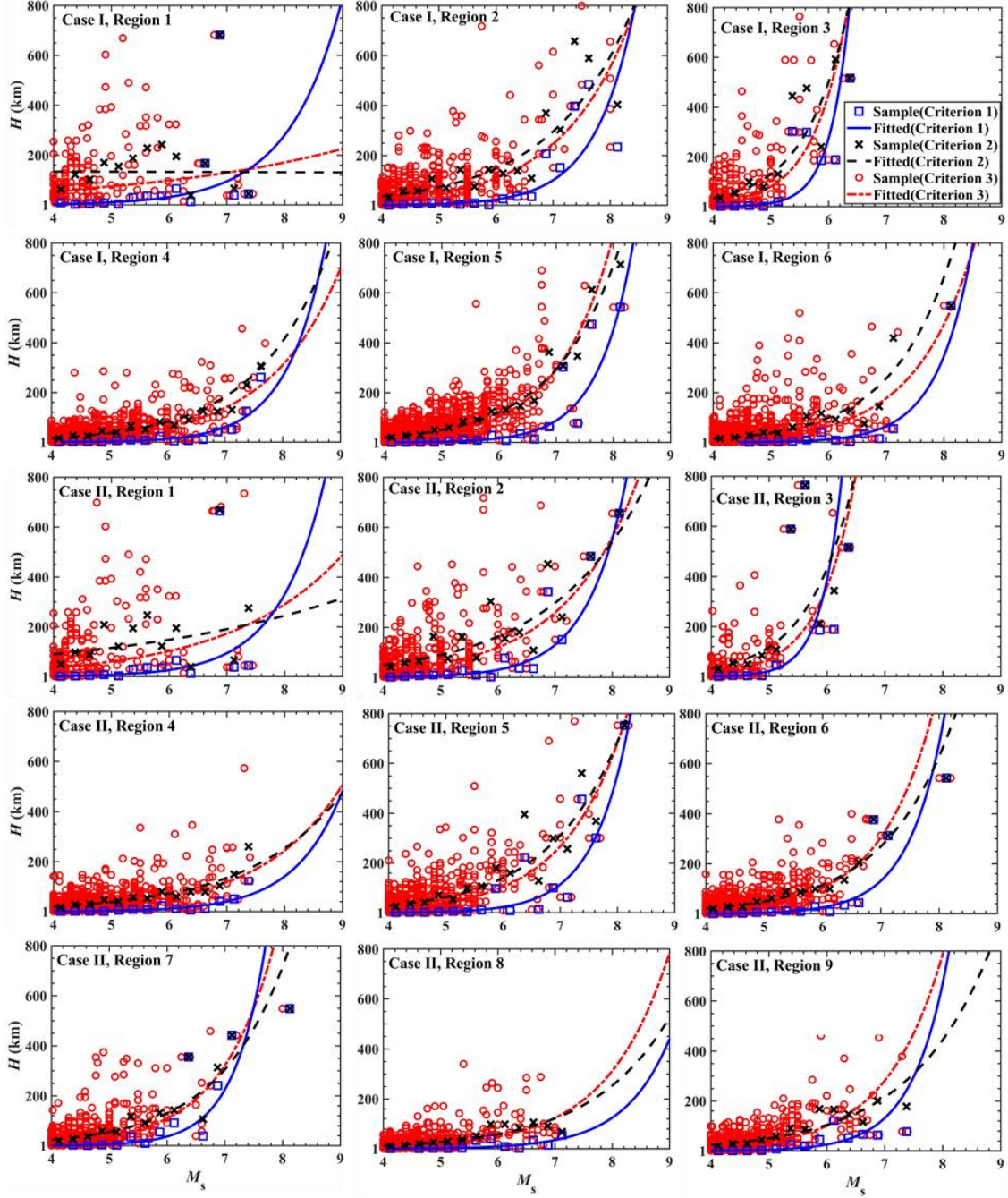
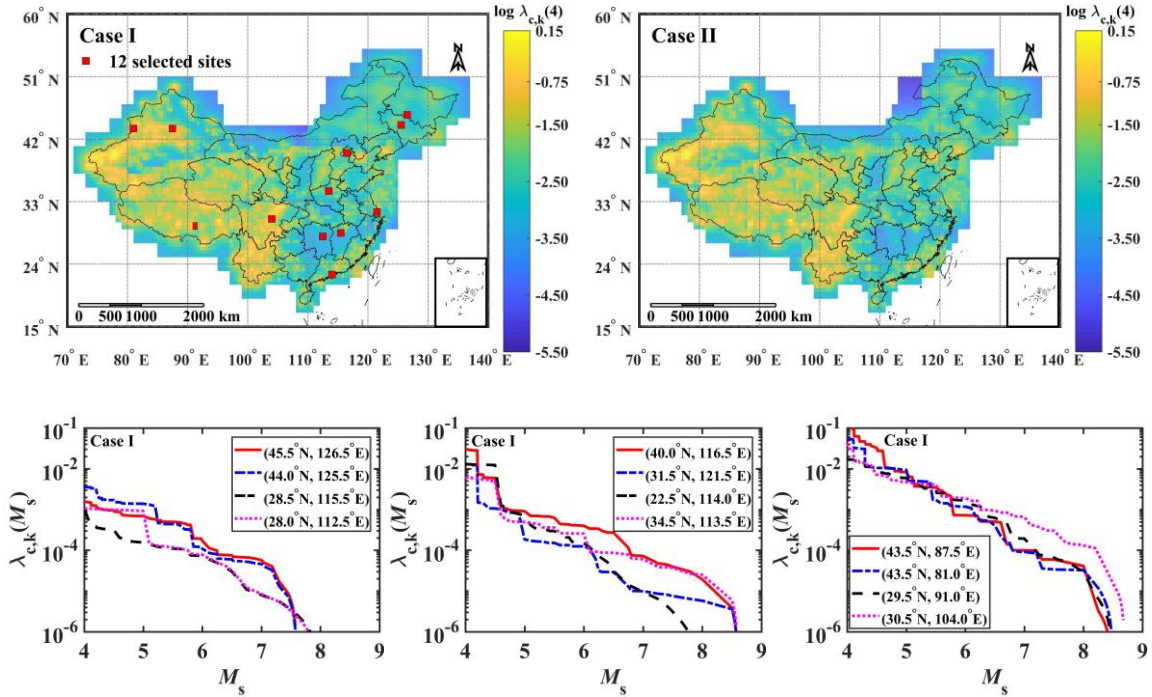


Figure 3.6. Fitted bandwidth function for Eq. (3.17) (Criteria 1, 2 and 3 shown in the plots refer to the criteria suggested by Molina et al. (2001), Zuccolo et al. (2013) and Goda et al. (2013), respectively).

By using the adopted model parameter and  $\lambda S$ , the spatial smoothing of the occurrence rate is carried out. The obtained  $\lambda_{c,k}(M_{s\min} = 4)$  is illustrated in the first row of the plots in

Figure 3.7 for Cases I and II. Also, the estimated  $\lambda_{c,k}(M_s)$  values for Cases I and II are presented in the Figure 3.7 for 12 selected sites, each located near the center of a city listed in Table 3.3 - the discussion of the estimated PGA values shown in the table 3.3 is deferred to the subsequent sections. The trends of the obtained  $\lambda_{c,k}(M_{s_{\min}} = 4)$  shown in the first row of Figure 3.7 are very similar for Cases I and II. A comparison of  $\lambda_{c,k}(M_s)$  values shown in the second and third rows in the Figure 3.7 indicates that  $\lambda_{c,k}(M_s)$  at a location is similar for Cases I and II, except when  $M_s$  is near  $M_{s_{\max}}$ . This can be explained by noting that a location may be classified in regions with different  $M_{s_{\max}}$  for Cases I and II. For the extrapolation of  $\lambda_{c,k}(M_s)$  from the maximum observed  $M_s$ ,  $M_{s_{\text{obs}}}$ , to the imposed  $M_{s_{\max}}$ , the model shown in Eq. (3.10) is used at each site but hinged at  $\lambda_{c,k}(M_{s_{\text{obs}}})$  with  $\beta$  estimated through regression analysis considering the occurrence rate such as those shown in Figure 3.7.



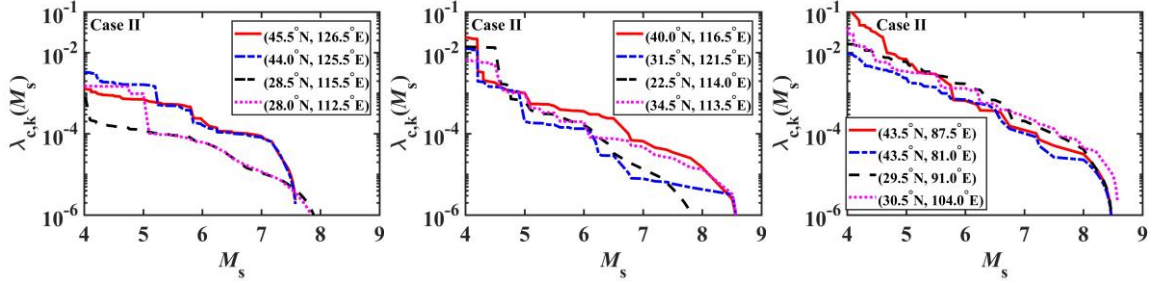


Figure 3.7. Spatially smoothed magnitude-recurrence relations using  $\lambda_S$  approach. Row 1 shows the estimated  $\lambda_{c,k}(M_{s_{\min}} = 4)$  for Case I and Case II. Rows 2 and 3 show  $\lambda_{c,k}(M_s)$  for twelve sites. Row 2 is for Case I and Row 3 is for Case II.

Table 3.3. Location of the selected twelve sites and the estimated PGA (g). For the estimated PGA, the first and second entries correspond to Case C1 = (Case I, nS,  $\beta$ -LSF and BSSA14-P) and Case C2 = (Case II,  $\lambda_S$  and BSSA14-P), respectively.

Location		Estimated return period value of PGA			GB18306 (Gao et al. 2015), for $P_E = 10\%$
Lat., Long.	City	$P_E = 63\%$	$P_E = 10\%$	$P_E = 2\%$	
45.5°N, 126.5°E	Harbin	0.04, 0.03	0.12, 0.10	0.24, 0.21	0.10
44.0°N, 125.5°E	Changchun	0.03, 0.04	0.11, 0.14	0.23, 0.28	0.10
28.5°N, 115.5°E	Nanchang	0.01, 0.02	0.06, 0.06	0.13, 0.12	0.05
28.0°N, 112.5°E	Changsha	0.01, 0.01	0.06, 0.08	0.15, 0.19	0.05
40.0°N, 116.5°E	Beijing	0.05, 0.06	0.18, 0.20	0.35, 0.35	0.20
31.5°N, 121.5°E	Shanghai	0.02, 0.04	0.11, 0.14	0.24, 0.28	0.10
22.5°N, 114.0°E	Shenzhen	0.02, 0.04	0.10, 0.18	0.22, 0.33	0.10
34.5°N, 113.5°E	Zhengzhou	0.04, 0.04	0.15, 0.15	0.30, 0.31	0.15
43.5°N, 87.5°E	Urumuqi	0.07, 0.05	0.23, 0.34	0.44, 0.55	0.20
43.5°N, 81.0°E	Yining	0.07, 0.07	0.27, 0.21	0.47, 0.38	0.20
29.5°N, 91.0°E	Lhasa	0.09, 0.08	0.24, 0.27	0.45, 0.48	0.20
30.5°N, 104.0°E	Chengdu	0.08, 0.10	0.35, 0.29	0.60, 0.51	0.10

## 3.4 Seismic hazard mapping

### 3.4.1 Ground-motion models

Two sets of GMMs are considered. The first set of GMMs for PGA is based on the geometric mean of the GMMs given by Yu et al. (2013) for long and short axes (i.e., along with and perpendicular to the fault line), which are used to develop the fifth-generation

CSHM. The GMMs, referred to as YLX13-G, for the four regions named in Table 3.4 and identified in the first plot in Figure 3.8 are expressed as,

$$\log Y = c_1 + c_2 M_s + c_3 M_s^2 + c_4 \log(R_{\text{epi}} + c_5 \exp(c_6 M_s)) + \varepsilon_Y, \quad (3.20)$$

where  $Y$  denotes PGA ( $\text{cm/s}^2$ ) or peak ground velocity ( $\text{cm/s}$ ;  $c_i, i = 1, \dots, 6$ , are the model coefficients with values shown in Table 3.4 for four regions denoted as ER, MR, XR, and TR; and  $\varepsilon_Y$  is the residual with zero mean and the standard deviation  $\sigma_{Y\varepsilon}$  of 0.236. Note that the constant  $\sigma_{Y\varepsilon}$  of 0.236 for different regions was suggested by Yu et al. (2013). They indicated that their GMMs is applicable for  $M_s$  up to 7.0 for MR.

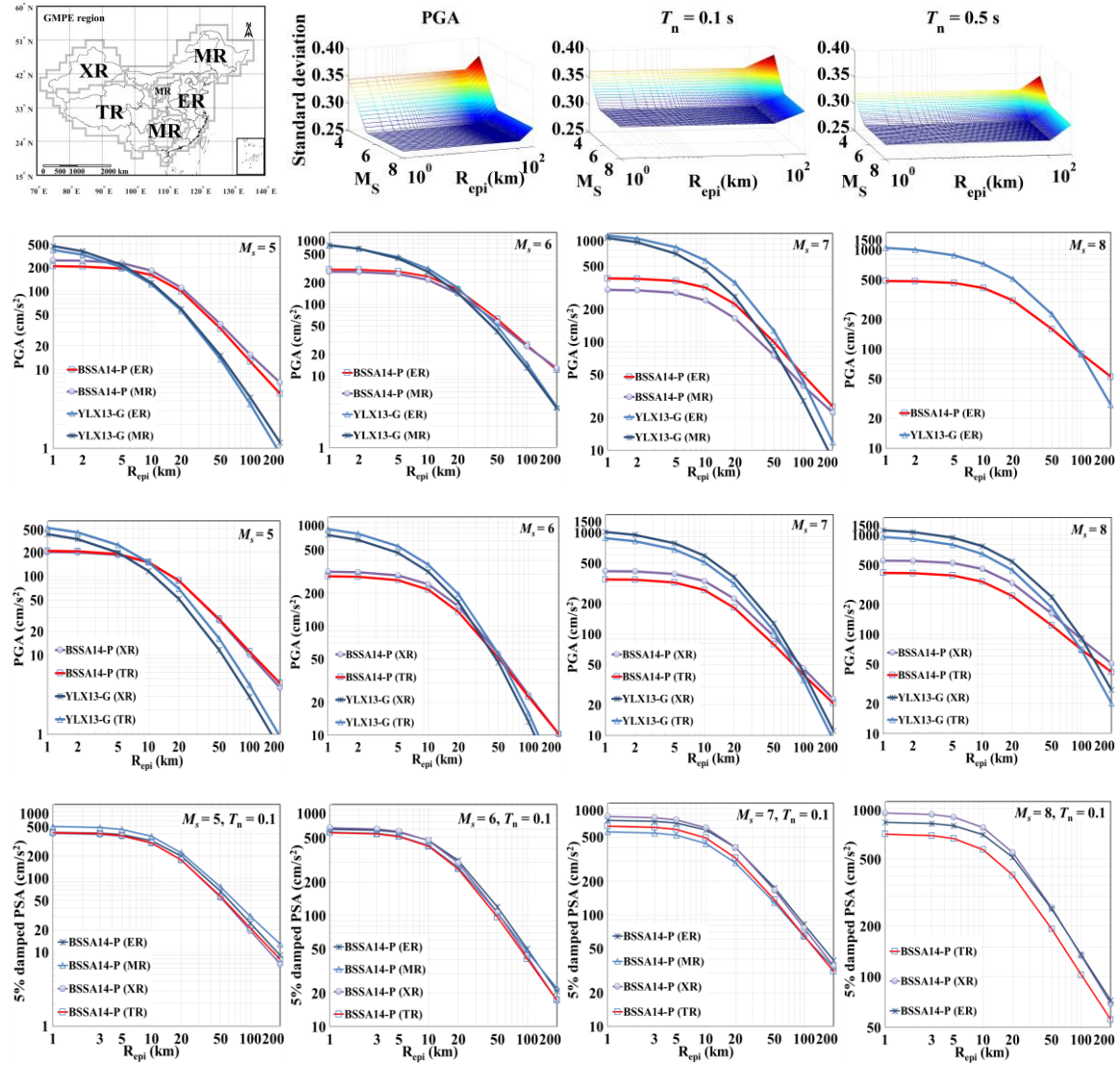
Table 3.4. GMMs for PGA for a random orientation estimated based on the geometric mean of the GMMs for long and short axes given in Yu et al. (2013) ( $c_3 = 0$ ).

Region	Parameter	$c_1$	$c_2$	$c_4$	$c_5$	$c_6$
Eastern seismic region (ER)	< 6.5	1.578	0.666	-2.160	1.516	0.423
	$\geq 6.5$	3.143	0.425	-2.160	1.516	0.423
Median seismic region (MR)	< 6.5	2.066	0.485	-1.901	2.049	0.313
	$\geq 6.5$	3.198	0.310	-1.901	2.049	0.313
Xinjiang seismic region (XR)	< 6.5	1.387	0.717	-2.254	1.299	0.445
	$\geq 6.5$	3.007	0.468	-2.254	1.299	0.445
Tibet seismic region (TR)	< 6.5	1.695	0.627	-2.135	1.630	0.412
	$\geq 6.5$	3.132	0.400	-2.135	1.630	0.412

The second set was developed in Hong and Feng (2019) based on the GMMs for PGA and SA given by Boore et al. (2014) (referred to as BSSA14) as the reference GMMs and applying the projection method (Hu and Zhang 1984) which was used to obtain the GMMs for mapping the fourth and fifth-generation CSHM (Hu et al. 2001; Yu et al. 2013; Gao et al. 2015). The projected GMMs in Hong and Feng (2019) is referred to as BSSA14-P in the following.

An illustration of the predicted PGA or SA by using YLX13-G and BSSA14-P as well as the standard deviation (i.e., sigma) for BSSA14-P is shown in Figure 3.8. The sigma values for BSSA14-P shown in the Figure 3.8 are to be multiplied by 0.91, 0.81, 0.93 and 1.04 to be used for ER, MR, XR, and TR. The results presented in the Figure 3.8 indicates

that the sigma values of the residuals for BSSA14-P are generally greater than the sigma associated with YLX13-G. The Figure 3.8 also shows that there are differences in the median of the predicted ground motion measures by the two sets of GMMs.



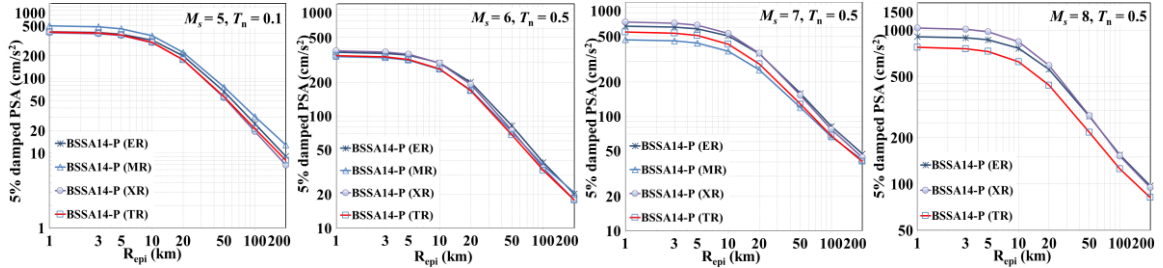


Figure 3.8. Comparison of the predicted ground motion measures by using YLX13-G and BSSA14-P for different regions (See Table 3.4). The sigma shown in the first row is for  $\log(\text{PGA})$  or  $\log(\text{SA})$  associated with BSSA14-P.

### 3.4.2 Hazard maps for PGA, SA and uniform hazard spectra

#### 3.4.2.1 Hazard maps for PGA

For the hazard mapping, combinations of spatial smoothed source model (Case I – nS, Case II –  $\lambda$ S shown in Figure 3.5), magnitude-recurrence relations ( $\beta$ -MLM,  $\beta$ -LSF shown in Table 3.2), and GMMs (YLX13-G, BSSA14-P), as well as the combinations of spatial smoothed source model (Case I –  $\lambda$ S, Case II –  $\lambda$ S shown in Figure 3.7) and GMMs (YLX13-G, BSSA14-P), are considered. By applying the simulation procedure for seismic hazard assessment (Hong et al. 2006), the seismic hazard is mapped for mainland China in terms of PGA by considering each of the mentioned combinations. For a few selected combinations, the maps are shown in Figures 3.9 and 3.10 for the exceedance probability,  $P_E$ , equal to 63%, 10% and 2% in 50 years (i.e., return period = 50, 475 and 2475 years). The results shown in Figure 3.9 are for the seismicity obtained based on nS, while the results depicted in Figure 3.10 are for the seismicity obtained based on  $\lambda$ S. For two selected combinations, C1 = (Case I, nS,  $\beta$ -LSF and BSSA14-P) presented in Row 2 in Figure 3.9, and C2 = (Case II,  $\lambda$ S and BSSA14-P) presented in Row 3 in Figure 3.10, the estimated PGA for 12 selected sites listed in Table 3.3 are also presented in the same table. Note that the estimated PGA for  $P_E = 10\%$  in 50 years corresponding to the fifth-generation Chinese seismic hazard map are tabulated in GB18306 (Gao et al. 2015). These tabulated values for the 12 sites listed in Table 3.3 are also included in the same table for comparison purposes.



From the results shown in Figures 3.9 and 3.10 and Table 3.3 for given combinations of the seismicity model and GMMs, it can be observed that:

- 1) Given a combination of seismicity model and GMMs, the spatial trends of the hazard are consistent for different exceedance probability (i.e., comparison of the plots within each row in Figures 3.9 and 3.10). On average, the ratio of the 2475-year to 475-year return period values of PGA is about 2; the ratio of the 2475-year to 50-year return period values of PGA is about 8. This can also be observed by using the reported return period values shown in Table 3.3 for the 12 selected sites. In all cases, the scatter of the ratio is very large. The fact that the ratio varies from site to site indicates that the coefficient of variation of PGA differs at different locations.
- 2) For the twelve selected sites shown in Figure 3.7, it is found that the estimated PGA based on C1 and C2 given in Table 3.3 are comparable for each other. It is found that the estimated PGA based on C2 is larger than that for C1, except for Harbin, Nanchang, Yining and Chengdu. This is attributed to the difference between magnitude-recurrence relations obtained by using  $nS$  and  $\lambda S$  approaches.
- 3) The estimated PGA values are consistent with or greater than those given by GB18306 (Gao et al. 2015) for  $P_E = 10\%$ . The estimated PGA values for Changchun, Changsha, Shanghai, Shenzhen, Urumqi, Lhasa, and Chengdu (especially, considering C1) are noticeably greater than the values given by GB18306 (Gao et al. 2015) which are obtained based on delineated seismic source zone and using GMMs with long and short axes. The observed difference can be attributed to the spatial smoothing of events with large magnitude and using GMMs for random orientation.
- 4) No concentrated seismic hazard near Haikou in Hainan island is shown in Figures 3.9 and 3.10. This differs from the fifth-generation Chinese seismic hazard map and can be explained by noting that a very concentrated seismic source near Haikou was adopted in Gao et al. (2015). Again, this is attributed to the differences between the assigned source models.

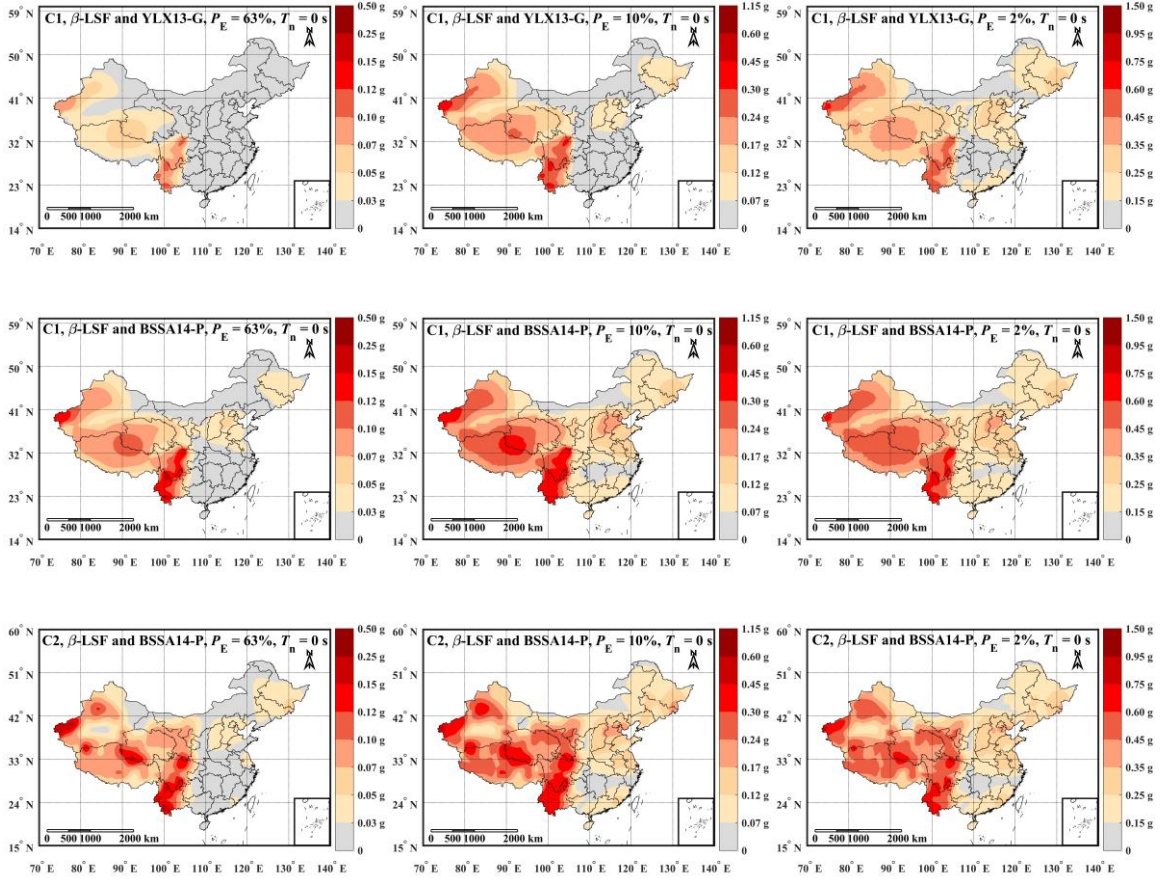
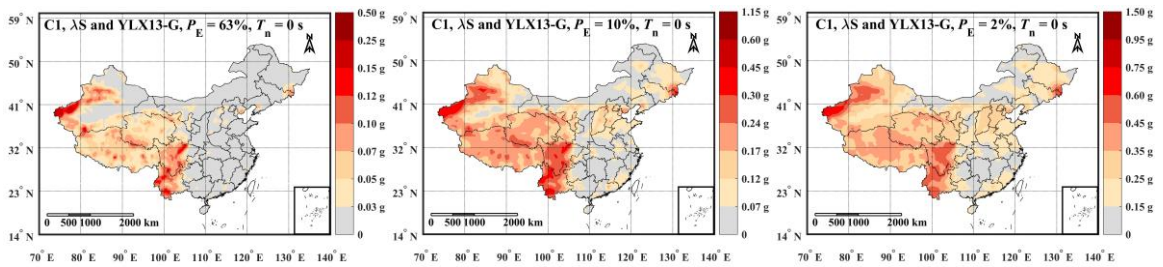


Figure 3.9. Estimated PGA by using  $nS$  for smoothing. : Row 1 for Case I,  $\beta$ -LSF and YLX13-G; Row 2 for Case I,  $\beta$ -LSF and BSSA14-P; and Row 3 for Case II,  $\beta$ -LSF and BSSA14-P. Columns 1 to 3 are for  $P_E = 63\%$ ,  $10\%$  and  $2\%$  in 50 years.



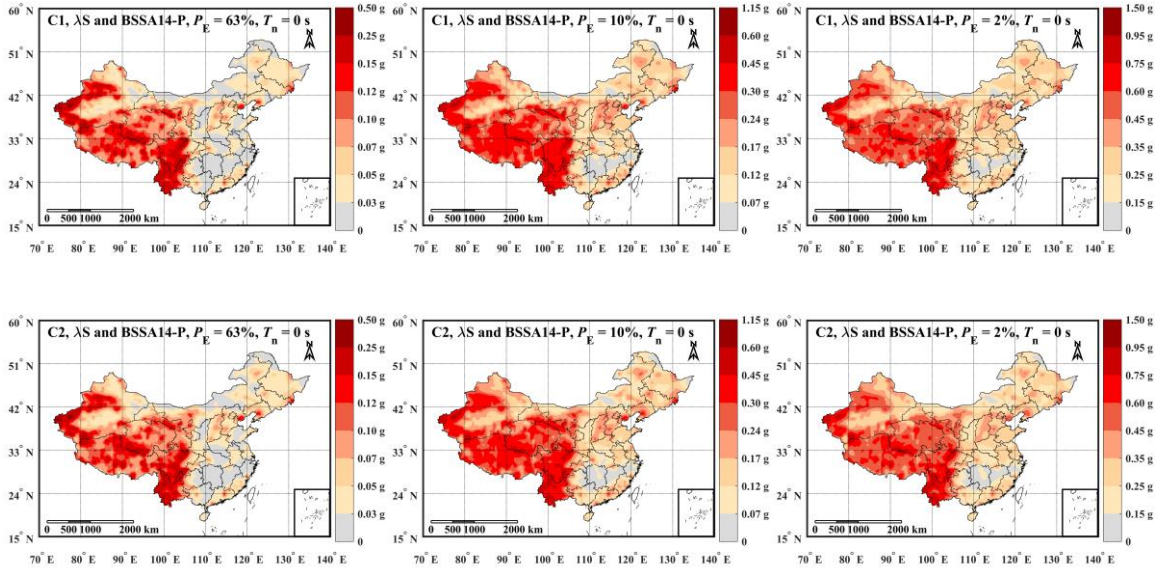


Figure 3.10. Estimated PGA using  $\lambda S$  for spatial smoothing. : Row 1 for Case I,  $\lambda S$  and YLX13-G; Row 2 for Case I,  $\lambda S$  and BSSA14-P; and Row 3 for Case II,  $\lambda S$  and BSSA14-P. Columns 1 to 3 are for  $P_E = 63\%$ ,  $10\%$  and  $2\%$  in 50 years.

- 5) A comparison of the results shown in Rows 1 and 2 in Figure 3.9 or in Figure 3.10 indicates that the use of YLX13-G leads to unconservative hazard estimates as compared to that obtained by using BSSA14-P. The values shown in Row 1 are, on average, about 36% to 80% of those of Row 2, depending on  $P_E$ . This is due to the differences in the sigma values and medians of the considered two sets of GMMs as shown in Figure 3.8.
- 6) Comparison of the results presented in Rows 2 and 3 indicates that the consideration of six regions versus nine regions (i.e., Case I and Case II) influences the estimated hazard. On average, the estimates by considering six regions lead to an increase of about 6% as compared to those by considering nine regions. The use of nine regions leads to a shaper spatially varying hazard with localized patches of significant hazard.
- 7) Comparison of the results shown in Figures 3.9 and 3.10 for the corresponding combinations but with different smoothing techniques indicates that the spatial trends of the estimated hazard are relatively consistent, although details vary. On average, the ratio between the results shown in Figure 3.9 to the corresponding results shown in

Figure 3.10 ranges from 0.78 to 0.92. The ratio increases as  $P_E$  increases, which can be explained by noting that  $M_{\text{min}}$  for nS equals 4.75 while that for  $\lambda S$  equals 4.0. Compared to nS, the use of  $\lambda S$  tends to provide a closer representation of the spatial distribution of the historical seismic hazard since it leads to less spatial smoothing.

### 3.4.2.2 Hazard maps for SA and uniform hazard spectra

Although each of the combinations of the spatial occurrence model, the magnitude-recurrence relation and a set of GMMs described in the previous section may be used as the basis to evaluate the seismic hazard, a slightly conservative estimate of seismic hazard is preferred for most engineering applications. Furthermore, it is desirable that the assessed seismic hazard reflects adequately the one that can be obtained based on historical observations and they should provide sufficient spatial details. Based on these considerations and to simplify the parametric analysis, only two combinations of the spatial seismic occurrence model, magnitude-recurrence relation, and a set of GMMs, defined as C1 and C2 in the previous section, are considered in this section to estimate the hazard in terms of SA and the UHS. Note that the estimated PSA for these two combinations are already presented in Figures 3.9 and 3.10, and Table 3.3 for 12 selected sites. The consideration of these two combinations with BSSA14-P instead of YLX13-G to assess SA is justified since YLX13-G can only be used to predict PGA.

The estimated hazard maps by using the simulation procedure (Hong et al. 2006) and the two combinations are shown in Figure 3.11 for three selected vibration period  $T_n$  values and a damping ratio of 5%. The results presented in Figure 3.11 indicates that:

- 1) For a given combination, the spatial trends of SA at a given  $T_n$  (i.e., for each row) are relatively consistent for different  $P_E$ . The ratio of the 2475-year to 50-year return period values of SA differs at different  $T_n$ . Moreover, the estimated SA for C1, on average, is about 20% greater than that obtained by using C2; the ratio varies slightly with  $T_n$ .
- 2) For different  $T_n$  values, the spatial trends in localized areas differ. This is partly attributed to that the GMMs for four regions differ and that SA at different  $T_n$  is affected

differently by earthquake magnitude (see Figure 3.8). An overall impression from the plots shown in Figure 3.11 is that the spatial trends of the estimated SA are similar for C1 and C2, although the maps for C2 are associated with more spatial variations than for C1.

- 3) For a given site, SA value decreases from  $T_n = 0.2$  s to 2 s. This agrees with the trends of the design spectra given in GB50011 (2010).

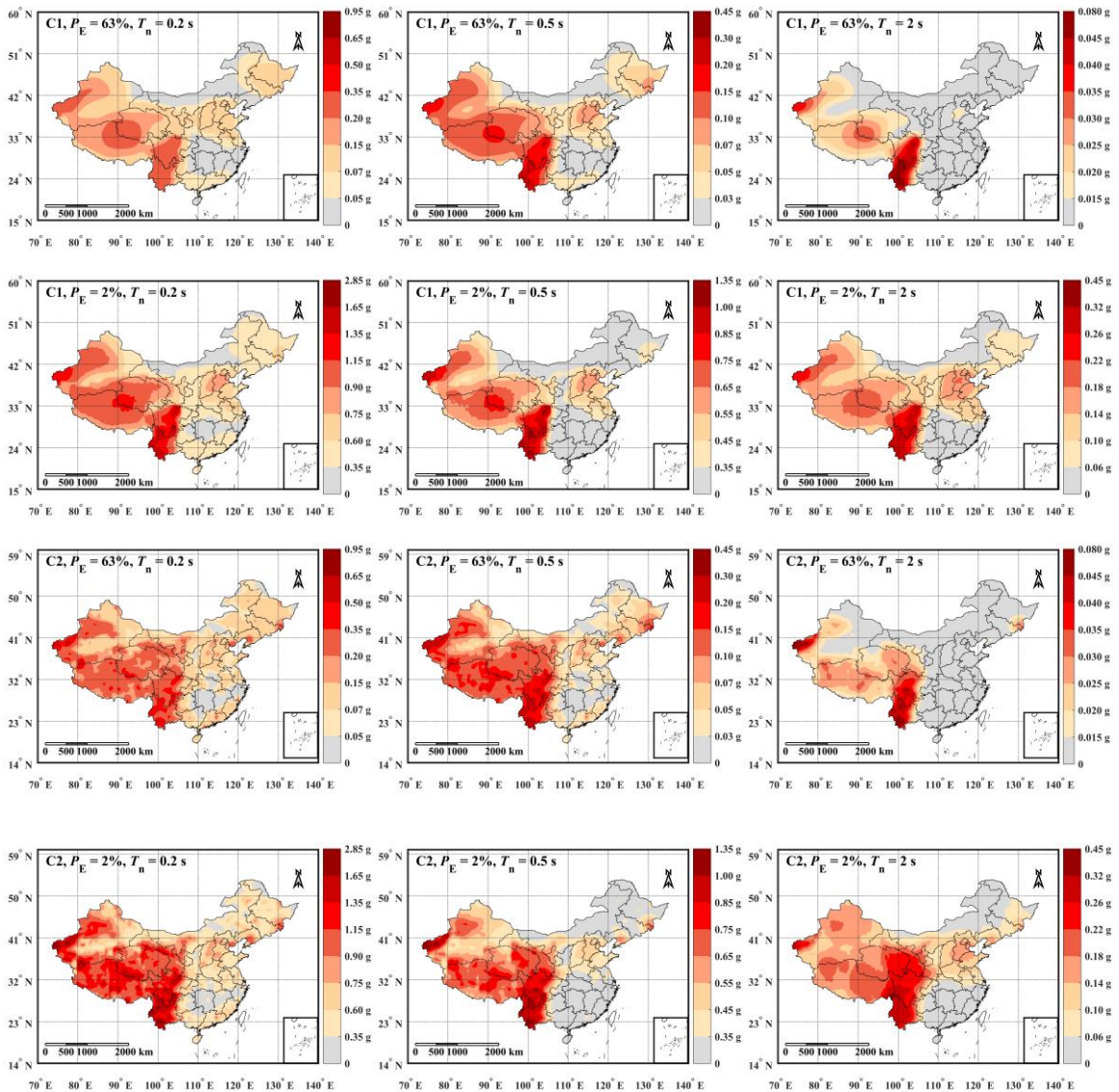
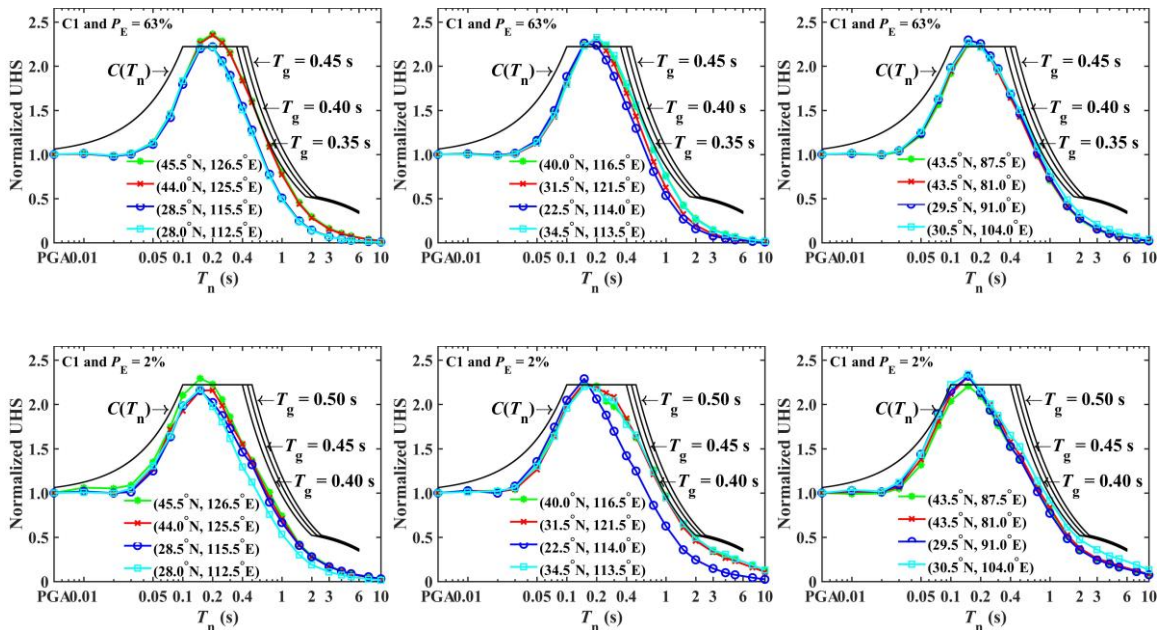


Figure 3.11. Estimated SA at  $T_n = 0.2, 0.5,$  and  $2$  s and damping ratio of 5% for different exceedance probability  $P_E$  in 50 years.

To see the shape of the UHS at different locations, the UHS for 12 sites considered in Figure 3.7 are evaluated and are shown in Figure 3.12 for C1 and C2. For comparison purposes, the normalized design spectrum recommended in GB50011 (2010),  $C(T_n)$ , is also presented in Figure 3.12. The results shown in the Figure 3.12 indicate that the normalized UHS are very similar for all considered sites whether  $P_E = 63\%$  or  $P_E = 2\%$  is considered. The normalized UHS for C1 closely resemble those for C2. This is partly due to that only BSSA14-P is used. In all cases, the code suggested design spectrum  $C(T_n)$  envelops the normalized UHS, except for  $T_n$  within 0.1 to 0.2 s. In other words, for  $T_n < 0.1$  s and  $T_n > 0.2$  s  $C(T_n)$  is conservative as compared to the normalized UHS. Since the ratio between  $C(T_n)$  and normalized UHS can be greater than 1.5 for  $T_n$  within 0.2 to 2 s, this conservatism can be important in setting the design SA for structures with relatively long vibration periods.



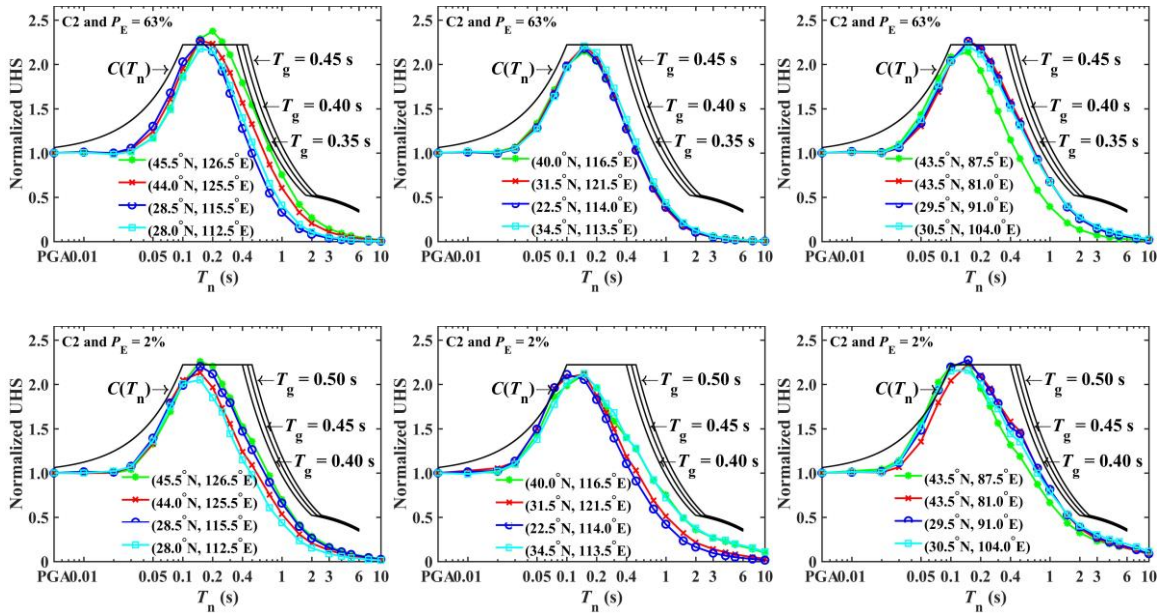


Figure 3.12. Plots of the obtained UHS normalized with its corresponding PGA (see Table 3.3).  $T_g$  is the characteristic period that depends on the site class as well as the site to source distance (GB50011 2010).

### 3.5 Conclusions

An assessment of seismic hazard for mainland China is carried out. The assessment starts with the historical earthquake catalogue and requires the assignment of regions in dealing with clustered earthquake occurrence. An application of the k-means cluster analysis is used to aid the assignment of the regions. The seismic occurrence rate model is obtained by applying one of the two spatial smoothing techniques: one smooths the cumulative event count ( $nS$ ), and the other smooths the earthquake magnitude dependent occurrence rate ( $\lambda S$ ). The use of the first one requires the estimation of parameters of the magnitude-recurrence model (i.e., G-R relation) for incomplete catalogue. Comparisons of the estimated parameters based on the maximum likelihood approach and least-squares fitting approach indicate that they lead to comparable G-R relations. It seems that the use of the least-squares approach in such a manner for incomplete catalogue has not been explored previously.

Probabilistic seismic hazard assessment was carried out by considering different combinations of the spatially smoothed source model, magnitude-recurrence relation, and GMM. The main observations that can be made include:

- 1) The use of the spatially smoothed source models provides competing and comparable seismic hazard maps to the fifth-generation CSHM that is developed based on delineated source models. The estimated return period values of PGA are consistent with or greater than that tabulated in GB18306 (e.g., see Table 3.3). For sites and regions where the seismic hazard given in the fifth-generation CSHM is lower than that estimated in this chapter, the assignment of the delineated source models should be further scrutinized.
- 2) Since the spatial smoothing requires the assessment of completeness of earthquake catalogue, some of the historical events with large magnitude may be removed in assessing the seismic hazard, it is suggested that an effort needs to be made in a future to incorporate the uncertainty in completeness assessment to estimate seismic hazard.
- 3) The application of  $nS$  and  $\lambda S$  (i.e., smoothing the cumulative event count and smoothing the occurrence rate) may result in a slightly different estimated return period value of seismic hazard. This is due to that  $nS$  approach requires the use of the fitted magnitude-recurrence relations while the  $\lambda S$  approach essentially uses empirical occurrence rate.
- 4) For a set of the adopted source model, the magnitude-recurrence relation and GMMs, the spatial trends of  $SA$  at a given  $T_n$  (i.e., for each row) are relatively consistent for different  $P_E$ , although for a localized area this may not be the case. The  $SA$  value attains its maximum value at the vibration period  $T_n$  near 0.2 s; the  $SA$  decreases as  $T_n$  increases for  $T_n$  greater than about 0.2 s. This agrees with the trends of the design spectrum given in GB50011 (2010).
- 5) The normalized design spectrum recommended in GB50011 (2010) envelops the normalized UHS developed in this chapter, except for  $T_n$  about within 0.1 to 0.2 s. The estimated normalized UHS are relatively insensitive to the site and to the exceedance



probability in 50 years. Therefore, for enhanced consistency in specifying seismic design load and economic efficiency, it is suggested to replace the design spectrum by the UHS.

### 3.6 References

- Albarelo D, Camassi R, Rebez A (2001). Detection of space and time heterogeneity in the completeness of a seismic catalog by a statistical approach: An application to the Italian area. *Bull. Seism. Soc. Am.*, 91(6): 1694-1703.
- Beauval C, Scotti O, and Bonilla F (2006). The role of seismicity models in probabilistic seismic hazard estimation: comparison of a zoning and a smoothing approach. *Geophysical Journal International*, 165(2): 584-595.
- Boore DM, Stewart JP, Seyhan E, and Atkinson GM (2014). NGA-west2 Equations for predicting PGA, PGV and 5% Damped PSA for Shallow Crustal Earthquakes. *Earthquake Spectra*, Vol. 30(3): 1057-1085.
- Bormann P, Liu R, Ren X, Gutdeutsch R, Kaiser D, Castellaro S (2007). Chinese national network magnitudes, their relation to NEIC magnitudes, and recommendations for new IASPEI magnitude standards. *Bull. Seism. Soc. Am.*, 97(1B): 114-127.
- Cornell CA (1968). Engineering seismic risk analysis. *Bull. Seism. Soc. Am.*, Vol. 58(5): 1583-1606.
- Esteva L (1968). "Bases para la formulación de decisiones de diseño sísmico.", Ph.D's thesis, Instituto de Ingeniería, Universidad Nacional Autónoma de México. (In Spanish)
- Frankel A (1995). Mapping seismic hazard in the central and eastern United State. *Seism. Res. Lett.*, Vol. 66(4): 8-21.
- Gao MT, Li XJ, Xu XW, Wei .B, Yu YX, Zhou BG, Zhao FX, Pan H, Lv, YJ, Zhou Q, Wu

- J, Lu DW, Chen K, Li YX, Gao ZW (2015) GB18306-2015: Introduction to the seismic hazard map of China. Standards Press of China, Beijing, China. (in Chinese).
- GB50011-2010. 2010. Code for seismic design of buildings, Ministry of Housing and Urban-Rural Development of the People's Republic of China (MOHURD), Beijing, China.
- Gardner JK, Knopoff L (1974) Is the sequence of earthquakes in Southern California, with aftershocks removed, Poissonian?. *Bull. Seism. Soc. Am.*, 64(5): 1363-1367.
- Goda K, Aspinall W, Taylor CA (2013). Seismic hazard analysis for the UK: Sensitivity to spatial seismicity modelling and ground motion prediction equations. *Seismological Research Letters*, 84(1): 112-129.
- Gu GX, Lin TH, Shi ZL, Li Q, Lu SD, Chen. HT, Wu HY, Yang YL, Wang SY (1983). *Catalog of Chinese Earthquakes 1831 B.C. – 1969 A.D.* Academia Sinica, Scientific Publishing House, Beijing.
- Hong HP, Feng C (2019). On the ground-motion models for Chinese seismic hazard mapping. *Bull. Seism. Soc. Am.* <https://doi.org/10.1785/0120180269>
- Hong HP, Goda K, Davenport AG (2006). Seismic hazard analysis: a comparative study. *Canadian Journal of Civil Engineering*, 33(9), 1156-1171.
- Hu YX, Zhang MZ (1984). A method of predicting ground motion parameters for regions with poor ground motion data. *Earthquake Engineering and Engineering Vibration*, Vol. 4(1): 1-11. (in Chinese)
- Hu YX, Gao MT, Du W, Jin Y, Zhao FX, Zou QJ, Tao YL, Zhou BG (2001). GB18306-2001: Introduction to China ground motion parameter zoning map. Standards Press of China, Beijing, China. (in Chinese).
- Huang WQ, Li WQ, Cao XF (1994). Completeness analysis of the seismic catalog for China mainland region – the basic completeness time for separate regions. *Acta Seismologica Sinica*, 16(4): 423-432 (in Chinese).

- Liu HX (1987). On the seismic zoning map China, Proceedings of International Seminar on Seismic Zonation, Guangzhou, China, pp. 35-42. (in Chinese)
- Liu RF, Chen YT, Ren X, Xu ZG, Sun L, Yang H, Liang JH, Ren KX (2007). Comparison between different earthquake magnitudes determined by China seismograph network. *Acta Seismologica Sinica*, Vol. 29(5): 467-476.
- Liu TJ, Pozos-Estrada A, Gomez R, Hong HP (2016). Seismic hazard estimation: directly using observations versus applying seismic hazard model. *Natural Hazards*, 80(1): 639-655.
- Liu J, Chen QF, and Chen Y (1996). Completeness analysis of the seismic catalog in North China region., *Earthquake*, Vol. 16(1), pp. 59-67.
- MacQueen J (1967). Some methods for classification and analysis of multivariate observations. In Proceedings of the fifth Berkeley symposium on mathematical statistics and probability, Vol. 1(4): 281-297, California.
- McGuire RK (2004). *Seismic Hazard and Risk Analysis*, EERI Monograph MNO-10, Earthquake Engineering Research Institute, Oakland, California.
- Milne WG and Davenport AG (1969). "Distribution of earthquake risk in Canada." *Bull. Seism. Soc. Am.*, Vol. 59(2): 729-754.
- Molina S, Lindholm CD, Bungum H (2001). Probabilistic seismic hazard analysis: zoning free versus zoning methodology. *Bollettino di Geofisica (selected papers from the 27th ESC, Lisbon, 2000)*, 42: 19-39.
- R Development Core Team, 2014. *R: A language and environment for statistical computing*, R Foundation for Statistical Computing, Vienna, Austria, available at <http://www.R-project.org>.
- Rosenblueth E and Ordaz M (1990). Maximum earthquake magnitude at fault. *Journal of engineering mechanics*, 116(1), 204-216.

- Silverman BW (2018). Density estimation for statistics and data analysis. Routledge.
- Vere-Jones D (1992). Statistical Methods for the Description and Display of Earthquake Catalogs. Statistics in Environmental and Earth Sciences, Edward Arnold, London, 220-246.
- Wand MP, Jones MC (1994). Kernel smoothing. Chapman and Hall/CRC.
- Wang S, Yu Y (2009). Research on Empirical Relationship of Earthquake Magnitude Scales and Its Influence on Seismicity Parameters, Technology for Earthquake Disaster Prevention, Vol. 4(2): 141—149.
- Weichert DH (1980). Estimation of the earthquake recurrence parameters for unequal observation periods for different magnitudes. Bull. Seism. Soc. Am., 70(4): 1337-1346.
- Woo G (1996). Kernel estimation methods for seismic hazard area source modeling. Bull. Seism. Soc. Am., 86(2): 353-362.
- Xu WJ, Gao MT (2012). Seismic hazard estimate using spatially smoothed seismicity model as spatial distribution function, Acta Seismological Sinica, 34(4): 525-536 (in Chinese).
- Xu WJ, Gao MT (2014). Statistical analysis of the completeness of earthquake catalog in China mainland, Chinese Journal of Geophysics, 57(8): 2802-2812 (in Chinese).
- Xu WJ (2019). Probabilistic seismic hazard assessment using spatially smoothed seismicity in North China seismic zone. Journal of Seismology, 23(3), 613-622.
- Yu, Y.X., Li, S.Y., and Xiao, L. (2013). Development of ground motion attenuation relations for the new seismic hazard map of China. Technology for earthquake disaster prevention, Vol. 8(1): 24-33 (in Chinese).
- Zuccolo E, Corigliano M, Lai CG (2013). Probabilistic seismic hazard assessment of Italy using kernel estimation methods. Journal of Seismology, 17(3): 1001-1020.

## Chapter 4

### 4 Projecting sets of ground motion models and their use to evaluate seismic hazard and UHS for mainland China

#### 4.1 Introduction

Ground motion models (GMMs) are used for seismic hazard evaluation. The models can be developed based on instrumental ground-motion data from past earthquakes such as those reported in NGA-West2 GMMs (Abrahamson et al. 2013, 2014; Boore et al. 2013, 2014; Campbell and Bozorgnia 2013, 2014; Chiou and Youngs 2013, 2014; and Idriss 2013, 2014). They could also be developed based on a physics-based stochastic model with well-calibrated model parameters (Atkinson and Boore 1995). As the instrumental ground-motion data of large magnitude seismic events for mainland China is very limited, the GMMs used for the fourth- and fifth-generation Chinese seismic hazard maps (CSHMs) (Hu et al. 2001; Yu et al. 2013; Gao et al. 2015) were developed based on the projection method (Hu and Zhang 1984). The models presented in Yu et al. (2013) were developed for four seismic regions (for GMMs) covering mainland China: Eastern seismic region (ER), Median seismic region (MR), Tibet seismic region (TR) and Xinjiang seismic region (XR). To develop GMMs for a target region, the projection method relies on the availability of the intensity prediction equations (IPEs) and GMMs for a reference region and of IPEs for the target region.

The CSHMs were only given in terms of the peak ground acceleration (PGA) with an exceedance probability of 10% in 50 years since the available GMMs used for the hazard mapping (Wang et al. 2000; Yu et al. 2013) were developed only for PGA. These maps are used as the basis to recommend the seismic design load requirements (GB 50011 2010). Moreover, the seismic design requirement in GB 50011 (2010) is based on a standardized response spectrum that may not mimic the uniform hazard spectrum (UHS) which by definition provides a probability consistent ground motion measure and has been adopted by other structural design codes (e.g., NBCC 2015). To overcome the lack of GMMs for the spectral acceleration (SA), Hong and Feng (2019) applied the projection method to develop the GMMs by using the GMMs given in Boore et al. (2014) for the reference

region. The model given in Boore et al. (2014) is one set of NGA-West2 GMMs; for simplicity, it is referred to as BSSA14 and its projected version is denoted as BSSA14-P. A comparison of the predicted values by using BSSA14-P and the GMMs given by Yu et al. (2013) (hereafter referred to as YLX13) indicates that, in general, they are similar. However, the use of BSSA14-P leads to a predicted median PGA value that is lower than that predicted by YLX13 for events of large magnitude and short epicentral distance. YLX13 is only applicable for PGA and peak ground velocity (PGV). Furthermore, the standard deviation of the residual (i.e., sigma) for the BSSA14-P varies with earthquake magnitude and source to site distance; this is not the case for YLX13.

It should be noted that the use of other sets of GMMs (Abrahamson et al. 2013, 2014; Campbell and Bozorgnia 2013, 2014; Chiou and Youngs 2013, 2014; and Idriss 2013, 2014), hereafter referred to as ASK14, CB14, CY14 and IM14, respectively, for the reference region to develop sets of projected GMMs were not explored. There are indications that these models could be adequate to represent the ground motion measures for the instrumental ground-motion data from past earthquakes that occurred in and near China (Dangkua et al. 2018; Huang and Galasso 2019), although the number of seismic events available and used for the validation is very limited.

The use of BSSA14-P to map the seismic hazard and UHS for mainland China was presented in Feng et al. (2020). For the mapping, they used spatially smoothed seismic source models developed based on incomplete historical earthquake catalogue and the procedures given in Frankel (1995) and Woo (1996). Their results indicate that the mapped quantiles (or return period value) of annual maximum PGA for some locations differ largely from those given in fifth-generation of CSHM which were estimated by using a delineated seismic source model (Gao et al. 2015). The use of the smoothed seismic source models to map seismic hazard for regions in different countries was presented in several studies, including Molina et al. (2001), Beauval et al. (2006), Xu and Gao (2012), Goda et al. (2013), Zuccolo et al. (2013) and Xu (2019). The application of the delineated source model was traditionally considered to develop CSHMs (Liu 1987; Hu et al. 2001); the uncertainty propagation analysis procedure by using the assigned delineated source models was pioneered by Cornell (1968) and Esteva (1968). The major dissimilarities

between these approaches include the manner in which the historical earthquake catalogue is used to define the seismic source models and to characterize the magnitude-recurrence relations. The study carried out in Feng et al. (2020) did not consider the uncertainty in the assignment of the (spatially smoothed) source model, the model parameters for the magnitude-recurrence relations, and the selection of sets of GMMs. This uncertainty referred to as epistemic uncertainty (Budnitz *et al.* 1997) could be taken into account in seismic hazard assessment by using the logic tree approach (McGuire 2004). The use of the logic trees with the smoothed source model has not been considered to assess CSHMs.

The main objectives of the present study are to develop sets of projected GMMs using the projection method for four target seismic regions (i.e., ER, MR, TR and XR) by considering ASK14, CB14, CY14 and IM14 as the GMMs for the reference region, and to evaluate UHS and map seismic hazard for mainland China. For the development of the projected GMMs, the overall procedure, including IPEs employed in Hong and Feng (2019), is adopted. The evaluation of UHS and the seismic hazard is carried out based on the logic trees with spatially smoothed seismicity models by using the procedure given in Woo (1996) that is less sensitive to the assigned area of the seismic source region, especially for large earthquake events. The constructed trees take into account the assigned weights for the smoothed seismic source models, the time period of the completeness of the catalogue obtained for selected probabilities and the sets of GMMs. Also, a sensitivity analysis of the estimated UHS and seismic hazard is carried out by considering different trees. The development of the projected GMMs is described in the following section. This is followed by the estimation of UHS and seismic hazard and by sensitivity analysis results. Observations are made by comparing the estimated results to those given in the fifth-generation CSHM (Gao et al. 2015) and the structural design code (GB 50011 2010). The potential impact of the obtained results on structural design is discussed.

## 4.2 New sets of ground motion models by using projection method

As mentioned in the introduction, GMMs used to develop the fourth- and fifth-generation of CSHM (Hu et al. 2001; Gao et al. 2015) were obtained based on the projection method (Hu and Zhang 1984). These GMMs were developed for PGA and PGV, and described in Wang et al. (2000) and Yu et al. (2013). The need for the use of the projection method is based on that the historical acceleration records for a sufficient number of large earthquakes are lacking in mainland China. In using the projection method to develop GMM for a target region, it is assumed that IPEs for the reference and target regions are known, and the GMM for the reference region is given. The projection method was applied in Hong and Feng (2019) to obtain BSSA14-P. For the application, they used IPE given in Howell and Schultz (1975) and BSSA14 for the reference region (i.e., California), and IPE given in Yu et al. (2013) for the target regions (i.e., seismic regions in China). Moreover, they considered the differences in the surface wave magnitude values reported by agencies in China and the U.S. (Liu et al. 2006), and the different source-to-site distance measures and magnitude measures used for IPEs and GMMs for the target and reference regions. The soil amplification term in GMMs for the reference region that is often assumed to be independent of the earthquake magnitude and distance is left out when assessing the projected GMMs. Once the projected GMMs are assessed, this term in the original GMMs is then incorporated in the projected GMMs.

The procedure for the projection method as presented in Figure 4.1 and IPEs used in Hong and Feng (2019) is employed in the present study to develop the projected GMMs by using ASK14, CB14, CY14 or IM14 as GMMs for the reference region. In the figure,  $I_{CA}(M_{Iref}, R_{Iref})$  and  $Y_A(M_{Gref}, R_{Gref})$  represent the IPE and GMM for the reference region while  $I_{CB}(M_s, R_{epi})$  and  $Y_B(M_{Itar}, R_{Itar})$  represent the IPE and GMM for the target region, where  $M$  and  $R$  with subscripts  $Iref$  and  $Gref$  are the magnitude and distance measures used in the IPE and GMM for the reference region, respectively;  $M_s$  and  $R_{epi}$  are the surface wave magnitude and epicentral distance, and  $M$  and  $R$  with subscripts  $Itar$  and  $Gtar$  are the magnitude and distance measures used in the GMM for the target region. The steps to develop the unknown  $Y_B(M_s, R_{epi})$  are to 1) find the predicted intensity using  $I_{CB}(M_s, R_{epi})$



for given values of  $M_s$  and  $R_{epi}$ ; 2) find the equivalent  $M_{Iref}$  based magnitude conversion and calculate the value of the distance measure  $R_{Iref}$  by equating  $I_{CB}(M_s, R_{epi})$  and  $I_{CA}(M_{Iref}, R_{Iref})$ ; 3) find the equivalent  $M_{Gref}$  and  $R_{Gref}$  based the magnitude conversion and distance conversion relation, and calculate the value of  $Y_A(M_{Gref}, R_{Gref})$  and 4) assign  $Y_B(M_s, R_{epi})$  equal to the value of  $Y_A(M_{Gref}, R_{Gref})$ . By repeatedly applying these steps and considering the uncertain residual terms in IPEs and GMMs as well as in the required transformations between different earthquake magnitudes and between different source-to-site distances, samples of  $Y_B(M_s, R_{epi})$  is established and used to find the projected GMMs through regression analysis.

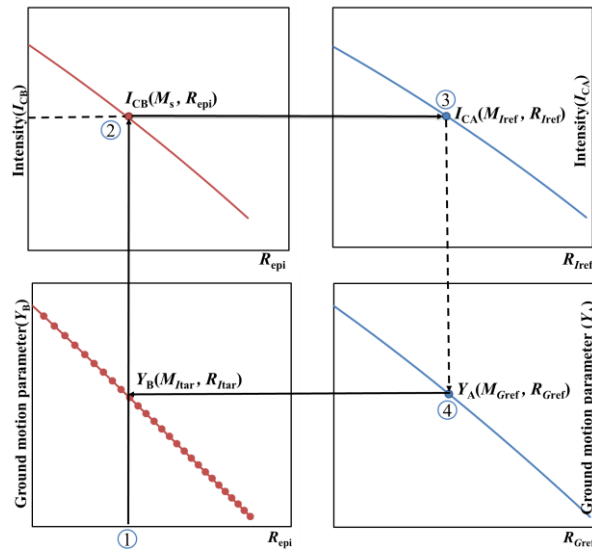


Figure 4.1. Schematic of the projection method by considering different earthquake magnitude and distance measures that are used for different regions.

Unlike BSSA14 which uses Joyner-Boore distance,  $R_{jb}$ , (defined as the closest distance to the surface projection of the fault) as the source to site distance measure, ASK14, CB14, CY14 and IM14 use the closest distance to the rupture plane,  $R_{rup}$ . In applying the projection method to develop BSSA14-P, it was considered that the difference between  $R_{jb}$  to  $R_{epi}$  could be considered as a Gamma distributed random variable (Scherbaum et al. 2004) with the mean and coefficient of variation (COV) of  $R_{epi} - R_{jb}$ , denoted as  $m_{e-jb}$  and  $\nu_{e-jb}$ , that are given by (Goda et al. 2010),

$$m_{e-jb} = \left[ 1 - \exp\left(- (0.458 - 0.0549M_w) \times R_{epi}^{1.046 - 0.0361M_w}\right) \right] \exp\left(-1.297 - 0.138M_w + 0.105M_w^2\right) \quad (4.1)$$

and,

$$v_{e-jb} = \left[ 1 + (0.227 - 0.0488M_w) \exp\left(1.921R_{epi}^{-0.0566}\right) \right] \exp\left(-2.109 - 0.0331M_w\right) \quad (4.2)$$

where  $M_w$  is the moment magnitude. However, there is no direct relation between  $R_{epi}$  and  $R_{rup}$  available in the literature but a relation between  $R_{rup}$  and  $R_{jb}$  was given Kaklamanos et al. (2014). Therefore, to apply the projection method to ASK14, CB14, CY14 and IM14, besides Eqs. (4.1) and (4.2) the relation given in Kaklamanos et al. (2014) is also adopted. Their relation for strike-slip events with dip of the fault,  $\delta$ , equal to  $90^\circ$  can be written as,

$$R_{rup} = \sqrt{R_{jb}^2 + Z_{tor}^2}, \quad (4.3)$$

where

$$Z_{tor} = \max\left[(Z_{hyp} - 0.6W \sin \delta), 0\right], \quad (4.4)$$

and  $Z_{hyp}$  and  $W$  represent the hypocenter depth and fault width, respectively. For strike-slip earthquake events,  $Z_{hyp}$  and  $W$  can be estimated using (Scherbaum et al. 2004; Wells and Coppersmith 1994),

$$Z_{hyp} = 5.63 + 0.68M_w + \varepsilon_{Z_{hyp}}, \quad (4.5)$$

and,

$$\log W = -0.76 + 0.27M_w + \varepsilon_{\log W}, \quad (4.6)$$

where  $\varepsilon_{Z_{hyp}}$  is a zero-mean normally distributed random variable with standard deviation  $\sigma_{Z_{hyp}} = 4.55$  km,  $Z_{hyp}$  is in the range of 3 to 24 km,  $\varepsilon_{\log W}$  is a zero-mean normally distributed random variable with standard deviation  $\sigma_{\log W} = 0.15$ .

Following the procedure described above, the projected GMMs corresponding to ASK14, CB14, CY14 and IM14, denoted as ASK14-P, CB14-P, CY14-P and IM14-P, are obtained for the strike-slip events and neglecting the hanging wall effect. It is considered that the natural logarithm of PGA or SA,  $\ln Y$ , for the projected GMM has the same mathematical form as its original version which is depicted in Table 4.1. In the table,  $R$  for ASK14 is defined by,

$$R = \sqrt{R_{\text{epi}}^2 + c_{4M_w}^2} \quad (4.7)$$

and

$$c_{4M_w}(M_w) = \begin{cases} c_{4\text{ASK}}, & \text{for } M_w > 5 \\ c_{4\text{ASK}} - (c_{4\text{ASK}} - 1)(5 - M_w), & \text{for } 4 < M_w \leq 5 \\ 1, & \text{for } M_w \leq 4 \end{cases} \quad (4.8)$$

Table 4.1. Magnitude scaling term and geometric attenuation anelastic attenuation term for the logarithm of PGA or SA in the GMMs.

	Magnitude scaling term	Geometric attenuation and anelastic attenuation term
ASK14-P	$\begin{cases} a_1 + a_5(M_w - M_1) + a_8(8.5 - M_w)^2, M_w > M_1, \\ a_1 + a_4(M_w - M_1) + a_8(8.5 - M_w)^2, M_2 \leq M_w < M_1, \\ a_1 + a_4(M_2 - M_1) + a_8(8.5 - M_w)^2 \\ + a_6(M_w - M_2) + a_7(M_w - M_2)^2, M_w < M_2, \end{cases}$	$\begin{cases} [a_2 + a_3(M_w - M_1)] \ln(R) + a_{17}R, \\ [a_2 + a_3(M_w - M_1)] \ln(R) + a_{17}R, \\ [a_2 + a_3(M_w - M_1)] \ln(R) + a_{17}R, \end{cases}$
CB14-P	$\begin{cases} c_0 + c_1M_w + c_2(M_w - 4.5), 4.5 < M_w \leq 5.5 \\ c_0 + c_1M_w + c_2(M_w - 4.5) + c_3(M_w - 5.5), 5.5 < M_w \leq 6.5 \\ c_0 + c_1M_w + c_2(M_w - 4.5) + c_3(M_w - 5.5) \\ + c_4(M_w - 6.5), M_w > 6.5 \end{cases}$	$\begin{cases} (c_5 + c_6M_w) \ln(\sqrt{R_{\text{epi}}^2 + c_7^2}) + c_{20}(R_{\text{epi}} - 80), R_{\text{epi}} > 80 \\ (c_5 + c_6M_w) \ln(\sqrt{R_{\text{epi}}^2 + c_7^2}), R_{\text{epi}} \leq 80 \end{cases}$
CY14-P	$c_1 + c_2(M_w - 6) + c_3 \ln(1 + e^{c_n(c_M - M_w)})$	$\begin{aligned} & c_4 \ln(R_{\text{epi}} + c_5 \cosh(c_6 \max(M_w - c_{\text{HM}}, 0))) \\ & + (c_{4a} - c_4) \ln(\sqrt{R_{\text{epi}}^2 + c_{\text{RB}}^2}) \\ & + \left( c_{\gamma 1} + \frac{c_{\gamma 2}}{\cosh(\max(M_w - c_{\gamma 3}, 0))} \right) R_{\text{epi}} \end{aligned}$
IM14-P	$\begin{cases} \alpha_1 + \alpha_2M_w + \alpha_3(8.5 - M_w)^2, M_w \leq 6.75 \\ \alpha_4 + \alpha_5M_w + \alpha_3(8.5 - M_w)^2, M_w \geq 6.75 \end{cases}$	$(\beta_1 + \beta_2M_w) \ln(R_{\text{epi}} + 10) + \gamma R_{\text{epi}}$

Note:  $a_1$  to  $a_6$ ,  $a_8$ ,  $a_{17}$  and  $c_{4M}$  are the regressed model coefficients for ASK14-P;  $c_0$  to  $c_7$  and  $c_{20}$  are the regressed model coefficients for CB14-P;  $c_1$  to  $c_5$ ,  $c_{4a}$ ,  $c_{\text{RB}}$  and  $c_{\gamma 1}$  are the regressed model coefficients for CY14-P;  $\alpha_1$  to  $\alpha_5$ ,  $\beta_1$ ,  $\beta_2$  and  $\gamma$  are the regressed model coefficients for IM14-P. For the soil amplification term, see the ASK14, CB14, CY14, and IM14.

According to Kanamori (1977) and Ekström and Dziewonski (1988),  $M_w$  is given by,

$$M_w = (2/3) \times \log M_0 - 10.73 \quad (4.9)$$

and,

$$\log M_0 = \begin{cases} 19.24 + M_{s-US} & M_{s-US} < 5.3 \\ 30.20 - \sqrt{92.45 - 11.40M_{s-US}} & 5.3 \leq M_{s-US} \leq 6.8 \\ 16.14 + 3/2 M_{s-US} & M_{s-US} > 6.8 \end{cases} \quad (4.10)$$

in which  $M_{s-US}$  representing the surface wave magnitude reported by the U.S. agency equals  $1.07M_s - 0.61$  (Liu et al. 2006) and  $M_s$  representing the surface wave magnitude reported by the Chinese agency.

The obtained coefficients for the projected GMMs are shown in Table 4.2 for a few selected values of the natural vibration period  $T_n$ , where the four seismic regions (ER, MR, TR and XR) are identified in Figure 4.2a. In developing the projected GMMs, convergence problem in nonlinear regression analysis was encountered when using CY14 as the reference GMM. Consequently, the coefficients  $c_6$ ,  $c_n$ ,  $c_M$ ,  $c_{r2}$ ,  $c_{r3}$  and  $c_{HM}$  for CY14-P are set equal to CY14. Moreover, if  $M_w$  is less than or equal to the  $c_M$  suggested in CY14, the value of  $c_M$  in CY14-P is taken equal to  $M_w$ . Plots of ASK14-P, CB14-P, CY14-P and IM14-P as well as ASK14, CB14, CY14 and IM14 for a few selected scenario events are shown in Figures 4.2 to 4.3. Also, for comparison purposes, BSSA14-P, BSSA14 and YLX13-G are included in the plots, where YLX13-G represents the geometric mean of YLX13 for the long and short axes (i.e., axes along and perpendicular to fault line). Since IM14 is only applicable for  $V_{S30} > 450$  m/s, and YLX13 was developed for sites with  $V_{S30} > 500$  m/s and considered to be applicable for site Class I<sub>1</sub> defined in GB 50011 (2010) (Yu et al. 2013),  $V_{S30} = 510$  m/s is employed for the plotting of the projected GMMs because this value represents for site Class I<sub>1</sub> (Lü and Zhao 2007).

Figure 4.2 shows that, in general, the predicted median PGA values by using the projected GMMs and by their corresponding original versions are relatively consistent. However, there are clear differences among IM14 (or IM14-P) and remaining GMMs from the

NGA-West2 for events with large magnitude and short epicentral distance. The same can be observed between YLX13-G and ASK14-P, BSSA14-P, CB14-P, and CY14-P. In all cases, the predicted median PGA values by using YLX13-G for four seismic regions are greater than those obtained by using the projected GMMs, except IM14-P, for  $R_{\text{epi}} \leq 100$  km. This trend is reversed for  $R_{\text{epi}} > 100$  km. The plot for this and remaining figures,  $M_s = 5$  and 7 rather than  $M_s = 5$  and 8 are used for MR because the magnitude  $M_s$  applicable for the region is considered to be 7 (Yu et al. 2013; Gao et al. 2015). There are differences between the original and projected GMMs. In general, the ratio of the predicted PGA by using the projected GMMs to that by using the original GMMs depends on the magnitude and epicentral distance. A simple calculation shows that the average ratio is about 1.17, 1.17, 1.30, 1.23 and 1.34 for  $M_s = 5$  and 0.88, 0.80, 0.83, 0.87 and 0.81 for  $M_s = 8$  (except that  $M_s = 7$  is considered for MR since for such a region the maximum applicable magnitude is 7) if ASK14, BSSA14, CB14, CY14, and IM14 are considered, respectively. Similar trends of the ratio are also observed if SA (shown in Figure 4.3) is considered.

Moreover, plots shown in Figure 4.3 indicate that the predicted median SA values by using the projected GMMs and by their corresponding original models follow very similar trends. It should be noted that IM14 was developed for  $V_{S30}$  greater than 450 m/s and for  $R_{\text{rup}} 150$  km. Since the seismic hazard assessment results reported in GB 50011 (2010) are for Class II that has a  $V_{S30}$  ranging from 260 to 510 m/s with an average of 385 m/s (Lü and Zhao, 2007), to be consistent and for comparison purposes, the assessment of seismic hazard and UHS to be carried out in the remaining part of this study is for site Class II (i.e.,  $V_{S30} = 385$  m/s). Consequently, IM14 and its projected version are not considered further.

Table 4.2. Model coefficients for the projected GMMs for selected  $T_n$ .

$T_n$ (s)	GMM (Region)	$a_1$	$a_2$	$a_3$	$a_4$	$a_5$	$a_6$	$a_8$	$a_{17}$	$C_{4ASK}$
0.2	ASK14-P (ER)	0.3719	-0.5106	0.2014	0.6460	0.2841	1.3873	0.0941	-0.0069	6.7101
	ASK14-P (MR)	-0.0900	-0.5681	0.1552	1.0399	0.7773	1.0581	0.2000	-0.0057	7.6297
	ASK14-P (TR)	0.2654	-0.5805	0.2012	0.7045	0.3570	1.2683	0.1188	-0.0060	6.4888
	ASK14-P (XR)	0.5809	-0.5569	0.2127	0.5737	0.2291	1.5325	0.0690	-0.0070	6.0098
0.5	ASK14-P (ER)	0.3289	-0.4643	0.2013	0.5673	0.1849	1.8338	0.0384	-0.0045	6.3030
	ASK14-P (MR)	-0.2064	-0.4807	0.1882	0.8779	0.5710	1.5074	0.1419	-0.0036	7.3719
	ASK14-P (TR)	0.2152	-0.5159	0.2055	0.6195	0.2411	1.7350	0.0608	-0.0035	6.0658
	ASK14-P (XR)	0.5248	-0.5083	0.2075	0.5048	0.1399	1.9677	0.0141	-0.0043	5.6388
2	ASK14-P (ER)	-0.9140	-0.4527	0.2009	0.5618	0.1670	2.2447	-0.0376	-0.0039	6.0923
	ASK14-P (MR)	-1.4619	-0.4593	0.1962	0.8436	0.5107	1.8919	0.0640	-0.0031	7.2941
	ASK14-P (TR)	-1.0289	-0.5002	0.2066	0.6108	0.2173	2.1386	-0.0156	-0.0030	6.0155
	ASK14-P (XR)	-0.7213	-0.4961	0.2058	0.5015	0.1244	2.3747	-0.0617	-0.0037	5.4570
		$c_0$	$c_1$	$c_2$	$c_3$	$c_4$	$c_5$	$c_6$	$c_7$	$c_{20}$
0.2	CB14-P (ER)	-6.2849	1.2700	0.4620	-1.6128	-0.2561	-1.6713	0.1354	8.0517	-0.0109
	CB14-P (MR)	-6.0680	1.2608	0.1360	-1.5164	-0.1395	-1.6318	0.1370	7.0369	-0.0103
	CB14-P (TR)	-6.2986	1.2609	0.3871	-1.6001	-0.1983	-1.6809	0.1382	7.0926	-0.0109
	CB14-P (XR)	-6.2763	1.2780	0.5314	-1.6344	-0.2791	-1.7493	0.1385	8.1678	-0.0103
0.5	CB14-P (ER)	-9.0343	1.7985	-0.1248	-1.4475	-0.2781	-1.6524	0.1429	7.6983	-0.0083
	CB14-P (MR)	-8.7839	1.7954	-0.5083	-1.3431	-0.1440	-1.7085	0.1612	6.6680	-0.0081
	CB14-P (TR)	-9.0496	1.7891	-0.2018	-1.4317	-0.2314	-1.6755	0.1488	6.7308	-0.0082
	CB14-P (XR)	-9.0589	1.8041	-0.0422	-1.4724	-0.3020	-1.7018	0.1428	7.7477	-0.0077
2	CB14-P (ER)	-13.6003	2.2001	0.1438	-1.3911	-0.6149	-1.5042	0.1209	7.5588	-0.0070
	CB14-P (MR)	-13.3023	2.2007	-0.2895	-1.2815	-0.4991	-1.6385	0.1524	6.5324	-0.0068
	CB14-P (TR)	-13.6124	2.1902	0.0583	-1.3746	-0.5785	-1.5411	0.1299	6.5229	-0.0067
	CB14-P (XR)	-13.6482	2.2042	0.2375	-1.4157	-0.6370	-1.5278	0.1174	7.5694	-0.0062
		$c_1$	$c_2$	$c_3$	$c_4$	$c_5$	$c_{4a}$	$c_{RB}$	$c_{r1}$	
0.2	CY14-P (ER)	-37.7153	0.9589	0.0075	-1.1484	16.2696	6.7082	182.7183	-0.0208	
	CY14-P (MR)	-63.9445	0.5615	-0.0099	-0.7639	53.2872	12.4796	152.9668	-0.0451	
	CY14-P (TR)	-34.1513	0.8979	0.0311	-1.1494	12.9504	6.1572	159.1684	-0.0221	
	CY14-P (XR)	-37.1224	1.0467	-0.0063	-1.2548	15.0634	6.5915	177.4143	-0.0211	
0.5	CY14-P (ER)	-37.1709	1.0894	-0.1454	-1.2854	24.3126	6.6547	161.4389	-0.0234	
	CY14-P (MR)	-56.6053	1.0255	-0.1258	-1.7416	114.7442	11.1253	145.5190	-0.0438	
	CY14-P (TR)	-33.5137	1.0449	-0.1175	-1.3370	20.2851	6.0474	141.9702	-0.0241	
	CY14-P (XR)	-37.6986	1.1308	-0.1714	-1.2879	20.2591	6.7526	158.2086	-0.0241	
2	CY14-P (ER)	-40.0744	1.1935	-0.5280	-1.3074	32.7644	7.0545	150.0259	-0.0253	
	CY14-P (MR)	-40.1454	2.4160	-0.1900	-4.5277	385.5502	8.6513	143.3593	-0.0429	
	CY14-P (TR)	-35.5509	1.1900	-0.4926	-1.4412	28.4295	6.2550	132.4801	-0.0251	
	CY14-P (XR)	-40.0332	1.1758	-0.5725	-1.2113	23.3424	7.0261	147.6983	-0.0252	
		$\alpha_1$	$\alpha_2$	$\alpha_3$	$\alpha_4$	$\alpha_5$	$\beta_1$	$\beta_2$	$\gamma$	
0.2	IM14-P (ER)	2.3051	0.8954	0.1292	5.7505	0.3849	1.8353	-0.1335	-0.0047	
	IM14-P (MR)	-0.0429	1.2282	0.2049	2.2786	0.8843	1.5244	-0.0667	-0.0025	
	IM14-P (TR)	2.5886	0.8855	0.1481	5.9997	0.3802	2.0455	-0.1408	-0.0024	
	IM14-P (XR)	3.0929	0.8337	0.1103	6.4662	0.3340	2.0221	-0.1473	-0.0043	
0.5	IM14-P (ER)	2.3595	0.8267	0.0820	6.7912	0.1701	1.8142	-0.1391	-0.0041	
	IM14-P (MR)	0.1351	1.1315	0.1596	3.5510	0.6254	1.5814	-0.0875	-0.0022	
	IM14-P (TR)	2.5364	0.8289	0.1010	6.9829	0.1702	2.0068	-0.1459	-0.0020	
	IM14-P (XR)	3.1380	0.7640	0.0630	7.4948	0.1186	1.9893	-0.1519	-0.0037	
2	IM14-P (ER)	-3.1278	1.1781	0.0673	3.3534	0.2179	1.6942	-0.1433	-0.0042	
	IM14-P (MR)	-5.3557	1.4867	0.1406	0.3683	0.6387	1.4646	-0.0936	-0.0024	
	IM14-P (TR)	-3.0726	1.1950	0.0863	3.4628	0.2268	1.8630	-0.1491	-0.0024	
	IM14-P (XR)	-2.3293	1.1053	0.0489	4.0819	0.1555	1.8649	-0.1575	-0.0039	

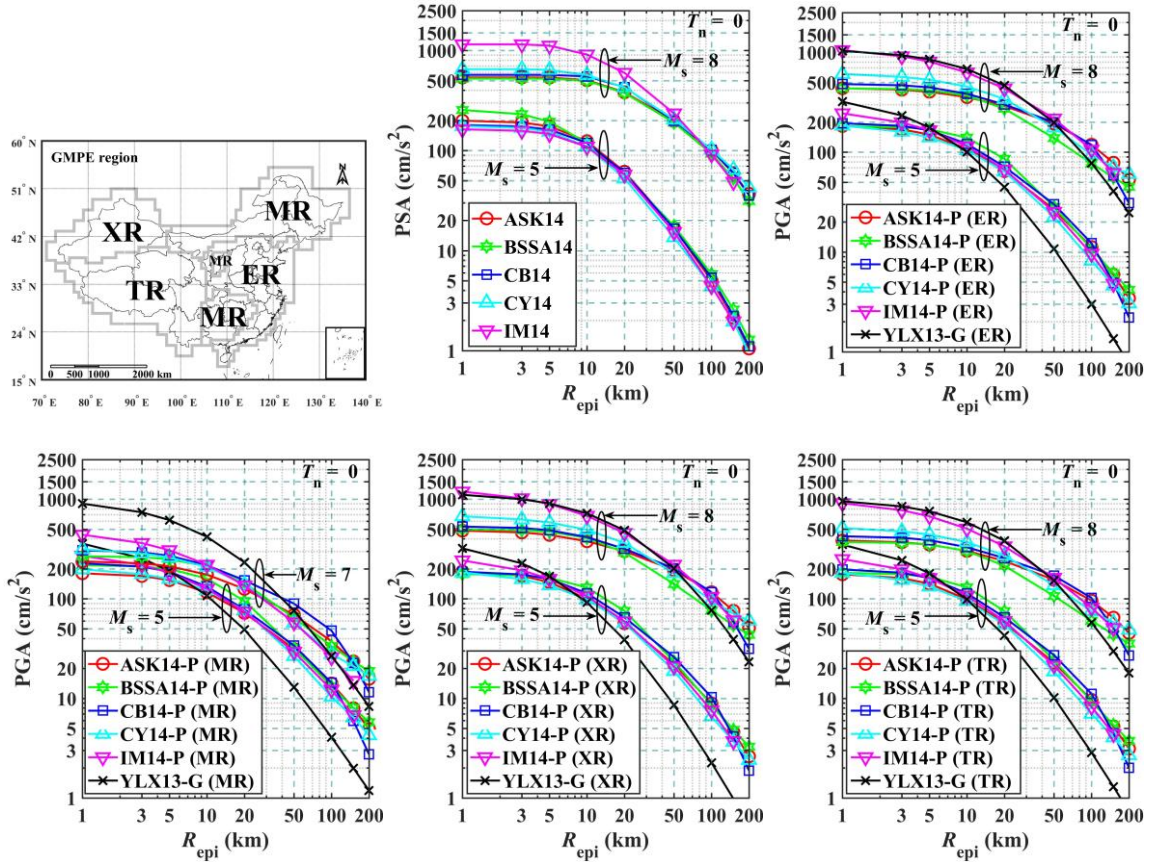
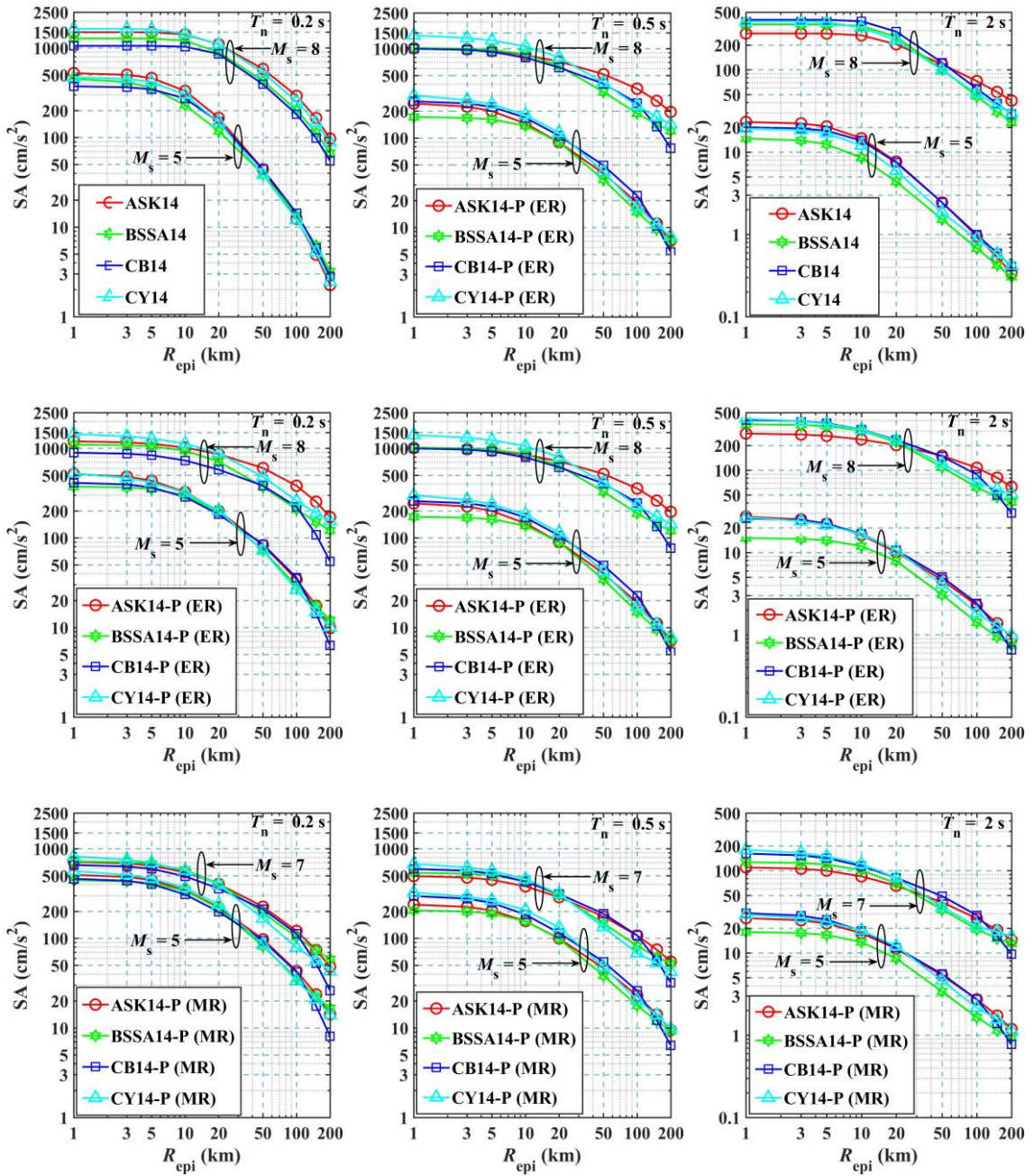


Figure 4.2. Identification of the four seismic regions for GMMs and comparison of predicted median PGA.





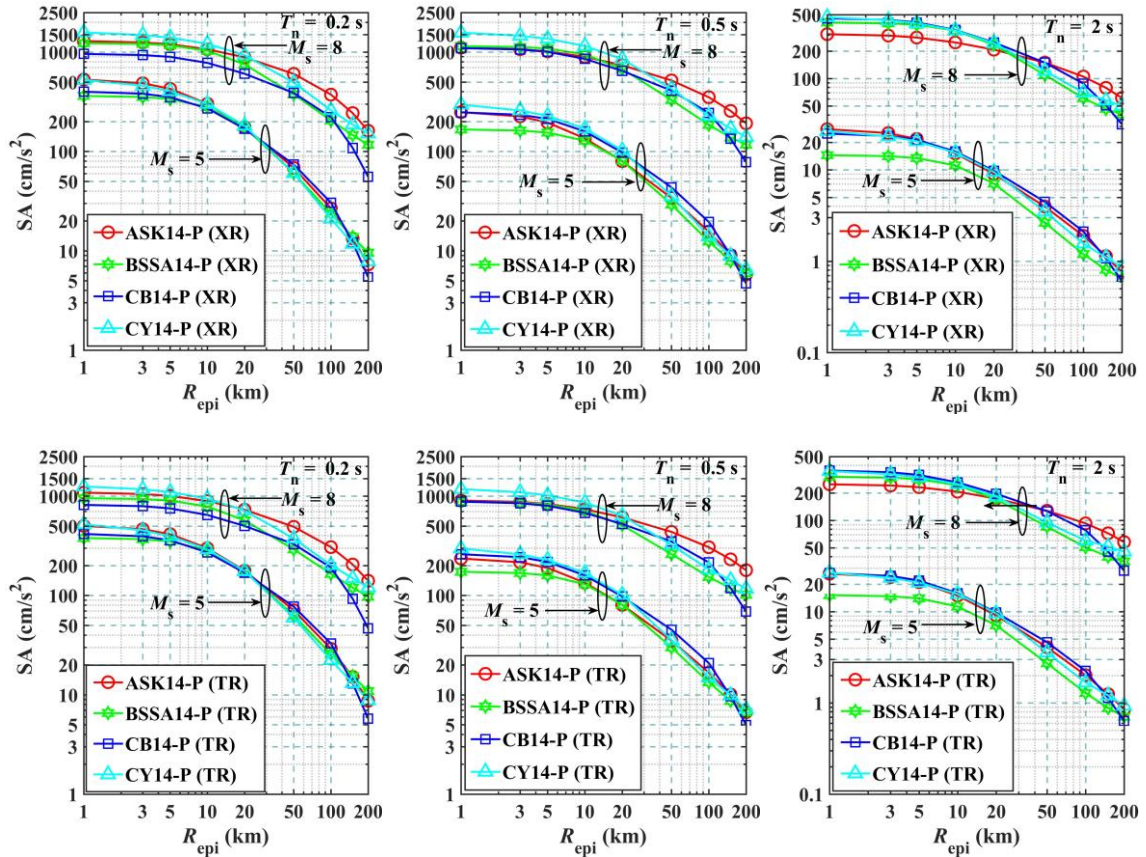


Figure 4.3. Comparison of predicted median SA at  $T_n = 0.2, 0.5$  and  $2$  s.

As mentioned in the introduction, Dangkua et al. (2018) compared the NGA-West2 GMMs to instrumental ground-motion data from past earthquakes that occurred in and near mainland China. As the data used in their study are unavailable to the present study, the predicted median PGA by using the projected GMMs is simply superimposed on their plots as shown in Figures 4.4a to 4.4e. The predicted median values presented in Figure 4.4a and 4.4b are obtained using the projected GMMs for ER, where the instrumental ground-motion data are for relatively small to moderate magnitude vertical strike-slip earthquakes occurred in China. Figures 4.4c and 4.4d compare the predicted median PGA values by using the projected GMMs for MR and TR to instrumental ground-motion data. The results shown in Figure 4.4e provide a comparison to records from Wenchuan earthquake (May 12, 2008) with  $M_s = 8.0$  (Li et al., 2008). In all cases, the projected models compare well to those calculated from the instrumental ground-motion data. No

comparison of the SA values is carried out since the SA values for the records are not reported in Dangkua et al. (2018).

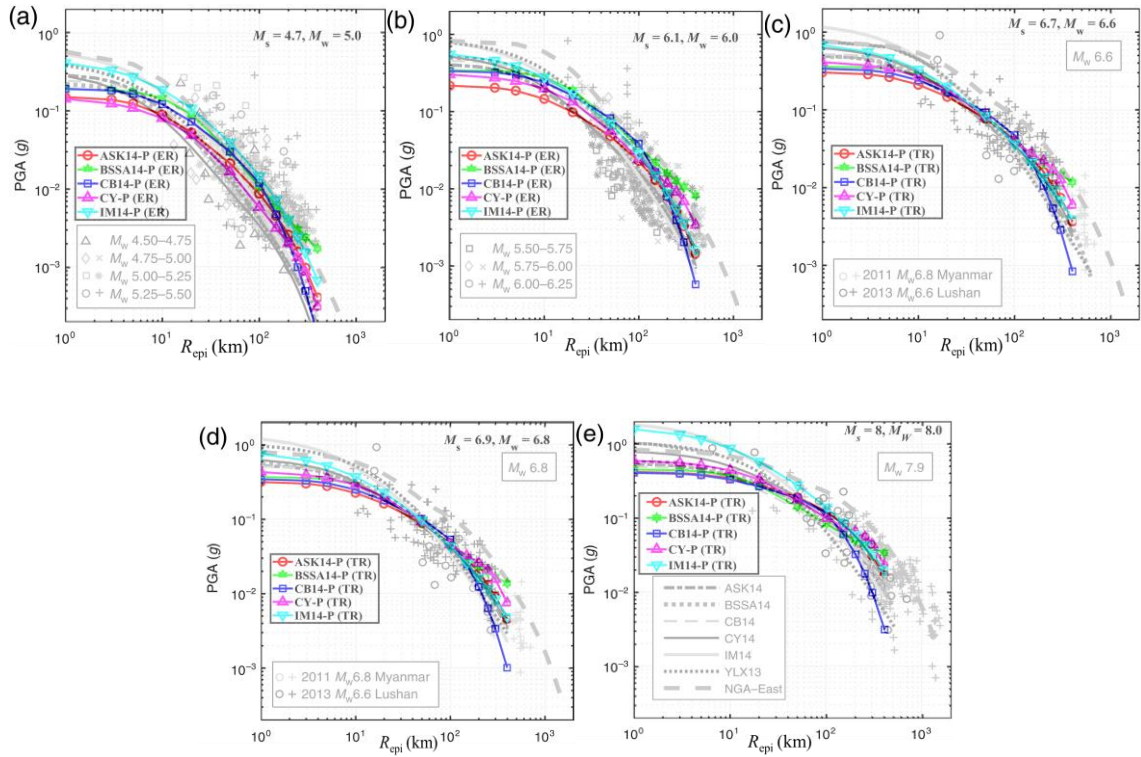


Figure 4.4. Comparison of the predicted median PGA by using projected GMMs to instrumental ground-motion data (the background data and plots are those from Dangkua et al. (2018)). For plots a) and b) the triangle, diamond, square and circle represent the data from the rock site and the remaining symbols are used to represent data from soil site; for plots c) to e) the circles and cross are used to represent data from rock and soil sites, respectively. a) PGA for ER and  $M_s = 4.5$ , b) PGA for ER and  $M_s = 6.1$ , c) PGA for MR and  $M_s = 6.7$ , d) PGA for TR and  $M_s = 6.7$ , and e) PGA for TR and  $M_s = 8.0$  ( $M_w = 8.0$  is obtained by using Eqs. (4.9) and (10)).

Besides the predicted median PGA and SA, the sigma of the residuals of the GMMs, which is considered to be normally distributed, is of importance for the seismic hazard assessment. The obtained sigma values for the projected GMMs are equal to those of the

original GMMs but scaled by a constant that depends on the considered region (Hong and Feng 2019). The constant equals 0.91, 0.81, 0.93 and 1.07, for ER, MR, TR and XR, respectively. The sigma for the original GMMs by considering PGA is illustrated in Figure 4.5 and compared to the sigma value of 0.53 associated with the predicted logarithm of PGA for YLX13-G. As can be observed in almost all cases, the former which varies with magnitude and epicentral distance is greater than the latter.

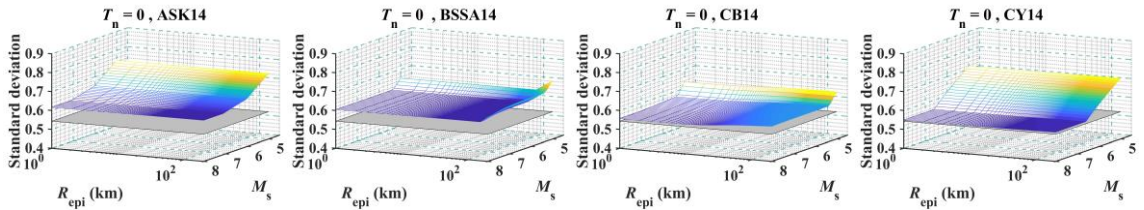


Figure 4.5. Sigma for ASK14, BSSA14, CB14, and CY14 and for YLX13-G.

### 4.3 Procedure to evaluate UHS and adopted source models

#### 4.3.1 Spatially smoothed seismic source models

Two smoothed earthquake source models considered for the numerical analysis to be carried out in the presented study are summarized in this section. The source models were developed by considering the historical seismic events shown in Figure 4.6a. These two source models (Feng et al. 2020), referred to as SM1 and SM2, are shown in Figures 4.6b and 4.6c. SM1 and SM2 use six and nine seismic source regions to cover mainland China, respectively. It must be emphasized that these seismic source regions in SM1 and SM2 differ from the four regions considered for the applicable GMMs. SM1 mimics that considered in Xu and Gao (2014) and SM2 is based on the results from cluster analysis using the events shown in Figure 4.6a. The cluster analysis is a statistical method that groups a set of objects such that objects in the same group (or cluster) are more similar to each other than to those in other groups (MacQueen 1967). It is considered that the assigned maximum magnitude  $M_{smax}$ , equals (7.6, 8.75, 7.6, 8.75, 8.5, 8.5) for the source regions 1 to 6 if SM1 is used, and (7.6, 8.75, 7.6, 8.75, 8.75, 8.5, 8.25, 8.5, 8.5) for the source regions 1 to 9 if SM2 is used. These values are based on those suggested for the

fifth-generation CSHM (Gao et al. 2015). These values are based on the largest magnitude of the maximum magnitude suggested by Gao et al. (2015) for the seismic regions and the maximum observed magnitude from the historical seismic events with a tolerance of 0.1.

Because the historical catalogue is associated with unequal observation periods for different earthquake magnitude intervals that influence the assessment of the magnitude recurrence relation, Feng et al. (2020) carried out the catalogue completeness analysis by using the procedure given in Albarello et al. (2001). For the  $j$ -th source region, they considered that the initial time  $T_{C,j}$  for which the events with magnitude greater than  $M_{\text{min},j}$  after  $T_{C,j}$  and before the most recent reporting time  $T_F$  is completed is uncertain. In other words, the period of completeness is  $\Delta T_{C,j} = T_F - T_{C,j}$  is uncertain. For a selected value of the cumulative distribution function of  $\Delta T_{C,j}$ ,  $p$ , the  $p$ -quantile of  $\Delta T_{C,j}$ , denoted as  $\Delta t_{C,j,p}$ , can be calculated, where the corresponding the  $p$ -quantile of  $T_{C,j}$ , denoted as  $t_{C,j,p}$ , is equal to  $T_F - \Delta t_{C,j,p}$ .

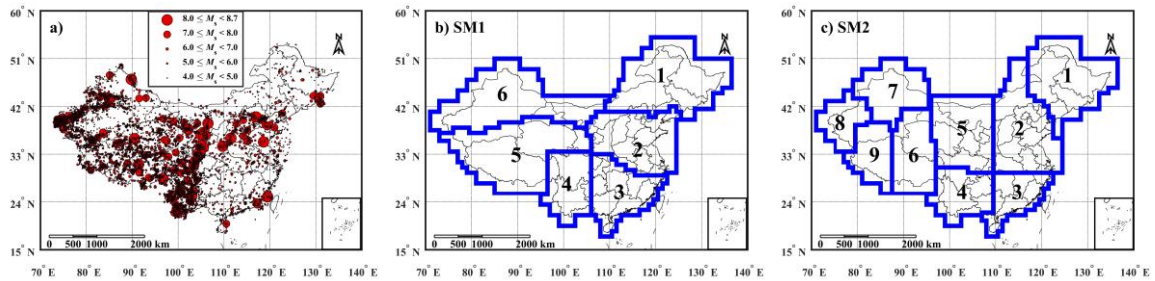


Figure 4.6. Assigned source regions and considered earthquake catalogue: a) Historical seismic events with  $M_s \geq 4.0$  after 1500 AD and excluding aftershocks (See Feng et al. 2020), replotted), b) SM1 with six seismic source regions; and c) SM2 with nine seismic source regions.

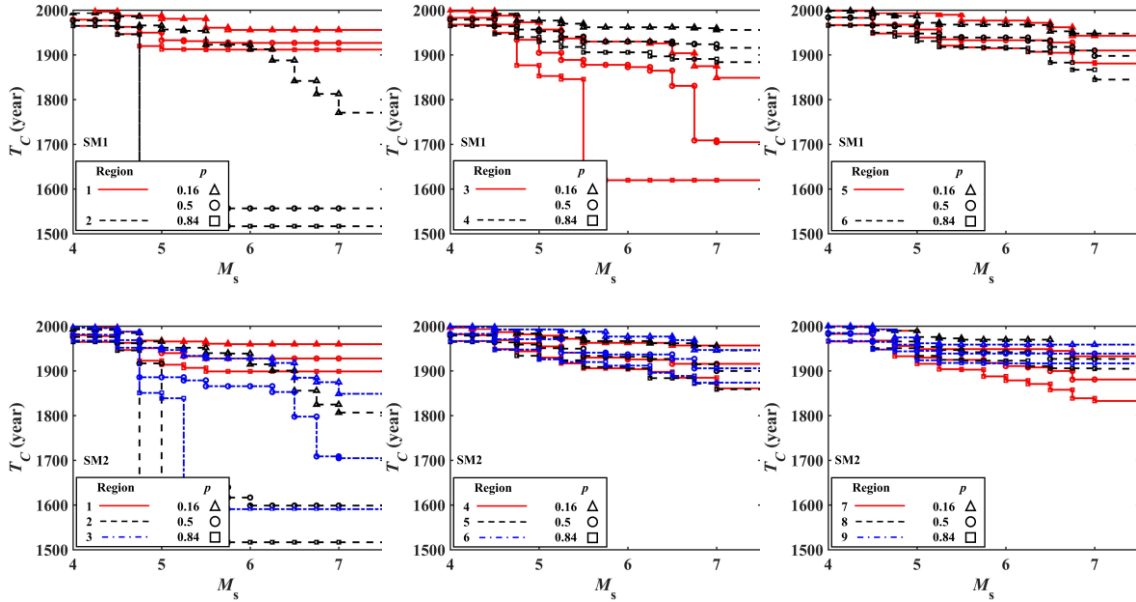


Figure 4.7. Estimated  $t_{C,j,p}$  for selected  $p$  values: The plots in the first and second rows are for SM1 and SM2.

For the analysis shown in Feng et al. (2020),  $p$  equal to 0.5 recommended in Albarello et al. (2001) was used by considering  $M_{s\min,j} = 4$ . By repeating such an analysis but considering  $p = 0.16$  and 0.84 for here, the obtained  $t_{C,j,p}$  is shown in Figure 4.7. An increased  $p$  leads to an decreased  $t_{C,j,p}$  (i.e., an increased observation period  $T_F - t_{C,j,p}$ ).

Given that the value of  $T_{C,j}$  for  $M_{s\min,j}$  is determined, the procedures in Frankel (1995) and in Woo (1996) could be used to evaluate the spatially smoothed magnitude recurrence relation for each of the nonoverlapping square cells covering the region of interest. The procedure in Frankel (1995) emphasizes the spatial smoothing of the total number of events within the seismic source region and the procedure in Woo (1996) is concentrated on spatially smoothing the magnitude dependent rate for each event within the considered catalogue. As mentioned in the introduction, the procedure given in Woo (1996) is adopted because the obtained occurrence rate of events with a large magnitude for sites near historical large seismic events is less sensitive to the assigned area of the source region. For the smoothing, the kernel function  $K(M_{s_j}, s - s_j)$ ,

$$K(M_{s_j}, s - s_j) = \frac{\alpha - 1}{\pi [H(M_{s_j})]^2} \left[ 1 + \left( \frac{|s - s_j|}{H(M_{s_j})} \right)^2 \right]^{-\alpha}, \quad (4.11)$$

suggested by Vere-Jones (1992) and used by others (Molina et al. 2001; Beauval et al. 2006; Xu and Gao 2012; Goda et al. 2013; Zuccolo et al. 2013; Feng et al. 2020) is considered, where  $M_{s_j}$  is the earthquake magnitude for the  $j$ -th event located at  $s_j$ ;  $s$  represents a point of interest within the considered seismic source region;  $\alpha$  equals 1.8 (Xu and Gao 2012); and,

$$H(M_{s_j}) = b_1 \exp(b_2 M_{s_j}), \quad (4.12)$$

in which  $b_1$  and  $b_2$  are model parameters to be estimated (Goda et al. 2013).

The earthquake annual occurrence rate for the  $k$ -th cell with its center defined by  $s_k$ ,  $\lambda_{c,k}(M_s)$ , is calculated using,

$$\lambda_{c,k}(M_s) = \sum_{j=1}^{n_E} I(M_{s_j} > M_s) \times K(M_{s_j}, s_k - s_j) / \Delta T_j, \quad (4.13)$$

where  $I(M_{s_j} > M_s)$  is an indicator function that equals 1 for  $M_{s_j} > M_s$  and 0 for  $M_{s_j} \leq M_s$ , respectively, and  $\Delta T_j = T_F - t_{C,j,p}$ . Typical values of  $\lambda_{c,k}(M_s = 4)$  and  $\lambda_{c,k}(M_s)$  by considering  $p = 0.16, 0.5$  and  $0.84$  and selected sites are shown in Figures 4.8 and 4.9.

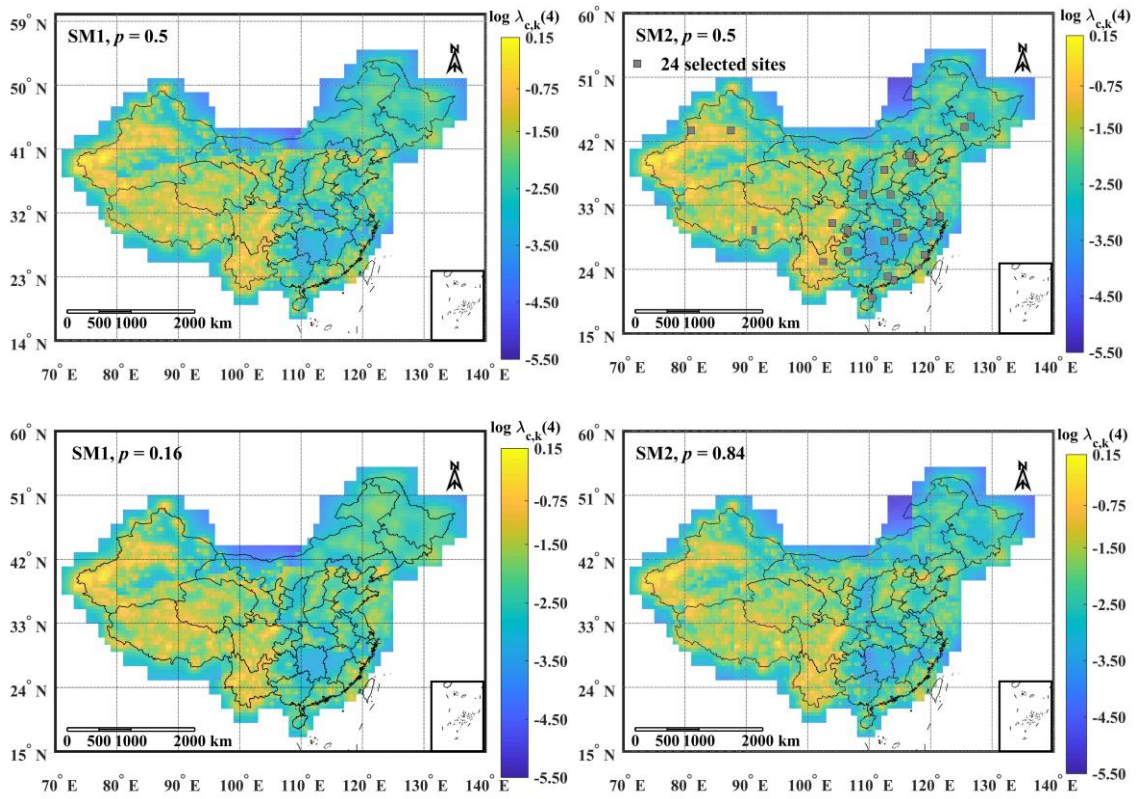


Figure 4.8. Spatially Smoothed  $\lambda_{c,k}(M_s = 4)$ . The first row is for  $p = 0.5$  and, SM1 and SM2. The left plot in the second row is for SM1 and  $p = 0.16$ , and the right plot for SM2 and  $p = 0.84$ .

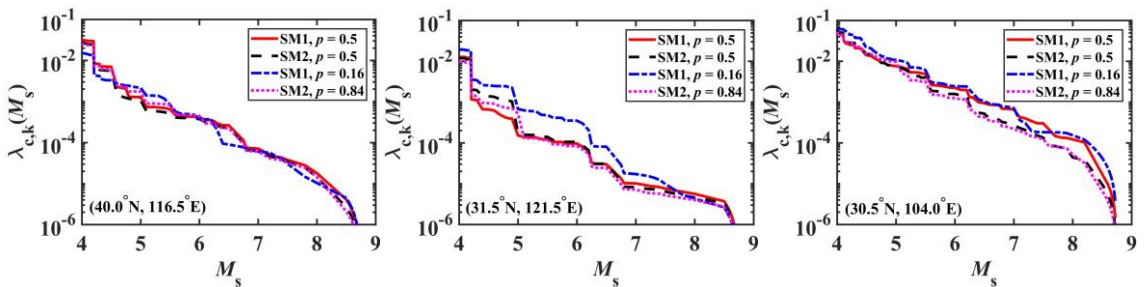


Figure 4.9.  $\lambda_{c,k}(M_s)$  for Beijing, Shanghai and Chengdu (from left to right) for selected  $p$  and seismic source model.

As can be observed from Figure 4.8, the spatial trends of  $\lambda_{c,k}(M_s = 4)$  for SM1 and SM2 are relatively consistent, although their values vary slightly for different  $p$  values. The



identified 24 cities on the map are to be considered in the following. The waving curves in Figure 4.9 representing  $\lambda_{c,k}(M_s)$  are typical of those obtained for spatially varying magnitude-recurrence relation. The plots illustrate that  $\lambda_{c,k}(M_s)$  is site-dependent and is a function of the selected  $p$  value. However,  $\lambda_{c,k}(M_s)$  is relatively insensitive to whether SM1 or SM2 is considered.

### 4.3.2 Seismic hazard assessment procedure

As can be observed from previous sections, an earthquake event occurs randomly in time and space with uncertain intensity. A combination of the source model, GMM and magnitude recurrence model that represents the seismic hazard model is uncertainty and is associated with a probability. The uncertainty in the selected models could be incorporated in assessing seismic hazard through a logic tree approach (McGuire 2004) as part of epistemic uncertainty (Budnitz *et al.*, 1997). The logic trees are shown in Figure 10 by considering the seismic source model (see Figures 4a and 4b), the magnitude recurrence relation model (see Figures 4.8 and 4.9), and the GMMs (e.g., ASK14-P, BSSA14-P, CB14-P, and CY14-P). These logical trees are considered in the present study.

Case 1 depicted in Figure 4.10 is used as the reference case. For this case, it is considered that each seismic source model presented in Figure 4.6 (i.e., SM1 and SM2) has an equal probability or weight of 0.5. The relative simple treatment of uncertainty in  $\lambda_{c,k}(M_s)$  caused by uncertainty in  $T_{C,j,p}$  is considered based on the two-point estimate method (Rosenblueth, 1975, 1981; Hong, 1998). This leads to using  $\lambda_{c,k}(M_s)$  based on  $t_{C,j,0.16}$  and  $t_{C,j,0.84}$  with an equal weight of 0.5. The considered GMMs are ASK14-P, BSSA14-P, CB14-P and CY14-P with an equal weight of 0.25. Although case 1 is the preferred case in the present study, additional trees that are considered as part of sensitivity analysis are also shown in Figure 4.10 and referred to as Cases 2 to 5. They are simplified versions of (or trimmed from) Case 1. Cases 2 to 5 are with decreased sophistication as compared to Case 1.

For the seismic hazard assessment, the simulation technique is employed and the earthquake occurrence is modelled as a Poisson process. In particular, for a given observation period of  $T_T$  years and a considered seismic source model (SM1 or SM2), following the simulation procedure for seismic hazard assessment in Hong et al. (2006), the occurrence of the earthquake events defined by their epicentral location, earthquake magnitude and occurrence time is simulated. For each event, an applicable GMM among all the considered models (i.e., ASK14-P, BSSA14-P, CB14-P and CY14-P), according to its epicentral location (i.e., whether it is located in ER, MR, XR or TR), is randomly selected based on the assigned weights. The simulated events together with their corresponding GMMs form the synthetic earthquake catalogue for the considered source model. Samples of PGA and SA for a site of interest is then calculated for each event in the synthetic catalogue using its corresponding GMM and a sampled value of its residual according to the probabilistic model of the residual. The samples are then used to form empirical probability distribution of the annual maximum of PGA or SA which is used to estimate their quantiles or return period values. For the case with multiple complete seismic source models such as Case 1 with SM1 and SM2, the empirical probability distributions of PGA and SA for SM1 and for SM2 are mixed according to the weights assigned to SM1 and SM2. The mixed empirical distribution of PGA or SA is then used to define the seismic hazard and UHS for the considered case.

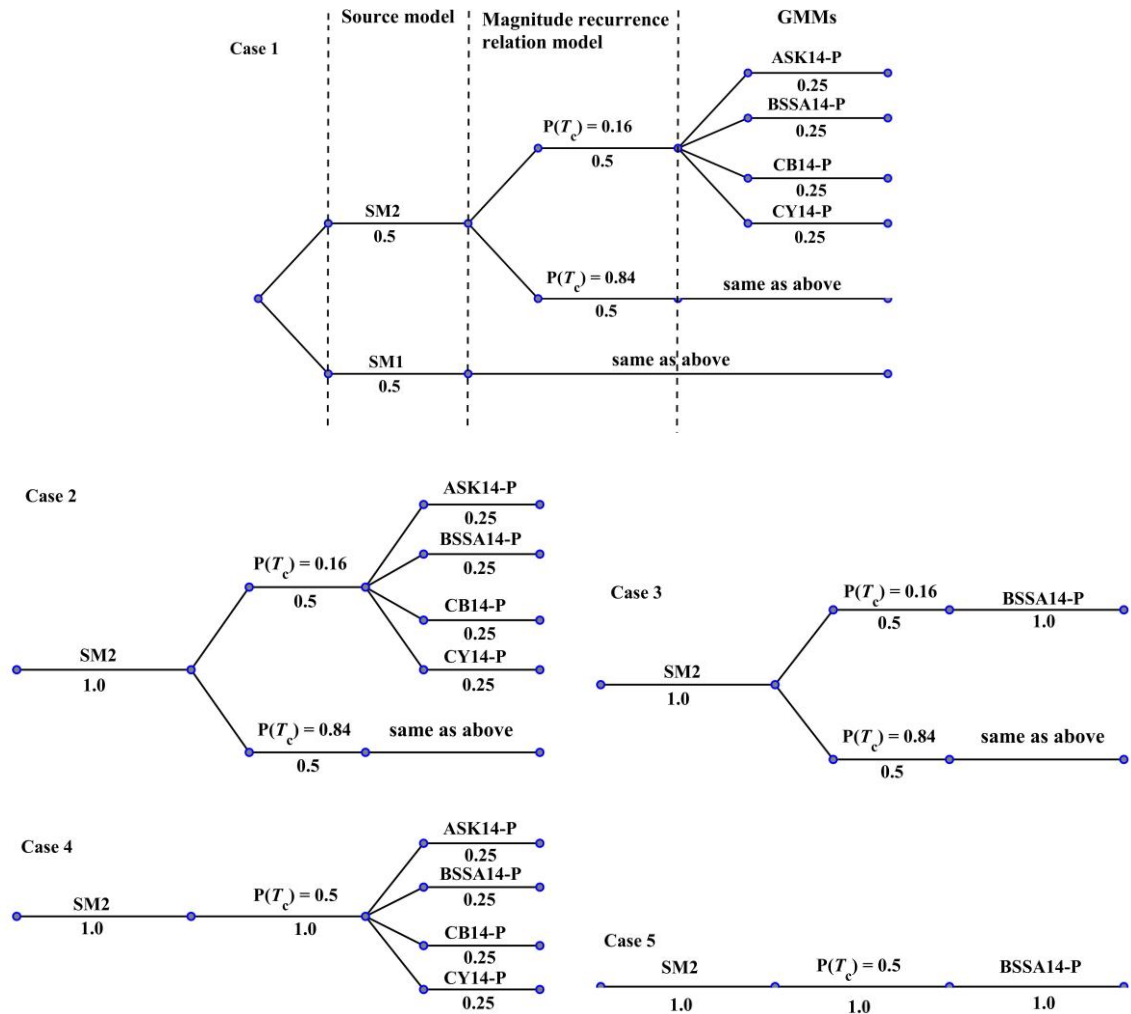


Figure 4.10. Considered five logic trees (Cases 1 to 5).

## 4.4 Estimated UHS and mapped seismic hazard

### 4.4.1 Estimated hazard and UHS for the reference case

Following the analysis procedure given in the previous section, an assessment of PGA is carried out for 24 selected sites that are identified in Figure 4.8 and listed in Table 4.3. Typical empirical probability distributions of the annual maximum PGA for a few of those identified sites are presented in Figure 4.11 on the lognormal probability paper. It can be observed from Figure 11. that the empirical probability distributions in the upper tail region could be approximated well by lognormally distributed random variables. The coefficient of variation (COV) of the distribution fitted to the upper tail region varies from

site to site. The estimated COV value from the fitted distribution to the upper tail ranges from 1.3 to 6.1 (see Table 4.3). The consideration of this spatially varying COV is important for the reliability-consistent calibration of seismic design load (Hong and Hong 2006).

Table 4.3. Estimated quantile values by considering 63%, 10% and 2% probability of exceedance in 50 years and 10% in 50 years value given in fifth-generation CSHM (Gao et al. 2015) (COV is calculated from the upper tail distribution fitting for Case 1).

City	(Lat °, Lon °)	COV	Case for $P_E = 63\%$					Case for $P_E = 10\%$					Case for $P_E = 2\%$					
			1	2	3	4	5	CSHM	1	2	3	4	5	1	2	3	4	5
			63%	63%	63%	63%	63%	10%	10%	10%	10%	10%	10%	2%	2%	2%	2%	2%
Harbin	(45.5°,126.5°)	2.5	0.03	0.03	0.04	0.03	0.03	0.10	0.10	0.10	0.11	0.10	0.10	0.21	0.20	0.23	0.19	0.22
Changchun	(44.0°,125.5°)	2.3	0.04	0.04	0.04	0.04	0.04	0.10	0.13	0.13	0.15	0.13	0.14	0.25	0.25	0.29	0.24	0.27
Nanchang	(28.5°,115.5°)	2.4	0.02	0.02	0.02	0.02	0.02	0.05	0.05	0.05	0.05	0.06	0.06	0.11	0.11	0.11	0.12	0.12
Changsha	(28.0°,112.5°)	6.1	0.01	0.01	0.01	0.01	0.01	0.05	0.06	0.06	0.06	0.07	0.08	0.13	0.13	0.14	0.17	0.20
Beijing	(40.0°,116.5°)	2.0	0.06	0.06	0.06	0.06	0.06	0.20	0.20	0.19	0.20	0.20	0.20	0.35	0.35	0.37	0.36	0.36
Shanghai	(31.5°,121.5°)	2.6	0.04	0.04	0.04	0.04	0.04	0.10	0.15	0.15	0.15	0.14	0.14	0.28	0.28	0.29	0.27	0.27
Shenzhen	(22.5°,114.0°)	2.8	0.04	0.04	0.04	0.04	0.04	0.10	0.16	0.16	0.18	0.16	0.18	0.30	0.30	0.33	0.31	0.33
Zhengzhou	(34.5°,113.5°)	3.1	0.04	0.04	0.04	0.04	0.04	0.15	0.15	0.14	0.15	0.14	0.15	0.29	0.29	0.30	0.28	0.30
Urumuqi	(43.5°,87.5°)	1.3	0.14	0.14	0.14	0.14	0.15	0.20	0.32	0.32	0.34	0.33	0.34	0.51	0.52	0.55	0.53	0.55
Yining	(43.5°,81.0°)	1.7	0.09	0.07	0.08	0.07	0.08	0.20	0.23	0.19	0.21	0.20	0.21	0.41	0.35	0.38	0.35	0.39
Lhasa	(29.5°,91.0°)	1.8	0.09	0.09	0.09	0.10	0.10	0.20	0.25	0.25	0.26	0.26	0.28	0.44	0.45	0.48	0.45	0.51
Chengdu	(30.5°,104.0°)	1.8	0.11	0.10	0.10	0.10	0.10	0.10	0.29	0.27	0.28	0.28	0.28	0.50	0.48	0.51	0.49	0.50
Tianjin	(39.0°,117.0°)	2.3	0.05	0.05	0.05	0.05	0.05	0.20	0.16	0.16	0.17	0.16	0.16	0.31	0.31	0.32	0.30	0.30
Chongqing	(29.5°,106.5°)	1.7	0.06	0.05	0.05	0.06	0.06	0.05	0.16	0.13	0.14	0.15	0.16	0.29	0.24	0.28	0.27	0.29
Xiamen	(24.5°,118.0°)	2.1	0.05	0.05	0.06	0.07	0.07	0.15	0.17	0.17	0.18	0.21	0.21	0.30	0.31	0.34	0.36	0.37
Guangzhou	(23.0°,113.0°)	2.8	0.03	0.03	0.03	0.03	0.03	0.10	0.12	0.12	0.12	0.12	0.13	0.24	0.23	0.25	0.23	0.25
Fuzhou	(26.0°,119.0°)	2.0	0.06	0.06	0.06	0.05	0.05	0.10	0.17	0.17	0.17	0.16	0.16	0.31	0.30	0.32	0.29	0.31
Taiyuan	(38.0°,112.5°)	1.7	0.08	0.08	0.09	0.10	0.10	0.20	0.24	0.24	0.25	0.26	0.26	0.41	0.41	0.42	0.43	0.44
Hangzhou	(30.5°,120.0°)	3.7	0.02	0.02	0.02	0.02	0.02	0.10	0.08	0.08	0.09	0.06	0.06	0.18	0.18	0.19	0.15	0.15
Xian	(34.5°,109.0°)	2.2	0.06	0.06	0.06	0.06	0.06	0.20	0.20	0.20	0.20	0.21	0.21	0.36	0.36	0.36	0.38	0.37
Kunming	(25.0°,102.5°)	1.5	0.13	0.13	0.13	0.13	0.14	0.20	0.32	0.32	0.34	0.32	0.35	0.54	0.56	0.58	0.54	0.58
Wuhan	(30.5°,114.5°)	2.9	0.02	0.03	0.03	0.02	0.02	0.05	0.08	0.08	0.09	0.07	0.07	0.17	0.17	0.19	0.15	0.16
Guiyang	(26.5°,106.5°)	2.3	0.03	0.03	0.03	0.03	0.03	0.05	0.08	0.09	0.09	0.09	0.09	0.16	0.17	0.18	0.17	0.19
Haikou	(20.0°,110.5°)	3.6	0.02	0.03	0.03	0.02	0.03	0.30	0.09	0.09	0.10	0.10	0.11	0.20	0.20	0.22	0.21	0.24

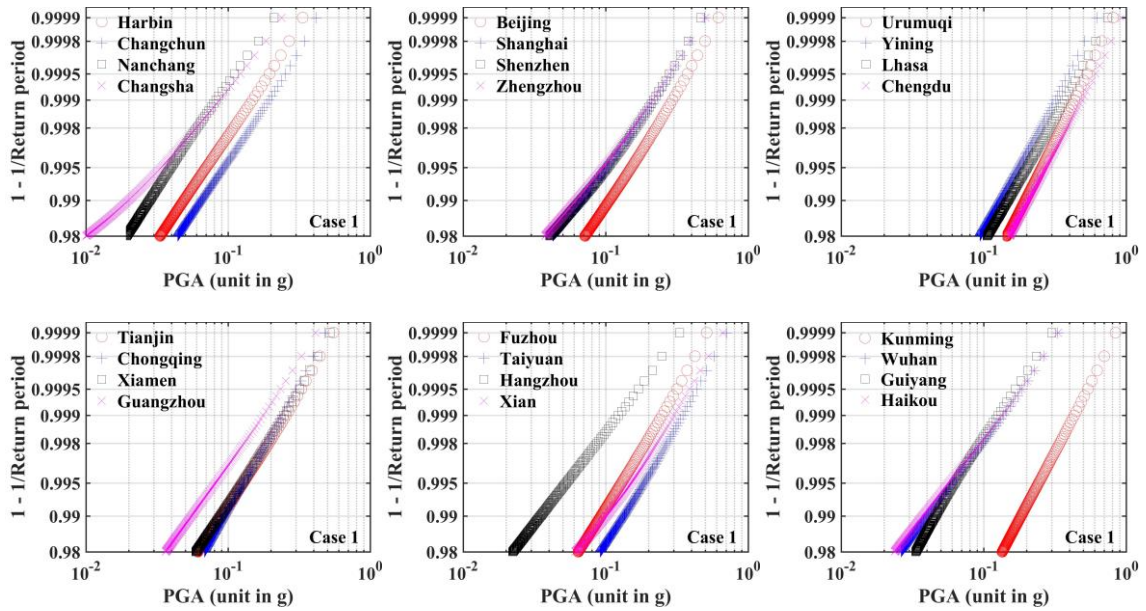


Figure 4.11. Empirical probability distributions of the annual maximum PGA at selected locations.

The estimated PGAs with an exceedance probability,  $P_E$ , equal to 63%, 10% and 2% in 50 years (i.e., 50-, 475-, and 2475-year return period values) are shown in Table 4.3 for the considered sites by using the empirical probability distributions obtained from the samples. In particular, 475-year return period values of PGA are compared with those suggested in the fifth-generation CSHM. The comparison indicates that, for most cases, the estimated values are close to those suggested in the fifth-generation CSHM. However, there are also large differences for some of the considered sites. For example, the estimated values for Chengdu and Chongqing are about 3 times of those suggested in the fifth-generation CSHM. Detailed inspection revealed that such large increases are due to the two historical events near Chengdu, the Wenchuan earthquake located at (31.01°N, 103.42°E) in 2008 and the Lushan earthquake located at (47.5°N, 30.3°E) in 2013. The epicentral distances to Chengdu are 99 and 79 km, respectively. For Chongqing, an earthquake with  $M_s$  of 5.3 and an epicentral distance of about 56 km occurred in 1989 contributed to the increased seismic hazard. The large decrease in the estimated seismic hazard for Haikou as compared to that given in the fifth-generation CSHM is caused by the removal of a historical event from the catalogue according to the completeness analysis results, where this event occurred in 1605

with an epicenter at about (20.0°N, 110.5°E),  $M_s$  of 7.5 and an epicentral distance of about 66 km to Haikou, Hainan island.

In general, the ratio of 2475-year return period value of PGA to that of 475-year return period value and to that of 50-year return period value varies spatially, with an average about 2 and 6 times, respectively.

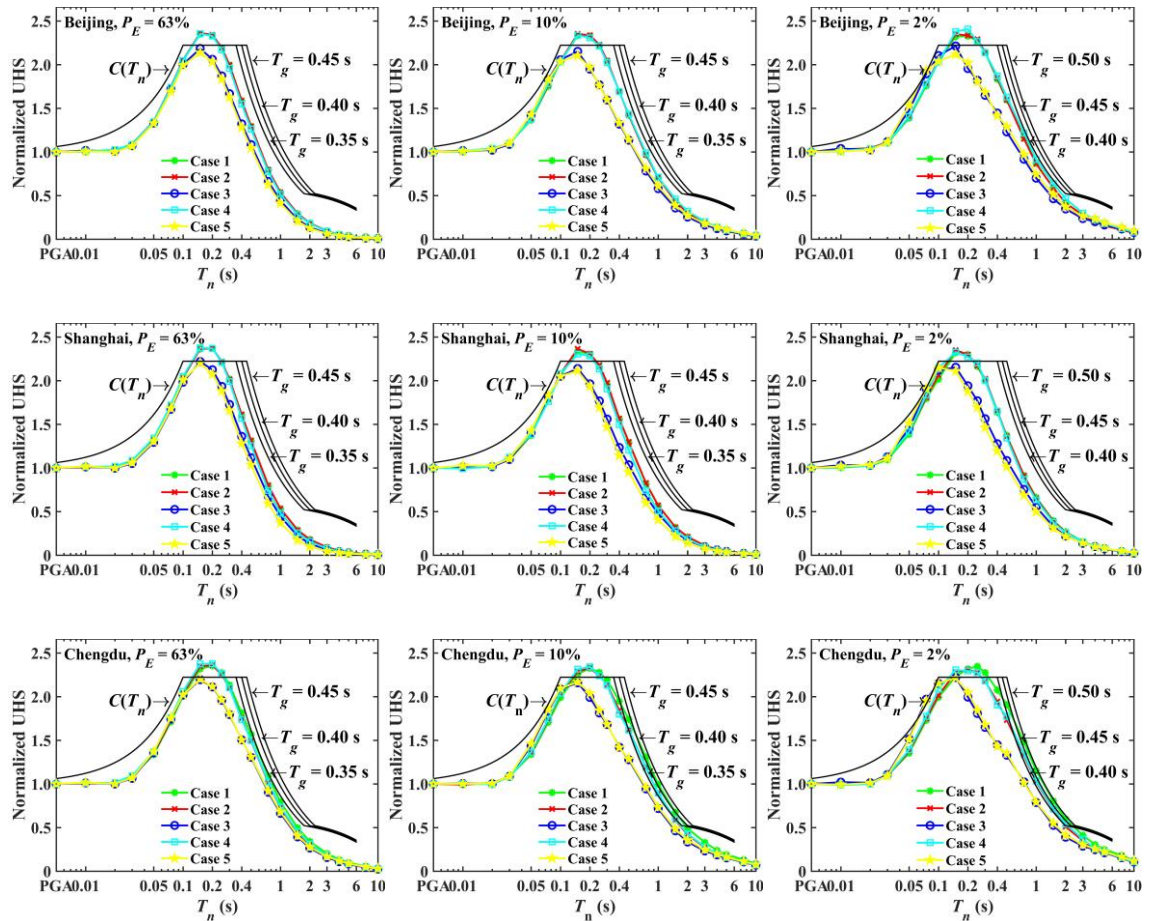


Figure 4.12. Standardized UHS for a few selected sites.

The analysis carried out for PGA is repeated for SA at different vibration periods. The estimated return period values of PGA and SA for each site are used to form UHS. Typical UHS are illustrated in Figure 4.12. For the plotting, the values of UHS are standardized by dividing its corresponding PGA value so the standardized UHS has a value of 1.0 at zero vibration period. Also, for comparison purpose the standard design spectrum  $C(T_n)$

recommended in GB50011 (2010) is also shown in the figure. The comparison suggests that the standardized UHS for the vibration period  $T_n$  outside of 0.1 to 0.2 s is always enveloped by  $C(T_n)$  which is consistent with that observed in Feng et al. (2020). For  $T_n$  within 0.1 to 0.2 s, the estimated UHS may exceed  $C(T_n)$ , the amplitude of exceedance is site-dependent. It must be emphasized that the results presented in Figure 4.12 alone cannot be used to infer that GB50011 (2010) is conservative or unconservative since the estimated PGA presented in Table 4.3 and the PGA suggested in GB50011(2010) differ. The results presented in Figure 4.12 simply indicates that the shape of the design spectrum in GB50011(2010) may not be appropriate and could be modified based on the obtained UHS for an improved reliability-consistent design.

By repeating the above mentioned seismic hazard assessment but for a squared grid system covering the mainland China, where the separation between two adjacent grid points equals  $0.5^\circ$ , the obtained hazard maps are presented in Figures 4.13 for PGA and in Figure 4.14 for SA. The results presented in the Figure 4.14. indicate that in general, the spatial trends of the seismic hazard map are similar for different exceedance probabilities, and for PGA and SA.

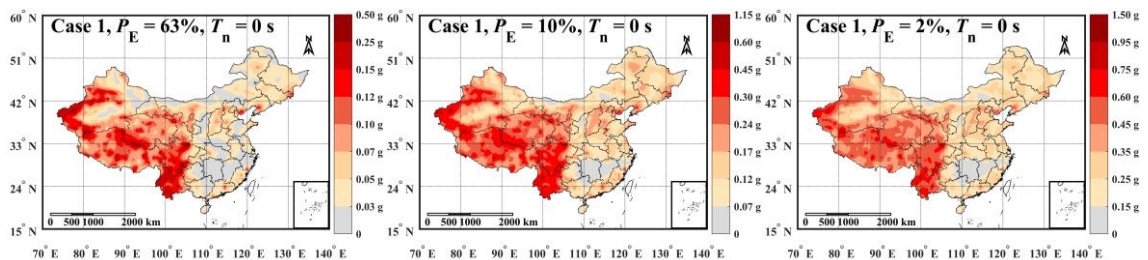


Figure 4.13. Seismic hazard map for Case 1 based on SA for  $P_E = 63\%$ , 10% and 2% in 50 years.



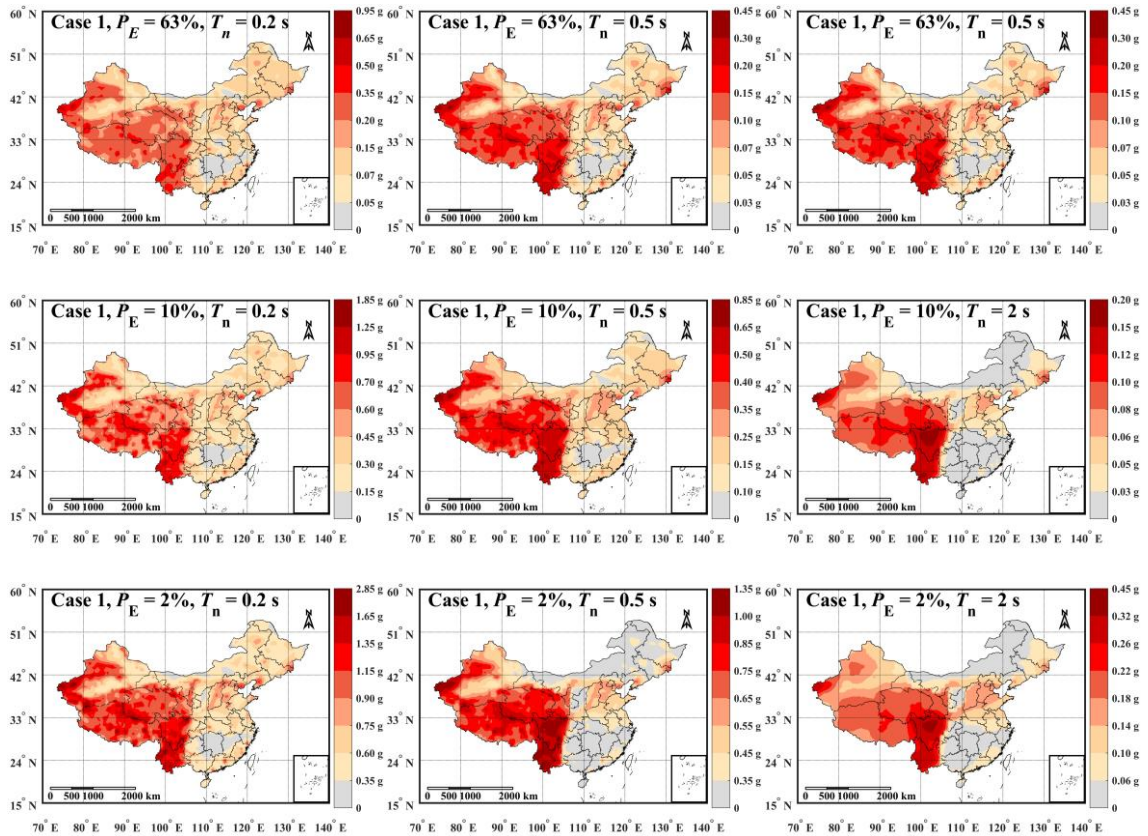


Figure 4.14. Seismic hazard map for Case 1 Based on SA  $P_E = 63\%$ ,  $10\%$  and  $2\%$  in 50 years.

#### 4.4.2 Sensitivity analysis and discussion

In this section, a sensitivity analysis is carried out by considering the logic trees shown in Figure 4.10 for Cases 2 to 5. The estimated seismic hazard in terms of PGA and for  $P_E = 63\%$ , for the 24 cities listed in Table 4.3 is also presented in Table 4.3. A clear feature of these results is that the results obtained by using simple or sophisticated logic trees shown in Figure 4.10 lead to a very consistent seismic hazard estimate. It reflects the consistency in the considered SM1 and SM2 (with their corresponding magnitude-recurrence options) and in the consistency of the GMMs.

The obtained seismic hazard values for Cases 2 to 5 are used to construct the normalized UHS and compared with Case 1 and  $C(T_n)$  shown in Figure 4.12. This comparison again

indicates the similarity among the results obtained by the considered Cases 1 to 5. Moreover, in all cases, the observations made earlier for the comparison of the results between Case 1 and  $C(T_n)$  are equally applicable to the results obtained for Cases 2 to 5. However, the estimated UHS may or may not exceed  $C(T_n)$  depending on the considered GMM and the considered site.

Finally, sets of seismic hazard maps are obtained based on the logic trees for Cases 2 to 5. Typical hazard maps are compared in Figure 4.15. A visual inspection of the results shown in Figures 4.14 and 4.15 indicates that their spatial trends are very similar. By calculating the relative difference between any pair of the maps of PGA shown in these figures, the relative difference is less than 15%.

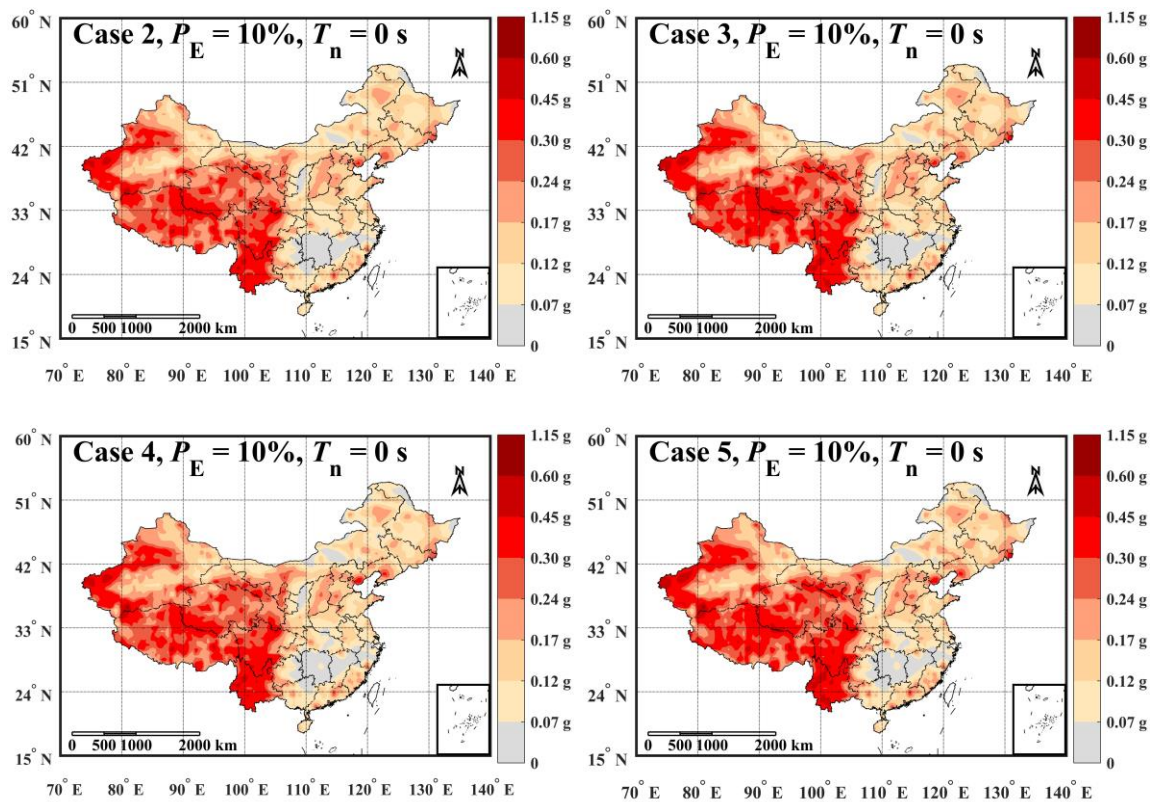


Figure 4.15. Comparison of seismic hazard maps for Cases 2 to 5  $P_E = 10\%$  in 50 years.

## 4.5 Conclusions

The lack of instrumental ground-motion data for sufficient moderate and large earthquakes

in mainland China hindered the development of the ground motion models (GMMs) and the so-called projection method has been applied to develop GMMs used in estimating the CSHMs. By following this procedure, sets of projected GMMs applicable to different seismic regions in mainland China was carried out by using the four sets of GMMs from the NGA-West2 as the reference GMMs. It was shown that, in general, these models are comparable. A comparison of the median value of the projected GMMs to the instrumental ground-motion data is used to support these newly projected GMMs. However, in terms of PGA, they differ from the GMMs employed for the mapping of the fifth generation of CSHM.

By using these projected GMMs, spatially smoothed seismicity based on historical earthquake catalogue, and developed logic trees, the estimation of the seismic hazard for mainland China is carried out. The results indicate that the estimated PGA for the probability of exceedance of 10% in 50 years agrees with that reported in the fifth-generation CSHM at many sites. However, discrepancies between the estimated PGA and that reported in the CSHM are also observed for several major cities (e.g., Chengdu, Chongqing, Haikou). The ratio between the former to the latter can be as high as 3 and as low as 0.3, which could impact the estimated seismic risk of these major cities.

In general, the coefficient of variation of the annual maximum PGA is spatially varying and ranges from 1.3 to 6.1, which is important to develop enhanced reliability consistent seismic design requirements. In addition, it was observed that the estimated shape of the UHS for regions with a significant seismic hazard is relatively consistent. However, the shape differs from the standardized seismic design spectrum recommended in the Chinese design codes. This suggests that an investigation on updating the standard design spectrum may be warranted.

In general, the spatial trends of the obtained seismic hazard maps by considering different logic trees presented in this chapter are similar. The trends also compare favourably to the fifth-generation of CSHM which is given in terms of PGA. Since an official seismic hazard map in terms of SA applicable to mainland China is currently unavailable, the maps of SA for the exceedance probability of 63% 10% and 2% in 50 years reported in the

presented study could serve as a yardstick for future endeavours in mapping seismic hazard in mainland China.

### **Data availability statement**

Some or all data, models or code generated or used during the study are available from the corresponding author by request. These include all model coefficients for the projected GMMs, estimated seismic hazard and site-specific standardized UHS.

## **4.6 References**

- Abrahamson, N.A., Silva, W.J., and Kamai, R. 2013. *Update of the AS08 ground motion prediction equations based on the NGA-Wet2 data set*. PEER Report No. 2013/04, Pacific Earthquake Engineering Research Center, University of California, Berkeley.
- Abrahamson, N.A., Silva, W.J., and Kamai, R. 2014. "Summary of the ASK14 ground motion relation for active crustal regions." *Earthquake Spectra*, 30 (3): 1025-1055.
- Albarelo, D., Camassi, R., and Rebez, A. 2001. "Detection of space and time heterogeneity in the completeness of a seismic catalog by a statistical approach: An application to the Italian area." *Bull. Seism. Soc. Am.* 91 (6): 1694-1703.
- Atkinson, G.M., and Boore, D.M. 1995. "Ground-motion relations for eastern North America." *Bull. Seismol. Soc. Am.* 85 (1): 17-30.
- Beauval, C., Scotti, O., and Bonilla, F. 2006. "The role of seismicity models in probabilistic seismic hazard estimation: comparison of a zoning and a smoothing approach." *Geophysical Journal International*. 165 (2): 584-595.
- Boore, D. M., J.P. Stewart, E. Seyhan, and G.M. Atkinson (2013). *NGA-West2 Equations for Predicting Response Spectral Accelerations for Shallow Crustal Earthquakes*, PEER Report No. 2013/05, Pacific Earthquake Engineering Research Center, University of California, Berkeley, CA.
- Boore, D.M., Stewart, J.P., Seyhan, E., and Atkinson, G.M. 2014. "NGA-west2 Equations for predicting PGA, PGV and 5% Damped PSA for Shallow Crustal Earthquakes."

*Earthquake Spectra*. 30 (3): 1057-1085.

Budnitz, R.J., Apostolakis, G., and Boore, D.M. 1997. *Recommendations for probabilistic seismic hazard analysis: guidance on uncertainty and use of experts*. OSTI.GOV Technical report No. NUREG/CR-6372-Vol. 1; UCRL-ID-122160. Nuclear Regulatory Commission, Washington, DC, United States. Div. of Engineering Technology; Lawrence Livermore National Lab., CA, United States; Electric Power Research Inst., Palo Alto, CA, United States; USDOE, Washington, DC, United States.

Campbell, K.W., and Bozorgina, Y. 2013. *NGA-West2 Campbell- Bozorgina ground motion model for the horizontal component of PGA, PGV, and 5%-damped elastic pseudo acceleration response spectra for periods ranging from 0.01 to 10 s*. PEER Report No. 2013/06, Pacific Earthquake Engineering Research Center, University of California, Berkeley.

Campbell, K.W., and Bozorgina, Y. 2014. "NGA-West2 ground motion model for the average horizontal component of PGA, PGV, and 5%-damped linear acceleration response spectra." *Earthquake Spectra*, 30 (3): 1087-1115.

Chiou, B.S.-J, and Youngs, R. 2013. *Update of the Chiou and Youngs NGA ground motion model for average horizontal components of peak ground motion and response spectra*. PEER Report No. 2013/07, Pacific Earthquake Engineering Research Center, University of California, Berkeley.

Chiou, B.S.-J, and Youngs, R. 2014. "Update of the Chiou and Youngs NGA model for the average horizontal components of peak ground motion and response spectra." *Earthquake Spectra*. 30 (3): 1117-1153.

Cornell, C.A. 1968. "Engineering seismic risk analysis." *Bull. Seism. Soc. Am.* 58 (5): 1583-1606.

Dangkua, D.T., Rong, Y., and Magistrale, H. 2018. "Evaluation of NGA - West2 and Chinese Ground - Motion Prediction Equations for Developing Seismic Hazard Maps of Mainland China". *Bull. Seism. Soc. Am.* 108 (5A): 2422-2443.

- Ekström, G., and Dziewonski, A.M. 1988. "Evidence of bias in estimation of earthquake size." *Nature*, 332: 319-324.
- Esteva, L. 1968. *Bases para la formulación de decisiones de diseño sísmico*. Ph.D's thesis, Instituto de Ingeniería, Universidad Nacional Autónoma de México. (In Spanish)
- Feng, C., Liu, T.J., and Hong, H.P. 2020. "Seismic hazard assessment for mainland China based on spatially smoothed seismicity." *J. of Seismology*, DOI: 10.1007/s10950-020-09918-3.
- Frankel, A. 1995. "Mapping seismic hazard in the central and eastern United State." *Seism. Res. Lett.* 66 (4): 8-21.
- Gao, M.T., Li, X.J., Xu, X.W., Wei, .B., Yu, Y.X., Zhou, B.G., Zhao, F.X., Pan, H., Lü, Y.J., Zhou, Q., Wu, J., Lu, D.W., Chen, K., Li, Y.X., Gao, Z.W. 2015 *GB18306-2015: Introduction to the seismic hazard map of China*. Standards Press of China, Beijing, China. (in Chinese).
- GB50011-2010. 2010. *Code for seismic design of buildings*. Ministry of Housing and Urban-Rural Development of the People's Republic of China (MOHURD), Beijing, China.
- Goda, K., Aspinall, W., and Taylor, C.A. 2013. "Seismic hazard analysis for the UK: Sensitivity to spatial seismicity modelling and ground motion prediction equations." *Seismological Research Letters*. 84 (1): 112-129.
- Goda, K., Hong, H.P., and Atkinson, G.M. 2010. "Impact of using updated seismic information on seismic hazard in Western Canada." *Canadian Journal of Civil Engineering*, 37 (4): 562-575.
- Hong, H.P., and Feng, C. 2019. "On the ground-motion models for Chinese seismic hazard mapping." *Bull. Seism. Soc. Am.* <https://doi.org/10.1785/0120180269>.
- Hong, H.P. and Hong, P. 2006 "Reliability-consistent seismic design load contour maps." 9<sup>th</sup> Canadian Conference on Earthquake Engineering, Ottawa, Ontario, Canada, 26-29,

June, 2007.

- Hong, H.P., Goda, K., and Davenport, A.G. 2006. "Seismic hazard analysis: a comparative study." *Canadian Journal of Civil Engineering*. 33 (9): 1156-1171.
- Hong, H.P. 1998. "An efficient point estimate method for probabilistic analysis." *Reliability Engineering & System Safety*. 59 (3): 261-267.
- Howell, B.F., and Schultz, T.R. 1975. "Attenuation of modified Mercalli intensity with distance from the epicenter." *Bull. Seismol. Soc. Am.* 65: 651-665.
- Hu, Y.X., Gao, M.T., Du, W., Jin, Y., Zhao, F.X., Zou, Q.J., Tao, Y.L., Zhou, B.G. 2001. *GB18306-2001: Introduction to China ground motion parameter zoning map*. Standards Press of China, Beijing, China. (in Chinese).
- Hu, Y.X., and Zhang, M.Z. 1984. "A method of predicting ground motion parameters for regions with poor ground motion data." *Earthquake Engineering and Engineering Vibration*. 4 (1): 1-11. (in Chinese)
- Huang, C., and Galasso, C. 2019. "A comparison of NGA-West2 ground-motion models to recent Chinese data." *Soil Dynamics and Earthquake Engineering*. 125 (10): 56-77.
- Idriss, I.M. 2013. *NGA-West2 model for estimating average horizontal value of pseudo-absolute spectral accelerations generated by crustal earthquakes*. PEER Report No. 2013/08, Pacific Earthquake Engineering Research Center, University of California, Davis.
- Idriss, I.M. 2014. "An NGA-West2 model empirical model for estimating the horizontal spectral values generated by shallow crustal earthquakes." *Earthquake Spectra*. 30 (3): 1155-1177.
- Kaklamanos, J., Baise, L.G., and Boore, D.M. 2014. "Technical note: Estimating unknown input parameters when implementing the NGA ground motion prediction equations in engineering practice." *Earthquake Spectra*. 27 (4): 1219-1235.

- Kanamori, H. 1977. "The energy release in great earthquakes." *Journal of Geophysical Research*, 82 (20): 2981-2987.
- Li, X.J., Zhou, Z.H., Yu, H.Y., Wen, R.Z., Lu, D.W., Huang, M., Zhou, Y.N., and Cui, J.W. 2008. "Strong motion observations and recordings from the great Wenchuan earthquake." *Earthquake Engineering and Engineering Vibration*. 7 (3): 235-246.
- Liu H.X. 1987. "On the seismic zoning map China." Proceedings of International Seminar on Seismic Zonation." Beijing, China, pp. 35-42, 6-10, December. (in Chinese)
- Liu, R.F., Chen, Y.T., Ren, X., Xu, Z.G., Sun, L., Yang, H., Liang, J.H., and Ren, K.X. 2006. "Comparison between different earthquake magnitudes determined by China seismograph network." *Acta Seismologica Sinica* 29 (5): 467-476.
- Lü, H.S., Zhao, F.X. 2007. "Site coefficients suitable to China site category." *Acta Seismologica Sinica*. 29 (1), 71 - 79.
- MacQueen J. 1967. Some methods for classification and analysis of multivariate observations. In Proceedings of the fifth Berkeley symposium on mathematical statistics and probability, Vol. 1(4): 281-297, California.
- McGuire, R.K. 2004. *Seismic Hazard and Risk Analysis*. EERI Monograph MNO-10, Earthquake Engineering Research Institute, Oakland, California.
- Molina, S., Lindholm, C.D., and Bungum, H. 2001. "Probabilistic seismic hazard analysis: zoning free versus zoning methodology." *Bollettino di Geofisica* (selected papers from the 27th ESC, Lisbon, 2000), 42: 19-39.
- NBCC. 2015. *National Building Code of Canada 2015*. Institute for Research in Construction, National Research Council of Canada, Ottawa, Ont.
- Rosenblueth, E. 1975. "Point estimates for probability moments." *Proceedings of the National Academy of Sciences*. 72 (10): 3812-3814.
- Rosenblueth, E. 1981. "Two-point estimates in probabilities." *Applied Mathematical*



- Modeling*. 5 (5): 329-335.
- Scherbaum, F., Schmedes, J., and Cotton, F. 2004. "On the conversion of source-to-site distance measures for extended earthquake source models." *Bull. Seismol. Soc. Am.* 94, 1053-1069.
- Vere-Jones, D. 1992. *Statistical methods for the Description and Display of Earthquake Catalogs*. Statistics in Environmental and Earth Sciences, Edward Arnold, London, 220-246.
- Wang, S.Y., Yu, Y.X., Gao, A.J., and Yan, X.J. 2000. "Development of attenuation relations for ground motion in China." *Earthquake Research in China*, 16 (2), 99-106. (in Chinese)
- Weichert, D.H. 1980. Estimation of the earthquake recurrence parameters for unequal observation periods for different magnitudes. *Bull. Seism. Soc. Am.*, 70(4): 1337-1346.
- Wells, D.L., and Coppersmith, K.J. 1994. New empirical relationships among magnitude, rupture length, rupture length, rupture width, rupture area, and surface displacement. *Bull. Seism. Soc. Am.* 84 (4): 974-1002.
- Woo, G 1996. "Kernel estimation methods for seismic hazard area source modeling." *Bull. Seism. Soc. Am.* 86 (2): 353-362.
- Xu, W.J. 2019. "Probabilistic seismic hazard assessment using spatially smoothed seismicity in North China seismic zone." *Journal of Seismology*. 23 (3): 613-622.
- Xu, W.J., and Gao, M.T. 2012. "Seismic hazard estimate using spatially smoothed seismicity model as spatial distribution function." *Acta Seismological Sinica*. 34 (4): 525-536 (in Chinese).
- Xu, W.J., and Gao, M.T. 2014. "Statistical analysis of the completeness of earthquake catalog in China mainland." *Chinese Journal of Geophysics*. 57 (8): 2802-2812 (in Chinese).
- Yu, Y.X., Li, S.Y., and Xiao, L. 2013. "Development of ground motion attenuation relations for the new seismic hazard map of China." *Technology for earthquake disaster prevention*. 8 (1): 24-33 (in Chinese).

Zuccolo, E., Mirko, C., and Lai, C.G. 2013. "Probabilistic seismic hazard assessment of Italy using kernel estimation methods." *Journal of Seismology*. 17 (3): 1001-1020.

## Chapter 5

### 5 Conclusions and Potential for Future Work

#### 5.1 Conclusions

In this thesis, new sets of GMMs are developed for mainland China based on the projection method, which transforms the GMMs for a reference region to the target region. For the development of the GMMs applicable to each of the four seismic regions in mainland China, the GMMs and IPE applicable to the Western U.S. are considered. Moreover, two seismic source models are developed based on the spatial smoothing technique and historical earthquake catalogue. The newly projected GMM and the spatial smoothed seismic source models are used to map seismic hazard for mainland China and to develop uniform hazard spectra (UHS).

The major conclusions from the study include:

1. A critical review of the GMMs used for developing the fourth-generation and fifth-generation CSHMs indicates that the assigned standard deviations of the residuals for the GMMs are consistently small.
2. The median of the mapped GMMs based on those given by Boore et al. (2013, 2014) (referred to as BSSA14-P) compare favorably to that used for the development of the fifth-generation CSHM. This provides confidence that the projected BSSA14-P for predicting SA could be applied for China.
3. It is found that the sigma for BSSA14-P is about 10%-20% greater than the GMMs used for the development of the CSHM. The effect of the sigma on the estimated seismic hazard for simple seismic source zones is investigated, and it is found that the increase in sigma is likely to cause an increase in the estimated return period value of the annual maximum PGA and affect the seismic hazard mapping.
4. Four additional sets of GMMs are projected based on the models reported in NGA-West2 (Abrahamson et al. 2013, 2014; Campbell and Bozorgnia 2013, 2014; Chiou

and Youngs 2013, 2014; Idriss 2013, 2014). These projected models are referred to as ASK14-P, CB14-P, CY14-P, and IM14-P. The comparison of the predicted PGA and SA by using all the projected GMMs indicates that they are similar, although there are differences. Most importantly, the predicted median agree well with those observed or calculated from the limited historical records applicable to mainland China. This, again, indicates that the use of the projected GMMs for mainland China is adequate.

5. Two seismic source models are developed based on the spatial smoothing technique. The first one is developed based on spatial smoothing of the occurrence rate and assuming that the magnitude-recurrence relation for an identified cluster (or a region) remains to be the same. The second one is developed by smoothing the historical events by considering its magnitude, resulting in that the magnitude-recurrence relation is spatially varying. There are similar spatial trends between earthquake occurrence rates predicted by these two models. However, the value of the occurrence rate can differ.

6. The use of the newly projected GMMs and developed seismic source models for hazard mapping is carried out for mainland China. The obtained return period values of PGA in most cases agree well with those given in the fifth-generation CSHM. As there are no maps of SA reported for mainland China, the hazard maps of SA given in this study are new.

7. New UHS applicable to mainland China are developed for the first time. By normalizing these UHS, it is shown that the normalized seismic design spectra given in GB50011 (2010) are conservative, except for  $T_n$  about within 0.1 to 0.2 s. This can be important since it suggests that the normalized seismic design spectra recommended in the code could be modified to provide a more hazard consistent design.

8. Parametric analysis by considering different combinations of GMMs, magnitude-recurrence relations indicates that, in general, the estimated seismic hazard agrees well with that reported by fifth-generation CSHM at many sites. However, a relatively large difference between the estimated seismic hazard and that reported by CSHM is observed at a few sites (e.g., at Chengdu, Chongqing, and Haikou). This suggests that the fifth-generation CSHM needs to be further scrutinized and validated.

## 5.2 Potential future work

The following future work could be of value:

- 1) An analysis of the standard deviation of the residual of the GMMs based on the historical records for events that occurred in China would be valuable once the data becomes well documented and available.
- 2) Valuable insights can be gained if the detailed information on the delineated source model used to develop the fifth-generation CSHM becomes available and is used together with the newly projected GMMs to map seismic hazard for mainland China.
- 3) An extension of the present study by including seismic risk and optimum structural design can provide valuable information to decision-makers to make informed decisions to reduce seismic risk, and to structural design code committees to improve current codified structural design practice.

## 5.3 References

- Abrahamson, N.A., Silva, W.J., and Kamai, R. (2013). Update of the AS08 ground motion prediction equations based on the NGA-Wet2 data set. PEER Report No. 2013/04, Pacific Earthquake Engineering Research Center, *University of California, Berkeley*.
- Abrahamson, N.A., Silva, W.J., and Kamai, R. (2014). Summary of the ASK14 ground motion relation for active crustal regions. *Earthquake Spectra*, 30 (3): 1025-1055.
- Boore, D. M., J.P. Stewart, E. Seyhan, and G.M. Atkinson (2013). NGA-West2 Equations for Predicting Response Spectral Accelerations for Shallow Crustal Earthquakes, PEER Report No. 2013/05, Pacific Earthquake Engineering Research Center, *University of California, Berkeley*.
- Boore, D.M., Stewart, J.P., Seyhan, E., and Atkinson, G.M. (2014). NGA-west2 Equations for predicting PGA, PGV and 5% Damped PSA for Shallow Crustal Earthquakes. *Earthquake Spectra*. 30 (3): 1057-1085.

- Campbell, K.W., and Bozorgina, Y. (2013). NGA-West2 Campbell- Bozorgina ground motion model for the horizontal component of PGA, PGV, and 5%-damped elastic pseudo acceleration response spectra for periods ranging from 0.01 to 10 s. PEER Report No. 2013/06, Pacific Earthquake Engineering Research Center, *University of California, Berkeley*.
- Campbell, K.W., and Bozorgina, Y. (2014). NGA-West2 ground motion model for the average horizontal component of PGA, PGV, and 5%-damped linear acceleration response spectra. *Earthquake Spectra*, 30 (3): 1087-1115.
- Chiou, B.S.-J, and Youngs, R. (2013). Update of the Chiou and Youngs NGA ground motion model for average horizontal components of peak ground motion and response spectra. PEER Report No. 2013/07, Pacific Earthquake Engineering Research Center, *University of California, Berkeley*.
- Chiou, B.S.-J, and Youngs, R. (2014). Update of the Chiou and Youngs NGA model for the average horizontal components of peak ground motion and response spectra. *Earthquake Spectra*. 30(3): 1117-1153.
- GB50011-2010. (2010). Code for seismic design of buildings. *Ministry of Housing and Urban-Rural Development of the People's Republic of China* (MOHURD), Beijing, China.
- Idriss, I.M. (2013). NGA-West2 model for estimating average horizontal value of pseudo-absoulte spectral accelerations generated by crustal earthquakes. PEER Report No. 2013/08, Pacific Earthquake Engineering Research Center, *University of California, Davis*.
- Idriss, I.M. (2014). An NGA-West2 model empirical model for estimating the horizontal spectral values generated by shallow crustal earthquakes. *Earthquake Spectra*. 30(3): 1155-1177.

## Appendix

### Appendix A: A summary for the Chinese GMMs

The available Chinese ground motion models (GMMs) are summarized in this Appendix , 37 GMMs proposed from 1984 to 2016 are given in this section. The summary focused on the employed recordings for the development of the GMMs, the range of applicability and the model coefficients for the GMMs.

#### **A1 Xu et al. (1984)**

The GMM is:

$$Y = A \exp(BM)(R + R_0)^C,$$

where  $Y$  represents the PGA in  $g$  and PGV in  $\text{cm/s}$ , respectively,  $A$ ,  $B$ ,  $C$  and  $R_0$  are the model coefficients, the coefficients of GMM for PGA,  $A = 0.1548$ ,  $B = 0.5442$ ,  $C = -1.002$ ,  $R_0 = 8$ ; and for PGV,  $A = 0.142$ ,  $B = 1.371$ ,  $C = -1.286$ ,  $R_0 = 2$ ,  $M$  denotes moment magnitude, note if moment magnitude is not available,  $M = M_L$  (local magnitude) is applied for  $M < 6.0$ ; and  $M = M_s$  is applied for  $M \geq 6.0$ ,  $R$  accounts for epicentral distance in km.

- The recordings that used for the developed GMMs are based on the aftershocks for 1975 Haicheng earthquake, mainshock and aftershocks for 1976 Tangshan earthquake. Note that most of the recordings are from the aftershocks for 1975 Haicheng earthquake.
- The applicable magnitude for the proposed GMM is ranging from 4 to 6.5, the applicable epicentral distance is no greater than 100 km.
- The recordings for the larger of the two horizontal components are used, and the recordings with peak acceleration smaller than 0.05g are excluded for the development of the GMMs.
- The number of the recordings that used for the development of the GMMs for PGA and PGV are 19 and 17. Due to the small number of the employed recordings, the simple linear regression approach is used to estimate the model coefficients.

- Compared with the GMMs that proposed by Boore and Joyner (1981) and Campbell (1981), the comparison suggested that the possibility of using western North America GMMs for earthquake events occurred in Northern China that exceed the applicable magnitude and distance range of the GMM.

## **A2 Peng et al. (1985a)**

The GMM is:

$$Y = \alpha \cdot 10^{(\beta M + \gamma R + \sigma)} / R,$$

- where the  $Y$  denotes PGA in  $g$ ,  $R = \sqrt{\Delta^2 + h^2}$  is in km and  $M$  is local magnitude,  $\Delta$  is epicentral distance,  $\alpha$ ,  $\beta$ , and  $\gamma$  are the model coefficients,  $\sigma$  accounts for the standard deviation of the logarithm of the predicated value,  $\sigma = 0.32$ ;  $h = 9.4$  and  $\sigma = 0.36$ ;  $h = 6.7$  are for logarithm of the predicated value based on horizontal and vertical GMMs, respectively.

For horizontal GMM:

$$\log A_m(H) = -1.49 + 0.31M - \log R - 0.0248R,$$

For vertical GMM:

$$\log A_m(V) = -1.92 + 0.29M - \log R - 0.0146R,$$

- 93 horizontal ground-motion recordings (larger of the two horizontal components) for 19 earthquakes with magnitudes ranging from 2.9 to 5.3 are used for the development of the horizontal GMM.
- 87 vertical ground-motion recordings for 19 earthquake events are employed for the development of the vertical GMMs.
- A description for the strong-motion array and a few representative near-source strong motion recordings recorded by the strong-motion array are presented in the study. There are 603 near-source three-component accelerograms that recorded by the strong-motion



array. The recordings are from 243 earthquakes with local magnitude ranging from 1.2 to 5.3 (25 events with magnitude larger than 4).

- Note the experimental strong-motion array is deployed in the meizoseismal area of 1976 Tangshan earthquake. All the instruments are installed in small, light shelters to minimize the effects that caused by the buildings.
- A two-stage regression method is employed based on Joyner and Boore (1981). Due to the observed severe bias for the regression results, the reported magnitudes of the earthquake events are reduced by 0.5 for events with magnitudes greater than 3.2 (except October 19, 1982 Lulong earthquake)
- Compared with the GMM given by Boore (1983) for western North America, it is found that the magnitude scaling factors for two regions are similar, while the distance attenuation factors for Tangshan region is larger than that for western North America.

### **A3 Hu et al. (1986)**

The GMM is:

$$\ln Y = c_0 + c_1 M + c_2 \ln(R + R_0),$$

where  $Y$  represents SA (spectral acceleration for SDOF system with damping ratio,  $\xi = 0.05$ ) or PGA in g,  $M$  is earthquake magnitude,  $R$  represents hypocentral distance in km,  $R_0$  is a constant value,  $c_0$ ,  $c_1$  and  $c_2$  are the model coefficients, the coefficients of GMM for PGA are  $c_0 = 1.078$ ,  $c_1 = 0.576$ ,  $c_2 = -1.88$ , and  $R_0 = 10$ .

- The GMMs are developed based on the projection method that proposed by Hu and Zhang (1984).
- The IPE is developed for Huabei region based on the isoseismal contour lines of the earthquake events occurred in Huabei.
- The GMMs are developed for rock site condition.

- Note the model coefficients of GMMs for SA are also given in Hu et al. (1996).
- The developed GMMs are comparable with the ground-motion recordings for the aftershocks of Tangshan earthquake.

#### **A4 Ding et al. (1988)**

The GMM is:

$$\ln Y = a + bM - c \ln R - dR$$

where  $Y$  is the PGA in  $\text{cm/s}^2$ ,  $a$ ,  $b$ ,  $c$  and  $d$  are the model coefficients to be estimated,  $R$  denotes as hypocentral distance in km,  $M$  is earthquake magnitude, the model coefficients for rock site condition are  $a = -3.066$ ,  $b = 0.2347$ ,  $c = -0.4137$ , and  $d = -0.00127$ .

- The GMM is developed for the loess regions of China.
- GMM for rock site condition is compared with the other GMMs that proposed for Tibet region, it is observed a slower attenuation rate for the developed GMM.
- The projection method given by Hu et al. (1986) is used for the development of the GMM.
- The isoseismal contour lines that obtained from the loess regions of China (Gansu, Shanxi, Shaanxi, Ningxia, Qinghai, Inner Mongolia Henan and Sichuan region) are employed for the development of the IPE.
- The coefficients for the GMMs that given for loess site condition are available in Ding et al. (1988).

#### **A5 Wang and Wu (1988)**

The GMM is:

$$\ln Y = c_1 + c_2 M + c_3 \ln(R + R_0) + \varepsilon,$$

where  $Y$  is PGA in  $\text{cm/s}^2$ ,  $M$  denotes earthquake magnitude,  $R$  is epicentral distance,  $\varepsilon$  is the residual term that followed a normal distribution with zero mean and standard deviation  $\sigma_\varepsilon$ ,  $c_i$ ,  $i = 1, 2, 3$ , and  $R_0$  are the model coefficients, for GMM with random fault orientation:  $c_1 = 6.623$ ,  $c_2 = 0.529$ ,  $c_3 = -1.468$ ,  $R_0 = 11$ , and  $\sigma_\varepsilon = 0.56$ .

- The GMMs are developed for Lunan region with rock site condition.
- The GMM are developed based on the projection method proposed by Hu and Zhang (1984). The IPE developed by Chandra (1979) for San Andres province and the GMM established by Boore et al. (1984) in terms of PGA are used for reference region IPE and GMM. It should be Noted that  $\sigma_\varepsilon$  for the established GMMs are set equal to that of the reference region GMM.
- 39 isoseismal lines of 10 earthquakes that occurred in the North China Plain are employed to develop the IPE for Lunan region. Note the range for the magnitude of the employed earthquakes is of 5.5-7.8, the earthquake events with magnitudes larger than 6.0 are selected in priority. If the isoseismal contour lines of mainshocks are selected, then the isoseismal contour lines of their aftershocks are excluded for regression analysis.
- Note the distance measurement of the IPE that developed for Lunan region is obtained by averaging the distance for long axis ( $R_a$ ) and the distance for short axis ( $R_b$ ) of the isoseismal contour lines:

$$R = \sqrt{R_a \cdot R_b}$$

### **A6 Guo and Wang (1990)**

The GMMs is:

$$Y = a \cdot \exp(bM)(R + \Delta)^c + \varepsilon,$$

The following GMMs are also proposed for comparison purpose:

$$Y = a \cdot \exp(bM)(\sqrt{R^2 + h^2} + \Delta)^c + \varepsilon,$$

$$Y = a \cdot \exp(bM)(R + c_1 \exp(c_2 M))^c + \varepsilon,$$

where  $Y$  is PGA in  $\text{cm/s}^2$ ,  $M$  accounts for earthquake magnitude,  $R$  is epicentral distance in km,  $a$ ,  $b$  and  $c$  are the model coefficients to be estimated based on regression analysis,  $\varepsilon$  denotes the residual term that followed a normal distribution with zero mean and standard deviation,  $\sigma_\varepsilon$ .  $\Delta$  is a factor that employed to consider the near-field saturation effect on the predicted ground motion,  $h$  is the pseudo depth and  $h$  is fixed at 10 km. The model coefficients for  $Y = a \cdot \exp(bM)(R + \Delta)^c + \varepsilon$  are  $a = 384$ ,  $b = 1.061$ ,  $c = -2.04$ ,  $\Delta = 20$ , and  $\sigma_\varepsilon = 0.602$ .

- 67 ground-motion recordings for mainshock and aftershocks of Tangshan earthquake and Haicheng earthquake, and 72 recordings for earthquakes occurred in Western U.S. are employed.
- The employed recordings are based on the larger of the two horizontal components. The  $M_L = M_s$  is considered for the recordings that collected from Western U.S. when  $M_s$  is not available.
- The regression procedure given by Wang and Guo (1990) is employed for the establishment of the GMM. Another set of GMMs are also developed based on the same function form given above but considering use moment magnitude  $M_w$  and  $R_{\text{rup}}$  (closest distance to the rupture surface) to replace the  $M$  and  $R$ .
- Note only the model coefficients for  $A = a \cdot \exp(bM)(R + \Delta)^c + \varepsilon$  are given here, the model coefficients for other developed GMMs are provided in Guo and Wang (1990).
- The GMMs are also developed by only using Huabei ground-motion recordings and compared with the GMMs developed based on Western U.S. ground-motion recordings, found comparable for each other.

### **A7 Huo and Hu (1992)**

The GMM is:

$$\log Y = c_1 + c_2 M + c_3 M^2 + c_4 \lg(R + c_5 \exp(c_6 M)),$$

where  $Y$  denotes as PGA in  $\text{cm/s}^2$ ,  $M$  is earthquake magnitude,  $R$  is  $R_{jb}$  distance (closest distance to the rupture plane) in km,  $\varepsilon$  is the residual term that followed a normal distribution with zero mean and standard deviation  $\sigma_\varepsilon$ ,  $c_i$ ,  $i = 1, \dots, 6$ , are the model coefficients to be estimated based on regression, the estimated coefficients for the GMM at rock site condition by considering  $R$ ,  $M$  and  $Y$  all as random variables are:  $c_1 = -1.8220$ ,  $c_2 = 1.448$ ,  $c_3 = -0.0520$ ,  $c_4 = -2.0180$ ,  $c_5 = 0.1818$ ,  $c_6 = 0.7072$ , and  $\sigma_\varepsilon = 0.1868$ .

- The ground-motion recordings of two horizontal components for 41 earthquakes that occurred in Western U.S. were employed for the development of the GMM. Note the  $M = M_s$  is considered for  $M \geq 6$ , and  $M = M_L$  or  $M = m_b$  (body-wave magnitude) is considered for  $M < 6$  in the regression analysis.
- The model coefficients of the GMMs are also estimated by setting  $c_3 = 0$ ; and the model coefficients of the GMMs are also estimated by setting  $c_3 = 0$  and  $c_5 = 0$ . The uncertainty of the  $M$ ,  $R$ , and  $Y$  are considered in the development of the GMMs.
- The GMMs are also given for PGV and PGD. The model coefficients for the GMMs based on PGV and PGD are given in the study.
- The GMMs for soil site condition are also considered and the corresponding model coefficients are also provided by the authors.

### **A8 Huo et al. (1992)**

The GMM is:

$$\log Y = c_1 + c_2 M + c_3 M^2 + c_4 \lg[R + c_5 \exp(c_6 M)] + \varepsilon,$$

where  $Y$  is PGA in  $\text{cm/s}^2$ ,  $M$  accounts for earthquake magnitude,  $R$  is epicentral distance in km,  $c_i$ ,  $i = 1, \dots, 6$ , are the model coefficients,  $\varepsilon$  denotes the residual term that followed a normal distribution with standard deviation  $\sigma_\varepsilon$ . The model coefficients of the GMM in

terms of PGA that given for Huabei region at rock sites along semi-major axis are,  $c_1 = 1.641$ ,  $c_2 = 0.8465$ ,  $c_3 = 0$ ,  $c_4 = -2.4456$ ,  $c_5 = 0.6274$ ,  $c_6 = 0.6121$ , and  $\sigma_\varepsilon = 0.260$ .

- The GMMs are developed based on the projection method given by Hu and Zhang (1984), the developed GMM and IPE for reference region are based on the same 41 earthquake events that occurred in Western U.S. The elliptical model given by Chen and Liu (1989) is considered for the IPEs that proposed for Huabei region, Northwest region, Southwest region, and Huanan region. Note that the developed IPEs are based on the original intensity database, while not the processed isoseismal contour lines.

- The model coefficients also estimated for GMMs with  $c_3 = 0$ .

- The projected GMMs for Huabei region and Southwestern China are compared with the available ground-motion recordings, found good agreement between the projected GMMs and recordings.

- The  $\sigma_\varepsilon$  are suggested as:  $(\sigma_{Y\varepsilon})_{\text{Target}} = \frac{(\sigma_{I\varepsilon})_{\text{Target}}}{(\sigma_{I\varepsilon})_{\text{Reference}}} \times (\sigma_{Y\varepsilon})_{\text{Reference}}$ , where  $(\sigma_{I\varepsilon})_{\text{Target}}$  and  $(\sigma_{I\varepsilon})_{\text{Reference}}$  represent the  $\sigma_\varepsilon$  for the IPE residual term for target and reference region respectively,  $(\sigma_{Y\varepsilon})_{\text{Reference}}$  denote the  $\sigma_\varepsilon$  for the GMM residual term for reference region.

- The model coefficients for GMMs based on PGV and PGD are given in Huo et al. (1992).

### **A9 Lin et al. (1993)**

The GMM is:

$$\ln Y = a + bM + c \ln(R + R_0) + \varepsilon,$$

where  $Y$  denotes as PGA,  $M$  is earthquake magnitude and  $R$  is the hypocentral distance given by:  $R = \sqrt{H^2 + D^2}$ ,  $H$  is the equivalent focal depth and  $D$  is epicentral distance unit in km,  $a$ ,  $b$ ,  $c$  and  $R_0$  are the to be estimated model coefficients. For rock site condition,  $a = 8.9654$ ,  $b = 0.4949$ ,  $c = -2.216$ ,  $R_0 = 25$ ,  $\varepsilon$  is the residual term followed a normal distribution

with zero mean and standard deviation  $\sigma_\varepsilon = 0.28$ , for soil site condition,  $a = 6.0092$ ,  $b = 0.5457$ ,  $c = -1.1963$ ,  $R_0 = 12$ , and  $\sigma_\varepsilon = 0.6838$ , for alluvium site condition,  $a = 6.903$ ,  $b = 0.3759$ ,  $c = -1.1033$ ,  $R_0 = 12$ , and  $\sigma_\varepsilon = 0.6838$ .

- Note  $H$  is set to be 10 km for the regression of the  $R_0$  term.
- The projection method given by Hu and Zhang (1984) is employed to derive the GMM, the IPE and GMM that proposed for Western U.S. at rock site condition are used. 73 isoseismal contour lines for 16 earthquake events with magnitude ranging from 5 to 8 are selected for the development of the elliptical IPE (Chen and Liu 1989) for Huabei region.
- The GMMs are also proposed for Western U.S. at soil site condition and alluvium site condition based on the recordings from 34 earthquake events with magnitude ranging from 5 to 7.6.
- Note the developed GMMs are not recommended to predict the near-field ground motion for large earthquake events.

### **A10 Xiang and GAO (1994)**

The GMM is:

$$Y = a \exp(bM_s)(R + \Delta)^c + \varepsilon,$$

where  $Y$  is PGA in  $\text{cm/s}^2$ ,  $a$ ,  $b$  and  $c$  are the model coefficients to be estimated based on regression method,  $R$  denotes as epicentral distance in km,  $\Delta$  is a constant,  $\varepsilon$  is the residual term,  $a = 252.9$ ,  $b = 0.5155$ ,  $c = -1.1516$ ,  $\Delta = 10$ , and  $\sigma_\varepsilon = 0.5258$  are the estimated model coefficients based on the recordings for Yunnan region,  $a = 129.07$ ,  $b = 0.5275$ ,  $c = -1.5785$ ,  $\Delta = 15$ , and  $\sigma_\varepsilon = 0.5203$  are the regressed coefficients based on the recordings for Western U.S. and Yunnan region.

- The GMMs are developed for Yunnan region.
- 131 recordings for the mainshocks and aftershocks of Luquan earthquake (1985,  $M_s = 6.3$ ), Lancang-Gengma earthquakes (1988,  $M_s = 7.2, 7.6$ ), Tonghai earthquake (1970,  $M_s =$

7.6), Longjing earthquakes (1976,  $M_s = 7.4, 7.2$ ) and Jianchuan earthquake (1982,  $M_s = 5.5$ ) are used. The employed recordings are obtained at rock site condition.

- The larger of the two horizontal components of ground-motion recordings is used. The distance for the employed recordings is ranging from 10 to 40 km.
- The IPEs proposed for Yunnan region and Western U.S. are compared, the comparison suggested that the Western U.S. recordings can be employed for the development of the GMM for Yunnan region. 114 ground-motion recordings for Western U.S. are used to overcome the shortage of larger earthquake recordings for Yunnan region.
- For employed Western U.S. ground-motion recordings, the local magnitude  $M_L$  will be used if  $M_s$  is not reported. The magnitudes for Western U.S. earthquake events are increased by 0.2 due to the difference of the magnitude reported by Chinese and U.S. earthquake agency.
- Two GMMs are developed, one GMM is developed only based on Yunnan region recordings, and another is based on recordings from Western U.S. and Yunnan region. The developed GMMs are compared with the those GMM that obtained using projection method (Hu and Zhang 1984), found the projected GMM is larger than the developed GMMs at  $M_s = 6.5$  and  $7.5$ .

### **A11 Wang et al. (1999)**

The GMM is:

$$\log Y = a + bM_s + c \lg R + dR + \varepsilon,$$

where  $Y$  accounts for PGA in  $\text{cm/s}^2$ ,  $R$  is epicentral distance in km.  $a$ ,  $b$ ,  $c$  and  $d$  are model coefficients to be estimated based on regression,  $\varepsilon$  is the residual term that expressed as a normal distribution with zero mean and standard deviation  $\sigma_\varepsilon$ .

- The employed ground-motion recordings of six aftershocks for Tangshan earthquake ( $M_s 7.8$ , July 28, 1976) with  $M_s$  ranging from 3.7 to 4.9 and  $R$  ranging from 2.1 to 41.3 km



are considered. The GMM that developed by using the ground-motion recordings obtained at both soil and rock site condition is:

$$\log Y = -0.122 + 0.452M_s - 0.311\log R - 0.0111R + \varepsilon, \sigma_\varepsilon = 0.277,$$

- The GMM by only using the recordings at soil site condition is:

$$\log Y = 0.430 + 0.428M_s - 0.764\log R - 0.00480R + \varepsilon, \sigma_\varepsilon = 0.271,$$

- The GMM based on the recordings at soil site condition for two aftershocks ( $M_s = 4.5$  and  $M_s = 4.9$ ) is,

$$\log Y = -1.184 + 0.849M_s - 0.737\log R - 0.0231R + \varepsilon, \sigma_\varepsilon = 0.120,$$

- The GMMs are all developed for North China.
- For the development of the GMMs, the larger of the two horizontal components of ground-motion recordings are used.
- The recordings from 3 stations with  $R < 2$  km are excluded in the regression analysis, as the large fitting error caused by those recordings.
- For earthquake events that not reported by  $M_s$ , the  $M_s = 1.13M_L - 1.08$  is applied, where  $M_L$  is local magnitude.
- The GMMs developed in this study are compared with that given by Peng et al. (1985), found comparable for each other.

## **A12 GAO et al. (2000)**

The GMM is:

$$\ln Y = c_1 + c_2M + c_3 \ln R + c_4R + \varepsilon,$$

where  $Y$  accounts for PGA,  $M$  represents for earthquake magnitude,  $R$  is epicentral distance in km,  $\sigma_\varepsilon$  is the standard deviation for residual term  $\varepsilon$  and  $c_i, i = 1, \dots, 4$ , are the model coefficients,  $c_1 = -2.1382$ ,  $c_2 = 0.4541$ ,  $c_3 = -0.8575$ ,  $c_4 = -0.0025$ , and  $\sigma_\varepsilon = 0.90$ .

- The GMM is developed for Eastern China based on the projection method given by Hu and Zhang (1984). The IPEs for target region are developed based on the isoseismal contour lines for 15 earthquakes with magnitude larger than 4.0 since 1904 that occurred in Anhui province and its neighboring region. The Western U.S. are selected for reference region.

- Note that the GMM are also proposed based on elliptical model (Hu and Zhang 1984), the GMM along long (semi-major) axis direction is:

$$\ln Y = -2.1382 + 0.454M - 0.8575 \ln \left( \sqrt{R_a^2 / 1.6 + 36} \right) - 0.0025 \left( \sqrt{R_a^2 / 1.6 + 36} \right), \sigma_\varepsilon = 0.90,$$

the GMM along short (semi-minor) axis direction is:

$$\ln Y = -2.1382 + 0.454M - 0.8575 \ln \left( \sqrt{1.6R_b^2 + 36} \right) - 0.0025 \left( \sqrt{1.6R_b^2 + 36} \right), \sigma_\varepsilon = 0.90$$

- Recommended to use the projection method to develop the GMMs for Eastern China due to the shortage of available instrumental ground-motion recordings.

### **A13 Shi and Shen (2003)**

The GMM is:

$$\log Y = c_1 + c_2 M + c_3 \log[R + c_4 \exp(c_5 M)] + \varepsilon,$$

where  $Y$  denotes PGA or SA in  $\text{cm/s}^2$ ,  $M$  denotes earthquake magnitude,  $R$  is epicentral distance in km,  $\varepsilon$  denotes the residual term that followed a normal distribution with zero mean and standard deviation,  $\sigma_\varepsilon$ .  $c_i, i = 1, \dots, 5$ , are the model coefficients,  $c_1 = 1.7662$ ,  $c_2 = 0.5536$ ,  $c_3 = -1.7738$ ,  $c_4 = -1.842$ ,  $c_5 = 0.418$ , and  $\sigma_\varepsilon = 0.2128$  are for GMM in terms of PGA along semi-major axis.

- The GMM is proposed for Shanghai and its neighboring region.
- The projection method proposed by Hu et al. (1996) is employed for the development of the GMM.
- The procedure given by Chen and Liu (1989) is followed to develop the elliptical IPEs, the IPEs are developed using 40 isoseismal contour lines for 13 aftershocks with magnitude ranging from 4.1 to 7.0 that occurred in Shanghai and its neighboring region.
- The Western U.S. is selected for reference region due to its intensity scale is comparable with that for China, the GMM is developed based on 204 ground-motion recordings from 24 earthquake events at rock site condition. The recordings for the two horizontal components are used. The magnitude and distance for the employed earthquake events are ranging from 4.0 to 7.2 and 6 to 230 km, respectively. The IPE is proposed by using 5423 original intensity database from 20 earthquake events.
- Note the coefficients of GMM for PGA along semi-minor axis direction are provided in their study.

#### **A14 Liu and Tao (2004)**

The GMM is:

$$Y = 3.16 \frac{\Delta\sigma}{\rho R} \sqrt{\frac{f_{\max}}{f_0}} \cdot \gamma_m,$$

where  $Y$  denotes PGA,  $\Delta\sigma$  accounts for stress drop (unit in bar),  $\rho$  is the density of the crustal for the considered source zones,  $f_0$  represents the corner frequency for the acceleration source spectra,  $f_{\max}$  is the frequency that the acceleration source spectra show a downtrend after  $f_{\max}$ ,  $R$  is epicentral distance,  $\gamma_m$  is the peak factor for stationary process. For Huabei region,  $\Delta\sigma = 100$  bars, shear-wave velocity is set to be 3.3 km/s,  $\rho$  is 2.8 g/cm<sup>3</sup>, for Southwestern region,  $\Delta\sigma = 150$  bars, shear-wave velocity is 3.5 km/s,  $\rho$  is 2.8 g/cm<sup>3</sup>.

- The development of the GMM is based on the stochastic point-source method and random vibration theory (Boore 1983).

- The developed GMMs and the selected GMMs developed based on projection method (Hu and Zhang, 1984) are compared with the obtained ground-motion recordings for earthquake events with magnitudes,  $M_w \leq 5.5$ , found that the obtained GMMs are in good agreement with the recordings.
- The GMMs for Southwestern region are compared with the ground-motion recordings for earthquake events with  $M_w \geq 6.0$ , found comparable with the PGA recordings.
- The values for the seismic source parameters that used in the development of the GMMs still need further discussion.

### **A15 Yu and Wang (2004)**

The GMM is:

$$\log Y = c_1 + c_2 M + c_3 M^2 + c_4 \log[R + c_5 \exp(c_6 M)] + \varepsilon ,$$

where  $Y$  is PGA or SA in  $\text{cm/s}^2$ ,  $M$  denotes earthquake magnitude,  $R$  is epicentral distance in km,  $\varepsilon$  is the residual term that followed a normal distribution with zero mean and the standard deviation  $\sigma_\varepsilon$ ,  $c_i$ ,  $i = 1, \dots, 6$ , are the model coefficients to be estimated based on regression, the coefficients for GMM in terms of PGA along semi-major axis are:  $c_1 = 0.617$ ,  $c_2 = 1.163$ ,  $c_3 = -0.046$ ,  $c_4 = -2.207$ ,  $c_5 = 1.694$ ,  $c_6 = 0.446$ , and  $\sigma_\varepsilon = 0.232$ .

- The GMMs are developed for northeastern Qinghai-Tibet Plateau.
- The GMMs are developed based on the projection method given by Hu et al. (1996) due to the insufficient instrumental ground-motion recordings for the considered region. The  $\sigma_\varepsilon$  for the projected GMMs are set to be equal to that for reference region.
- For target region, the isoseismal contour lines for 31 earthquake events occurred in Ningxia, Gansu and Qinghai province with  $M \geq 5.0$  are used to develop the elliptical IPEs (Chen and Liu 1989).

- For reference region, the IPE proposed by Chandra (1976) for San Andreas province is employed, the GMM is developed by using both the ground-motion recordings for Western U.S. and the ground-motion recordings for Southern California. The developed GMMs for reference region is compared with the GMMs that given by Huo (1989) for Western U.S., found the developed GMMs perform better than the GMMs given by Huo (1989).
- The coefficients of the GMMs based on SA are available in their study.

### **A16 Yu and Wang (2006)**

The GMM is:

$$\log Y = c_1 + c_2 M + c_4 \log[R + c_5 \exp(c_6 M)] + \varepsilon,$$

where  $Y$  is PGA or SA in  $\text{cm/s}^2$ ,  $M$  denotes surface-wave magnitude,  $R$  is epicentral distance in km,  $\varepsilon$  is the residual term that followed a normal distribution with zero mean and standard deviation  $\sigma_\varepsilon$ ,  $c_i$ ,  $i = 1, \dots, 6$ , are the model coefficients to be estimated. The coefficients of the GMM that proposed for Eastern China in terms of PGA along semi-major axis are  $c_1 = 2.027$ ,  $c_2 = 0.548$ ,  $c_4 = -1.902$ ,  $c_5 = 1.700$ ,  $c_6 = 0.425$ , and  $\sigma_\varepsilon = 0.240$ ; for Western China, the coefficients for GMM in terms of PGA along semi-major axis are  $c_1 = 2.206$ ,  $c_2 = 0.532$ ,  $c_4 = -1.954$ ,  $c_5 = 2.018$ ,  $c_6 = 0.406$ , and  $\sigma_\varepsilon = 0.240$ .

- The GMMs are given for Eastern China and Western China at rock site condition. Note the boundary for the Eastern China and Western China is defined approximately by the longitude line of  $105^\circ\text{E}$ .
- The projection method given by Hu et al. (1996) is employed for the development of the GMMs in this study. The procedure considered for the development of the GMM is based on Wang et al. (2000).
- For reference region, the IPE given by Chandra (1979) for San Andreas province is employed, the GMMs are developed based on the ground-motion recordings for Western U.S. and Southern California.

- For target region, 718 isoseismal contour lines for 258 earthquake events with magnitudes larger than 5.0 are employed for the development of the elliptical IPEs (Chen and Liu 1989).
- The GMMs are not recommended to predict ground motion in near field due to the limited near-field ground-motion recordings that collected from reference region, the coefficients given here are only for GMM in terms of PGA, the coefficients for SA are available in Yu and Wang (2006).

### **A17 Lei et al. (2007)**

The GMM is:

$$\log Y = c_1 + c_2 M + c_3 M^2 + c_4 \log[R + c_5 \exp(c_6 M)] + \varepsilon ,$$

where  $Y$  is PGA or SA in  $\text{cm/s}^2$ ,  $M$  denotes surface-wave magnitude,  $R$  is epicentral distance in km,  $\varepsilon$  is the residual term that followed a normal distribution with zero mean and standard deviation  $\sigma_\varepsilon$ ,  $c_i$ ,  $i = 1, \dots, 6$ , are the model coefficients to be estimated based on regression. For Southwestern China, the coefficients for the GMM based on PGA along semi-major axis are  $c_1 = -0.3349$ ,  $c_2 = 1.3807$ ,  $c_3 = -0.0665$ ,  $c_4 = -2.1920$ ,  $c_5 = 2.5292$ ,  $c_6 = 0.3334$ , and  $\sigma_\varepsilon = 0.232$ . For Sichuan Basin region, the coefficients for the GMM based on PGA along semi-major axis are  $c_1 = -1.8244$ ,  $c_2 = 1.5408$ ,  $c_3 = -0.0845$ ,  $c_4 = -1.6392$ ,  $c_5 = 0.8691$ ,  $c_6 = 0.3844$ , and  $\sigma_\varepsilon = 0.232$ .

- Two sets of GMMs are developed for Southwestern China and Sichuan Basin region at rock site condition.
- The projection method (Hu et al., 1996) is considered and the procedure given by Wang et al. (2000) is followed for the development of the GMMs.
- The IPEs for Southwestern China is developed by using 236 isoseismal contour lines with magnitudes ranging from 4.0 to 7.8 that occurred from 1950 to 2006; the IPEs for Sichuan Basin region is developed based on 91 isoseismal contour lines for 40 earthquake

events with magnitude in the range of 3.8 to 7.1 that occurred from 1932 to 2004. The IPEs are developed based on the elliptical model given by Chen and Liu (1989).

- The IPE proposed by Chandra (1979) for San Andreas province and the GMMs given by Yu and Wang (2004) for Western U.S. are used as reference region IPE and GMMs.
- The difference for the surface-wave magnitude (Liu et al. 2006) that reported by China ( $M_s$ ) and U.S. agency ( $M_{s-US}$ ) is considered by  $M_{s-US} = 1.07M_s - 0.61$  in the development of the GMMs for target region.
- Note that only the coefficients of the GMM for PGA along semi-major axis are given here, the coefficients for GMMs based on SA are presented in Lei et al. (2007).

### **A18 Tang et al. (2007)**

The GMM is:

$$\log Y = c_1 + c_2 M + c_3 \log(R + R_0) + \varepsilon,$$

where  $Y$  denotes PGA in  $\text{cm/s}^2$ ,  $M$  is earthquake magnitude,  $R$  represents epicentral distance in km,  $R_0$  is represents near-field correction term,  $c_1$ ,  $c_2$  and  $c_3$  are the model coefficients to be estimated based on regression,  $\varepsilon$  is the residual term that followed a normal distribution with zero mean and standard deviation  $\sigma_\varepsilon$ . For the horizontal GMM in PGA,  $c_1 = 2.427$ ,  $c_2 = 0.259$ ,  $c_3 = -1.398$ ,  $R_0 = 14$ , and  $\sigma_\varepsilon = 0.354$ ; for the vertical GMM in PGA,  $c_1 = 2.078$ ,  $c_2 = 0.345$ ,  $c_3 = -1.596$ ,  $R_0 = 12$ , and  $\sigma_\varepsilon = 0.378$ .

- The GMM is developed for the Bachu-Jiashi region at soil site condition.
- The GMM is developed based on 126 ground-motion recordings for earthquake events with  $M \geq 4.0$  that occurred from 1996 to 2003. The applicable magnitude range for the horizontal GMM and the vertical GMM are 4.0 - 6.9 and 4.0 - 5.9, respectively. The applicable distance range for the two GMMs is 15 - 60 km.

### **A19 Lü et al. (2009)**

The GMM is:

$$\log Y = c_1 + c_2 M + c_4 \log[R + c_5 \exp(c_6 M)] + \varepsilon ,$$

where  $Y$  is PGA or SA in  $\text{cm/s}^2$ ,  $M$  accounts for earthquake magnitude,  $R$  is epicentral distance in km,  $c_i$ ,  $i = 1, \dots, 6$ , are the model coefficients to be estimated based on regression,  $\varepsilon$  denotes residual term that defined by a normal distribution with zero mean and standard deviation,  $\sigma_\varepsilon$ . The coefficients of GMM for PGA along semi-major axis are:  $c_1 = 2.759$ ,  $c_2 = 0.397$ ,  $c_4 = -1.890$ ,  $c_5 = 2.723$ ,  $c_6 = 0.311$ , and  $\sigma_\varepsilon = 0.240$ .

- The GMMs are given for Jiangxi and its neighboring region at rock site condition.
- The projection method proposed by Hu and Zhang (1984) is considered for the development of the GMMs.
- For target region, the elliptical model given by Chen and Liu (1989) is considered for the development of the IPEs. The isoseismal contour lines for 26 earthquakes that occurred in Jiangxi and its neighboring region (Guangdong, Fujian, Zhejiang, Anhui, Hubei and Hunan province) are used.
- For reference region, the IPE given by Chandra (1979) for San Andreas province is considered, the GMMs given by Yu and Wang (2004) for Western U.S. are employed.

### **A20 Lu et al. (2009)**

The GMM is:

$$\log Y = c_1 + c_2 M + c_3 M^2 + c_4 \log[R + c_5 \exp(c_6 M)] + \varepsilon ,$$

where  $Y$  is PGA or SA in  $\text{cm/s}^2$ ,  $M$  accounts for earthquake magnitude,  $R$  is epicentral distance in km,  $c_i$ ,  $i = 1, \dots, 6$ , are the model coefficients to be estimated based on regression,  $\varepsilon$  denotes residual term that defined by a normal distribution with zero mean and standard deviation,  $\sigma_\varepsilon$ .

- The GMMs are proposed for median-strong seismic motion region at rock site condition.



- The GMMs are developed based on the projection method (Hu et al., 1996).
- For target region, 126 isoseismal contour lines for 51 earthquake events that occurred in Northeast region, Huazhong region and Huanan region are employed for the development of the elliptical IPEs (Chen and Liu 1989), the procedure for the development of the IPEs is based on Wang et al. (2000).
- The IPE given by Chandra (1979) for San Andreas province is used for reference region IPE. The GMMs given by Huo (1989) and Yu and Wang (2004) for Western U.S. are considered for the reference region GMMs.
- The coefficients for the developed GMM along semi-major axis by using reference region GMM given by Huo (1989) are  $c_1 = 1.4118$ ,  $c_2 = 0.7711$ ,  $c_3 = 0.0234$ ,  $c_4 = -2.0293$ ,  $c_5 = 0.95$ ,  $c_6 = 0.45$ , and  $\sigma_\varepsilon = 0.085$ . The coefficients for the developed GMMs along semi-major axis by using the reference region GMMs given by Yu and Wang (2004) are  $c_1 = 2.9793$ ,  $c_2 = 0.6247$ ,  $c_3 = 0$ ,  $c_4 = -2.5682$ ,  $c_5 = 2.789$ ,  $c_6 = 0.451$ , and  $\sigma_\varepsilon = 0.134$ .
- The predicted PGA based on the proposed GMM is larger than that based on the GMM given by Wang et al. (2006) for earthquake events with  $M \leq 4$ .

### **A21 Jin et al. (2009)**

The GMM is:

$$\ln Y = a + b \ln(\Delta + 10) + c\Delta + dM,$$

where  $Y$  denotes as SA (spectral acceleration for SDOF system with damping ratio,  $\xi = 0.02$ ),  $M$  accounts for local earthquake magnitude,  $\Delta$  is epicentral distance in km,  $a$ ,  $b$ ,  $c$  and  $d$  are model the coefficients, for the horizontal GMM based on SA at nature vibration period  $T_n = 0.26$  s,  $a = -8.8997$ ,  $b = -0.6581$ ,  $c = -0.0063$ , and  $d = 1.7549$ .

- The GMM is developed for Fujian region at rock site condition.
- 92 earthquakes of 1932 broadband velocity ground-motion recordings (1288 horizontal and 644 vertical recordings) on rock sites from 7 stations located in Fujian province are

employed for the development of the GMM. The epicentral distance for the employed recordings is ranging from 13 km to 462 km, and local magnitude for the employed recordings is ranging from 2.8 to 4.8. The velocity recordings are transferred to acceleration recordings based on the approach given by Jin et al. (2003).

- The two components of the horizontal recordings are used.
- The obtained GMMs are compared with the GMMs given by Huo (1989), found the GMMs are similar for distance larger than 100 km, while relatively large difference is observed for distance smaller than 100 km at  $M_L = 5$ .

## **A22 Kang and Jin (2009)**

The GMM is:

$$\ln Y = a + bM_L + (c + dM_L) \ln(R + R_0),$$

where  $Y$  is PGA in  $\text{cm/s}^2$ ,  $M_L$  denotes local magnitude,  $R$  is epicentral distance in km,  $a$ ,  $b$ ,  $c$ , and  $d$  are the coefficients to be estimated based on regression.  $R_0$  was set to be 10 km. For the horizontal GMM based on PGA,  $a = 1.6683$ ,  $b = 1.4315$ ,  $c = -1.7457$ , and  $d = 0.0289$ , for the vertical GMM based on PGA,  $a = 2.6607$ ,  $b = 0.8246$ ,  $c = -1.9301$ , and  $d = 0.1296$ .

- The GMM is developed for the Sichuan region at rock site condition.
- The 8505 broadband velocity recordings for 105 earthquake events from 27 earthquake recording stations in Sichuan region were employed, the  $M_L$  is ranging from 4.0 to 6.4, the epicentral distance is in the range of 26 - 462 km. The velocity recordings are transferred to the acceleration recordings based on the approach given by Jin et al. (2003).
- The two components of the horizontal ground-motion recordings are employed for the development of the horizontal GMMs.
- The developed GMMs are suggested for  $M_L$  of 4.0 - 6.4 and  $R$  of 26 km - 462 km for rock site condition.

### A23 Yang et al. (2011)

The GMM is:

$$\ln Y = a + bM + c \ln(R + k_1 \exp(k_2 M)) + \varepsilon ,$$

where  $Y$  is PGA in  $\text{cm/s}^2$ ,  $M$  accounts for earthquake magnitude,  $R$  is epicentral distance in km,  $a$ ,  $b$ ,  $c$ ,  $k_1$  and  $k_2$  are the model coefficients to be estimated based on regression,  $\varepsilon$  denotes the residual term that followed a normal distribution with zero mean and standard deviation,  $\sigma_\varepsilon$ . For the horizontal GMM based on PGA at soil site condition,  $a = 4.96$ ,  $b = -0.88$ ,  $c = -1.40$ ,  $k_1 = 0.99$ ,  $k_2 = 0.45$ , and  $\sigma_\varepsilon = 0.53$ , for the vertical GMM based on PGA at soil site condition,  $a = 6.04$ ,  $b = 1.07$ ,  $c = -1.90$ ,  $k_1 = 0.99$ ,  $k_2 = 0.52$ , and  $\sigma_\varepsilon = 0.49$ .

- The GMM is developed for loess region.
- The mainshock and aftershocks for Wenchuan earthquake are considered in the study, 1221 ground-motion recordings for 49 earthquakes at soil site condition and 6 ground-motion recordings for 6 earthquakes at rock site condition are employed. The recordings are collected in Shaanxi, Gansu, Ningxia, Qinghai, and Ningxia province.
- The considered recordings for soil site condition are converted to the recordings for rock site condition based on the site amplification function; the converted recordings are then used for the development of the GMMs for rock site condition.
- The developed GMMs are compared with the other GMMs that proposed based on projection method, found better performance for the developed GMMs.

### A24 Cui et al. (2012)

The GMM is:

$$\log Y = c_1 + c_2 M + c_3 \log(R + R_0) + c_4 S + \varepsilon ,$$

where  $Y$  denotes for PGA, PSA in  $\text{cm/s}^2$  or PGV in  $\text{cm/s}$ ,  $M$  is earthquake magnitude,  $R$  denotes epicentral distance in km,  $S$  represents the site factor, for soil site condition,  $S = 1$ ;

for rock site condition,  $S = 0$ ;  $\varepsilon$  accounts for the residual term that followed a normal distribution with zero mean and standard deviation  $\sigma_\varepsilon$ .  $c_i$ ,  $i = 1, \dots, 4$  are the model coefficients to be estimated based on regression analysis.

- Note  $Y$  is based on geometric mean of the two components of the horizontal recordings.
- The GMMs are developed for the mountain area of Sichuan and Yunnan region.
- The recordings employed for the development of the GMMs are selected based on: (1)  $R$  less than 110 km; (2)  $M \geq 4.5$ ; (3) the two components of the horizontal ground-motion recordings are both available. If the PGA for the two components of the horizontal recordings are both all less than 0.01 g, then such recordings are excluded for the analysis.
- Three different regression approaches are considered, for unweighted regression:  $R_0 = 10$  km,  $c_1 = 1.827$ ,  $c_2 = 0.3506$ ,  $c_3 = -1.2775$ ,  $c_4 = -0.1370$ , and  $\sigma_\varepsilon = 0.3445$ ; for weighted regression (recordings for Wenchuan aftershocks are excluded),  $R_0 = 8$  km,  $c_1 = 2.4911$ ,  $c_2 = 0.3647$ ,  $c_3 = -1.7654$ ,  $c_4 = -0.0575$ , and  $\sigma_\varepsilon = 0.3902$ ; for unweighted regression (recordings for Wenchuan aftershocks are excluded),  $R_0 = 15$  km,  $c_1 = 2.7831$ ,  $c_2 = 0.4956$ ,  $c_3 = -2.6029$ ,  $c_4 = 0.4220$ , and  $\sigma_\varepsilon = 0.3546$ .
- A large difference is observed for the established GMMs at  $M_s = 5.5$  and  $M_s = 6.5$ . The developed GMMs are compared to the recordings for Ninger earthquake events with  $M_s = 6.4$ , found the proposed GMM based on weighted regression approach gives best agreement.
- Compare with the GMMs given by Cui et al. (2006), found the GMMs developed for this study are more reasonable.
- The site effects for the developed GMMs needs further discussion.
- The model Coefficients for GMMs based on PGV and PSA are available in their study.

## **A25 Fan et al (2012)**

The GMM is:

$$\log Y = c_1 + c_2 M + c_3 M^2 + c_4 \log[R + c_5 \exp(c_6 M)] + \varepsilon ,$$

where  $Y$  is PGA, PSA in  $\text{cm/s}^2$  or PGV in  $\text{cm/s}$ ,  $M$  denotes surface-wave magnitude,  $M_s$ ,  $R$  is epicentral distance in km,  $\varepsilon$  is the residual term that followed a normal distribution with zero mean and standard deviation,  $\sigma_\varepsilon$ ,  $c_i$ ,  $i = 1, \dots, 6$ , are model the coefficients to be estimated based on regression. For GMM with PGA along semi-major axis,  $c_1 = -0.35$ ,  $c_2 = 1.159$ ,  $c_3 = -0.05$ ,  $c_4 = -1.679$ ,  $c_5 = 0.263$ ,  $c_6 = 0.634$ , and  $\sigma_\varepsilon = 0.232 \sim 0.292$ , the coefficients are estimated based the assumption that earthquake events for reference region and target region could cause the same intensity for an interested site, and the magnitudes of the events for reference region and target region are same.

- The GMMs are developed for Guanzhong Plain at rock site condition.
- Four sets of GMMs are developed based on the four different assumptions for the projection method (Hu et al., 1996). The difference for the  $M_s$  reported by Western U.S. agency and China are considered based on Liu et al. (2006).
- For reference region, the GMM given by Yu et al. (2002) for Western U.S. is employed, the IPE given by Chandra (1979) for San Andreas province is considered.
- For target region (i.e., Guanzhong Plain), the IPEs are developed based on the elliptical model given by Chen and Liu (1989). Following the projection procedure that considered by Wang et al. (2000), 87 isoseismal contour lines for 30 earthquake events are considered for the development of the target region IPEs in this study.
- The projected GMMs based on different assumptions are compared, found the developed GMMs are similar.
- The coefficients for GMMs that developed based on different assumptions are available in Fan et al. (2012).

## **A26 Liu and Li (2012)**

The GMM is:

$$\log Y = b_0 + b_1 R + b_2 \log R + \varepsilon,$$

where  $Y$  is PGA in  $\text{cm/s}^2$ ,  $R$  represents  $R_{jb}$  (closest distance to the rupture plane) in km,  $\varepsilon$  denotes the residual terms that followed a normal distribution with zero mean and standard deviation  $\sigma_\varepsilon$ ,  $b_0$ ,  $b_1$  and  $b_2$  are the model coefficients,  $b_0 = 3.0016$ ,  $b_1 = -0.0027$ , and  $b_2 = -1.1047$  are considered for the horizontal GMM with PGA at hanging wall sites;  $b_0 = 4.3278$ ,  $b_1 = -0.001$ , and  $b_2 = -0.3387$  are used for the horizontal GMM with PGA at footwall sites.

- The GMMs are developed based on the ground-motion recordings for mainshock of Wenchuan earthquake that recorded by 107 stations.
- 154 horizontal recordings and 77 vertical recordings are collected from 70 recording stations located at hanging wall sites. 60 horizontal recordings and 30 vertical recordings are collected from 30 recording stations at for footwall sites. The  $R_{jb}$  for the employed recordings are ranging from 0 to 500 km. Note the two components of the horizontal recordings are considered as two independent recordings.
- Note most of the stations are placed at soil site condition, but the recordings are not classified for rock sites and soil sites. The soil amplification effect is not considered by the developed GMMs.
- The developed horizontal GMMs are compared with the GMM given by Huo (1989), found the GMM given by Huo (1989) may underestimate the PGA.
- The both the horizontal GMMs for hanging wall sites and footwall sites are larger than vertical GMMs.
- Note the coefficients for the vertical GMMs are available in Liu and Li (2012).
- Concluded that the other GMMs (Huo 1989; Campbell 1981) are not applicable for large earthquakes, such as Wenchuan earthquake.

## **A27 Liu et al. (2012)**

The GMM is:

$$\ln Y = c_1 + c_2 M + c_3 \ln(R + c_4 \exp(c_5 M)) + \varepsilon,$$

where  $Y$  denotes as ground motion parameters,  $M$  represents earthquake magnitude,  $R$  is epicentral distance in km,  $\varepsilon$  is the residual term that followed a normal distribution with zero mean and standard deviation  $\sigma_\varepsilon$ ,  $c_i$ ,  $i = 1, \dots, 5$ , are the model coefficients, the coefficients of horizontal GMM for PGA are  $c_1 = 5.7632$ ,  $c_2 = 0.4524$ ,  $c_3 = -1.1129$ ,  $c_4 = 14.9122$ ,  $c_5 = 0.0056$ , and  $\sigma_\varepsilon = 0.6623$ .

- The GMMs are developed for Yunnan region.
- A two-stage regression approach (Joyner and Boore 1981) is employed to estimate the coefficients for GMM.
- 72 ground-motion recordings for earthquake events with magnitudes ranging from 3 to 7.6 are considered, most of the recordings are in the epicentral distance range of 8 - 50 km. It should be noted that the number of the far-field recordings for small earthquakes and near-field recordings for larger earthquakes are small.
- The obtained horizontal GMM for PGA are compared with other GMMs proposed for Yunnan region, found the predicted ground motion based on the developed GMMs is smaller than the other GMMs at near field, while the trend is reversed for far field.
- The estimated coefficients for GMMs with PGV and PSA are available in Liu et al. (2012).

### **A28 Liu and Luo (2013)**

The GMM is:

$$\ln Y = A_2 - B_2 \ln(R_m + R_2) + \varepsilon,$$

where  $Y$  denotes PGA,  $R_m$  is epicentral distance for the circular model,  $A_2$  and  $B_2$  are the estimated coefficients,  $R_2$  represents the distance saturation term,  $\varepsilon$  is residual term that

followed a normal distribution with zero mean and standard deviation  $\sigma_\varepsilon$ , the coefficients for vertical GMM with PGA are:  $A_2 = 11.533$ ,  $B_2 = 1.597$ ,  $R_2 = 12$ ,  $\sigma_\varepsilon = 0.318$ ; the coefficients for horizontal GMM with PGA are:  $A_2 = 12.232$ ,  $B_2 = 1.604$ ,  $R_2 = 20$ ,  $\sigma_\varepsilon = 0.465$ .

- The GMMs are developed using a so-called “mapping circular model”.
- 261 ground-motion recordings for the mainshock of Wenchuan earthquake event at soil site conditions are considered. The recordings are recorded by the stations located in Sichuan, Shaanxi, Gansu, Ninxia, Qinghai, Shanxi, and Yunnan provinces.

### **A29 Jiang et al (2013)**

The GMM is:

$$\ln Y = c_1 + c_2 M + c_3 \ln(R + c_4 \exp(c_5 M)) + \varepsilon,$$

where  $Y$  denotes PGA in cm/s,  $M$  is surface-wave magnitude,  $R$  is epicentral distance,  $\varepsilon$  is the residual term that followed a normal distribution with zero mean and standard deviation  $\sigma_\varepsilon$ ,  $c_i$ ,  $i = 1, \dots, 5$  are the model coefficients. For vertical GMM,  $c_1 = 1.8433$ ,  $c_2 = 1.2897$ ,  $c_3 = -1.6366$ ,  $c_4 = 2.1529$ ,  $c_5 = 0.4514$ , and  $\sigma_\varepsilon = 0.3276$ ; for horizontal GMM,  $c_1 = 1.6235$ ,  $c_2 = 1.3214$ ,  $c_3 = -1.8043$ ,  $c_4 = 1.9238$ ,  $c_5 = 0.4638$ , and  $\sigma_\varepsilon = 0.3412$ .

- 6783 ground-motion recordings for the aftershocks of Wenchuan earthquake are considered.
- The epicentral distance and the magnitudes for the considered recordings are of  $R < 150$  km and  $M_s$  3.3 - 6.4.
- Note that for earthquake events not reported by  $M_s$ , the  $M_s$  is estimated based on  $M_s = 1.13M_L - 1.08$ , where  $M_L$  is local magnitude.
- The proposed GMMs are only applicable for Sichuan region.



- Compared to the GMMs given by Kang and Jin (2009), relatively large difference is observed.

### **A30 Sun et al. (2013)**

Three GMMs are considered:

$$\log Y = C_1 + C_2 M + C_3 R + \varepsilon ,$$

the coefficients of the horizontal GMM for PGA are  $c_1 = -0.6929$ ,  $c_2 = 0.4898$ ,  $c_3 = -0.0063$ , and  $\sigma_\varepsilon = 0.7739$ .

$$\log Y = C_1 + C_2 M + C_3 M \log(R + R_0) + C_4 \log(R + R_0) + \varepsilon ,$$

the coefficients of the horizontal GMM for PGA are  $c_1 = 0.6382$ ,  $c_2 = 0.4689$ ,  $c_3 = 0.0122$ ,  $c_4 = -1.1458$ ,  $R_0 = 2$ , and  $\sigma_\varepsilon = 0.2175$ ;

$$\log Y = C_1 + C_2 M + C_3 M \log(R + R_0) + C_4 \log(R + R_0(M)) + C_7 R + \varepsilon ,$$

and  $R_0(M) = C_5 \exp(C_6 M)$ ,

the coefficients of the horizontal GMM for PGA are  $c_1 = 1.9268$ ,  $c_2 = 0.5898$ ,  $c_3 = -0.0081$ ,  $c_4 = -1.9944$ ,  $c_5 = 10.1340$ ,  $c_6 = 0.1237$ ,  $c_7 = 0.0023$ , and  $\sigma_\varepsilon = 0.2175$ ;  $Y$  denotes as PGA in cm/s,  $M$  represents earthquake magnitude,  $R$  is epicentral distance in km, and  $c_i$ ,  $i = 1, \dots, 7$ , are the model coefficients to be regressed,  $\varepsilon$  is the residual term that followed a normal distribution with zero mean and standard deviation  $\sigma_\varepsilon$ .

- The two-stage regression method (Joyner and Boore 1981) is applied to estimate the model coefficients, 169 horizontal and 168 vertical ground-motion recordings at rock site condition are employed for the development of the GMMs.
- The employed recordings are based on earthquake events occurred after 1976 with magnitude ranging from 1.2 to 7.8, note that only one recording with  $M > 6$ .

- The developed GMMs are compared with the recordings for earthquake events occurred in May 28, 2012 with  $M = 4.8$ , found that the GMMs are comparable with the recordings.
- Note the estimated coefficients for vertical GMMs are available in Sun et al. (2013).

### **A31 Wang et al (2013)**

The GMM is:

$$\log Y = C_1 + C_2 M + C_3 M^2 + (C_4 + C_5 M) \log[R + C_6 \exp(C_7 M)] + \varepsilon$$

where  $Y$  is PGA or SA,  $M$  denotes as surface-wave magnitude,  $R$  accounts for closest distance to the rupture plane,  $\varepsilon$  is the residual term that followed a normal distribution with zero mean and standard deviation  $\sigma_\varepsilon$ ,  $c_i$ ,  $i = 1, \dots, 6$ , are the model coefficients, the coefficients of the horizontal GMM for PGA are,  $c_1 = 3.569$ ,  $c_2 = 0.117$ ,  $c_3 = 0$ ,  $c_4 = -2.274$ ,  $c_5 = 0.140$ ,  $c_6 = 0.996$ ,  $c_7 = 0.375$ , and  $\sigma_\varepsilon = 0.289$ .

- The GMMs are developed for Sichuan-Yunnan region.
- The two horizontal components of the ground-motion recordings are decomposed by considering the angles for  $0^\circ$  to  $180^\circ$  (Hong and Goda 2007), then the PGA of the recordings that oriented the major axis is employed.
- In total 951 ground-motion recordings for earthquake events with  $M_s > 4.5$  and  $R < 200$  km are used; 64 recordings for the mainshock of Wenchuan earthquakes, 26 recordings for Panzhihua earthquake, 17 recordings for Ninger earthquake, 19 recordings for Yaoan earthquake and 825 recordings for 86 aftershocks of Wenchuan earthquake.
- Due to the limited number for the available instrumental ground-motion recordings, the obtained GMMs are not recommended for earthquake events with  $M_s$  ranging from 6.6 to 7.9 and large earthquake events with  $R_{rup} < 30$  km.
- The regression procedure is summarized as:

1. The coefficients for  $C_6 \exp(C_7 M)$  term are estimated based on the 64 recordings for the mainshock of Wenchuan earthquake and 62 recordings for Panzhihua earthquake, Ninger earthquake and Yaoan earthquake.

2. The coefficients for  $(C_4 + C_5 M)$  term are estimated using non-linear regression method based on the 825 aftershock recordings.

3. Then  $C_1$ ,  $C_2$  and  $C_3$  are estimated based on the considered recordings.

- Compared with the GMMs given by Yu and Wang (2006) for Western China, found relatively large difference for SA at natural vibration period,  $T_n > 0.3$  s and  $T_n < 0.2$  s.

- Coefficients for GMMs based on SA are given in Wang et al. (2013).

### A32 Zhang et al. (2013)

The GMM is:

$$\ln Y = f_B(M, R_{rup}) + b_1 SS + b_2 RS + b_3 NS + f_{site}(V_{S30}) + F_{HW} f_{HW}(M, R_{rup})$$

- The terms considered in the model are:

Base model

$$f_B(M, R_{rup}) = \begin{cases} \alpha_0 + \alpha_1 + (M - M_c) - [\beta_1 + \beta_2(M - M_c)] \ln R, & M \leq M_c \\ \alpha_0 + \alpha_2 + (M - M_c) - [\beta_1 + \beta_2(M - M_c)] \ln R, & M > M_c \end{cases}$$

$$R = \sqrt{R_{rup}^2 + h^2},$$

where  $Y$  is PGA or PSA,  $M$  accounts surface-wave magnitude,  $M_c$  is the hinged magnitude,  $R_{rup}$  represents the closest distance to the fault rupture plane unit in km,  $c_i$ ,  $i = 0, \dots, 2$ ,  $\beta_1$ , and  $\beta_2$  are the model coefficients to be estimated based on regression.

Fault rupture mechanism model

$$F = b_1 SS + b_2 RS + b_3 NS,$$

For strike-slip events,  $SS = 1$ ,  $RS = NS = 0$ , for reverse-slip events,  $RS = 1$ ,  $SS = NS = 0$ , for normal-slip events,  $NS = 1$ ,  $SS = RS = 0$ .

Site response model

$$f_{\text{site}}(V_{S30}) = \begin{cases} c \ln(V_{S30}) + d, & V_{S30} < V_1 \\ c \ln(V_1) + d, & V_{S30} \geq V_1 \end{cases}$$

$$V_1 = \begin{cases} 3000, & T < 0.2 \\ \exp[8.0 - 0.9024 \ln\left(\frac{T}{0.2}\right)], & 0.2 \leq T < 1, \\ 700, & T \geq 1 \end{cases}$$

where  $c$  and  $d$  are model parameters.

Hanging-wall model

$$f_{\text{HW}}(M, R_{\text{rup}}) = T_1(M)T_2(R_{\text{rup}}),$$

$$T_1(M) = \begin{cases} 0, & M < 6 \\ M - 6, & 6 \leq M < 7, \\ 1, & M \geq 7 \end{cases}$$

$$T_2(R_{\text{rup}}) = \begin{cases} \gamma_1 R_{\text{rup}} (R_{\text{rup}} - \gamma_2), & R_{\text{rup}} < \gamma_2 \\ 0, & R_{\text{rup}} \geq \gamma_2 \end{cases}$$

- The coefficients of GMM for PGA along fault orientation are,  $\alpha_1 = -0.277$ ,  $h = 10.36$ ,  $\beta_1 = 1.144$ ,  $\beta_2 = -0.239$ ,  $b_1 = 3.57$ ,  $b_2 = 3.63$ ,  $b_3 = 3.39$ ,  $c = -0.301$ , and  $M_c = 6.25$ .

- The GMM is proposed for Western China.

- 1315 ground-motion recordings for 39 earthquake events with  $M_s$  ranging from 5 to 8 with  $R_{\text{rup}} < 200$  km are employed. Mainshock and 18 aftershocks for Wenchuan earthquake, and 20 earthquake events occurred in other countries with magnitude range of 6.0 - 8.0. The two horizontal components of the ground-motion recordings are

decomposed into two directions: along the fault orientation and normal to the fault orientation.

- The model coefficients of the GMM for PGA and PSA along and normal to the fault orientation are presented in Zhang et al. (2013).
- The obtained GMMs are compared with the GMMs proposed by Abrahamson et al. (2008), Boore and Atkinson (2008), Campbell and Bozorgnia (2008) and Chiou and Youngs (2008), found that the predicted ground motion based on the developed GMMs is smaller than that based on those GMMs, and the predicted ground motion based on the developed GMMs agrees with the average of that from the considered four GMMs at  $T_n < 1$  s.

### **A33 Yu et al. (2014)**

The GMM is:

$$\log Y = c_1 + c_2 M + (c_4 + c_3 M) \log(R + R_0) + \varepsilon ,$$

where  $Y$  is PGA, SA in  $\text{cm/s}^2$  or PGV in  $\text{cm/s}$ ,  $M$  denotes surface-wave magnitude,  $R$  is epicentral distance in km,  $\varepsilon$  is the residual term that followed a normal distribution with zero mean and standard deviation  $\sigma_\varepsilon$ ,  $c_i$ ,  $i = 1, \dots, 5$ , are the model coefficients to be estimated based on regression, the coefficients of the GMM for PGA at rock site condition are  $c_1 = -7.019$ ,  $c_2 = 1.372$ ,  $c_4 = 2.284$ ,  $c_5 = -0.663$ , and  $\sigma_\varepsilon = 0.310$ .

- The GMMs are developed for Sichuan-Yunnan region.
- $R_0$  is set to be equal to 5 km in the regression analysis.
- 332 ground-motion recordings for 24 earthquakes events with  $M$  ranging from 4.7 to 6.7 occurred in Sichuan-Yunnan region since 2007 are employed, 36 recordings with epicentral distance less than 75 km are for rock sites condition. The recordings for aftershocks of Wenchuan earthquake are not considered, only the recordings for the aftershocks of Panzhihua earthquake are used.

- The GMMs given by Yu and Wang (2006) along semi-minor axis are used for comparison purpose, found that the difference is small for  $M$  in the range of 5.0 - 6.0 at natural vibration period  $T_n < 0.3$  s for rock site condition, also found that the predicted ground-motion based on the obtained GMM at soil site condition is close to considered GMM (Yu and Wang 2006).
- The predicted ground-motion based on the developed GMMs for soil site condition and the developed GMMs for rock site condition are similar for  $T_n < 0.8$  s.
- The GMMs given by Kang and Jin (2009) and Wang et al. (2013) are compared with the developed GMMs at rock site condition, large difference is observed among the GMMs at  $M_s = 5.5$ . The difference could be attributed to the distance attenuation properties of Sichuan and Yunnan region.
- Due to insufficient near-field recordings ( $R < 20$  km) that employed for the development of the GMMs, the obtained GMMs are recommended for  $20 \leq R \leq 200$  km and  $4.7 \leq M_s \leq 6.0$ .
- The model coefficients for the GMMs based on PGA, PGV and SA are given in Yu et al. (2014).

### **A34 Tao et al. (2014)**

The stochastic point source model is:

$$FA(M_0, f, R) = C \cdot S(M_0, f) \cdot G(R) \cdot D(R, f) \cdot A(f) \cdot P(f) \cdot I(f),$$

where  $M_0$  is moment of magnitude and  $R$  is hypocentral distance in km,  $f$  represents frequency in Hz,  $C$  is the scaling factor given by  $\frac{R_{\theta\phi} FV}{4\pi R \rho_s \beta_s^3}$ ,  $R_{\theta\phi}$  is the radiation pattern of 0.6,  $F$  accounts for free surface effects equal to 2.0,  $V$  represents the partition of a vector into horizontal components of  $\frac{1}{\sqrt{2}}$ ,  $\rho_s = 2.9$  g/cm<sup>3</sup> and  $\beta_s = 3.5$  km/s represent the density and the shear velocity in the source region,  $A(f)$  denotes the exemplify factor for the near

ground site.  $I(f)$  accounts for the type of the ground motion.  $S(M_0, f)$ ,  $G(R)$ ,  $D(R, f)$  and  $P(f)$  are the source terms to be determined based on the ground-motion recordings for small earthquake events,  $\Delta\sigma = 100$  bars,  $Q_0 = 241$ ,  $\eta = 0.8113$ ,  $R_1 = 69$  km,  $R_2 = 122$  km, and  $k_0 = 0.0613$ s.

- The GMMs are proposed for Huabei region.
- The details of the source model are given by Wang (2001).
- 1995 ground-motion recordings recorded by 156 stations for 28 earthquake events that occurred from Feb. 2002 to Sep. 2012 are employed to estimate the source parameters. The employed recordings are with moment magnitude ( $M_w$ ) ranging from 3.5 to 4.5 and with  $R < 30$  km.
- Recordings for 46 earthquake events that occurred from 1976 to 2012 with  $M_w$  ranging from 4.5 to 7.4 are compared with the proposed GMMs, found agreement with the considered recordings for  $M_w = 5$  and 7, while the predicted ground motion based on the developed GMM are larger than the recordings with  $M_w = 6$

### **A35 Tan (2015)**

The stochastic point source model is:

$$FA(M_0, f, R) = C \cdot S(M_0, f) \cdot G(R) \cdot D(R, f) \cdot A(f) \cdot P(f) \cdot I(f),$$

the definition of the parameters in the stochastic point source model followed as Tao et al. (2014). The estimated parameters is obtained based on the ground-motion recordings for small earthquake events that occurred in the considered regions, for Sichuan region,  $\Delta\sigma = 50$  bars,  $Q_0 = 173$ ,  $\eta = 0.4524$ ,  $R_1 = 92$  km, and  $R_2 = 126$  km, for Yunnan region,  $\Delta\sigma = 43$  bars,  $Q_0 = 180$ ,  $\eta = 0.3300$ ,  $R_1 = 87$  km, and  $R_2 = 141$  km.

- The employed ground-motion recordings are with moment magnitude  $M_w$  range of 3.5-4.5, 147 recordings for 82 earthquakes events occurred in Sichuan, 863 recordings

from 154 earthquakes events occurred in Yunnan. The distance range for the employed recordings are of 50 km - 300 km.

- The developed GMMs are compared with the ground-motion recordings obtained from the considered regions, found that the GMMs are comparable with the recordings for  $M_w = 5, 6, \text{ and } 7$ .
- The comparisons are made for the GMMs proposed for Sichuan region and Yunnan region, found that the obtained GMMs are in the middle of the other GMMs.

### **A36 Tian et al. (2015)**

The GMM is:

$$\log Y = c_1 + c_2 M + c_3 M^2 + c_4 \log[R + c_5 \exp(c_6 M)] + \varepsilon ,$$

where  $Y$  is PGA or PSA in  $\text{cm/s}^2$ ,  $M$  denotes earthquake magnitude,  $R$  is epicentral distance in km,  $\varepsilon$  is the residual term that followed a normal distribution with zero mean and standard deviation  $\sigma_\varepsilon$ ,  $c_i, i = 1, 2, 4, 5, 6$  are the model coefficients to be estimated based on regression analysis,  $c_3$  is set to be equal to 0 for the regression, the coefficients of the horizontal GMM for PGA along semi-major axis are  $c_1 = 2.387, c_2 = 0.689, c_4 = -2.395, c_5 = 1.331, c_6 = 0.537$ , and  $\sigma_\varepsilon = 0.207$ .

- The GMM is developed for Eastern China at rock site condition.
- Note the coefficients for GMM along semi-major axis and semi-minor axis for PGA and PSA are given in Tian et al. (2015).
- The projection method given by Hu and Zhang (1984) is considered for the development of the GMMs. For target region, the IPEs given by Wang et al. (2000) are considered.
- For reference region, the IPE given by Chandra (1979) for San Andreas province is considered, and the GMMs proposed by Zheng (2012) based on ground-motion recordings that considered for NGA-west project are employed.



- Compared to the GMMs given by Yu and Wang (2006), found they are very similar.

### **A37 Mu and Yuen (2016)**

The GMM is:

$$\log Y = F_M + F_D + F_S + \varepsilon ,$$

$$F_M = b_1 + b_2(M - M_0) + b_3(M - M_0)^2 + b_4(M - M_0)^3 ,$$

$$F_D = [b_5 + b_6(M - M_0) + b_7(M - M_0)^2 + b_8(M - M_0)^3] \log R + b_9 R ,$$

$$F_S = b_{10} \log(V_S / V_A) ,$$

where  $Y$  is PGA in cm/s,  $F_M$ ,  $F_D$  and  $F_S$  denote magnitude, distance and site amplification terms, respectively.  $\varepsilon$  is a zero-mean of Gaussian error term with standard deviation  $\sigma_\varepsilon$ ,  $M$  is moment magnitude,  $M_0$  is a shifting constant,  $R$  represents hypocentral distance in km,  $V_S$  is the shear wave velocity for the site profile, for rock sites,  $V_S = 700$  m/s, for soil sites,  $V_S = 400$  m/s, for soft soil sites,  $V_S = 200$  m/s,  $V_A$  is the reference velocity and set to be equal to 1200 m/s,  $b_1 = 2.333$ ,  $b_2 = 2.473$ ,  $b_3 = -1.867$ ,  $b_4 = -0.378$ ,  $b_5 = -0.873$ ,  $b_6 = -1.079$ ,  $b_7 = 0.990$ ,  $b_8 = -0.195$ ,  $b_{10} = -0.049$ ,  $\sigma_\varepsilon = 0.122$ .

- The ground-motion recordings are obtained from China Earthquake Data Center for earthquake events occurred in Tangshan area with magnitude  $M \geq 4.0$ .
- 132 horizontal ground-motion recordings for 72 earthquake events recorded by 29 stations are employed for the development of the GMMs.
- The coefficients are estimated based on the HEteRogeneous BAYesian Learning (HERBAL) approach.
- The coefficients for the GMMs based on different variance models are provided in their study.

## Reference

- Abrahamson, N. and Silva, W. (2008) Summary of the Abrahamson & Silva NGA ground-motion relations. *Earthquake Spectra*, 24(1), pp. 67-97.
- Boore, D.M. and Atkinson, G.M. (2008) Ground-motion prediction equations for the average horizontal component of PGA, PGV, and 5%-damped PSA at spectral periods between 0.01 s and 10.0 s. *Earthquake Spectra*, 24(1), pp. 99-138.
- Boore, D. M. (1983) Stochastic simulation of high-frequency ground motions based on seismological models of the radiated spectra. *Bulletin of the Seismological Society of America*, 73(6A), pp. 1865-1894.
- Campbell, K.W. (1981). Near-source attenuation of peak horizontal acceleration. *Bulletin of the Seismological Society of America*, 71(6), pp. 2039-2070.
- Chiou, B.S.J. and Youngs, R.R. (2014) Update of the Chiou and Youngs NGA model for the average horizontal component of peak ground motion and response spectra. *Earthquake Spectra*, 30(3), pp. 1117-1153.
- Cui, J.W., Zhang, J.G., Gao, D., Duan, J.X., and Wang, T. (2012) The ground motion attenuation relation for the mountainous area in Sichuan and Yunnan. *Proceedings of 15th World Conference on Earthquake Engineering*, Lisbon, Portugal, 24-28, September 2012, pp. 668-678.
- Ding, B.Y., Lei, Z.S., and Fang, S.L. (1988). Experimental attenuation relationship of ground motion on basement rock in Chinese loess region. *Northwestern Seismological Journal*, 10 (3), pp. 58-65 (in Chinese).
- Fan, W., D, L.S., Shao, H.C., Liu, J., He, L.P., and Wen, Y. (2012) Study on seismic acceleration attenuation relationship of Guanzhong Plain using different transformation methods. *Seismology and Geology*, 34(1), pp. 129-137 (in Chinese).

- Gao, Y.F., Xie, K.H., and Zeng, G.X. (2000) The seismic attenuation regularities in the moderate-strong earthquake area. *Journal of Zhejiang University*, 34(4), pp. 404-408 (in Chinese).
- Guo, Y.X., and Wang, G.X. (1990). Attenuation of horizontal peak value of acceleration on rock site in North China. *Earthquake Engineering and Engineering Vibration*, 10(1), pp. 41-50 (in Chinese).
- Hong, H.P. and Goda, K., (2007) Orientation-dependent ground-motion measure for seismic-hazard assessment. *Bulletin of the Seismological Society of America*, 97(5), pp. 1525-1538.
- Huo, J.R., Hu, Y.X., and Feng, Q.M. (1992). Study on estimation of ground motion from seismic intensity. *Earthquake Engineering and Engineering Vibration*, 12(3), pp. 1-15 (in Chinese).
- Huo, J.R., and Hu, Y.X. (1992) Study on attenuation laws of ground motion parameters. *Earthquake Engineering and Engineering Vibration*, 12(2), pp. 1-11 (in Chinese).
- Hu, Y.X., Wang, S.Y., Liu, X.H., and Zhu, L. (1986). Attenuation relationship of ground motion for north China partly based on data from Tangshan earthquake, *Chinese Civil Engineering Journal*, 19(3), pp. 1-10 (in Chinese).
- Hu, Y.X., and Zhang, M.Z. (1984) A method of predicting ground motion parameters for regions with poor ground motion data. *Earthquake Engineering and Engineering Vibration*, 4(1), pp. 1-11. (in Chinese).
- Hu, Y.X., Zhou, K.S., and Yan, X.J. (1996) A method for evaluation of ground motion in regions with few acceleration observation data. *Earthquake Engineering and Engineering Vibration*, 16(3), pp. 2-10 (in Chinese).
- Jiang, Q., Guo, M.Z., Hu, Z.M., and Zhai, C.D. (2013) Research on attenuation relationship of ground motion for Wenchuan earthquake aftershocks. *Journal of Institute of Disaster Prevention*, 15(2), pp. 6-10 (in Chinese).

- Jin, X., Kang, L.C., and Ou, Y.P. (2009) Acceleration spectrum attenuation relation for small and moderate earthquakes in Fujian region. *Journal of Earthquake Engineering and Engineering Vibration*, 29(5), pp. 52-58 (in Chinese).
- Joyner, W.B. and Boore, D.M., (1981) Peak horizontal acceleration and velocity from strong-motion records including records from the 1979 Imperial Valley, California, earthquake. *Bulletin of the seismological Society of America*, 71(6), pp. 2011-2038.
- Kang, L.C., and Jin, X. (2009) Ground motion attenuation relation for small to moderate earthquakes in Sichuan region. *Acta Seismologica Sinica*, 31(4), pp. 403-410 (in Chinese).
- Lei, J.C., Gao, M.T., and Yu, Y.X. (2007) Seismic motion attenuation relations in Sichuan and adjacent areas, *Acta Seismologica Sinica*. 29 (5): 500-511 (in Chinese).
- Liu, B.Y., Liang, Y.H., and Wen, Y.B. (2012) Research on attenuation characteristic of seismic motion in Yunnan. *Journal of Seismological Research*, 35(2), pp. 226-235 (in Chinese).
- Liu, L., and Li, X.J. (2012) Peak ground acceleration attenuation relationship of Wenchuan 8.0 earthquake. *Journal of Beijing University of Technology*, 38(2), pp. 173-179 (in Chinese).
- Liu, C, and Tao, X.X. (2004). Simplified attenuation relationship of PGA based on random vibration theory, *Proceedings of Seismic Prevention and Disaster Mitigation, Beijing, China*, December, 18-20, 2004, pp. 109-114 (in Chinese).
- Liu, P., and Luo, Q.F. (2013) Wenchuan 8.0 magnitude earthquake peak acceleration attenuation relationship based on a model of mapping circle. *Journal of Vibration and Shock*, 32(3), pp. 75-78 (in Chinese).
- Lin, J.Y., Cai, H.C., and Zhao, J. (1993) Analysis and determination of the equation of ground motion attenuation in Hebei province and its nearby areas. *North China Earthquake Science*, 11(3), pp. 19-29 (in Chinese).

- Lu, J.Q., Li, S.Y., and Li, W. (2009) Study on ground motion attenuation relationship of moderate earthquake risk areas. *World Earthquake Engineering*, 25(4), pp. 33-43 (in Chinese).
- Lü, J., Yu, Y.X., Tang, L.R., Gao, J.H., and Lu, F.Y. (2009) Seismic motion attenuation relation in Jiangxi province and its adjacent areas. *Seismology and Geology*, 31(1), pp. 122-132 (in Chinese).
- Mu, H.Q. and Yuen, K.V. (2016) Ground motion prediction equation development by heterogeneous Bayesian learning. *Computer Aided Civil and Infrastructure Engineering*, pp. 1-16.
- Peng, K.Z., Xie, L.L., Li, S.B., Boore, D.M., Iwan, W.D., and Teng, T.L. (1985) The near-source strong-motion accelerograms recorded by an experimental array in Tangshan, China. *Physics of the Earth and Planetary Interiors*, 38, pp. 92-109.
- Shi, S.Z., and Shen, J.W. (2003) A study on ground acceleration attenuation relationship in Shanghai and its adjacent region. *Earthquake Research in China*, 19(4), pp. 315-323 (in Chinese).
- Sun, L.N., Qi, Y.Y., Lü, G.J., Peng, Y.Q., Guo, Q.N., and Tian, L. (2013) A study on bedrock ground motion attenuation relation in Tangshan region, China. *Technology for Earthquake Disaster Prevention*, 8(5), pp. 261-274 (in Chinese).
- Tao, Z.R., Tao, X.X., and Li, W.Q. (2014) Strong ground motion attenuation relationship for North China from small earthquake records by earthquake monitoring networks. *Earthquake Engineering and Engineering Dynamics*, 34.Suppl, pp. 202-205 (in Chinese).
- Tan, L.C. (2015) Improvement in inversion of source spectrum and attenuation parameters for ground motion attenuation in Sichuan and Yunnan region, *master thesis, Harbin Institute of Technology, Harbin, Heilongjiang* (in Chinese).

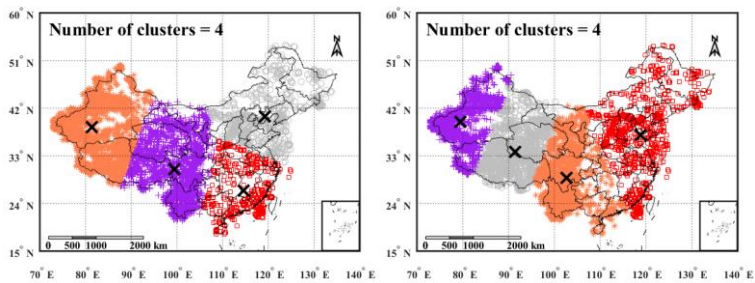
- Tang, L.H., Li, M., and Wang, H.T. (2007) Research on the acceleration attenuation relationship of moderate-strong earthquake in Jiashi-Bachu region. *Northwestern Seismological Journal*, 29(4), pp. 377-384 (in Chinese).
- Tian, L., Gai, X., and Tao, J.Q. (2015) Study on acceleration response spectra based on ground motion attenuation relation at base rock in east China. *Journal of Guangzhou University (Natural Science Edition)*, 14(5), pp. 44-48, 82 (in Chinese).
- Wang, B.Q., Wu, D.M., and Bian, Y.J. (1999) Attenuation characteristics of peak acceleration in North China and comparison with those in the eastern part of North America. *Acta Seismologica Sinica*, 12(1), pp. 26-34.
- Wang, Y.S., Li, X.J., and Zhou, Z.H. (2013) Research on attenuation relationship for horizontal strong ground motions in Sichuan-Yunnan region. *Acta Seismologica Sinica*, 35(2), pp. 238-249 (in Chinese).
- Wang, S.Y., and Wu, H.Y. (1988) Attenuation relation for Lunan region. *Earthquake Research in China*, 4(3), pp. 182-186 (in Chinese).
- Xu, Z.X., Shen, X.B., and Hong, J.R. (1984) Attenuation relation of ground motion in northern China. *Proc. of 8th World Conference on Earthquake Engineering, San Francisco, California*, Volume II, 21-28 July, 1984, pp. 335-342,.
- Xiang, J.G., and Gao, D. (1994) The attenuation law of horizontal peak acceleration on the rock site in Yunnan Area. *Earthquake Research in China*, 8(4), pp. 209-516.
- Yang, F., Luo, Q.F., Li, B.Q., and Che, W. (2011) Acceleration peak attenuation relationship of loess region in Northwestern China on the basis of Wenchuan earthquake. *Journal of Beijing University of Technology*, 37(10), pp. 1487-1483 (in Chinese).
- Yu, Y., Cui, J.W., Li, X.J., and Yang, L.W. (2014) Analysis of ground motion attenuation characterization for moderate earthquakes in Sichuan-Yunnan region. *Earthquake research in China*, 30(3), pp. 409-418 (in Chinese).

- Yu, Y.X., and Wang, S.Y. (2004) Attenuation relations for horizontal peak ground acceleration and response spectrum in Northeastern Tibetan Plateau region. *Acta Seismologica Sinica*, 26(6), pp. 591-600 (in Chinese).
- Yu, Y.X., and Wang, S.Y. (2006) Attenuation relations for horizontal peak ground acceleration and response spectrum in Eastern and Western China. *Technology for Earthquake Disaster Prevention*, 1(3), pp. 206-217 (in Chinese).
- Zhang, Q., Hu, J.J., Xie, L.L., and Jiang, Z.J. (2013) Next generation ground motion attenuation model for Western China. *Journal of Tianjin University (Science and Technology)*, 46(12), pp. 1079-1088 (in Chinese).
- Zheng, T. (2012) Attenuation relationship for acceleration spectra in the northeast seismic zone of China, master thesis. Institute of Engineering Mechanics, China Earthquake Administration, Harbin, China (in Chinese).

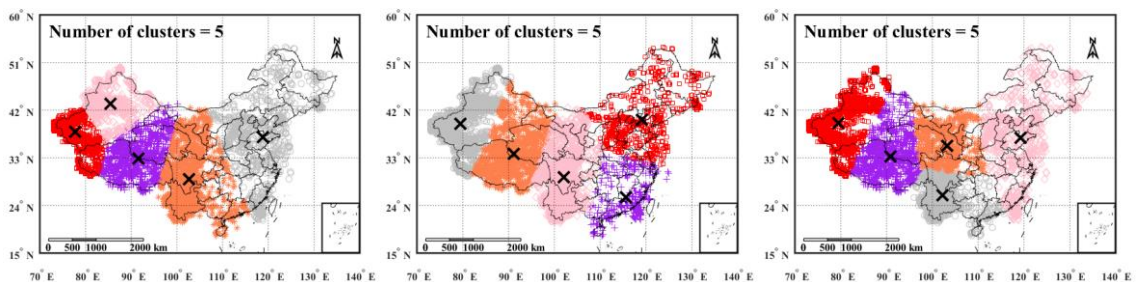
## Appendix B: k-means cluster analysis results

The k-means cluster analysis is used for the development of the nine seismic source regions (setting the number of clusters equal to 9) that considered as the seismic source model for Case II in Chapter 3. The results of the k-means cluster analysis based on the number of clusters ranging from 4 to 10 are given in this appendix for complementary. The “x” symbols in the figure denote the central for the obtained clusters. Some approaches for selecting the best number of the clusters that used for the analysis are available in Wu (2012), and the estimated best number of clusters by considering different approaches may vary, therefore, the selection for the best number of the clusters in this study is based on the inspection of the results in this Appendix B, and the number of the clusters equal to 9 gives a relatively better result to reduce the inhomogeneity of geographically varying seismicity. The following results are obtained using the MATLAB with code “kmeans”. For each considered cluster number, the non-repetitive obtained results are shown in the figures below.

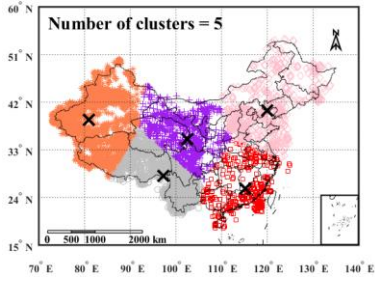
Results based on the considered cluster number = 4:



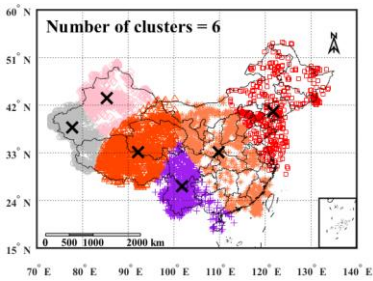
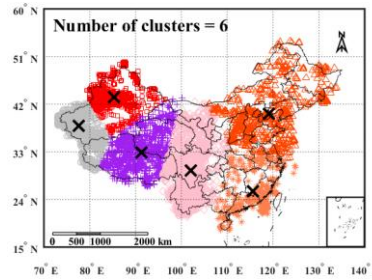
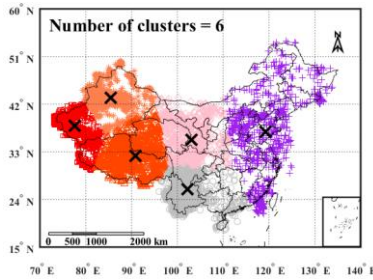
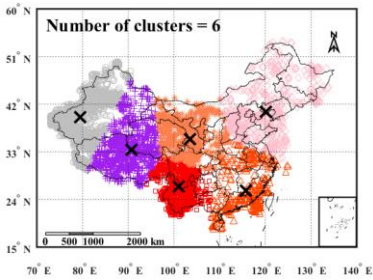
Results based on the considered cluster number = 5:



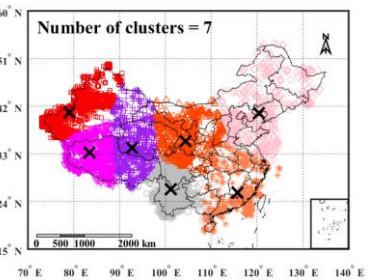
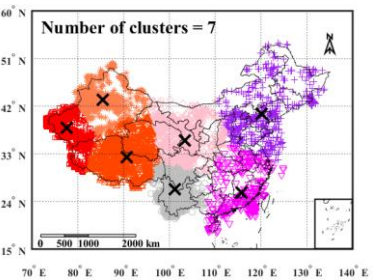
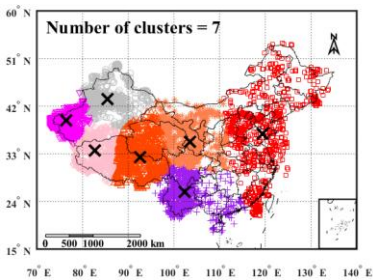




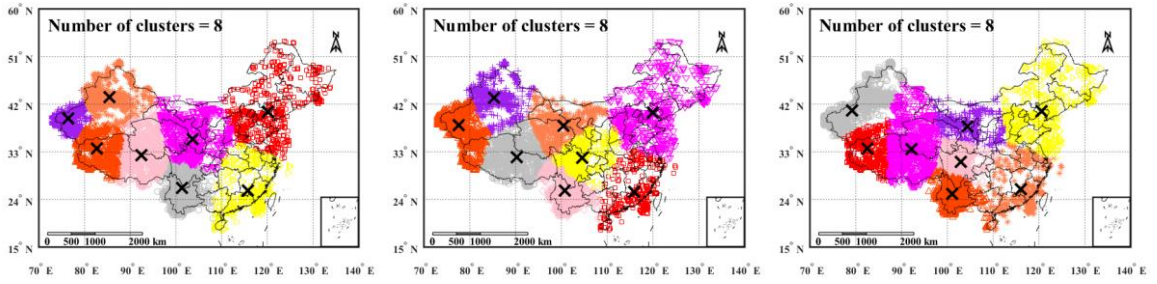
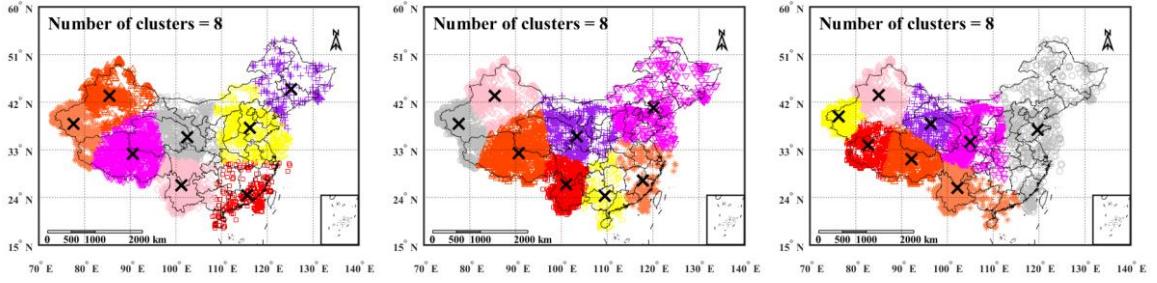
Results based on the considered cluster number = 6:



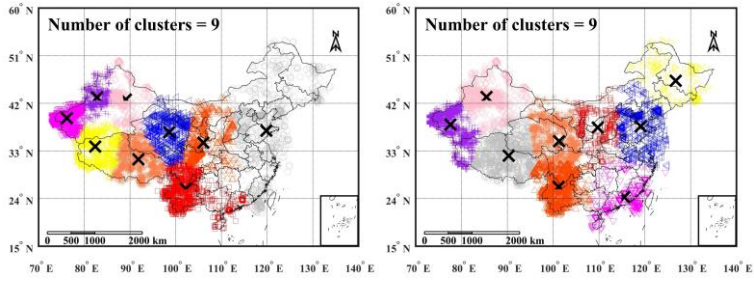
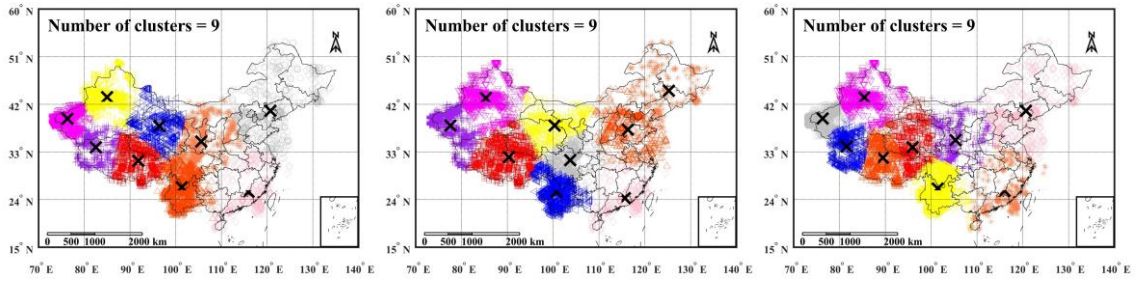
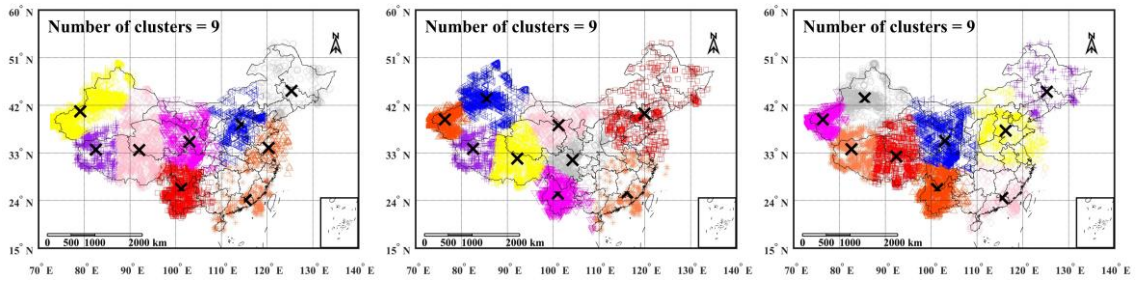
Results based on the considered cluster number = 7:



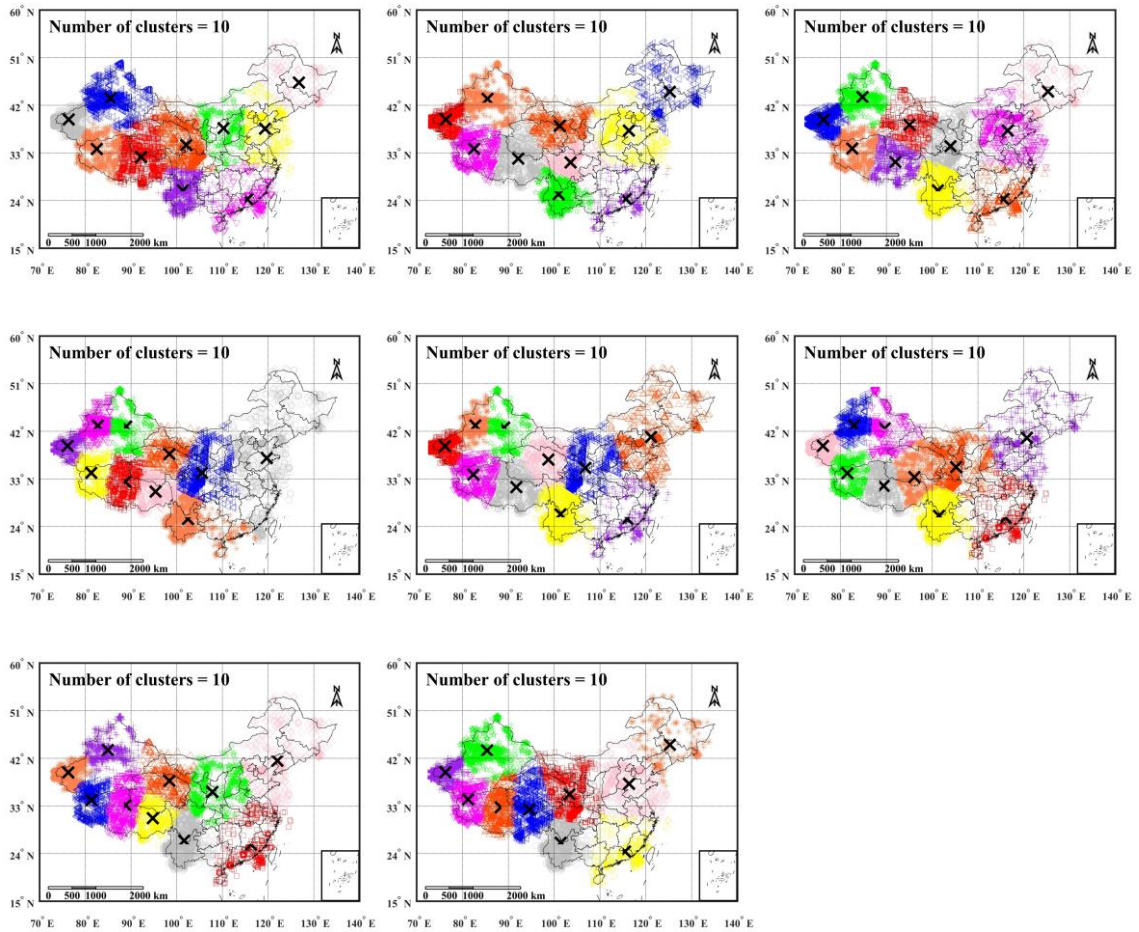
Results based on the considered cluster number = 8:



Results based on the considered cluster number = 9:



Results based on the considered cluster number = 10:



## Reference

Wu, J. (2012). *Advances in K-means clustering: a data mining thinking*. Springer Science & Business Media.

MATLAB. (2017). version 9.2.0.538062 (R2017a). Natick, Massachusetts: The MathWorks Inc.

## Curriculum Vitae

**Name:**

Chao Feng

**Post-secondary**

Northeast Agricultural University

**Education and**

Harbin, Heilongjiang, China

**Degrees:**

2008-2012 B.E.Sc.

Northwest A&F University  
Yangling, Shaanxi, China  
2012-2015 M.Eng.Sc.

The University of Western Ontario  
London, Ontario, Canada  
2015-2020 Ph.D.

**Honours and**

2015-2019 Chinese Government Scholarship

**Awards:****Related Work**

Teaching Assistant

**Experience**

The University of Western Ontario  
2015-2019

**Publication in Referred Journal:**

Hong, H.P, and C. Feng. (2019). On the ground motion model for Chinese seismic hazard mapping, *Bulletin of Seismological Society of America*, 109(5), 1912-1921.  
[doi.org/10.1785/0120180269](https://doi.org/10.1785/0120180269)

Feng, C., Liu, T. J., and Hong, H. P. (2020). Seismic hazard assessment for mainland China based on spatially smoothed seismicity. *J Seismol*, 24, 613–633, doi.org/10.1007/s10950-020-09918-3.

**Publication in Conference Proceedings:**

Feng, C, T.J, Liu, and H.P. Hong (2019). Application of kernel smoothing approach to assess seismic hazard for selected regions in Canada, *12<sup>th</sup> Canadian Conference on Earthquake Engineering*, June 17-20, 2019, Quebec, QC.